

CRANFIELD UNIVERSITY

VICENTE MARTÍNEZ MARTÍNEZ

Modelling of the Flight Dynamics of a Quadrotor Helicopter

SCHOOL OF ENGINEERING

MSc THESIS

CRANFIELD UNIVERSITY

SCHOOL OF ENGINEERING

DEPARTMENT OF AEROSPACE SCIENCES

MSc THESIS

Academic Year 2006-2007

VICENTE MARTÍNEZ MARTÍNEZ

Modelling of the Flight Dynamics of a Quadrotor Helicopter

Supervisor: Dr. Alastair K. Cooke

September 2007

This thesis is submitted in partial fulfilment of the requirements for the degree of
Master of Science by Research

©Cranfield University 2007. All rights reserved. No part of this publication may be reproduced
without the written permission of the copyright owner.

ABSTRACT

Historically, helicopters with four rotors (quadrotors) have not been very common, mainly because most of the usual payloads could be lifted using one or two rotors. However, the quadrotor possesses some special characteristics that make it attractive. One, of course, is the superior payload capacity. The other is the simplicity of its control system: just by independently adjusting the speed of each rotor it is possible to control both the attitude and the horizontal/vertical motion. This system is particularly suitable for small UAVs, because it reduces the mechanical complexity of the rotors (saving volume and weight) and simplifies the control algorithms required for autonomous flight.

Although much progress has been made in the field of quadrotor UAVs, it is still a great challenge to build a quadrotor capable of fully autonomous flight. In order to be successful in selecting the appropriate control algorithms it is essential to have a complete understanding of quadrotor flight dynamics.

This Report presents a detailed physical model to describe quadrotor flight dynamics. It is based on a real quadrotor, the Draganfly XPro, but retains the necessary flexibility to be applied to other quadrotors.

The model relies on standard helicopter theories, although these have been severely modified to account for the particularities of the quadrotor. The level of detail is above that which was common in previous quadrotor models: rotor in-plane forces and moments have been included, as well as blade flapping dynamics. To obtain the necessary experimental data, a series of wind tunnel tests has been carried out.

On the final part of this Report, the model is coded into Matlab/Simulink. The simulator is then used to study open loop flight dynamics. In the future, this simulator will also be used to test potential control algorithms.

To my parents, who have always supported me

LIST OF CONTENTS

List of Figures.....	9
List of symbols and acronyms	13
1. Introduction	19
2. Fundamentals of the quadrotor	24
3. The Draganfly XPro	36
4. Equations of motion	38
5. Estimation of mass and inertial properties	57
6. Equations of the D.C. motors	61
7. Estimation of the constants of the motors	66
8. Selection of the model for the rotor	70
9. Modelling of the rotor	75
10. Induced flow model	107
11. Aerodynamics of the airframe	114
12. Wind tunnel tests	120
13. Analysis of the experimental data. Rotor model validation	133
14. The Matlab/Simulink model of the quadrotor	156
15. Limitations of the model.....	169
16. Running the Matlab/Simulink model of the quadrotor.....	173
17. Conclusions	203
References	211
Appendix A: Matlab/Simulink Model	219
Appendix B: Mass and inertial properties	221
Appendix C: Technical data of the motor	225
Appendix D: Motor tests	227
Appendix E: Wind tunnel tests.....	228
Appendix F: Coefficients of forces and moments	241
Appendix G: Matlab files	272
Appendix H: Simulink blocks	281

LIST OF FIGURES

Fig 1.1. The Yuri I, a human powered quadrotor (Ref 2.12).	31
Fig 2.2. Pitch control.	32
Fig 2.3. Yaw control.	33
Fig 2.4. “Heave” control.	34
Fig 3.1. Image of the CAD model of the Draganfly XPro.	37
Fig 4.1. Moments over the armature.	44
Fig 4.2. Body axes.	46
Fig 5.1. CAD model of the Draganfly XPro.	58
Fig 5.2. Schematic of the simplified model to estimate the moments of inertia.	59
Fig 8.1. Picture of the blades of the XPro	73
Fig 9.1. Detail of the hub-blade assembly.	75
Fig 9.2. Real blade (up), Offset-hinge and spring (middle), Offset-hinge with no spring (down) (Ref 9.3).	78
Fig 9.3a. Set of axes $P_i x_w y_w z_w$	80
Fig 9.3b. Forces on the rotor(quantities positive as shown).	81
Fig 9.3c. Moments on the rotor (quantities positive as shown).	81
Fig 9.4. Azimuthal angle ψ in a conventional helicopter (Ref 9.4).	83
Fig 9.5. Flapping angles in a conventional helicopter (Ref 9.4).	84
Fig 9.6 Lateral view of the quadrotor. The thrust \mathbf{T} and the torque vector \mathbf{Q} are perpendicular to the Tip Path Plane (TPP). The force \mathbf{H} is parallel to it	91
Fig 10.1. Induced Velocity Ratio vs Climb Velocity Ratio in axial flight.	110
Fig 11.1. $Oxyz$ and $Ox_w y_w z_w$ axes.	114
Fig 9.3b. Forces on the rotor (quantities positive as shown).	121
Fig 9.3c. Moments on the rotor (quantities positive as shown).	121
Fig 12.1. Picture of the test installation showing how the support of the rotor can rotate around the axis of the balance.	122
Fig 12.2. Measuring equipment in the wind tunnel.	123
Fig 12.3. IR transmitter-receiver already installed.	124
Fig 12.4. Detail of the position of the point O_i	125
Fig 12.5(a). Motor-rotor performance: comparison between the “smoothed” experimental curve (solid line) and the results estimated. R_a, K were taken as the average of the nine obtained values.	127
Fig 12.5(b). Motor-rotor performance: comparison between the “smoothed” experimental curve (solid line) and the results estimated. R_a, K were taken as the average of the two last obtained values.	128

Fig 13.1. Thrust coefficient C_T (or C_{f_z}) plotted against λ_z , in axial flight ($\mu = 0$)...	138
Fig 13.2. Dependence of the measured C_T on the spinning speed.	139
Fig 13.3. C_T values measured by Felker and McKillip.	141
Fig 13.4. $-C_Q$ (or $-C_{m_z}$) plotted against λ_z	143
Fig 13.5. Coning angle a_0 in hover.....	145
Fig 13.6. $C_{f_z}(\lambda_z, \mu)$ surface.....	147
Fig 13.7. $-C_{m_z}(\lambda_z, \mu)$ surface	148
Fig 13.8. $a_0 + a_{1s}$, against Ω (rotor horizontal, free stream velocity of 15.5m/s)	151
Fig 13.9. $a_0 + a_{1s}$ against μ (rotor horizontal, free stream velocity of 15.5m/s)	151
Fig 14.1. Interior of block “Motor”	159
Fig 14.2. Detail of Block “Dynamics” showing how the angular rates are calculated.	161
Fig 14.3. Interior of Block “Euler”	162
Fig 16.1. Heave: step input.....	174
Fig 16.2. Heave: vertical speed (step input).	174
Fig 16.3. Heave: altitude (step input).	175
Fig 16.4. Heave: effect of C_T on the vertical speed (step input).	176
Fig 16.5. Heave: pulse input.....	176
Fig 16.6. Heave: vertical speed (pulse input).	177
Fig 16.7. Heave: altitude (pulse input).	177
Fig 16.8(a). Pitch up: step input.	179
Fig 16.8(b). θ (step input).....	179
Fig 16.9(a). Pitch up: pulse input.	179
Fig 16.10(a). Pitch up: double pulse input.	179
Fig 16.9(b). θ (pulse input).....	179
Fig 16.10(b). θ (double pulse input).....	179
Fig 16.11. Quadrotor pitching up.	180
Fig 16.12. Pitch up: effect of f_x and m_y (pulse input).....	182
Fig 16.13(a). Pitch up: vertical speed.	183
Fig 16.13(b): Pitch up: altitude.....	183
Fig 16.14. Pitch up: q (step input, gimbal support).....	183
Fig 16.15. Pitch up: θ (step input, gimbal support).....	184
Fig 16.16. Quadrotor with gimbal support.	184
Fig 16.17. Pitch up: effect of C_T and m_y on q (step input, gimbal support).....	185
Fig 16.18. Pitch up: q (pulse input, gimbal support).....	186
Fig 16.19. Pitch up: θ (pulse input, gimbal support).....	186
Fig 16.20. Pitch up: effect of the spring strength on θ (pulse input, gimbal support).	187
Fig 16.21. Yawing: step input (Signal 1).	188
Fig 16.22. Yawing: r (step input).....	189
Fig 16.23. Yawing: ψ (step input).....	189
Fig 16.24. Yawing: effect of f_x on r (step input).....	190
Fig 16.25. Yawing: r (pulse input).....	191
Fig 16.26. Yawing: ψ (pulse input).....	191
Fig 16.27. Yawing: ϕ and θ (pulse input).	192

Fig 16.28. Vertical gust velocity, relative to the ground.	195
Fig 16.29. Vertical gust: quadrotor vertical velocity.	196
Fig 16.30. Vertical gust: altitude.	196
Fig 16.31. Horizontal gust velocity.	197
Fig 16.32. Horizontal gust: pitch angle.	197
Fig 16.33. Effect of the inductance on the pitch up manoeuvre.	198

LIST OF SYMBOLS AND ACRONYMS

Symbols

All magnitudes are given in S.I. units, unless otherwise stated.

\mathbf{a}_G	acceleration of the centre of mass of the airframe, in an inertial frame
\mathbf{a}_{Gi}	acceleration of the centre of mass of the hub, in an inertial frame
\mathbf{a}_{Gj}	acceleration of the centre of mass of the armature, in an inertial frame
\mathbf{a}_O	acceleration of the point O , in an inertial frame
A_l	longitudinal cyclic pitch parameter
a	slope of the lift coefficient curve
a_0	coning angle
a_{1s}	longitudinal flapping angle
B_l	lateral cyclic pitch parameter
b	number of blades per rotor
b_{1s}	lateral flapping angle
C_{fx}, C_{fy}, C_{fz}	coefficients corresponding to f_x, f_y, f_z
C_{mx}, C_{my}, C_{mz}	coefficients corresponding to m_x, m_y, m_z
$(C_{mx})_{hub}, (C_{my})_{hub}$	coefficients corresponding to $(m_x)_{hub}, (m_y)_{hub}$
$C_{fxa}, C_{fya}, C_{fza}$	coefficients corresponding to f_{xa}, f_{ya}, f_{za}
$C_{mxa}, C_{mya}, C_{mza}$	coefficients corresponding to m_{xa}, m_{ya}, m_{za}
C_H	H force coefficient
C_Q	torque coefficient
C_T	thrust coefficient
c	“mean” blade chord
c_{d0}, c_{d1}, c_{d2}	coefficients of the drag polar
e	effective hinge offset
e_j	offset of the joint between the blade and the hub
F	friction coefficient
$\mathbf{F}_{\text{airframe}}$	aerodynamic forces over the airframe
\mathbf{F}_i	aerodynamic forces applied to the b-blades system at its centre of mass,
	P_i
F_{xi}, F_{yi}, F_{zi}	components of \mathbf{F}_i in body axes
f_x, f_y, f_z	components of \mathbf{F}_i in $P_i x_w y_w z_w$ axes
f_{xa}, f_{ya}, f_{za}	components of $\mathbf{F}_{\text{airframe}}$ in $O x_w y_w z_w$ axes
\mathbf{g}	gravitational acceleration vector

g	gravitational acceleration
g_r	gear ratio
G	centre of mass of the airframe
G_i	centre of mass of the hub
G_j	centre of mass of the armature
G_T	centre of mass of the quadrotor
\mathbf{H}_G	angular momentum of the airframe, at its centre of mass, measured in an inertial frame
\mathbf{H}_{Gi}	angular momentum of the hub, at its centre of mass, measured in an inertial frame
\mathbf{H}_{Gj}	angular momentum of the armature, at its centre of mass, measured in an inertial frame
\mathbf{H}_{Pi}	angular momentum of the b-blades system, at its centre of mass, measured in an inertial frame
H	aerodynamic force on the Tip Path Plane
h	distance between O_i and P_i
\mathbf{I}_G	inertia tensor of the airframe at its centre of mass, in body axes $Oxyz$
\mathbf{I}_{Gi}	inertia tensor of the hub at its centre of mass, in a set of axes parallel to $Oxyz$
\mathbf{I}_{Gj}	inertia tensor of the armature at its centre of mass, in a set of axes parallel to $Oxyz$
$I_x, I_y, I_z, I_{xy}, I_{yz}, I_{xz}$	components of \mathbf{I}_G
I_{xi}, I_{yi}, I_{zi}	components of \mathbf{I}_{Gi}
I_{xj}, I_{yj}, I_{zj}	components of \mathbf{I}_{Gj}
I_{yb}	inertia of the blade around the effective hinge
I_{zb}	inertia of the blade around the axis of the hub
i_a	armature current
K	voltage-rotational speed constant
K_c	constant of Glauert's inflow model
k_β	blade spring strength
L	armature inductance
m	mass of the airframe
m_b	mass of the blade
m_i	mass of the hub
m_j	mass of the armature
m_T	total mass of the quadrotor
$\mathbf{M}_{\text{airframe}}^O$	aerodynamic moments over the airframe, at O
\mathbf{M}^{Pi}	aerodynamic moments applied to the b-blades system at its centre of mass, P_i

M_b	first static moment
M_{xi}, M_{yi}, M_{zi}	components of \mathbf{M}^{Pi} in body axes
$(M_{xi})_{hub}, (M_{yi})_{hub}, (M_{zi})_{hub}$	components of the moment transmitted by the b blades to the hub, in body axes
m_x, m_y, m_z	components of \mathbf{M}^{Pi} in $P_i x_w y_w z_w$ axes
$(m_x)_{hub}, (m_y)_{hub}, (m_z)_{hub}$	components of the moment transmitted by the b blades to the hub, in $P_i x_w y_w z_w$ axes
m_{xa}, m_{ya}, m_{za}	components of $\mathbf{M}_{\text{airframe}}^0$ in $Ox_w y_w z_w$ axes
O	reference point of the airframe
O_i	reference point of the hub
p, q, r	components of the angular velocity of the airframe in body axes
P_w, q_w, r_w	components of the angular velocity of the airframe in $P_i x_w y_w z_w$ axes
P_i	centre of mass of the b-blades system
\mathbf{Q}	aerodynamic torque vector
Q	torque vector modulus
R	rotor disc radius
R_a	armature resistance
r	longitudinal coordinate of the blade station
r_{Gb}	longitudinal coordinate of the centre of mass of the blade
\mathbf{T}	thrust vector
T	thrust vector modulus
u, v, w	components of the velocity of O in body axes
u_e, v_e, w_e	components of the velocity of O in ground axes
u_i, v_i, w_i	components of the velocity of O_i in $Oxyz$ axes
V	Speed of the free stream in the wind tunnel
v_a	armature voltage
\mathbf{v}_G	velocity of the centre of mass of the airframe, in an inertial frame
v_{ind}	average induced velocity or local induced velocity at $\psi = \pm \frac{\pi}{2}$ (Glauert's inflow model)
$(v_{ind})_{local}$	local induced velocity
V_x	in-plane component of the velocity
V_z	velocity component perpendicular to the Hub Plane
x_e, y_e, z_e	coordinates of O in ground axes
α	angle of attack of the rotor
α_a	angle of attack of the airframe
α_1	first coefficient of Southwell
β	flapping angle

β_{ss}	sideslip angle of the rotor
β_{ssa}	sideslip angle of the airframe
γ	Lock number
ϕ, θ, ψ	Euler angles (roll, pitch, yaw)
ψ	blade azimuthal angle
κ	corrective factor for λ_{ind}
λ_1	frequency ratio of the first blade flapping mode
λ_{ind}	v_{ind} to tip speed ratio
λ_z	V_z to tip speed ratio
μ	V_x to tip speed ratio
Ω	rotational speed of the rotor
ρ	air density
σ	rotor solidity
τ_j	EM torque
θ_0	Pitch angle at the blade root
θ_1	Blade twist
ω	rotational speed of the motor
$\mathbf{\omega}$	angular velocity of the rigid airframe, measured in an inertial frame
$\mathbf{\omega}_i$	angular velocity vector of the hub, measured in an inertial frame
$\mathbf{\omega}_j$	angular velocity vector of the armature, measured in an inertial frame
ω_{nr}	blade non-rotating flap frequency

Subscripts

i	rotor number. $i = 1$ for the front rotor (Rotors are numbered clockwise)
j	motor number $j = 1$ for the front motor (motors are numbered clockwise)

Dressings

$\dot{x}_e = \frac{dx_e}{dt}$	differentiation with respect to time
\bar{V}_z	non-dimensionalized with the induced velocity in hover

Acronyms

BET	Blade Element Momentum Theory
HP	Hub Plane
MT	Momentum Theory

MMT	“Modified” Momentum Theory
TPP	Tip Path Plane
TWS	Turbulent Wake State
VRS	Vortex Ring State
WBS	Windmill Brake State

1. INTRODUCTION

1.1 Background

A quadrotor is a rotorcraft equipped with four rotors laid up symmetrically around its centre. It is capable of hover, forward flight and vertical take off and landing, therefore it should be classified as a rotary-wing VTOL aircraft.

Traditionally the quadrotor configuration has not been used in the aerospace industry, mainly because most of the usual payloads could be lifted using one or two rotors. However, the quadrotor possesses some special characteristics that make it attractive. One, of course, is the superior payload capacity. The other is the simplicity of its control system: just by independently adjusting the speed of each rotor it is possible to control both attitude and linear velocity. This system is particularly suitable for small UAVs, because it reduces the mechanical complexity of the rotors (saving volume and weight) and simplifies the control algorithms required for autonomous flight.

1.2 Problem statement

Although much progress has been made in the field of quadrotor UAVs, it is still a great challenge to build a quadrotor capable of fully autonomous flight. To do so, it is necessary to implement the appropriate control algorithms and to have a suitable set of sensors. As for the design of the control algorithms, in order to be successful in that task it is essential to have a complete understanding of quadrotor flight dynamics. Failure to adequately model these dynamics may lead to the selection of an unsuitable controller.

The aim of this Research Project is to produce a quadrotor model that can be later used as a tool for the study of Stability and Control. This model will be programmed in Matlab/Simulink and will be based around the Draganfly XPro quadrotor. In order to enable this quadrotor to fly autonomously, several controllers have been proposed. It is expected that these controllers will be tested in the model before implementing them in the real vehicle. Hence, the accuracy of the model (and thus the level of detail) has to be in accordance with the requirements of this task. Ideally, the model should have enough flexibility to be adapted in the future to simulate other quadrotors apart from the XPro.

1.3 Description of the key objectives

As a part of the global aim, several objectives are pursued:

- To study and summarize all the published information about quadrotors in general and quadrotor flight dynamics in particular
- To create a physical model of the vehicle
- To study the aerodynamics of the rotor
- To program the model using Matlab/Simulink
- To investigate the flight handling characteristics in open-loop

These objectives are explained below.

To study and summarize all the published information about quadrotors in general and quadrotor flight dynamics in particular

Prior to starting to study in detail the flight dynamics of the quadrotor, it is necessary to have some basic knowledge about this type of helicopter: how is it controlled, what are its potential applications, what are its main advantages over other types of rotorcraft, etc.

Even more important is to gather all the published information about quadrotor modelling and flight dynamics. Although there are already several reports that look at these subjects in depth (Refs 1.1 to 1.7), most of the information available is still scarce and incomplete. It would be convenient to unite all this information into a single piece of work that could later be used as a starting point for future research.

Creating a physical model of the quadrotor

To be able to accurately predict the flight dynamics of the quadrotor, a detailed physical model is necessary. This model should be as general as possible, making the minimum number of assumptions and hypotheses. Nevertheless, the model will be particularized for a specific quadrotor, the Draganflyer XPro, although it should be easily customizable to suit a different type of quadrotor. The elements that constitute this model are the following:

- A set of equations of motion
- A model of the rotor
- A set of equations to describe the dynamics of the motors

Additionally, a simple gust model will also be included.

Most of the works published about quadrotors focus on Control issues (see Refs 1.8 to 1.14); they use fairly simple models to describe the Flight Dynamics of the vehicle. Although this is very convenient to simplify the mathematics, it can lead to the omission of important effects that may significantly affect flight handling.

An example of this is rotor modelling. Many works (see Refs 1.8 to 1.10 and Ref 1.14, for example) consider that the rotors are rigid, that the thrust and torque coefficients are constant and that there are no in-plane forces and moments. But nothing of this is true: the blades are flexible and so the thrust is not parallel to the axis of the rotor; the thrust and torque coefficients are not constant but heavily depend on the airflow through the rotor; and there are in-plane forces and moments that may contribute to de-stabilize the vehicle.

Fortunately, this trend is already starting to reverse. Researchers are turning their eyes to helicopter theory to seek for clues on how to produce better models of quadrotor

dynamics (Refs 1.2, 1.4 and 1.7). However, application of helicopter theory to quadrotors is not straightforward. There are many important differences between conventional helicopters and quadrotors and this has to be addressed. For instance, conventional helicopters keep rotor speed constant. Hence, traditional helicopter theories are optimized for the normal values of this rotor speed. On the other hand, most quadrotors (except those which are capable of adjusting the pitch angle of their blades) are controlled by independently modifying the speeds of the four rotors. These speeds can be a 50% higher or lower than the value corresponding to hover. Traditional helicopter theories might fail at the lower end of this range, and they do not predict the effect on the rotor wake of constant speed changes.

It will be seen that most of the limitations of traditional helicopter theories can be circumvented. In the case of rotor speed, by keeping far from the lower limit and by assuming quasi-steady conditions during each revolution.

This Research Project will try to produce a quadrotor model with a higher level of detail than that of already existing models. It will also try to determine whether such a model is accurate enough to be used to test those controllers which are planned to be implemented in the real vehicle.

Studying the aerodynamics of the rotor

This is a consequence of the need to produce an accurate physical model of the whole vehicle. It is obvious that the rotors are the most important element and thus modelling them correctly is critical. In order to do so, several theories will have to be reviewed and numerous tests will have to be conducted at the wind tunnel. In fact, large portions of this Report will be devoted to this subject.

Producing a Matlab/Simulink model of the quadrotor

As it has been already mentioned, the physical model of the quadrotor will be programmed in Matlab/Simulink. The main requirements of the simulation are:

- Acceptable execution times
- Robustness
- Modular architecture, to make it as flexible as possible and easy to modify

No graphics engine will be used. It is preferred to concentrate efforts on the development the physical model.

Studying the open-loop flight dynamics

A quadrotor is not likely to be flown in open loop. It is very unstable; corrections have to be made constantly and at very high frequencies. As a result, only close-loop flying is feasible. However, it is still important to study open-loop flight dynamics, so that we

can have a better understanding of the challenges that any stabilization/control system will have to face. It will be seen that these “challenges” include: very fast dynamics (short time constants), coupling between attitude and linear velocity, sensitivity to pitch/roll disturbances, etc.

1.4 Overview of the work undertaken

In order to fulfil the objectives previously described, a clear sequence of tasks had to be carried out. A complete description of the work undertaken will be done in the following Sections. At this point, it will be enough with briefly describing the tasks that were performed.

First of all, an extensive work of research was done in order to fulfil the first of the objectives, which was to acquire a basic understanding about the characteristics of quadrotor machines. This research gave a considerable importance to the resources available on the Internet, since the traditional resources (books, articles...) contained detailed information about specific subjects (control techniques, dynamic models...) but little about the basic issues, such as the history of the quadrotor concept or its potential applications.

In the next place came the task of building the physical model of the quadrotor. This meant writing down the equations of motion and the equations of the motors. As for the rotor model, several options were examined. Finally, it was decided to use a model based on those from Prouty and Young (see Section 9).

Although the rotor model was entirely theoretical, experimental data were needed to adjust several parameters and to validate the model itself. In order to obtain these experimental data a complete sequence of tests with the rotor in the wind tunnel was conceived and carried out. These tests proved successful, providing data about thrust, torque and even about flapping dynamics. However, no reliable information about rotor in-plane forces and moments could be obtained.

The tests in the wind tunnel also served to obtain some experimental data about the dynamics of the electric motors, which were required for the model.

Another important task was to obtain the mass and inertial properties of the quadrotor. To do so, all the elements of the XPro were carefully measured and weighed. Then, a complete CAD model of the quadrotor was made. This model was later used to obtain the position of the centre of mass and the moments and products of inertia of the complete assembly and its sub-assemblies.

Once the physical model was ready and the mass and inertial properties had been obtained, it was possible to build the Matlab/Simulink model of the Draganflyer XPro. This simulation did not introduce other simplifications apart from those which were already included in the physical model. The result was a simulation in six degrees of freedom of the quadrotor.

Finally, the Matlab/Simulink model was used to investigate open-loop flight dynamics. Potential control problems were identified, previously known results were confirmed and new flight characteristics were observed.

2. FUNDAMENTALS OF THE QUADROTOR

2.1 Introduction




As it was stated in Section 2.1, this Project is focused on a particular quadrotor, the Draganflyer XPro. But before commenting in detail the characteristics of this rotorcraft, it is necessary to have a general knowledge about quadrotors: operating principles, advantages, drawbacks and potential applications.

2.2 The quadrotor concept

A quadrotor is a rotorcraft composed of four rotors laid up symmetrically around its centre. It is capable of hover, forward flight and vertical take off and landing. Hence, it should be classified as a rotary-wing VTOL aircraft.

Although the term “quadrotor” is the most common, other terms are used to refer to this vehicle, such as “quadrocopter” (german) or simply “four-rotor helicopter”. Other terms are trademarked, like “quad copter” or “quattrocopter”.

This configuration is relatively rare amongst helicopters. Most helicopters, no matter what size, are fitted with just one main rotor and a tail rotor to compensate the reaction torque. The table below possibly includes all the existing configurations, including the two already mentioned:

Configuration	Description	Figure
Conventional/Single rotor	One main rotor + one tail rotor	
Tandem	Two counter-rotating rotors: front and rear	
Side by side	Two counter-rotating rotors: left and right	



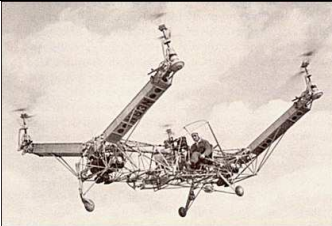
Coaxial	Two coaxial counter-rotating rotors	
“Intermeshing” or “Synchropter”	Two counter-rotating rotors, mechanically linked	
“Quadrotor”	Two pairs of counter-rotating rotors	

Table 2.1. Helicopter configurations.

As it has been said, the single rotor solution is by far the most extended, at least among manned helicopters. The tandem configuration is also used in some well-known cases, such as the CH-47 “Chinook”, and the side by side type is known for being the one chosen for the world’s largest helicopter, the MIL V-12. There are several helicopters with coaxial rotors too, such as those manufactured by Kamov. In unmanned helicopters, the coaxial configuration is at least as widespread as the single-rotor one. On the other hand, Kaman is a well-known manufacturer of helicopters that use the “Synchropter” configuration. But the quadrotor configuration is extremely rare.

There are two basic reasons for this. The first one is that the majority of the usual payloads can be lifted using one or at most two main rotors, hence there is no need for more rotors, which increase the weight and the complexity of the vehicle. The other is the lack of experience in designing helicopters of this type, which is of course a consequence of the first.

Because of these issues, the quadrotor configuration has traditionally been restricted to a few experimental vehicles. However, this trend has started to change in recent years, and the future of the quadrotor looks now much more promising. To understand why, it is necessary to take a look at the advantages of this configuration, as opposed to its drawbacks.

2.4 Major advantages of the quadrotor concept

These advantages, compared to the other configurations, are the following:

- Higher payload capacity
- Simplicity of the control system
- Reduced gyroscopic effects
- Improved stability

Higher payload capacity

The more obvious advantage is the first one. The thrust developed by a rotor increases with its diameter (Refs 2.1 and 2.2). Thus, by increasing the diameter it is possible to increase the thrust and therefore the payload which can be lifted. However, there is a limit as to how much the diameter can be increased, which is imposed by the compressibility effects that occur at the tip of the blade when it is moving so fast that it approaches the transonic region. Even then, it is possible to augment the thrust by adding more blades to the rotor, but this also has a limit, imposed both by the increasing mechanical complexity and by the interaction between the wakes of the blades.

So if the thrust has to be raised even more, it is necessary to add more rotors. This is precisely what was done in the CH-47 “Chinook”, a tandem rotor helicopter which was designed to lift very large payloads. And there is no special reason why the number of rotors should be limited to two. However, as the number of rotors increases the empty weight of the helicopter rises too, and so the ratio payload/weight is reduced. It would be possible to reach a point in which no payload can be carried because all the thrust is used to lift the empty vehicle.

It should be noted that the configurations with an odd number of rotors are unadvisable, because it is not possible to arrange them in pairs, with one rotating in the opposite direction of the other. Since it is not possible to arrange them in pairs, it is more complicated to balance all the reaction torques.

Simplicity of the control system

In sub-section 2.7 it will be explained that it is possible to control the attitude of the quadrotor just by adjusting separately the rpm of each rotor. There are also other control methods which will be explained when appropriate, and which do not consist in varying the rpm. But what it is said here applies only to the first method. In all the other mentioned configurations (single rotor, tandem, side by side, coaxial) the attitude control is achieved by varying the pitch angle of the blade, while the rotational speed of the rotors remains constant. In order to vary the pitch angle complex mechanical systems are required. These systems are prone to failure, increase the weight and need frequent maintenance. But if the attitude control can be achieved just by modifying the rpm of the rotors, then there is no need for those systems, saving costs, weight and

volume. In particular, the reduction in weight and volume can be very interesting for some applications, such as small UAVs.

On the other hand, the conceptual simplicity of this control system makes it easy to automate, which is another reason why the quadrotor configuration is so attractive for UAVs.

Reduced gyroscopic effects

Gyroscopic effects can affect every rotating body, including the rotor of a helicopter. However, depending on the type of rotor, these gyroscopic effects will be different (Ref 2.3).

An articulated rotor (see Section 9) will tend to behave like an ideal gyroscope, which means that its angular momentum vector will tend to keep the same orientation when the helicopter changes its attitude. On the other hand, a perfectly rigid rotor (see Section 9) will introduce a gyroscopic moment on the airframe when there is a change in attitude. Other types of rotors will behave in an intermediate way.

In all the cases, the gyroscopic effects will depend on the rpm and the direction of rotation of the rotor.

In a quadrotor, two rotors are turning clockwise and the other two, counter clockwise. If the rpm are identical in the four rotors then the gyroscopic effects will cancel out. In practice, these gyroscopic effects might not cancel out because of the tolerances in the position of the rotors, their masses, etc. But in any case the gyroscopic effects will be much smaller than in a single rotor helicopter.

Improved stability and controllability

For the same mass, a quadrotor has larger moments of inertia around its three axes, compared to a single rotor helicopter (Ref 2.4). On the other hand, it can be demonstrated that the time constant associated to the motion around each of those axes is proportional to the square root of the corresponding moment of inertia. For example, if we consider a pitch up manoeuvre, the equation of moments around the centre of mass of the vehicle will be:

$$M = I_y \ddot{\theta}$$

Where M is the external moment applied, I_y is the moment of inertia around the y axis and θ is the pitch angle. If we estimate the orders of magnitude:

$$M \sim I_y \frac{\theta_c}{t_c^2}$$

Where θ_c is the pitch angle obtained and t_c is the time constant. Therefore:

$$t_c \sim \sqrt{\frac{\theta_c}{M}} I_y$$

As we wanted to prove.

Hence, the quadroptor will have larger time constants than the single rotor helicopter, at least in theory. Larger time constants mean that the pilot has more time to react to divergent modes and to make the necessary corrections or, in other words, that the controllability is better. Full scale helicopters are easier to pilot than their reduced scale counterparts because the moments of inertia of the former are much larger.

The author of this report tried to find the opinion to this respect of experienced pilots of helicopters. As to the difference between full scale helicopters and aeromodels, there is consensus about the fact that the latter are more difficult to pilot. However, as for the difference between quadroptor and single-rotor aeromodels, there is no such consensus. In fact, some pilots think that the quadroptor may be more difficult to pilot. This issue should be investigated in more detail.

2.5 Major drawbacks of the quadroptor concept

These drawbacks, compared to the other configurations, could be summarized in the next list:

- Higher weight. Lower payload/weight ratio
- Bigger power consumption
- Coupling between controllability and motor dynamics
- Technology in its infancy

Higher weight. Lower payload/weight ratio

As for the higher take off weight, it is an obvious conclusion of the fact that, instead of one or two main rotors, there are four.

Regarding the low payload/take off weight ratio, it is not so obvious. On the one hand, the take off weight is larger, as it has been explained. But on the other hand, the payload is also larger, because the thrust available is bigger. In the end it is more an empirical evidence than a conclusion of theoretical studies.

Bigger power consumption

This is another consequence of having more rotors. Bigger power consumption implies bigger power plants and bigger energy reserves (either batteries or fuel tanks), and this in turn implies higher take off weight, which was already high because of the increased number of rotors.

In small, unmanned quadrotors powered by electric motors this issue can be very important. The power consumption is indeed very large and this reduces significantly their flight endurance. In the case of the Draganflyer XPro, for instance, the batteries will allow flying for not more than 15-18 min, as stated in the website of the manufacturer: www.draganfly.com (accessed 10th January 2007). The reduced flight endurance is a serious limitation and one of the reasons why quadrotor UAVs have not seen yet widespread usage. This problem will have to be solved in order to make full use of the potential of the quadrotor.

Coupling between controllability and motor dynamics

It has already been said that the possibility of controlling the attitude of the quadrotor just by independently modifying the speeds of each rotor was a great advantage, because it rendered unnecessary all the complex mechanical systems needed to change the blade pitch angle.

However, it should not be forgotten that the speed of the rotors depends strongly on the dynamics of the motor(s) driving them. Any motor or engine, no matter of what type (electric, internal combustion, gas turbine, steam powered) has a certain inertia to changes in its regime (i.e., speed). The larger the inertia, the larger the time lag. Depending on the type of motor/engine and its size, the time lag may differ in several orders of magnitude, but it will never be zero (no engine has an instantaneous response). Because of this, whenever a change in the speed of the rotor (motor) is demanded, there will be a time lag until this change is fully implemented, its length being of the same order of magnitude as the time constant of the motor.

The flight dynamics of the quadrotor are characterised by several time constants, as it was first said when referring to its stability. If the value of the time lag of the motor gets close to one of these, then the control of the quadrotor will become very difficult, or even impossible. Usually this is not a problem with electrical motors, because their time lag is very small, but it could be with internal combustion engines, which have a larger inertia. This is the reason why all the quadrotors powered by internal combustion engines are controlled by other methods rather than rpm control, or by a combination of those methods with rpm control.

In those quadrotors controlled solely by means of the rpm of the rotors, such as the XPro, the issue of time lag remains critical, and because of that one of the aims of this Project will be to accurately model this lag in the XPro.

If each of the rotors is driven by a different motor, like in the XPro, the rpm-based control technique poses another problem, which is its sensitivity to small differences in the performance of each of the motors (Ref 2.5). Little differences in the response of each motor may be enough to make it completely unstable and nearly impossible to fly without the aid of electronic stabilization systems. This issue will be mentioned again in Section 16.

Technology in its infancy

This problem has also been commented before. Unlike the rest of the disadvantages, this will disappear as soon as many quadrotors are designed and operated. Until then it remains a primary concern, especially for manned vehicles, where reliability is essential.

2.6 Advantages vs Drawbacks. Applications of the quadrotor concept

In the confrontation between advantages and drawbacks, it is evident that the winner will be decided depending on the application we are aiming at. Many different applications are possible, but here we will only summarize those in which the quadrotor has better chances to succeed.

Heavy lift VTOL aircraft

This application is the more obvious since it takes advantage of the higher thrust that the quadrotor can deliver compared to other helicopters. However, to this date, the only serious attempt that was made to build a quadrotor of this type was the Piasecki PA-39 MHLS or *Multiple Helicopter Heavy Lift System* (Ref 2.6). The idea of this project was to create a quadrotor by joining four Sikorsky CH-53 helicopters using a large structure. If it had been carried out, it would have been capable of lifting cargoes that no other helicopter could lift, such as ballistic missiles or armoured vehicles. However, the concern about the lack of experience with this type of configuration prevailed and the project was cancelled.

Heavy lift Tiltrotor

The idea of a tiltrotor fitted with two wings in tandem, each with two rotors, was first put into practice in the Bell X-22. Although some prototypes did fly, the model never went into serial production. Recently, the same concept was revisited for the proposed Bell QTR (*Quad TiltRotor*) project. This project intends to use much of the elements of the V-22 Osprey to save costs in design and manufacturing (Ref 2.7). To this date, it remains the only manned, full scale rotorcraft that could use of the quadrotor configuration in the near future.

Fully autonomous VTOL UAV

Contrary to the two previous applications, this one does not focus only on the higher payload capacity of the quadrotor, but on its other advantages.

An autonomous VTOL UAV could perform an extraordinary amount of different missions: camera surveillance, aerial filming, military reconnaissance, search and rescue, building inspection...It could perform these missions both indoors and outdoors,

taking advantage of its small size to fly in cramped spaces full of obstacles. Being autonomous, there would be no need to keep a communications link with the base, and it could manoeuvre very fast without waiting for instructions from the pilot. Because of this, extensive research is being conducted to develop autonomous VTOL UAV's.

However, to this date many of the attempts have proven unsuccessful, for different reasons: instability, lack of power, inadequate sensors, unsuitable control algorithms, inadequate CPU's, etc (Ref 2.4). In this context, the quadrotor appears as a very interesting option. Its high payload capacity could allow it to carry cameras, sensors...Its mechanical simplicity, due to the fact that it does not require complex systems to change the pitch angle of the blades, could allow it to be very small and cheap. From the perspective of the control algorithms, the rpm control technique is also interesting, because of its simplicity.

In brief, the quadrotor is particularly well suited for this application, and that is why there is an increasing interest on it. In fact, contrary to the full scale, manned quadrotors, the technology of their small sized counterparts passed its infancy long ago. There are many remote-controlled quadrotors commercially available, such as the different Draganflyer models, the Roswell Flyer, the X-UFO, etc. Apart from that, many universities have already built their own models (such as the X4-flyer —see Ref 2.8). Some aeronautical companies have their own quadrotors too, like the “Quattrocopter” from EADS (Refs 2.9 and 2.10) or the “Quad Copter”, from Atair Aerospace (Ref 2.11). But there is still a long way to go until fully autonomous quadrotors are operational.

Other applications

The strangest application of the quadrotor concept is perhaps the Yuri I, a human powered vehicle designed and built by a team from the Nihon Aero Student Group (NASG) lead by Dr Akira Naito (Ref 2.12):

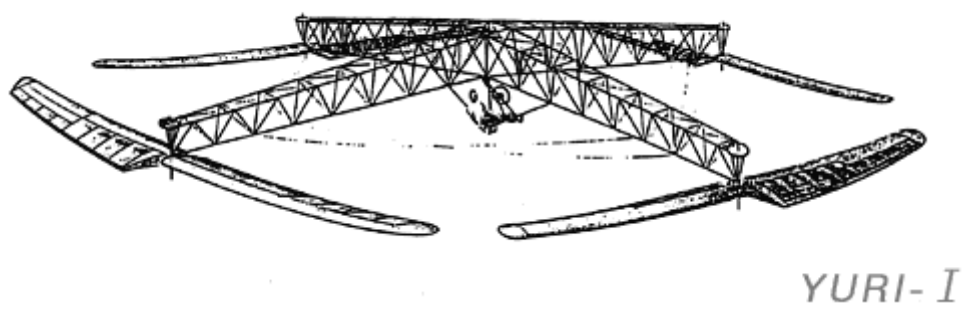


Fig 1.1. The Yuri I, a human powered quadrotor (Ref 2.12).

2.7 Control of the quadrotor

Now the most common method to control the attitude and translation of the quadrotor will be described. It assumes that the configuration of the aircraft is as follows: There is

one rotor at the front and one at the rear, while the two others are on the sides. The front and rear rotors turn likewise (usually counter clockwise) whilst the left and right rotors turn the opposite way in order to cancel the torques. This is the configuration of the Draganflyer XPro as well as of most of the quadrotors. But some quadrotors, such as the Convertawings model A, the Piasecki PA-39 or the Curtiss-Wright VZ-7AP, did use a different configuration, in which there was no rotor at the front or the rear, but instead two rotors on the right side and two on the left. The attitude control, however, was basically analogous.

Attitude control

Pitch control

To pitch up thrust in the front rotor is increased in a certain quantity while thrust in the rear rotor is decreased in the same quantity (see Figure below). By doing so a pitch moment is created while keeping global thrust and torque unchanged. Pitching down is analogous.

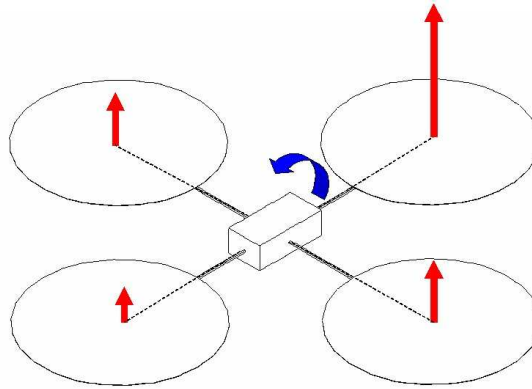


Fig 2.2. Pitch control.

It should be noted that, for a given trim condition, even if the global thrust remains unchanged, as soon as the pitch angle departs from the trim value, the balance of forces will be broken and the quadrotor will start to descend. This behaviour will be discussed in detail in Section 16, where a possible way of avoiding it will also be presented.

Roll control

Roll control is performed in a similar manner, increasing thrust in one of the side rotors and decreasing in the other. As in the previous case, as soon as the roll starts the quadrotor will begin to descend.

Yaw control

Yaw control is achieved by breaking the balance of torques that has been mentioned before. For instance, to yaw to the right thrust and therefore torque are reduced in the

rotors rotating clockwise and increased in those rotating counter clockwise. This is done in such a way that the global thrust remains unchanged. In the figure below, the reaction torque has been increased in the rotors turning counter clockwise, and reduced in the rotors turning clockwise. Since the reaction torque is opposite to the direction in which the rotors turn, the overall result is a yawing moment to the right.

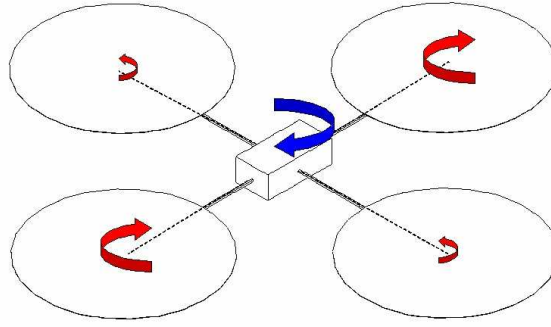


Fig 2.3. Yaw control.

It should be noted that this way of attitude control is only possible because the thrust and the torque in each rotor are proportional. If they were not, it would not be possible to modify the thrusts without breaking the balance of torques, and vice versa. The thrust T and the torque Q may be defined as follows (see Section 9):

$$T = \rho \pi R^4 \Omega^2 C_T \quad Q = \rho \pi R^5 \Omega^2 C_Q$$

Where ρ is the air density, R is the rotor radius, Ω is the rotational speed and C_T , C_Q are two coefficients. Although these coefficients are not proportional (because they behave differently for the same variations of the parameters that affect them), their influence in T, Q is small compared to that of Ω . Hence, T and Q can be assumed to be proportional.

Translation control

From a trimmed, steady hovering condition, to ascend or descend thrust is modified by equal in the four rotors.

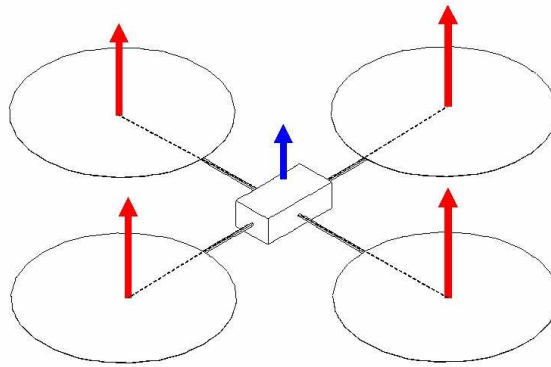


Fig 2.4. “Heave” control.

To move forward or backwards a certain pitch angle has to be reached and maintained. Lateral translation is analogous.

In steady, horizontal flight the quadrotor keeps a negative pitch angle so that there is a horizontal component of thrust which overcomes drag.

Thrust control

As it has been seen, to control the attitude it is necessary to independently modify the thrust of each rotor. According to Blade Element Theory (see Section 9), there are two possible methods to vary the thrust: either by increasing the pitch angle of the blade (which increases its angle of attack) or by augmenting the rotational speed of the rotor (i.e., the rpm). Both methods have already been mentioned. The latter has the advantage of its simplicity, but it also introduces a time lag, because the motors cannot change its regime instantaneously. The pitch angle technique, on the other hand, provides a faster, nearly instantaneous response, although it increases the mechanical complexity of the vehicle.

The Draganflyer XPro, as well as many other remotely piloted quadrotors, uses the rpm control technique because of its simplicity. Some quadrotors, though, use other techniques (Ref 2.4).

2.8 Some comments about the terminology used in this Section

Many authors consider that the term “helicopter” should be reserved for those types of rotorcraft where it is possible to control the pitch angle of the blades both collectively and cyclically. From that point of view, those quadrotors which are controlled exclusively by adjusting the rpm of the rotors (that is, the vast majority) should not be classified as “helicopters”. However, the author considers that, since the term “helicopter” is universally known, it can be more clarifying for the non-specialized

reader. Besides, a quadrotor is capable of performing all the tasks which can be done with a conventional helicopter.

Another issue that needs to be addressed is the use of the terms “rotor” and “propeller”. In this case, the author agrees that it is necessary to make the difference. In a propeller, the component of the air velocity vector is usually aligned with the axis. On the other hand, in a rotor the velocity vector can have any orientation. In fact, in horizontal flight it will be parallel or nearly parallel to the rotor disk. Besides, in a rotor, blade flapping is very important, whereas in a propeller it is usually ignored.

3. THE DRAGANFLY XPRO

3.1 Description of the Draganfly XPro

As it has been explained, the quadrotor that will be modelled here is the Draganfly XPro. It has an empty weight of 2.36kg and can carry a payload of up to 0.5kg. The flight endurance is about 15-18 min.

The airframe consists of four carbon fibre arms attached to a central platform which houses the electronics and the battery. Each rotor is situated at the end of one of the arms. The front and rear rotors turn counter clockwise, whereas the left and right turn clockwise.

Each rotor is composed of two or three blades, depending on the version. These are cambered, tapered and untwisted, and have a positive pitch angle of about 20°. They are made of carbon fibre and are quite flexible. The blades are attached to a pulley, the pulley being driven by a strap that is rotated by a motor. The motor is also placed at the end of the arm. The pulley has 120 teeth, and the gear installed in the shaft of the motor has 12. Therefore the gear ratio is exactly 10.

The motor is a Mabuchi RS-545SH. It works with direct current and it is of the conventional type, which means that it is fitted with brushes. The electric power is supplied by a 14.8V Li-Poly battery or by a NiMH battery.

The Draganflyer XPro is remotely operated using a 9 channel FM transmitter, which sends signals to the onboard receiver (Ref 3.1). The vehicle is fitted with a CPU which is in charge of sending the control signals to each of the motors. It receives inputs from the receiver as well as from three piezoelectric oscillation gyros. The quadrotor always works in closed loop, which means that it is the CPU, and not the pilot, the one that determines the rpm in each rotor. To do so it uses the inputs from the three gyros. Without the aid of the CPU, the quadrotor would be very unstable and therefore extremely difficult to fly.

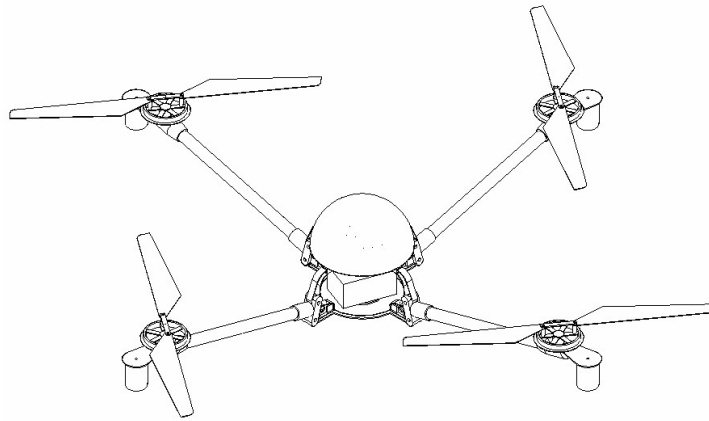


Fig 3.1. Image of the CAD model of the Draganfly XPro (note that the straps that link the pulleys with the motors have not been represented).

4. EQUATIONS OF MOTION

4.1 Introduction

In order to build a model to predict the dynamics of any mechanical system, the first step is obviously to write down the equations of motion of the system. The quadrotor is no exception.

At the end of this Section, a full set of equations that describe the dynamics of the quadrotor will have been obtained. These equations will be the core of the model of the quadrotor and will be used in the Simulink simulation.

Unless it is said otherwise, the notation used in this Section will be maintained through the rest of the report. As for the units, S.I. will always be used.

To illustrate the importance of this Section it is noted that extensive reference will be made to it throughout the whole report. The importance of estimating mass and inertial properties, the description of the structure of the Simulink model...these are all issues that cannot be fully understood without a thorough analysis of the Equations of Motion.

4.2 Equations of motion of a rigid body

The equations of motion of a rigid body, in an inertial frame of reference (Ref 4.1):

$$\mathbf{F} = m\mathbf{a}_G \quad (4.1)$$

$$\mathbf{M}^O = \frac{d}{dt}\mathbf{H}_G + \mathbf{OG} \times m\mathbf{a}_G \quad (4.2)$$

Where:

m is the mass of the rigid body

O is an arbitrary point and G is the centre of mass of the body

\mathbf{F} is the sum of all the external forces acting on the body

\mathbf{a}_G is the absolute acceleration of the centre of mass

\mathbf{M}^O is the resultant of all the moments at O

\mathbf{H}_G is the angular momentum of the body at its centre of mass G

4.3 Equations of motion of a system of bodies

Usually, mechanical devices are composed not by one but many different rigid bodies. That is the case of the quadrotor, for instance, where there is the airframe, the rotors, etc. The equations of motion of a system of rigid bodies, using the Newton-Euler formulation (Ref 4.1):

$$\mathbf{F} = \sum_i m_i \mathbf{a}_{G_i} \quad (4.3)$$

$$\mathbf{M}^O = \sum_i \frac{d}{dt} \mathbf{H}_{G_i} + \sum_i (\mathbf{OG}_i \times m_i \mathbf{a}_{G_i}) \quad (4.4)$$

Where:

m_i is the mass of the rigid body i

O is an arbitrary point

G_i is the centre of mass of the rigid body i

\mathbf{F} is the resultant of the *external* forces applied to the system

\mathbf{M}^O is the resultant of the *external* moments applied to the system, applied at O

\mathbf{H}_{G_i} is the angular momentum of the rigid body i , at G_i

It should be noted that all magnitudes are measured in an inertial frame of reference $O_e x_e y_e z_e$ (e.g., the ground).

Taking into account that:

$$m_T = \sum_i m_i \quad (4.5)$$

$$m_T \mathbf{OG}_T = \sum_i m_i \mathbf{OG}_i \quad (4.6)$$

Eq (4.3) can be re-written:

$$\mathbf{F} = m_T \mathbf{a}_{G_T} \quad (4.7)$$

Eq (4.4) is not very useful because it is coupled with (4.3) through \mathbf{a}_{G_i} . It would be interesting to get rid of \mathbf{a}_{G_i} . This can be easily done *provided that O and every G_i are fixed relative to a given reference frame*. Usually, this reference frame will be attached to one of the rigid bodies and the origin of axes will be placed at O . Therefore, it will be called $Oxyz$. In the most general case the body will have an accelerated motion relative to $O_e x_e y_e z_e$ and thus $Oxyz$ will be non-inertial.

From now on, we will assume that all the vector magnitudes are expressed with the unit vectors $\mathbf{i}, \mathbf{j}, \mathbf{k}$, which are those associated with the $Oxyz$ axes. This does not mean that those magnitudes are relative to the $Oxyz$ frame. On the contrary, the vector magnitudes, unless otherwise stated, will always be relative to the inertial $O_e x_e y_e z_e$ frame.

Since we have considered G_i to be fixed relative to $Oxyz$:

$$\mathbf{a}_{G_i} = \mathbf{a}_O + \frac{d\boldsymbol{\omega}}{dt} \times \mathbf{OG}_i + \boldsymbol{\omega} \times (\boldsymbol{\omega} \times \mathbf{OG}_i) \quad (4.8)$$

Where $\boldsymbol{\omega}$ is the angular velocity vector of $Oxyz$ relative to $O_e x_e y_e z_e$.

Another consequence of G_i being fixed relative to $Oxyz$ for every i is that the centre of mass of the system G_T is also fixed relative to $Oxyz$. Therefore:

$$\mathbf{a}_{G_T} = \mathbf{a}_O + \frac{d\boldsymbol{\omega}}{dt} \times \mathbf{OG}_T + \boldsymbol{\omega} \times (\boldsymbol{\omega} \times \mathbf{OG}_T) \quad (4.9)$$

Finally, we should consider the following identities:

$$\begin{aligned} \mathbf{OG}_i \times \left(\frac{d\boldsymbol{\omega}}{dt} \times \mathbf{OG}_i + \boldsymbol{\omega} \times (\boldsymbol{\omega} \times \mathbf{OG}_i) \right) &= \\ = (\mathbf{OG}_i^2 \mathbf{U} - [\mathbf{OG}_i, \mathbf{OG}_i]) \cdot \frac{d\boldsymbol{\omega}}{dt} + \boldsymbol{\omega} \times (\mathbf{OG}_i^2 \mathbf{U} - [\mathbf{OG}_i, \mathbf{OG}_i]) \cdot \boldsymbol{\omega} \end{aligned} \quad (4.10)$$

$$\begin{aligned} \mathbf{OG}_T \times \left(\frac{d\boldsymbol{\omega}}{dt} \times \mathbf{OG}_T + \boldsymbol{\omega} \times (\boldsymbol{\omega} \times \mathbf{OG}_T) \right) &= \\ = (\mathbf{OG}_T^2 \mathbf{U} - [\mathbf{OG}_T, \mathbf{OG}_T]) \cdot \frac{d\boldsymbol{\omega}}{dt} + \boldsymbol{\omega} \times (\mathbf{OG}_T^2 \mathbf{U} - [\mathbf{OG}_T, \mathbf{OG}_T]) \cdot \boldsymbol{\omega} \end{aligned} \quad (4.11)$$

$$\text{Where } \mathbf{U} = \begin{bmatrix} 1 & 0 & 0 \\ 0 & 1 & 0 \\ 0 & 0 & 1 \end{bmatrix}$$

And where $[\mathbf{OG}_i, \mathbf{OG}_i]$ and $[\mathbf{OG}_T, \mathbf{OG}_T]$ are dyadic products.

With (4.9) and it is possible to re-write (4.7) as:

$$\mathbf{F} = m_T \left(\mathbf{a}_O + \frac{d\boldsymbol{\omega}}{dt} \times \mathbf{OG}_T + \boldsymbol{\omega} \times (\boldsymbol{\omega} \times \mathbf{OG}_T) \right) \quad (4.12)$$

On the other hand, with eqs (4.8) to (4.11) in (4.4):

$$\begin{aligned}
 \mathbf{M}^0 - \mathbf{OG}_T \times \mathbf{F} &= \\
 &= \sum_i \frac{d}{dt} \mathbf{H}_{Gi} + \left\{ \sum_i m_i (\mathbf{OG}_i^2 \mathbf{U} - [\mathbf{OG}_i, \mathbf{OG}_i]) - m_T (\mathbf{OG}_T^2 \mathbf{U} - [\mathbf{OG}_T, \mathbf{OG}_T]) \right\} \cdot \frac{d\boldsymbol{\omega}}{dt} + \\
 &+ \boldsymbol{\omega} \times \left\{ \sum_i m_i (\mathbf{OG}_i^2 \mathbf{U} - [\mathbf{OG}_i, \mathbf{OG}_i]) - m_T (\mathbf{OG}_T^2 \mathbf{U} - [\mathbf{OG}_T, \mathbf{OG}_T]) \right\} \cdot \boldsymbol{\omega}
 \end{aligned} \tag{4.13}$$

In order to simplify the notation, we define the following:

$$\mathbf{I}_{OG_i} = \sum_i m_i (\mathbf{OG}_i^2 \mathbf{U} - [\mathbf{OG}_i, \mathbf{OG}_i]) \tag{4.14}$$

$$\mathbf{I}_{OG_T} = m_T (\mathbf{OG}_T^2 \mathbf{U} - [\mathbf{OG}_T, \mathbf{OG}_T]) \tag{4.15}$$

Therefore, the final equations are as follows:

$$\mathbf{F} = m_T \left(\mathbf{a}_O + \frac{d\boldsymbol{\omega}}{dt} \times \mathbf{OG}_T + \boldsymbol{\omega} \times (\boldsymbol{\omega} \times \mathbf{OG}_T) \right) \tag{4.16}$$

$$\mathbf{M}^0 - \mathbf{OG}_T \times \mathbf{F} = \sum_i \frac{d}{dt} \mathbf{H}_{Gi} + \left(\sum_i \mathbf{I}_{OG_i} - \mathbf{I}_{OG_T} \right) \cdot \frac{d\boldsymbol{\omega}}{dt} + \boldsymbol{\omega} \times \left(\sum_i \mathbf{I}_{OG_i} - \mathbf{I}_{OG_T} \right) \cdot \boldsymbol{\omega} \tag{4.17}$$

(4.16) and (4.17) are the equations of motion of a system of rigid bodies where the centre of mass G_i of each body is fixed relative to the common $Oxyz$ frame. We will need these equations to describe the motion of the quadrotor.

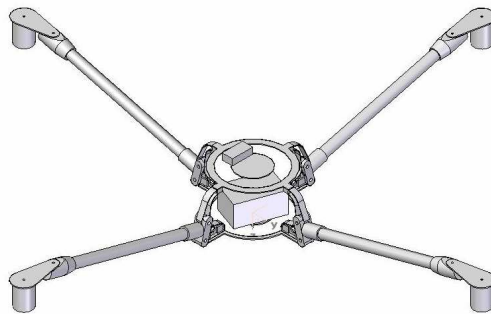
(4.16) and (4.17) can also be used when the rigid body i is replaced by a system of new rigid bodies with its centre of mass at G_i , provided that this centre of mass remains fixed relative to $Oxyz$.

4.4 Particularization for the quadrotor

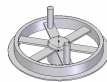
As stated before, the quadrotor itself is not a rigid body, but a system of rigid bodies. Therefore eqs (4.16) and (4.17) can be applied to it with only minor modifications.

We will consider the quadrotor as a system composed of the following rigid bodies.

- The airframe



- The hub of the rotor



- The blades of the rotor



- The armature of each motor, also called “rotor” (as opposed to the “stator” of the motor)



In order to avoid confusions, the armature will always be referred by this name and the term “rotor” will be reserved for the hub-blades assembly.

Modelling the armature as a separate rigid body is an important difference with other models that ignore its influence on vehicle dynamics (see Refs 1.1, 1.4, 1.7, 1.9, for example). Although the rotor (hub+blades) has a larger inertia around its axis of rotation, the armature rotates ten times faster (see below) and its mass is two times bigger. Hence, the effect on vehicle dynamics of armature rotation can be as important as that of the rotor.

blades

As it was explained in Section 3, the rotors of the XPro have two or three blades. In order not to lose generality, here we will consider a rotor with b blades, unless otherwise stated.

The kinematics of the blades in relation to the rigid airframe is fairly complex because it is the combination of several types of motion:

- *Rotation*. Around the axis of the rotor. This is the main and most obvious motion.
- *Feathering*. Around the longitudinal axis of the blade.
- *Flapping*. The motion of the blade on a vertical plane.
- *Lead-Lag (or Lagging)*. The motion of the blade on its plane.

These types of motion will be the subject of a detailed study in Section 9. For the moment, it will be enough to say that they are the result of the different forces and moments acting on the blade. These are:

- The aerodynamic forces and moments exerted by the airflow.
- The forces and moments exerted by the hub.
- The weight force.

If we analyze the dynamics of the blade on a reference frame attached to it then we will have to add the inertial forces and moments, since that frame is a non-inertial one.

hub

The hub is the rotating element to which the blades are attached. In the XPro the hub consists of several parts (see Figure 9.1), the most prominent of which is the gear. A strap links this gear to another one which is on the shaft of the motor (see Section 3 and Figure 9.1). The purpose of this strap is to transmit the motion of the motor to the hub.

The hub is subjected to four different types of actions:

- The forces and moments exerted by the blades.
- The forces and moments exerted by the rigid airframe.
- The forces and moments transmitted through the strap.
- The weight force.

The forces and moments exerted by each blade will be applied at the joint between the blade and the hub. This means several sets of forces and moments, one for each blade. However, in some cases it will be useful to replace these sets by a single one consisting of a force vector and a moment vector applied at the centre of mass of the system composed by the b blades. In the most general case, none of the three components of these vectors will be zero. Due to the flapping/lagging motion, the position of the centre of mass where they are applied will not be fixed relative to the hub. Nevertheless, it will be possible to define its *mean* position in one turn of the rotor.

As for the actions exerted by the rigid airframe, there will be the following:

- A force defined by a vector with 3 components (x, y, z directions).
- A moment defined by a vector contained in the plane of the rotor (x, y directions). There will not be a component in the z direction because the rotor is allowed to turn around its axis.

Finally, there are the forces and moments transmitted through the strap that links the hub and the motor. In the study of the dynamics of the system, the only action which will be relevant is the torque around the rotor axis. We will not consider the rest of the forces and moments transmitted through the strap.

Armature of the motor

This part can be modelled as a rotating cylinder.

As a result of the existing constraints, the following reactions are exerted by the rigid airframe over the armature:

- A force with 3 components (x, y, z directions).
- A moment of force defined by a vector contained in a plane perpendicular to the longitudinal axis (x, y directions).
- A friction torque defined by a vector parallel to the longitudinal axis. This friction torque is due to the contact with the brushes of the motor.

There will also be an electromagnetic torque defined by a vector parallel to the longitudinal axis. This torque, together with the friction torque and the rotational speed, are displayed on the figure below.

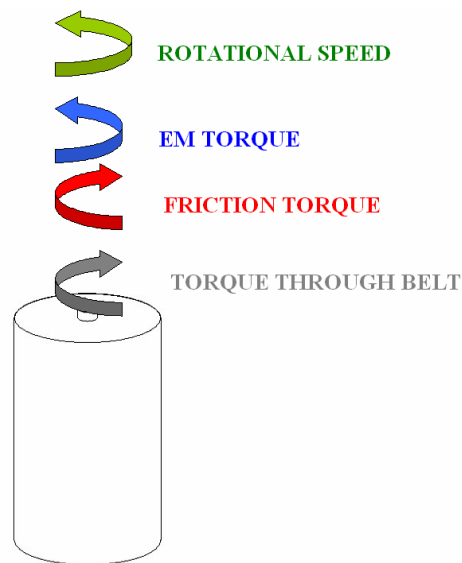


Fig 4.1. Moments over the armature. Notice that the moments exerted by the airframe around the axes perpendicular to the spinning axis have not been included.

The nature of the electromagnetic torque and the way of calculating it will be discussed in Section 6. As for the friction torque, there are several models in the literature that

allow estimating it. Here it will be assumed that the friction torque is linear in the motor speed, i.e., that only *viscous* friction is present (see Ref 6.2).

There is as well the moment transmitted by the hub through the strap. Since the gear ratio is 10 (because the gear of the hub has 120 teeth and that of the motor has 12), the moment over the armature will be a tenth of the one moment the hub. For the same reason, the armature will rotate 10 times faster.

Finally, the weight force cannot be forgotten, especially if it is considered that the mass of the armature is quite significant.

Rigid Airframe

The rigid airframe is subjected to the following actions:

- The forces and moments exerted by the hubs and armatures.
- The aerodynamic forces and moments exerted by the airflow (most notably, the drag).
- The weight force.

The aerodynamic forces and moments over the airframe are extremely difficult to estimate. Fortunately, in Section 11 it will be shown that in many cases they can be neglected.

4.5 Choice of body axes

It will be seen later that it is convenient to define a set of axes, attached to the rigid airframe, in which the different vector magnitudes can be expressed. These body axes may have its origin at any point of the airframe. Due to the double symmetry of the quadrotor, it is interesting to set the origin O in some position on the central vertical axis of the vehicle. Arbitrarily, O will be placed at the intersection between this axis and the bottom surface of the carbon fiber plate. When the quadrotor is horizontal, O is the lowest point.

If the Draganflyer XPro is observed carefully, it can be noted that the central vertical axis is parallel to the axes of the rotors. Moreover, it is also parallel to the rotating axes of the motors. This characteristic, which could seem trivial, is going to greatly simplify the geometry and, by extension, it is going to reduce the complexity of the equations of motion. Some authors (see Ref 1.2) have explained that the stability of the quadrotor can be improved by slightly tilting the rotors to the centre. It should be realised that a change like that would bring an additional complexity to the model of the vehicle.

Choosing the directions of the axes according to the conventions of the literature, what results is a set of axes which is shown in the next figure:

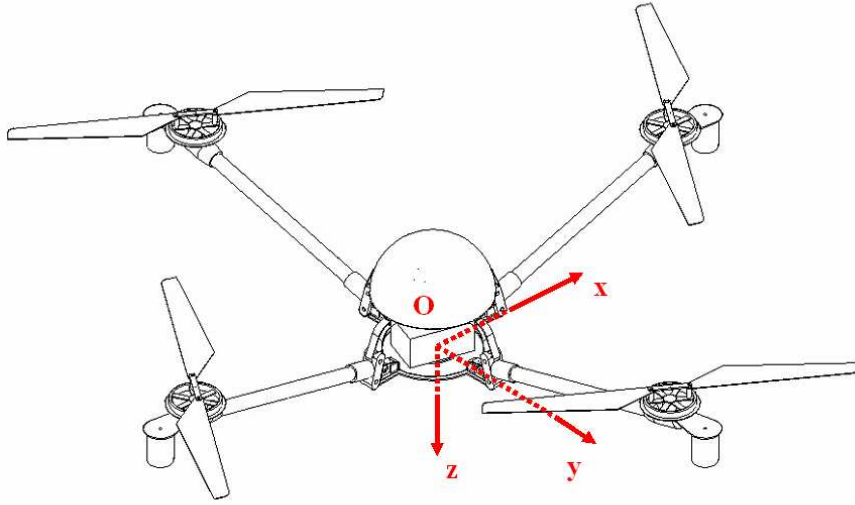


Fig 4.2. Body axes.

Where $\mathbf{i}, \mathbf{j}, \mathbf{k}$ are the unit vectors associated to those axes.

4.6 Calculations of the derivatives of the angular momenta

In order to be able to use eqs (4.16) and (4.17) it is necessary to calculate first these derivatives.

Hub

We will begin by considering the hub. A subscript i will be assigned to each rotor. The rotors will be numbered clockwise, starting with the front one, which will have $i=1$. The centre of mass of the hub will be named G_i .

\mathbf{H}_{Gi} will be the angular momentum of the hub, at its centre of mass, measured in an inertial frame (i.e., the ground). This can be calculated as (Ref 4.1):

$$\mathbf{H}_{Gi} = \mathbf{I}_{Gi} \cdot \boldsymbol{\omega}_i \quad (4.18)$$

Where \mathbf{I}_{Gi} is the inertia tensor at G_i and $\boldsymbol{\omega}_i$ is the angular velocity vector of the rotor, measured in an inertial frame. The above magnitudes can easily be expressed in a set of axes parallel to $Oxyz$ but with origin in G_i .

These axes roughly correspond to the principal directions of inertia of the hub, thanks to the axial-symmetry of the hub and the fact that its spinning axis is parallel to Oz .

Therefore:

$$\mathbf{I}_{Gi} = \begin{bmatrix} I_{xi} & 0 & 0 \\ 0 & I_{yi} & 0 \\ 0 & 0 & I_{zi} \end{bmatrix} \quad (4.19)$$

On the other hand, we can define $\boldsymbol{\omega} = p\mathbf{i} + q\mathbf{j} + r\mathbf{k}$ as the angular velocity of the rigid airframe. Then, the absolute angular velocity of the propeller will be:

$$\boldsymbol{\omega}_i = \boldsymbol{\omega} + \Omega_i \mathbf{k}_i = p\mathbf{i} + q\mathbf{j} + (r - \Omega_i)\mathbf{k} \quad (4.20)$$

Where Ω_i will be positive if the rotor is spinning counter clockwise and negative if spinning clockwise.

To calculate $\frac{d}{dt}\mathbf{H}_{Gi}$ we need to use the Theorem of Coriolis, since \mathbf{H}_{Gi} is expressed with $\mathbf{i}, \mathbf{j}, \mathbf{k}$. Then:

$$\frac{d}{dt}\mathbf{H}_{Gi} = \mathbf{I}_{Gi} \cdot \frac{d\boldsymbol{\omega}_i}{dt} + \boldsymbol{\omega} \times \mathbf{I}_{Gi} \cdot \boldsymbol{\omega}_i \quad (4.21)$$

Which can be rewritten as:

$$\frac{d}{dt}\mathbf{H}_{Gi} = I_{xi}\dot{p}\mathbf{i} + I_{yi}\dot{q}\mathbf{j} + I_{zi}(\dot{r} - \dot{\Omega}_i)\mathbf{k} + (p\mathbf{i} + q\mathbf{j} + r\mathbf{k}) \times (I_{xi}p\mathbf{i} + I_{yi}q\mathbf{j} + I_{zi}(r - \Omega_i)\mathbf{k}) \quad (4.22)$$

This can be re-written as:

$$\frac{d}{dt}\mathbf{H}_{Gi} = (I_{zi}q(r - \Omega_i) - I_{yi}qr + I_{xi}\dot{p})\mathbf{i} + (-I_{zi}p(r - \Omega_i) + I_{xi}pr + I_{yi}\dot{q})\mathbf{j} + I_{zi}(\dot{r} - \dot{\Omega}_i)\mathbf{k} \quad (4.23)$$

Since the spinning speed is usually much larger than r it is possible to assume that $\omega_{zi} \approx -\Omega_i$. By taking all this into account we arrive to:

$$\frac{d}{dt}\mathbf{H}_{Gi} = (-I_{zi}q\Omega_i - I_{yi}qr + I_{xi}\dot{p})\mathbf{i} + (I_{zi}p\Omega_i + I_{xi}pr + I_{yi}\dot{q})\mathbf{j} + I_{zi}(\dot{r} - \dot{\Omega}_i)\mathbf{k} \quad (4.24)$$

It is interesting to note that the terms involving Ω_i correspond to the gyroscopic effects, whereas the terms involved with $\dot{\Omega}_i$ correspond to the so-called inertial counter-torques.

It is also worth noting that, although Ω_i is much larger than p, q, r , this does not imply that the same is going to be applicable for the time derivatives. For this reason, \dot{r} has been retained in (4.24).

Blades

\mathbf{F}_i is the resultant of the forces exerted by the airflow.

According to what was explained before, \mathbf{F}_i will be applied at the centre of mass of the system composed by the b blades, which we will name P_i . In addition, \mathbf{M}_i will be the corresponding moment vector at P_i .

In order to calculate the derivative of the angular momentum of each of the blades it could be possible to follow the same procedure used for the hub. However, there is an important reason that make this unadvisable, which is that the motion of the blade relative to the airframe is much more complex than that of the hub. As a result, the mathematical problem becomes virtually unassailable unless several simplifications are introduced.

Hence, another approach is required. This will be explained in detail in Section 9. For the moment, it will be enough to know that:

$$\left(\frac{d}{dt} \mathbf{H}_{\mathbf{P}_i} \right)_{mean} \approx (-M_{xi} + \dots)\mathbf{i} + (-M_{yi} + \dots)\mathbf{j} + bI_{zb}(\dot{r} - \dot{\Omega}_i)\mathbf{k} \quad (4.25)$$

Armature

A subscript j will be assigned to each armature. For each armature, it will be equal to the value of i of the associated rotor.

The mathematical procedure is completely analogous to the one followed with the hub.

$$\mathbf{I}_{Gj} = \begin{bmatrix} I_{xj} & 0 & 0 \\ 0 & I_{yj} & 0 \\ 0 & 0 & I_{zj} \end{bmatrix} \quad (4.26)$$

$$\boldsymbol{\omega}_j = \boldsymbol{\omega} - g_r \Omega_i \mathbf{k} = p\mathbf{i} + q\mathbf{j} + (r - g_r \Omega_i)\mathbf{k} \quad (4.27)$$

Where it has been taken into account that the spinning speed of the armature relative to the airframe is equal to that of the associated rotor, multiplied by the gear ratio g_r .

Hence, using the Theorem of Coriolis:

$$\frac{d}{dt} \mathbf{H}_{Gj} = \mathbf{I}_{Gj} \cdot \frac{d\boldsymbol{\omega}_j}{dt} + \boldsymbol{\omega} \times \mathbf{I}_{Gj} \cdot \boldsymbol{\omega}_j \quad (4.28)$$

Which can be rewritten as:

$$\frac{d}{dt} \mathbf{H}_{Gj} = (-I_{zj} q g_r \Omega_i - I_{yj} q r + I_{xj} \dot{p}) \mathbf{i} + (I_{zj} p g_r \Omega_i + I_{xj} p r + I_{yj} \dot{q}) \mathbf{j} + I_{zj} (\dot{r} - g_r \dot{\Omega}_i) \mathbf{k} \quad (4.29)$$

Rigid airframe

The angular momentum:

$$\mathbf{H}_G = \mathbf{I}_G \cdot \boldsymbol{\omega} \quad (4.30)$$

Where \mathbf{I}_G is the inertia tensor of the rigid airframe at G , expressed in body axes.

$$\mathbf{I}_G = \begin{bmatrix} I_x & -I_{xy} & -I_{xz} \\ -I_{xy} & I_y & -I_{yz} \\ -I_{xz} & -I_{yz} & I_z \end{bmatrix} \quad (4.31)$$

To calculate $\frac{d}{dt} \mathbf{H}_G$ we need to use again the Theorem of Coriolis. Therefore:

$$\frac{d}{dt} \mathbf{H}_G = \mathbf{I}_G \cdot \frac{d\boldsymbol{\omega}}{dt} + \boldsymbol{\omega} \times \mathbf{I}_G \cdot \boldsymbol{\omega} \quad (4.32)$$

4.7 Complete sets of equations of motion

As it has been indicated before, (4.16) and (4.17) can be applied to the quadrotor, with some slight modifications.

Equation of forces

Equation (4.16) was:

$$\mathbf{F} = m_T \left(\mathbf{a}_O + \frac{d\boldsymbol{\omega}}{dt} \times \mathbf{OG}_T + \boldsymbol{\omega} \times (\boldsymbol{\omega} \times \mathbf{OG}_T) \right) \quad (4.16)$$

Where G_T is the centre of mass of the complete vehicle (airframe + hubs + blades + armatures) and m_T , its total mass.

We define the velocity of the point O as:

$$\mathbf{v}_O = u\mathbf{i} + v\mathbf{j} + w\mathbf{k} \quad (4.33)$$

Therefore it will be:

$$\mathbf{a}_O = \dot{u}\mathbf{i} + \dot{v}\mathbf{j} + \dot{w}\mathbf{k} \quad (4.34)$$

It should be borne in mind that (4.16) is valid because the point G_T is fixed relative to the airframe. And this is true because we have assumed that the centre of mass of the system composed by the blades, that is, P_i , is fixed relative to the airframe. However, it should not be forgotten that this is a simplification. P_i is not fixed relative to the airframe. Even its mean position in one turn will change with time, because of blade flapping (see Section 9). The centres of mass of the hub and the armature need also to be fixed for (4.33) to be true, but is the case in reality, unlike what happens with P_i .

\mathbf{F} was the resultant of all the external forces exerted on the vehicle. These are the weight and the aerodynamic forces (both over the blades and over the other elements). Therefore:

$$\mathbf{F} = \sum_i \mathbf{F}_i + m_T \mathbf{g} + \mathbf{F}_{\text{airframe}} \quad (4.35)$$

Where:

\mathbf{F}_i is the resultant of the forces exerted by the airflow over the b-blades system

\mathbf{g} is the gravitational acceleration

$\mathbf{F}_{\text{airframe}}$ is the resultant of the forces exerted by the airflow over the airframe

Finally:

$$\sum_i \mathbf{F}_i + m_T \mathbf{g} + \mathbf{F}_{\text{airframe}} = m_T \left(\mathbf{a}_O + \frac{d\boldsymbol{\omega}}{dt} \times \mathbf{OG}_T + \boldsymbol{\omega} \times (\boldsymbol{\omega} \times \mathbf{OG}_T) \right) \quad (4.36)$$

On the other hand:

$$\mathbf{g} = -\sin \theta \mathbf{i} + \sin \phi \cos \theta \mathbf{j} + \cos \phi \cos \theta \mathbf{k} \quad (4.37)$$

Where ϕ, θ, ψ are the Euler angles (roll, pitch, yaw). Since these angles are going to appear in the above equations, we will need additional equations to obtain them. These equations are (Ref 4.2):

$$\begin{aligned}
\dot{\phi} &= p + (q \sin \phi + r \cos \phi) \tan \theta \\
\dot{\theta} &= q \cos \phi - r \sin \phi \\
\dot{\psi} &= (q \sin \phi + r \cos \phi) \sec \theta
\end{aligned} \tag{4.38}$$

Equation of Moments

\mathbf{M}^O was the resultant, applied at O , of the *external* moments exerted on the quadrotor. These are the aerodynamic moments (both over the blades and over the other elements) and the moment due to the weight force. Hence:

$$\mathbf{M}^O = \sum_i (\mathbf{M}^{Pi} + \mathbf{OP}_i \times \mathbf{F}_i) + \mathbf{M}_{\text{airframe}}^O + \mathbf{OG}_T \times m_T \mathbf{g} \tag{4.39}$$

Where:

\mathbf{M}^{Pi} are the moments exerted by the airflow over the b-blades system, at P_i

$\mathbf{M}_{\text{airframe}}^O$ are the aerodynamic moments over the airframe and the hubs, at O

Then, with (4.35) and (4.39):

$$\begin{aligned}
\mathbf{M}^O - \mathbf{OG}_T \times \mathbf{F} &= \sum_i (\mathbf{M}^{Pi} + \mathbf{OP}_i \times \mathbf{F}_i) + \mathbf{M}_{\text{airframe}}^O + \\
&+ \mathbf{OG}_T \times m_T \mathbf{g} - \mathbf{OG}_T \times \left(\sum_i \mathbf{F}_i + m_T \mathbf{g} + \mathbf{F}_{\text{airframe}} \right) = \\
&= \sum_i (\mathbf{M}^{Pi} + \mathbf{OP}_i \times \mathbf{F}_i) + \mathbf{M}_{\text{airframe}}^O - \mathbf{OG}_T \times \left(\sum_i \mathbf{F}_i + \mathbf{F}_{\text{airframe}} \right)
\end{aligned} \tag{4.40}$$

Now, basing on eq (4.17):

$$\begin{aligned}
&\sum_i (\mathbf{M}^{Pi} + \mathbf{OP}_i \times \mathbf{F}_i) + \mathbf{M}_{\text{airframe}}^O - \mathbf{OG}_T \times \left(\sum_i \mathbf{F}_i + \mathbf{F}_{\text{airframe}} \right) = \\
&= \sum_i \left(\frac{d}{dt} \mathbf{H}_{Pi} \right)_{\text{mean}} + \sum_i \frac{d}{dt} \mathbf{H}_{Gi} + \sum_j \frac{d}{dt} \mathbf{H}_{Gj} + \frac{d}{dt} \mathbf{H}_G + \\
&+ \left(\sum_i \mathbf{I}_{OPi} + \sum_i \mathbf{I}_{OGi} + \sum_j \mathbf{I}_{OGj} + \mathbf{I}_{OG} - \mathbf{I}_{OG_T} \right) \cdot \frac{d\boldsymbol{\omega}}{dt} + \\
&+ \boldsymbol{\omega} \times \left(\sum_i \mathbf{I}_{OPi} + \sum_i \mathbf{I}_{OGi} + \sum_j \mathbf{I}_{OGj} + \mathbf{I}_{OG} - \mathbf{I}_{OG_T} \right) \cdot \boldsymbol{\omega}
\end{aligned} \tag{4.41}$$

Where:

$$\begin{aligned}
\mathbf{I}_{\text{OPi}} &= \sum_i b m_b (\mathbf{OP}_i^2 \mathbf{U} - [\mathbf{OP}_i, \mathbf{OP}_i]) \\
\mathbf{I}_{\text{OGi}} &= \sum_i m_i (\mathbf{OG}_i^2 \mathbf{U} - [\mathbf{OG}_i, \mathbf{OG}_i]) \\
\mathbf{I}_{\text{OGj}} &= \sum_j m_j (\mathbf{OG}_j^2 \mathbf{U} - [\mathbf{OG}_j, \mathbf{OG}_j])
\end{aligned} \tag{4.42}$$

$$\mathbf{I}_{\text{OG}} = m_T (\mathbf{OG}^2 \mathbf{U} - [\mathbf{OG}, \mathbf{OG}])$$

$$\mathbf{I}_{\text{OG}_T} = m_T (\mathbf{OG}_T^2 \mathbf{U} - [\mathbf{OG}_T, \mathbf{OG}_T])$$

Where m_b is the mass of a blade, m_i is the mass of the hub, m_j is the mass of the armature and b is the number of blades per rotor.

We should also consider the following relations:

$$\boldsymbol{\omega}_i = \boldsymbol{\omega} - \Omega_i \mathbf{k} \tag{4.43}$$

$$\boldsymbol{\omega}_j = \boldsymbol{\omega} - g_r \Omega_i \mathbf{k} \tag{4.44}$$

Using them and expressions (4.21), (4.28) and (4.32), eq (4.41) can be re-written in the following way:

$$\begin{aligned}
& \sum_i (\mathbf{M}^{\text{Pi}} + \mathbf{OP}_i \times \mathbf{F}_i) + \mathbf{M}_{\text{airframe}}^{\text{O}} - \mathbf{OG}_T \times \left(\sum_i \mathbf{F}_i + \mathbf{F}_{\text{airframe}} \right) = \sum_i \left(\frac{d}{dt} \mathbf{H}_{\text{Pi}} \right)_{\text{mean}} + \\
& + \left(\sum_i \mathbf{I}_{\text{OPi}} + \sum_i \mathbf{I}_{\text{Gi}} + \sum_i \mathbf{I}_{\text{OGi}} + \sum_j \mathbf{I}_{\text{Gj}} + \sum_j \mathbf{I}_{\text{OGj}} + \mathbf{I}_G + \mathbf{I}_{\text{OG}} - \mathbf{I}_{\text{OG}_T} \right) \cdot \frac{d\boldsymbol{\omega}}{dt} + \\
& + \boldsymbol{\omega} \times \left(\sum_i \mathbf{I}_{\text{OPi}} + \sum_i \mathbf{I}_{\text{Gi}} + \sum_i \mathbf{I}_{\text{OGi}} + \sum_j \mathbf{I}_{\text{Gj}} + \sum_j \mathbf{I}_{\text{OGj}} + \mathbf{I}_G + \mathbf{I}_{\text{OG}} - \mathbf{I}_{\text{OG}_T} \right) \cdot \boldsymbol{\omega} - \\
& - \sum_i \mathbf{I}_{\text{Gi}} \cdot \dot{\Omega}_i \mathbf{k} - \boldsymbol{\omega} \times \sum_i \mathbf{I}_{\text{Gi}} \cdot \Omega_i \mathbf{k} - \sum_j \mathbf{I}_{\text{Gj}} \cdot g_r \dot{\Omega}_i \mathbf{k} - \boldsymbol{\omega} \times \sum_j \mathbf{I}_{\text{Gj}} \cdot g_r \Omega_i \mathbf{k}
\end{aligned} \tag{4.45}$$

Eq (4.45) has the advantage of contributing to separate the terms with $\boldsymbol{\omega}$ from those with Ω_i or $\dot{\Omega}_i$ (although $\left(\frac{d}{dt} \mathbf{H}_{\text{Pi}} \right)_{\text{mean}}$ still contains terms both with $\boldsymbol{\omega}$ and $\dot{\Omega}_i$). This will be interesting when designing the algorithm to solve the equations of motion of the vehicle (see Section 14).

4.8 Balance of torques over the spinning axis

It will be seen in Section 6 that another equation is required in order to complete the physical model of the quadrotor. This is the equation that is obtained when the balance of torques around the longitudinal axis of the armature is considered. This scalar equation, in fact, is included in the vector equation (1.2), which applies to the armature when we consider it as an isolated rigid body.

Using (4.2), with the appropriate changes in notation:

$$\mathbf{M}^{G_j} = \frac{d}{dt} \mathbf{H}_{G_j} \quad (4.46)$$

Where G_j has been chosen as the point where the resultant of moments is applied.

$\frac{d}{dt} \mathbf{H}_{G_j}$ has already been calculated (eq 4.29).

As it has been indicated, we are only interested in the equation for the z axis. Taking into account what was explained in sub-section 4.4 about the moments acting on the armature, we can produce the following equation:

$$-\tau_j + Fg_r\Omega_i + \frac{M''_{zi}}{g_r} = I_{zj}(\dot{r} - g_r\dot{\Omega}_i) \quad (4.47)$$

Where:

τ_j is the electromagnetic torque over the armature (same sign as Ω_i , that is, positive when the armature spins counter clockwise and negative if contrary).

$Fg_r\Omega_i$ is the friction torque.

M''_{zi} is the torque exerted by the hub over the strap. Therefore $\frac{M''_{zi}}{g_r}$ will be the torque exerted by the strap over the armature.

It can be assumed, with no loss of generality, that the interaction between the armature and the hub is restricted to the M''_{zi} torque transmitted through the strap.

Equation (4.2) can also be applied to the hub in a totally analogous way as that of the armature. The equation for the z axis is then:

$$M'_{zi} - M''_{zi} = I_{zi}(\dot{r} - \dot{\Omega}_i) \quad (4.48)$$

Where M'_{zi} is the moment around the spinning axis exerted by the b-blades system over the hub.

Finally, we apply eq (4.2) to the b-blades system. The equation for the z axis is then:

$$M_{zi} - M'_{zi} = bI_{zb}(\dot{r} - \dot{\Omega}_i) \quad (4.49)$$

Where M_{zi} is the third component of \mathbf{M}^{Pi} .

With (4.48) and (4.49) in (4.47):

$$-\tau_j + Fg_r\Omega_i + \frac{M_{zi} - (bI_{zb} + I_{zi})(\dot{r} - \dot{\Omega}_i)}{g_r} = I_{zj}(\dot{r} - g_r\dot{\Omega}_i) \quad (4.50)$$

It will be seen in Section 6 that the electromagnetic torque is governed by the following equation:

$$\pm v_{aj} = Kg_r\Omega_i + \frac{R_a}{K}\tau_j + \frac{L_a}{K}\dot{\tau}_{aj} \quad (6.7)$$

(+ for motors turning counter clockwise, – for motors turning clockwise)

Where the meaning of the symbols in the above equation will be explained in the corresponding section.

4.9 Coupling of the equations of the quadrotor. Solving methods

At this point, it is convenient to remember all the equations that we have obtained:

- The equation of forces (eq 4.36)
- The 3 kinematic relations (eq 4.38)
- The equation of moments (eq 4.45)
- The 4 balances of torques around the spinning axis of the armatures (eq 4.50)
- The 4 equations of the d.c. motors (eq 6.7)

Eqs (4.36), (4.45) and (4.50) require knowing the aerodynamic forces and moments exerted by the airflow over the blades and the airframe. These will be the subject of study of sections 9, 10, 11 and 13. Until then, it will be enough to know that those forces and moments depend exclusively on the following variables: $p, q, r, u, v, w, \Omega_1, \Omega_2, \Omega_3, \Omega_4$.

Therefore once we know how to calculate those forces and moments, we can use the previous set of equations to obtain:

$$p, q, r, \phi, \theta, \psi, u, v, w, \Omega_1, \Omega_2, \Omega_3, \Omega_4$$

These variables are the only ones needed to describe the kinematic state of the vehicle at any given time.

4.10 “Navigation” equations

We will want to know as well the position x_e, y_e, z_e and velocity u_e, v_e, w_e of the point O of the quadrotor, relative to an inertial frame of reference attached to the ground (Earth axes). To do so, the following equations will be needed (Ref 4.2):

$$\begin{aligned}
 u_e &= \dot{x}_e \\
 v_e &= \dot{y}_e \\
 w_e &= \dot{z}_e \\
 u_e &= u \cos \theta \cos \psi + v(\sin \phi \sin \theta \cos \psi - \cos \phi \sin \psi) + w(\cos \phi \sin \theta \cos \psi + \sin \phi \sin \psi) \\
 v_e &= u \cos \theta \sin \psi + v(\sin \phi \sin \theta \sin \psi + \cos \phi \cos \psi) + w(\cos \phi \sin \theta \sin \psi - \sin \phi \cos \psi) \\
 w_e &= -u \sin \theta + v \sin \phi \cos \theta + w \cos \phi \cos \theta
 \end{aligned} \tag{4.51}$$

The three last equations can be re-written using pseudo-matrix notation:

$$(\mathbf{v}_O)_e = \mathbf{M}_{DC}^T \cdot \mathbf{v}_O \tag{4.52}$$

$(\mathbf{v}_O)_e$ is the velocity vector whose components are u_e, v_e, w_e

\mathbf{M}_{DC} is the Direction Cosine Matrix and \mathbf{M}_{DC}^T is its transpose:

$$\mathbf{M}_{DC}^T = \begin{bmatrix} \cos \theta \cos \psi & \sin \phi \sin \theta \cos \psi - \cos \phi \sin \psi & \cos \phi \sin \theta \cos \psi + \sin \phi \sin \psi \\ \cos \theta \sin \psi & \sin \phi \sin \theta \sin \psi + \cos \phi \cos \psi & \cos \phi \sin \theta \sin \psi - \sin \phi \cos \psi \\ -\sin \theta & \sin \phi \cos \theta & \cos \phi \cos \theta \end{bmatrix} \tag{4.53}$$

Once that ϕ, θ, ψ and u, v, w have been obtained by means of (4.38) and (4.36) respectively, we can use (4.51) to calculate $u_e, v_e, w_e, x_e, y_e, z_e$ for any given time.

It should be noted that the $O_e z_e$ axis of the inertial frame points downwards (to the ground). Thus, a positive z_e will imply that the quadrotor is *below* its initial altitude, (which here we will arbitrarily define as $z_e = 0$).

4.11 Conclusions

A complete set of equations of motion has been produced using Newton-Euler formulation. The effect of rotor and armature rotation on the dynamics of the vehicle has been taken into account.

Before the equations can be integrated, it will be necessary to study and model the aerodynamic forces and moments over the rotors and the airframe. This will be done in Sections 9, 10, 11 and 13.

Then, in Section 14, it will be seen how the equations can be integrated to determine the attitude, velocity and position of the quadrotor.

5. ESTIMATION OF MASS AND INERTIAL PROPERTIES

5.1 Introduction

To successfully build a model of the flight dynamics of the quadrotor it is essential to know its mass and inertial properties. It was shown in the section devoted to the Equations of Motion that the following information, from each of the moving parts (rotor, armature, rigid airframe), was needed:

- Mass
- Coordinates of the centre of mass
- Moments and products of inertia, in a set of axes parallel to $Oxyz$, and with origin in the centre of mass of the rigid body

It is evident that, the more accurate these data are, the better the results of the model will be.

5.2 Proposed methods. Use of a commercially available CAD tool

As for the masses they are relatively easy to obtain just by disassembling the vehicle and weighing each of the components. The masses of the components of the Draganflyer XPro are shown in Appendix B.

Obtaining the position of the centre of mass and the values of the moments and products of inertia is a different issue. There are two ways of obtaining these values, either experimentally or theoretically. If properly carried out, the first way should be more accurate, since it gives the values for the *real* quadrotor, not for an idealization of it. However, the experiments to measure these values on the full scale vehicle can be very complicated and may turn out not to be cost-effective. Hence, the theoretical approach was preferred (to get a complete description of the methods to measure these properties experimentally, check references 5.1 to 5.5).

The most efficient way to proceed, once we have decided to leave aside the experimental methods, is to use one of the many CAD software packages that are commercially available. In particular, it was chosen to use SolidEdge v18. With this software it is possible to model each component of the quadrotor and then assign it a mass or a density value. The program is then able to calculate its volume, its centre of mass, the principal moments of inertia, the orientation of the principal axes and the moments and products of inertia in any given set of axes. Moreover, assemblies can be created using the different components and then the program can calculate the previous properties for those assemblies. This way it is possible to obtain the mass and inertial properties of the rotor, the rigid airframe and even the whole quadrotor.

The major drawback of this method is that to produce good results it is necessary to accurately know the dimensions and geometry of each component, as well as its mass (or density). To obtain that information, thorough measurements were carried out on *every* component of the quadrotor. With this set of measurements a CAD model was built (see Fig 5.1). The results obtained with this model are shown on Appendix B.

It should be mentioned that this CAD model is not completely detailed. Some components have a simplified geometry while some others, the smallest, have not been modelled. In the case of the armatures of the motors, since it was not possible to measure their weight or dimensions without disassembling the motors (something that was not advisable), the following assumptions were made:

- The armature is a cylinder with the same density as the stator
- The mass of the armature is $\frac{2}{3}$ of the mass of the whole motor

An image of this simplified CAD model is shown below:

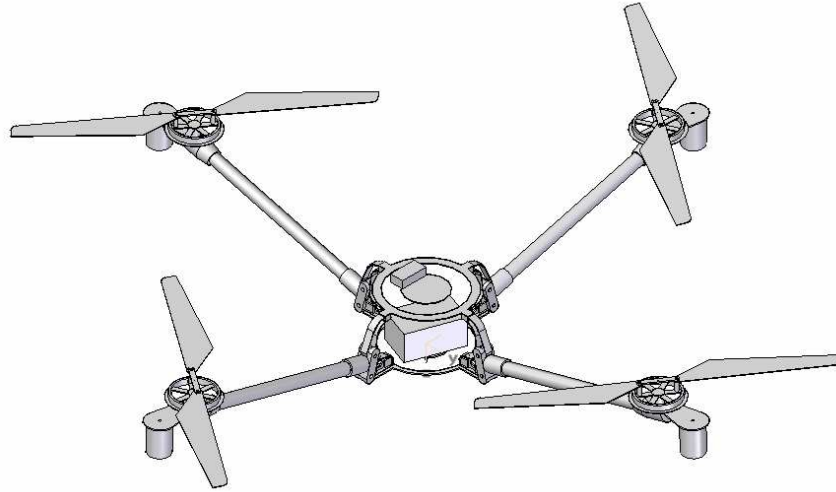


Fig 5.1. CAD model of the Draganfly XPro (note that the dome over the centre of the airframe has not been represented).

5.3 Verification of the results by a different method

In order to clarify if the previous results were realistic, they were compared to others obtained with a much more primitive method, which is now explained. The method consists in idealizing the quadrotor as a central homogeneous cuboid, which represents the battery, surrounded by four individual particles which occupy the same positions as the motors (see Fig 5.2). Each of these particles has a mass equal to that of the rotor plus the motor and half of the arm. On the other hand, the cuboid is given a mass equal to the sum of the masses of the battery and those of all the rest of elements, including the four other halves of the arms. The reasoning behind this model is that a very significant part of the mass of the quadrotor comes from the battery and the four motors so it is valid to represent the whole quadrotor only with these few items.

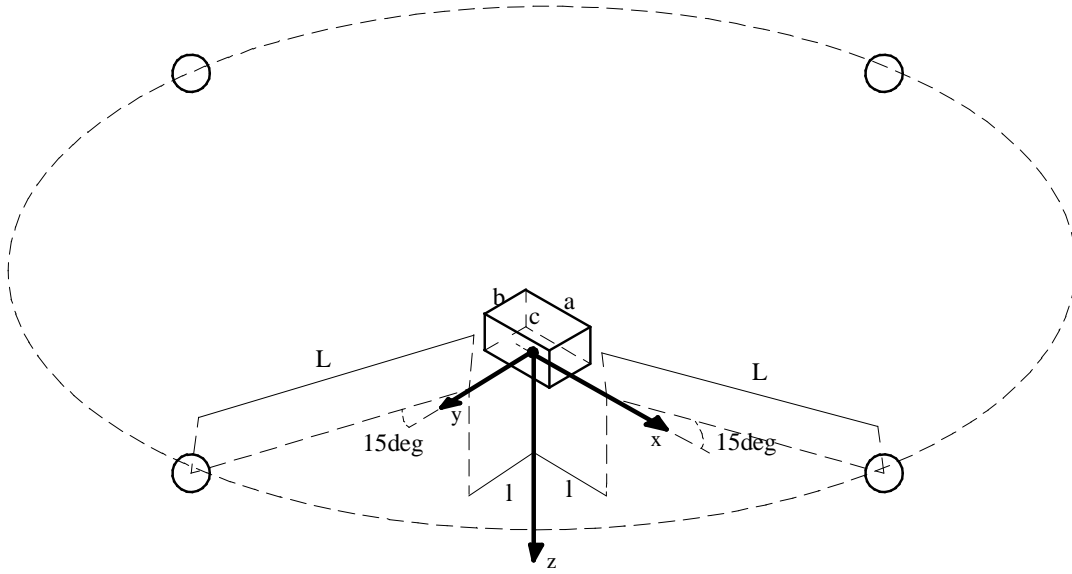


Fig 5.2. Schematic of the simplified model to estimate the moments of inertia.

Where:

$$L = 422.15\text{mm}, l = 113.5\text{mm}, a = 97\text{mm}, b = 62\text{mm}, c = 48\text{mm}$$

The masses are (see Appendix B):

$$M = 634 + 23 + 129 + 4 \times 26 + 45 + 19 + 4 \times \frac{119}{2} = 1192\text{g}$$

$$m = 168 + 30 + 2 \times 13 + \frac{119}{2} = 283.5\text{g}$$

$$4M + m = 2326\text{g}$$

The coordinates of the centre of gravity are then:

$$x_{CG} = y_{CG} = 0$$

$$z_{CG} = -\frac{\frac{c}{2}M + 4mL \sin 15^\circ}{M + 4m} = -65.57\text{mm}$$

There is some difference with the results predicted by the CAD software. In the case of x_{CG}, y_{CG} it is due to the fact that this simple model does not include some components (mainly the receiver) which are placed slightly off the central vertical axis, and whose effect is to move the cg laterally. As for the coordinate z_G , there is a difference of about 10mm probably because there is a certain amount of mass which is placed quite higher than the cg of the battery.

The moments and products of inertia can be calculated with simple formulae for the cuboid and using the parallel axis theorem:

$$I_z = \frac{1}{12} M (a^2 + b^2) + 4m(l + L \cos 15^\circ)^2 = 0.3094 \text{ kgm}^2$$

$$I_x = I_y = 2m(L \sin 15^\circ)^2 + 2m[(L \sin 15^\circ)^2 + (l + L \cos 15^\circ)^2] + \frac{1}{12} M (c^2 + b^2) + M \left(\frac{c}{2} \right)^2 = 0.1689 \text{ kgm}^2$$

$$I_{xy} = 0$$

$$I_{xz} = I_{yz} = -m(l + L \cos 15^\circ)L \sin 15^\circ + m(l + L \cos 15^\circ)L \sin 15^\circ = 0$$

In this case, the difference between the results produced by this simple model and those obtained from the CAD design is very small: about 4% for I_z and around 1% for I_x and I_y . As for the products of inertia, the values in the CAD design are not zero, but get really close.

It can be seen that this primitive model has confirmed that the products and moments of inertia obtained with the CAD design are certainly correct, or at least very close to the actual values. It should be noted that this results correspond to the complete vehicle, including the rotors and the armatures of the motors. However, it is reasonable to expect that, if the results obtained from the CAD model for the whole assembly are basically correct, the results obtained for any of its sub-assemblies, like the rigid airframe or the rotor, will also be.

As for the position of the centre of gravity, this simplified model probably is not the most suitable, although it gives an estimate close to that of the CAD design.

5.4 Blade modelling

Although the CAD model that has been presented here is fairly accurate, some elements have been modelled in more detail than others. The blades of the XPro are one example of an element that has been modelled in a simplified way: the real blades have camber but the ones of the model do not. However, it will be seen in Section 9 that the impact of this simplification is minimal.

6. EQUATIONS OF THE D.C. MOTORS

6.1 Introduction

It has been already indicated that the Draganflyer XPro is fitted with four Mabuchi RS-545SH conventional D.C. motors. Appendix C contains all the technical information about these motors.

Section 7 will deal with how to calculate the different parameters of the motors. This Section, however, is devoted to explaining the theoretical model of the dynamics of a conventional D.C. motor, both in transient and steady state.

Having an accurate theoretical model of the D.C. motor is essential for the same reason that it was essential to have an accurate set of equations of motion for the quadrotor, that is, because the Matlab/Simulink model will require it in order to simulate adequately the flight dynamics of the XPro. As in every other aspect of Engineering, the better the theoretical model, the better the resulting predictions.

The issue of the control variable

In Section 2 it was explained that the control of small, remotely-piloted quadrotors like the XPro is achieved just by varying the rpm of the rotors. This was in fact one of the main advantages of the quadrotor over other small helicopters, because it made unnecessary the complex mechanical systems that were needed to control the pitch angle of the blades.

However, it is important to realise that the rotational speed of each motor, and thus of each rotor, cannot be controlled directly. The rotational speed of the motor is the result of the interaction of different moments applied to the armature of the motor. In the section devoted to the equations of motion it was explained that the armature is the rotating part of the motor, and that the moments exerted over it, around its spinning axis, were three:

- An electromagnetic torque τ in the direction of rotation.
- A friction torque opposed to the rotation of the armature.
- A torque transmitted through the strap that links the motor and the rotor, also opposed to the rotation (from the perspective of the armature).

The interaction of these moments with each other and with the forces of inertia that affect the armature will result in a certain rotational speed. The only torque which can be controlled to modify this speed is the electromagnetic torque τ . This is controlled in turn by a combination of voltages and currents applied to the wiring of the motor.

Hence, determining the control variable that will finally be used to govern the quadrotor is not obvious at all. The following sub-sections will explain which are the “candidates” and which one is in the end the one that is used in the quadrotor.

6.2 Brief description of the architecture of a conventional D.C. motor

As any other electric motor, the D.C. motor has two different parts: the *rotor*, which is the element that rotates, as its name indicates; and the *stator*, which remains fixed. In a D.C. motor, the rotor is also called the *armature*, term which was introduced Section 4 and which is preferred because it avoids confusions with the *other* rotor, that is, the one composed by the blades and the hub.

The rotation of the armature is achieved thanks to the electromagnetic torque τ , as it was indicated before. To generate this torque, the stator is fitted with permanent magnets or with electromagnets, and the armature is fitted with its own electromagnet (essentially a coil or winding). When the current passes through this coil, the resultant electromagnetic force pushes the armature, making it rotate. To prevent the armature from reversing its motion as the poles of the armature electromagnet pass the poles of the stator, a commutator reverses the polarity of the armature electromagnet. In order to do so, the armature is fitted with brushes that press against the commutator. Incidentally, these brushes are the main source of friction torque.

We will represent the voltage and the current in the coils of the armature by v_a and i_a , respectively.

6.3 Electrical Equations of the D.C. motor

The equations of the two equivalent circuits that represent the motor are (Ref 6.1):

$$\tau = K_I i_f i_a \quad (6.1)$$

$$v_f = R_f i_f + L_f \frac{di_f}{dt} \quad (6.2)$$

$$v_a = K_I i_f \omega + R_a i_a + L_a \frac{di_a}{dt} \quad (6.3)$$

Where:

τ is the electromagnetic torque over the armature

v_f, i_f are the field voltage and current, respectively

v_a, i_a are the voltage and current in the coil of the armature, respectively

ω is the rotational speed of the motor (Using the notation of Section 4, it will be $\omega = g_r \Omega$)

L_f, L_a are the inductances of the windings of the stator and the armature, respectively

R_f, R_a are the resistances of the windings of the stator and the armature, respectively (the windings of the stator and the armature are electromagnets)

K_I is a constant of the motor to be determined

We have then six variables $\tau, \omega, v_a, i_a, v_f, i_f$ and 3 equations. There is an additional equation which is required to solve the problem, the equation of moments around the rotating axis of the armature, eq 4.50. This equation is necessary because it includes τ . Hence, this leaves us with two degrees of freedom or, in other words, with two control variables.

From the six variables listed, the only ones which can be controlled directly are v_a, i_a, v_f, i_f . Therefore any possible method of governing the motor will have to control two of these variables. We will summarize the possible methods now.

6.4 Control of the D.C. motor

There are three basic methods to control the regime of the D.C. motor (Ref 6.2):

Stator voltage control with constant armature current

In this method, i_a is kept constant by using a constant current generator rather than a voltage generator to supply the armature coils (note that if i_a is kept constant, v_a cannot be kept constant). The speed is then controlled with v_f .

Stator voltage control with constant armature voltage

Now, v_a is kept constant by using a constant voltage generator to supply the coils of the armature (note that if v_a is kept constant, i_a cannot be kept constant). The control variable is again v_f .

Armature-current control

In this case the aim is to keep the magnetic flux in the field constant, that is to keep i_f constant. To do this, either v_f is kept constant or the stator coils are replaced by permanent magnets. From a mathematical point of view, this means that equation (6.2)

can be dropped off and that $K_i i_f$ can be considered as a single constant which will be named K . The control variable is now v_a .

From the three methods, this is the one used in most applications, and the quadrotor is no exception. The main reason is that this method allows replacing the electromagnets of the stator with simpler, and cheaper, permanent magnets. In applications where small D.C. motors are needed, like in the XPro, this is in fact the only method which can be used, because it would be very difficult to fit the stator with electromagnets in such small motors.

The Mabuchi RS-545SH again is no exception. Its stator is fitted with a permanent magnet rather than an electromagnet.

6.5 Equations of the D.C. motors of the XPro. Control of the motors of the XPro

Considering all what has been said before it is clear that the set of equations for the motor of the XPro will be the following:

$$\tau_j = K i_{aj} \quad (6.4)$$

$$v_{aj} = K g_r \Omega_i + R_a i_{aj} + L_a \frac{di_{aj}}{dt} \quad (6.5)$$

Where the subscript j to identify the motor has already been included, and where it has been taken into account that the rotational speed of the motor is $g_r \Omega_i$ (Ω_i being the rotational speed of the rotor and g_r , the gear ratio).

If we obtain i_{aj} from (6.4) and enter in (6.5) the result is:

$$v_{aj} = K g_r \Omega_i + \frac{R_a}{K} \tau_j + \frac{L_a}{K} \frac{d\tau_j}{dt} \quad (6.6)$$

In this way, we have reduced the mathematical model of the motor of the XPro to a single equation with 3 variables τ_j, Ω_i, v_{aj} .

The variable used to control the motor will be v_{aj} .

Clockwise and counter clockwise motors

Until now, it has been implicitly assumed that Ω_i and τ_j were positive and the direction of turn of the motor has been ignored. However, the XPro has motors rotating in different directions and we have to account for this in the physical model. To do so, Ω_i and τ_j is positive if the rotor turns counter clockwise and negative if contrary. If we

use this criteria in (6.6) we will get negative voltages in the motors which turn clockwise. It is preferable to avoid this because of the lack of physical meaning and to do so it is enough to slightly modify this equation:

$$\pm v_{aj} = Kg_r \Omega_i + \frac{R_a}{K} \tau_j + \frac{L_a}{K} \frac{d\tau_j}{dt} \quad (6.7)$$

Where + is used in motors turning counter clockwise and – in the other case.

6.6 Some considerations about the electronics of the Draganfly XPro

As it was explained in Section 3, the commercially available Draganfly XPro is remotely controlled by a pilot using a transmitter. This transmitter sends radio signals to a receiver aboard the quadrotor. This receiver transforms these radio signals into electric signals which then go to the CPU of the quadrotor. This CPU also receives electric inputs from the gyrometers. Taking both into account the CPU calculates the v_{aj} required by each motor.

Thus, before v_{aj} there is a whole set of physical variables, algorithms and control loops that still have not been modelled. And they will not be. It is evident that modelling in detail the transmitter, the receiver, the CPU and the gyrometers is beyond the scope of this Project. Besides, the aim of this Project was to serve as a help for the development of an autonomous version of the XPro, and this autonomous version will not use the transmitter or the receiver. In addition, it might be fitted with a different CPU and different gyrometers. It would be useless to model the default components before knowing whether or not they are going to be kept in the autonomous version.

7. ESTIMATION OF THE CONSTANTS OF THE MOTORS

7.1 Introduction

In the Section 6 the following equations were obtained for the D.C. motor of the XPro:

$$\tau_j = K i_{aj} \quad (6.4)$$

$$v_{aj} = K g_r \Omega_i + R_a i_{aj} + L_a \frac{di_{aj}}{dt} \quad (6.5)$$

To be able to solve the mathematical problem, another equation was required, the “mechanical equation”, which was eq 4.50.

A quick look at these equations reveals that there are certain constants that have to be determined before we can introduce the equations in the model of the XPro. It is the same situation as with the equations of motion, when the mass and inertial properties were required prior to adopting those equations for the model of the XPro.

In the case of the motors, the constants to be determined are K, R_a, L_a, F . What follows is an explanation of how to obtain these values. It should be noted that, in reality, those constants will be different for each motor, because the motors are not exactly identical, even if the four are of the same model (there are small variations in the dimensions, the masses, the wiring, and even in the cleanliness of the brushes). In fact, because of these differences the response of each motor will be slightly different from the others, making it more difficult to control the quadrotor (see Section 16). For the moment, it will be assumed that the four motors, and so their constants, are exactly identical.

7.2 Estimation of the constants of the motor. Theoretical background

The electric equations, once again:

$$\tau = K i_a \quad (6.4)$$

$$v_a = K g_r \Omega + R_a i_a + L_a \frac{di_a}{dt} \quad (6.5)$$

Where the subscript j has been omitted for the sake of clarity and where Ω is the rotational speed of the rotor, in rad/sec.

Constants determined in the steady state regime

If the motor is working in a *steady state condition*, which is easy to reproduce in a test bench:

$$\tau = K i_a \quad (7.1)$$

$$v_a = K g_r \Omega + R_a i_a \quad (7.2)$$

And the “mechanical equation”:

$$\tau = \tau_{load} + F g_r \Omega \quad (7.3)$$

Where τ_{load} is the load torque or, in other words, the output mechanical torque of the motor.

It should be noted that this equation is valid regardless of whether the motor is installed in the quadrotor, in a test bench or in any other situation in which it is driving a load, provided that it is in a steady state regime.

Merging (7.1) and (7.3):

$$K i_a = \tau_{load} + F g_r \Omega \quad (7.5)$$

(7.2) and (7.5) are two and the constants to be determined are three: K, R_a, F . On the other hand, the variables are $v_a, i_a, \tau_{load}, \Omega$. If we knew those variables in two different functioning points, it would be possible to determine K, R_a, F . The values of the variables at those points can be obtained experimentally or using the data provided by the manufacturer (see Appendix C).

However, there are certain points that are less convenient for being used to determine the constants. One point which should not be used is the stalling point, that is, the point at which the speed of the motor suddenly drops because the load torque is too high. This point should be avoided because the rotational speed is difficult to specify (it is not zero) and because we can hardly say that it is in the steady state regime (the speed is dropping). Besides, in this point the current i_a is maximum, so if this point is been studied experimentally, extra precautions have to be taken to avoid equipment damage or personal injuries.

A useful advice would be not to use points too close to the stalling point or to the “no load” point, because in those regions there are several non-linear effects which are not covered by our equations. It should not be forgotten that the model described by (7.2) and (7.5) is a simplified model that makes several assumptions, for instance, that the friction is linear in the rotational speed.

Estimation of the inductance

K, R_a, F affect the dynamics of the motor in both a steady state condition or in a transient state one. But the inductance L is only relevant in the second case.

Because L affects only the transient response, it can only be determined by studying the transient state regime of the motor. Since the manufacturer does not provide information about the transient states of the motor, L can only be determined experimentally.

A simple method would be to feed the motor with a sinusoidal v_a of frequency ω and to measure the amplitude and phase of Ω and i_a . It should be noted that this ω is *not* the rotational speed of the motor.

Using complex number algebra (j is the imaginary unit):

$$v_a = v_{a0} e^{j\omega t} \quad (7.6)$$

Then, it will be:

$$i_a = i_{a0} e^{j\omega t} e^{j\phi} \text{ and } \Omega = \Omega_0 e^{j\omega t} e^{j\phi} \quad (7.7)$$

Entering in (6.5):

$$v_{a0} = K g_r \Omega_0 e^{j\phi} + R_{a0} e^{j\phi} + L i_{a0} j \omega e^{j\phi} \quad (7.8)$$

If $\Omega_0, \phi, i_{a0}, \phi$ are known, then we can obtain L as:

$$L = \operatorname{Re} \left(\frac{v_{a0} - R_{a0} e^{j\phi} - K g_r \Omega_0 e^{j\phi}}{i_{a0} j \omega e^{j\phi}} \right) \quad (7.9)$$

(The phases ϕ, ϕ should not be confused with the Euler angles of the equations of motion of the quadrotor).

7.3 Estimation of the constants of the motor using the information provided by the manufacturer

Appendix C shows the information about the RS-545SH motor provided by Mabuchi, the manufacturer. It gives data from three different points of the steady state regime: the no load point, the maximum efficiency point and the stalling point. The latter will not be used in the estimation of the constants for the reasons explained before. Using the first two we can obtain the values of K, R_a, F :

These values are:

$$R_a = 0.267 \text{ ohm}$$

$$K = 0.00464 \text{ volts} \cdot \text{s} \cdot \text{rad}^{-1}$$

$$F = 2.035\text{E} - 06 \text{ N} \cdot \text{m} \cdot \text{s} \cdot \text{rad}^{-1}$$

In Section 12 new estimates will be obtained using experimental data.

8. SELECTION OF THE MODEL FOR THE ROTOR

8.1 Introduction

Obtaining a physical model of the rotor is essential for the study of the flight dynamics of the quadrotor. In particular, this model will have to provide \mathbf{F}_i and \mathbf{M}^{Pi} , as well as $\left(\frac{d}{dt}\mathbf{H}_{Pi}\right)_{mean}$, all of which are required by the equations of motion that were obtained in Section 4. This model will be restricted to the blades. More precisely, it will be a model of the physical system formed by the b blades of the rotor. The other element of the rotor, the hub, will not be part of this model.

Since the selection of this model will greatly influence the outcome of the whole simulation of the quadrotor, it is worth taking some time to examine the different choices available, its advantages and its limitations.

Many reports that aim at modelling quadrotor flight dynamics do not justify the selection of one model or another, nor do they take into account its limitations when establishing conclusions. We should avoid making this mistake here too.

8.2 Empirical models vs Theoretical models

Empirical models

Under this term we refer to all the models that are almost exclusively based on empirical data, typically obtained in the wind tunnel.

In order to obtain the large amounts of data which are required, many wind tunnel tests have to be carried out. Statistical software packages have then to be used to identify trends and find correlations. Ideally, the result of all this work will be a series of empirical functions to calculate the relevant magnitudes (induced velocity, thrust, torque, flapping angles, etc).

The main advantage of this method is that, if properly done, the obtained model will be very accurate on its predictions, since it is closely based on the *real* system, not on an idealization. On the other hand, these models have four basic disadvantages. Firstly, they require a very large amount of experimental data, and an equally large amount of time to analyze them. Secondly, their accuracy is directly proportional to the accuracy of these data; any errors in the measures will be directly transmitted to the models. Thirdly, they do not provide information on how each design parameter (blade pitch, chord, twist, aerofoil, etc) is affecting the behaviour of the rotor. And finally, they lack flexibility, because they are limited to the rotor of the tests. This is linked to the previous point and means that these models cannot be used with rotors other than the one that has been tested.

Theoretical models

These are the models based on one or several of the theories that aim at explaining the physical behaviour of a rotor. Among these theories are, ordered by increasing complexity (Ref 8.1):

- Blade Element Theory (BET) + Momentum Theory (MT)
- Prescribed Wake Methods
- Free Wake Methods
- Solving methods for the Navier-Stokes equations

From these, only the first one is affordable in terms of effort and resources considering the scope of this Project and the time assigned to it.

The main disadvantage of these models is that they all simplify the real system to a certain extent. More complex models will make fewer assumptions and thus be more accurate. But there will always be some error due to the inevitable simplifications that have to be made. This is an important issue because it might happen that the resulting accuracy is smaller than that which was desired.

On the other hand, these models are much more flexible than their empirical counterparts. They provide information about how the design parameters affect the performance of the rotor, they require less work to be tuned, and they need few experimental data.

Conclusion

Given the scope of this Project, theoretical models are more convenient. But we still need to know if they are capable of producing accurate results. Possibly the best way to know that is to look at the published reports on the same topic.

One of the best works on quadrotor modelling has been done by Pounds *et al* (Refs 8.2, 8.3). They developed a theoretical model of the rotor based on the results obtained by Prouty for conventional helicopters (Ref 8.4). According to them, the results obtained were reasonably accurate, at least so as to be used to evaluate controllers for the vehicle, which is basically the same requisite of our model. Later, G.M. Hoffmann *et al* (Ref 8.5) used a similar but simpler model for their own quadrotor. They showed that this model was capable of predicting several physical effects that had been observed in flight.

Other published reports deal with quadrotor modelling too, but they use much simpler models (to the extent of considering the thrust and torque coefficients to be constant, for example; see Section 1).

According to all what has been said, it can be stated that a theoretical model is capable of making satisfactory predictions, provided that its level of detail is enough. Since theoretical models are more convenient because of their simplicity, as explained before, it will be one of these that will be used in our simulation.

It should be borne in mind that theoretical models also required a certain amount of experimental data, which have to be obtained in the wind tunnel. This issue will be explained in detail in the following sections.

8.3 Overview of the models available

As it has been previously said, theoretical models based on wake methods or on Navier-Stokes equations are completely out of the scope of this Project. We will therefore be limited to models based on Momentum Theory combined with Blade Element Theory. Within these, there are still plenty of options. Among the ones which were reviewed were the following:

Local-Differential Momentum Theory (Blade Element-Momentum Theory)

This theory simultaneously calculates the induced velocity and the coefficients of forces and moments. It was initially considered but was quickly rejected because the formulation that was found in the published works was not detailed enough. For example, we were interested in modelling the blade flapping and the influence on it of the blade stiffness, but no book or article was found describing how to do so with this theory.

Therefore it was decided to use the Momentum Theory (or a variation of it) for the modelling of the induced flow and Blade Element Theory (BET) for the coefficients of forces and moments. Even then, there were still many possibilities depending on the assumptions made for BET:

No flapping model

This model is one of the simplest ones. It ignores blade flapping by assuming that the rotor is perfectly rigid. But the rotors of the XPro are far from being perfectly rigid (see Figure 8.1 on next page), and so this model is too simple.

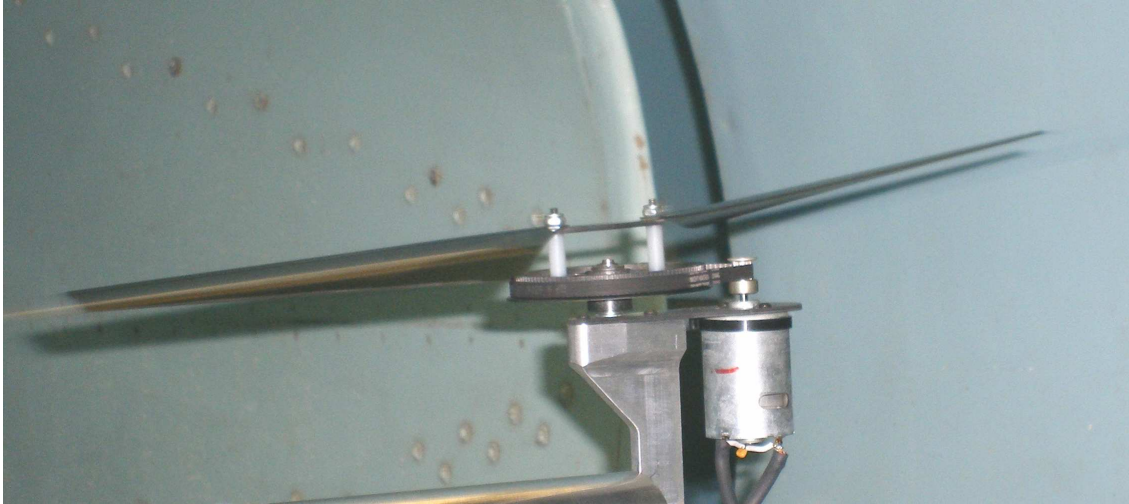


Fig 8.1. Picture of the blades of the XPro taken in the wind tunnel while the rotor was turning at high speed. Blade flapping is obvious: the blade on the left is bent downwards whereas the one on the right is bent upwards.

1st order flapping

This means that the flapping angle is assumed to be a first order series of sines and cosines of the azimuthal angle of the blade. Models that assume first order flapping are by far the most extended, at least for non-commercial applications. There are several particularly well-known:

Newman:

Newman (Ref 8.6) developed a simple model where real blade flapping dynamics are simulated by means of an equivalent system composed by a rigid blade with a zero-offset hinge. To simplify the formulation, other hypotheses are made. Because of its simplicity, this model is very widespread. This model was used by Hoffmann *et al* (Ref 8.5) for their quadrotor, with satisfactory results. For this Research Project, though, this model is considered to be too simple.

Prouty:

Prouty (Ref 8.4) developed a very detailed mathematical model of the rotor of a conventional helicopter. A very simplified version of this model was later used by Pounds *et al* (Refs 8.2, 8.3) for their quadrotor. This model uses an offset hinge with no spring to simulate the stiffness of the blade. It considers the effect of the angular rates on the flapping angles, but not on the coefficients of forces and moments. It can produce very satisfactory results, as shown by Pounds *et al* (Refs 8.2, 8.3).

Padfield:

Padfield's model (Ref 8.7) includes the effect of the angular rates on the coefficients and gives even more attention to the problem of determining the flapping angles. It uses

a hinge with spring and no offset to simulate the dynamics of the blade. Overall, this model is more detailed than the previous one, yet lacks its popularity, possibly because it is more complex.

Bramwell:

Bramwell's model (Refs 8.8, 8.9) is similar to that of Prouty, although less detailed in some aspects.

2nd order flapping

One well-known model of this type is the one developed by Wheatley (Ref 8.10) and Bailey (Ref 8.11). It might be expected that the inclusion of second order harmonics would increase the accuracy of the results. However, Bramwell (Ref 8.10) disagrees with this, indicating that the effects of higher modes of blade bending (which are not considered here) are at least as important as the effects of second order harmonics.

All the models which have been reviewed here can be further improved by including the effect of the reverse flow region (in a simple way, though) and by using a drag coefficient linear or quadratic with the angle of attack. All this can be done thanks to the flexibility of these models.

8.4 Selection of the model

It was decided to reject second order flapping models because the benefits of including second order harmonics probably did not compensate for the additional complexity.

As for the first order flapping models, Padfield's was the most detailed, but perhaps excessively complex and slightly obscure. On the other hand, Newman's was too simple. Between Bramwell's model and that of Prouty, the latter was more comprehensive and more detailed in some aspects. Besides, Prouty's model had the advantage of having already been used for quadrotor modelling (Refs 8.2, 8.3) with acceptable results.

Therefore, it was decided to follow Prouty to develop the rotor model. However, it will be seen that important modifications were made on Prouty's model before applying it to the XPro. The most important one was to add a torsional spring, which is not included in the original model.

As it has been said before, Prouty's model has already been applied to quadrotors by Pounds *et al.* But they made important simplifications on the original model (such as ignoring the force H , for example) that might be compromising the accuracy of the results. Because of this, here we will not simplify the original model. In fact, as we have seen, we will expand it.

9. MODELLING OF THE ROTOR

INTRODUCTION

9.2 Description of the rotor

The rotor of the XPro is composed by two or three blades and a hub to which they are attached.

Each blade is attached to the hub by means of a single screw (see Fig 9.1). The joint offset e_j , that is, the distance between the axis of the hub and the axis of the bolt, is $26mm$. If we define the radius of the rotor R as the distance between the axis of the hub and the tip of the blade, then the joint offset is approximately a 10% of R . It is important not to confuse the radius of the rotor, R , with the length of the blade. According to what has been said, the length of the blade is approximately 90% of R .

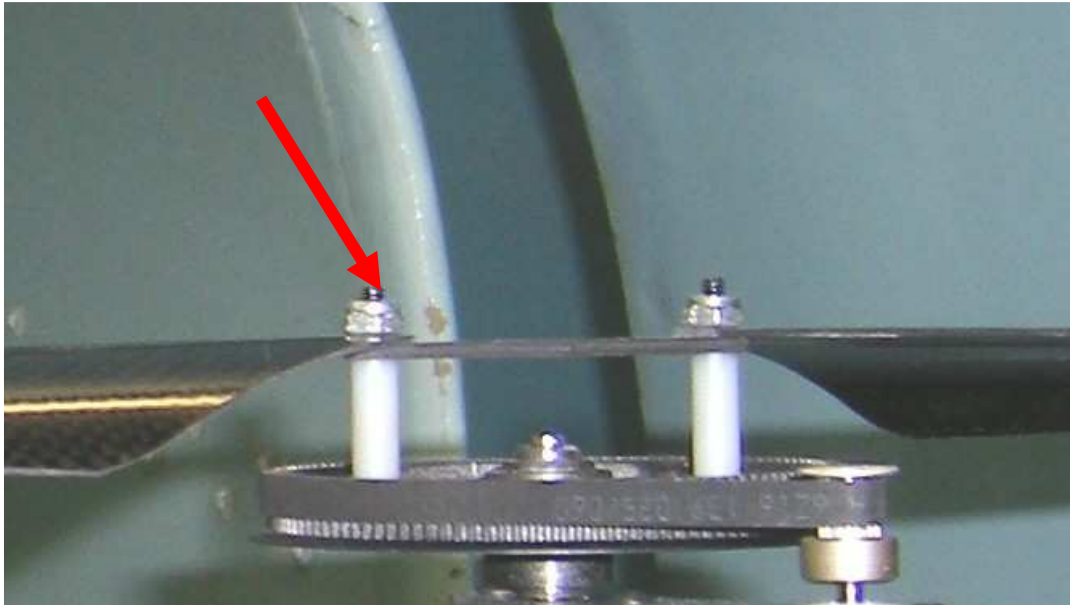


Fig 9.1. Detail of the hub-blade assembly. The arrow points at the screw that secures the blade to the hub.

9.3 Description of the motion of the blades

As it was indicated in Section 4, the kinematics of the blades relative to the airframe is fairly complex, resulting from the combination of several types of motion.

Rotation

The motion of the blade around the axis of the rotor or, in other words, the motion of the hub around its axis. This is the most obvious type of motion. The speed of rotation is represented by Ω_i as indicated in Section 4.

Contrary to conventional helicopters, where this speed is maintained invariable for different reasons (ref 9.1), in the quadrotor it is constantly being modified in order to control the attitude (see Section 2). In the XPro the typical values range between 100 and 200 rad/s.

Feathering

The motion of the blade around its longitudinal axis. In conventional helicopters, where control is achieved by collective and cyclic variations of the pitch, the feathering motion is controlled by the position of the swashplate. The XPro, on the contrary, is not capable of controlling the pitch angle of the blade, since this feature is not required to control the vehicle (control is achieved by independently adjusting the speed of the four rotors, as explained). Therefore, the blade will be free to feather and the feathering motion will be the result of the moments acting around the longitudinal axis of the blade. It should be noted, however, that the feathering motion is constrained by the stiffness of the blade around its longitudinal axis. If the blade was completely rigid, there would be no feathering motion.

Although feathering is important, specially because of its influence on the flapping motion (see sub-section 9.19), *it will not be modelled*. The main reason is that, in order to satisfactorily model the feathering, it is necessary to estimate both the aerodynamic moment around the longitudinal axis of the blade and the stiffness of the blade around that axis, and these are very difficult tasks.

However, in sub-section 9.19 a method to model the feathering motion will be described, and the influence of this motion on flapping will be explained.

Flapping

The motion of the blade on a plane which contains the axis of rotation of the rotor. It will be seen that, as in any other rotorcraft, blade flapping has a decisive influence on quadrotor dynamics. The origin of this motion lies on the cyclic variations of lift seen by the blade. The blade of a rotor in hover produces the same lift as it turns. However, under other flight conditions, the lift varies as the blade turns around the axis of the rotor. This makes the blade move up or down as the lift changes.

Obviously, the flapping motion is constrained because the blade is attached to the hub and because it is rigid. In fact, a perfectly rigid blade attached to the hub by a perfectly rigid joint would not flap. However, in real life the blade will not be perfectly rigid. Moreover, in order to alleviate stresses, the joint between the blade and the hub will

either be designed to be flexible or just be replaced by a hinge. The consequence of all this is that the blade will be able to flap.

This leads to the issue of how to model the flapping. A detailed model that represents the blade and its joint to the hub with fidelity is not practical for a real-time simulation of a rotorcraft. It is necessary to make some simplifications. Padfield (Ref 9.2) offers a comprehensive list of the most common models. All these models assume the blade to be perfectly rigid and replace the real joint between the blade and the hub by a hinge. Additionally, some models add a torsion spring to the hinge. What makes the difference between the models is the method use to determine the hinge offset and the spring strength.

The flapping angle β is difficult to define in a real rotor (see Figure 9.2). However, in these simplified models β can be easily defined as the angle between the rigid blade and the plane of the hub (see Figure 9.2).

It is important to understand that β cannot be controlled, at least directly. It is the result of the equilibrium between the different moments acting at the blade hinge. This will be more clear when it is explained how to calculate this angle.

Lead-Lag (or Lagging)

This is the motion of the blade on its plane. It is a consequence of the flapping motion. When the blade rotates and flaps in the same time, each blade element is subjected to the Coriolis force. This force is perpendicular to the plane of the flapping motion.

One of the main consequences of lagging is that the centre of mass of the rotor will no longer be on the axis of rotation. Instead, it will move around it. This will induce vibrations on the vehicle, which can be very intense under certain circumstances (Ref 9.2). However, this phenomenon is of no importance for the determination of the attitude and trajectory of the vehicle, which is our task. Therefore *the lead-lag motion will be ignored* in our model of the quadrotor.

9.4 Description of the simplified model

As it has been said before, an exact model which considers the flexibility of the blade is too complicated for a real-time simulation. It is therefore necessary to find a simplified model. It has been anticipated that all the models available assume that the blade is rigid and include a hinge, no matter if the real rotor does not have it (as in the case of the XPro). Depending on the model, a torsion spring will be placed at the hinge. The hinge offset and the spring stiffness will be chosen so that one or more physical characteristics of the idealized rotor match with those of the real one. In any case, it is essential that the model accurately predicts the moments and forces transmitted to the hub.

The most common models are:

- Centre hinge with spring
- Offset-hinge and spring
- Offset-hinge with no spring

Depending on the type of rotor, one of the models can be much better suited. For instance, with an articulated rotor the third model will be used. With a teetering rotor the first model will be used, but with no spring. However, a hingeless rotor (such as the one in the XPro) can be represented with any of the three models. All what follows refers to this type of rotor, except when stated otherwise.

The purpose of the torsional spring is to simulate the stiffness of the blade at the joint with the hub.

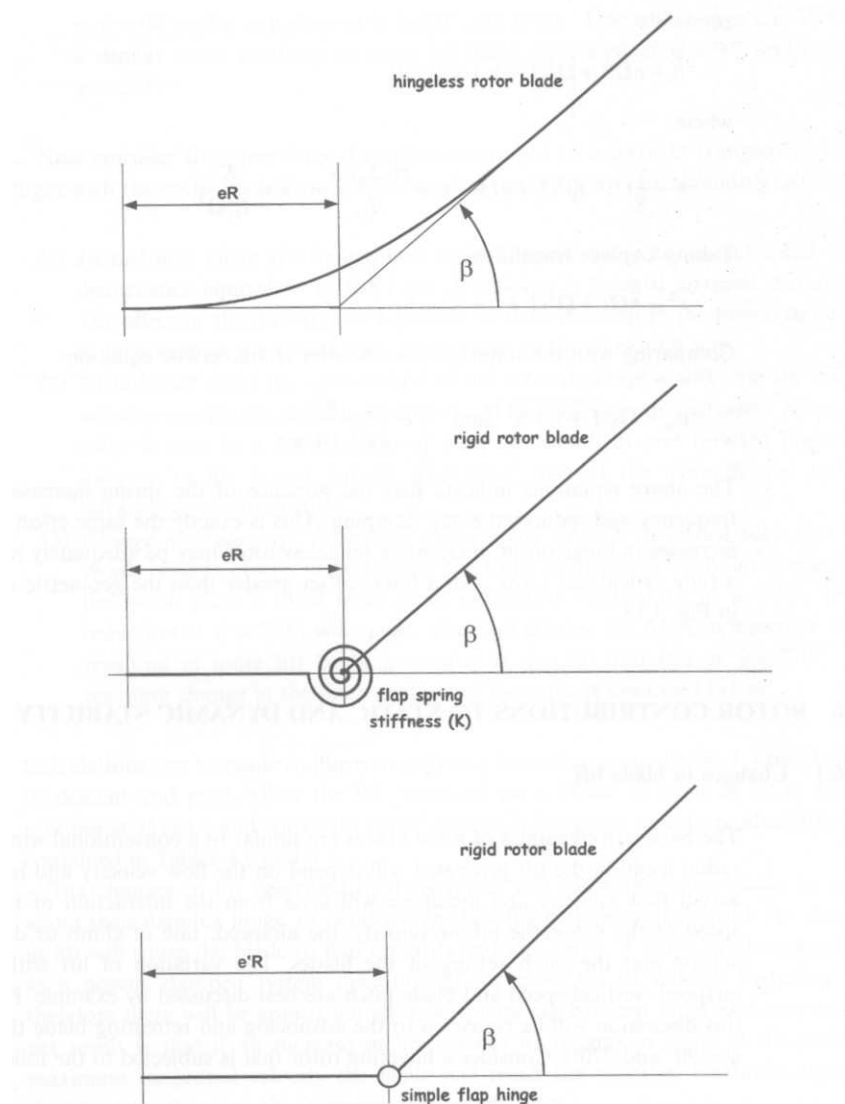


Fig 9.2. Real blade (up), Offset-hinge and spring (middle), Offset-hinge with no spring (down) (Ref 9.3).

Offset-hinge with no spring

In this model the spring is simulated by increasing the offset of the hinge. An “effective hinge offset” is thus defined. The advantage of eliminating the spring is that the mathematical expressions become simpler. This type of model is very common and it has been developed in great detail by Prouty (Ref 9.4).

However, an extra offset is not a perfect replacement for a spring, for several reasons. One of them is that this offset will depend on the rotating speed of the rotor Ω . In a conventional helicopter, where Ω is kept almost constant, the offset can be assumed to be constant too. But in the XPro, where Ω is changing all the time, this cannot be done; the offset will have to change in accordance. The other disadvantage is that for $\Omega=0$ the model fails. This is because of the lack of spring. When there is no spring, the only forces on which the model relies to prevent the blade from “falling” are the aerodynamic and centrifugal. But when $\Omega=0$ they are both zero. Obviously, real articulated rotors have mechanical constraints to restrict the movement around the hinge and keep the blades straight when $\Omega=0$. But this is not represented in the model. Therefore, as Ω approaches zero, the predicted flapping angles become unrealistic.

Offset-hinge with spring

In this model the hinge offset and the spring strength are chosen so that they match one or several of the physical characteristics of the blade. Young (Ref 9.5) suggested selecting the spring strength so that the resulting non-rotating flap frequency matched with the real one. Then, the hinge offset should be chosen so to match the rotating flap frequency.

The advantages of including a torsional spring have already been explained. Because of these advantages, here we will use this model.

Centre hinge with spring

This is an alternative model proposed by Padfield (Ref 9.2). In the case of the XPro, though, it is difficult to use. The root of the real blade has an offset, and therefore between the hub axis and the blade root there is no lift generation. This would have to be taken into account if we wanted to use Padfield’s model, thus complicating the formulation. In the quadrotor the blade root is as far as a 10% from the hub axis, so this effect is important.

9.5 Auxiliary axes

When studying the aerodynamics of the rotor, usually is more convenient to define new set of axes $P_i x_w y_w z_w$, which is shown in Fig 9.3a. In this Figure we can also see an additional set of axes $P_i xyz$, which is parallel to $Oxyz$:

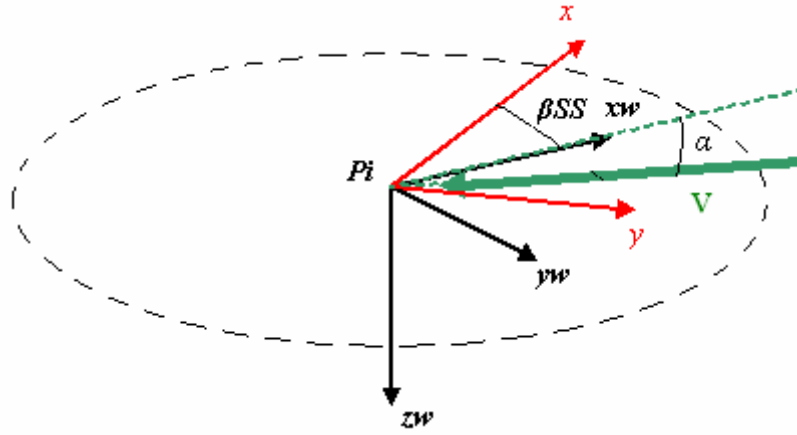


Fig 9.3a. Set of axes $P_i x_w y_w z_w$. The dashed circle is the projection of the TPP on the HP.

The origin of the set of axes is at P_i , which was the centre of mass of the system formed by the b blades. It should be remembered that P_i is assumed to be fixed relative to the airframe.

We will use low-case letters for the forces and moments at P_i when expressed in $P_i x_w y_w z_w$ axes, whereas the upper-case letters will represent the forces and moments at P_i but expressed in $Oxyz$ axes. For example, m_x is the moment at P_i around $P_i x_w$ while M_x is the moment at P_i around an axes parallel to Ox .

We will define the forces and moments in the new set of axes so that (see Figures 9.3b and 9.3c:

$$\mathbf{F}_i = F_x \mathbf{i} + F_y \mathbf{j} + F_z \mathbf{k} = -f_x \mathbf{i}_w + f_y \mathbf{j}_w - f_z \mathbf{k}_w \quad (9.1)$$

$$\mathbf{M}^{Pi} = M_x \mathbf{i} + M_y \mathbf{j} + M_z \mathbf{k} = m_x \mathbf{i}_w + m_y \mathbf{j}_w + m_z \mathbf{k}_w \quad (9.2)$$

And therefore:

$$\begin{aligned} F_{xi} &= -f_{xi} \cos \beta_{SSi} - f_{yi} \sin \beta_{SSi} \\ F_{yi} &= f_{yi} \cos \beta_{SSi} - f_{xi} \sin \beta_{SSi} \\ F_{zi} &= -f_{zi} \end{aligned} \quad (9.3)$$

$$\begin{aligned} M_{xi} &= m_{xi} \cos \beta_{SSi} - m_{yi} \sin \beta_{SSi} \\ M_{yi} &= m_{yi} \cos \beta_{SSi} + m_{xi} \sin \beta_{SSi} \\ M_{zi} &= m_{zi} \end{aligned} \quad (9.4)$$

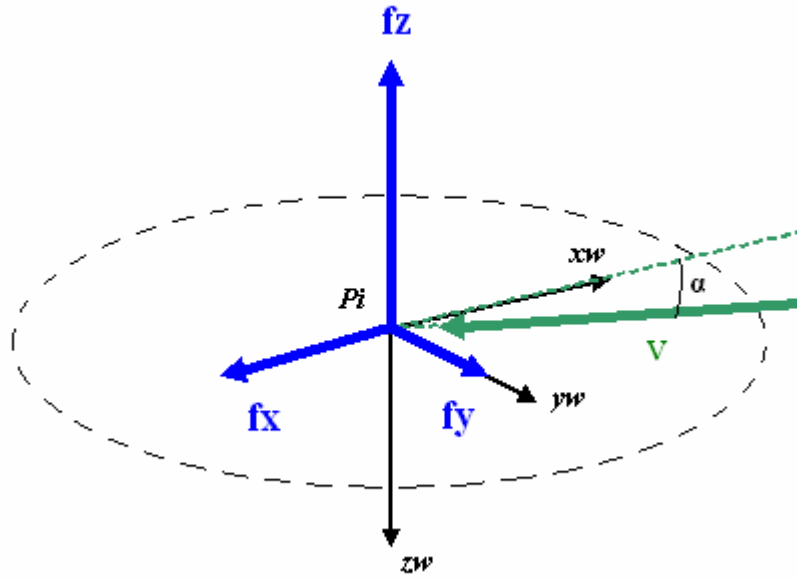


Fig 9.3b. Forces on the rotor (quantities positive as shown).

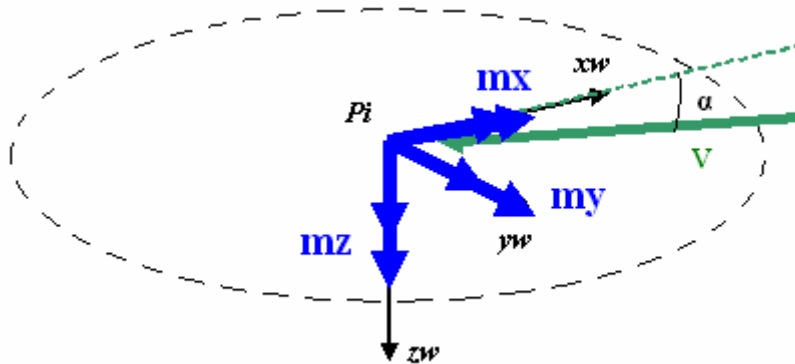


Fig 9.3c. Moments on the rotor (quantities positive as shown).

It can be seen that if there is no free stream or if the free stream is parallel to the axis of the rotor ($\alpha = \frac{\pi}{2}$) then the set of axes is not defined. However, it will be seen that in this case $f_{xi} = f_{yi} = m_{xi} = m_{yi} = 0$.

The sideslip angle β_{ss} and the angle of attack α can be obtained using the following expressions:

$$\beta_{ss} = \arctg \frac{v_i}{u_i} \quad (9.5)$$

$$\alpha = \arctg \frac{V_z}{V_x} \quad (9.6)$$

The sideslip angle β_{ss} should not be confused with the flapping angle, which is represented with the β symbol.

Where $V_x = +\sqrt{u_i^2 + v_i^2}$ and $V_z = -w_i$.

Attention will have to be paid to the cases in which the denominator of the above expressions is zero. This will be important when building the Simulink model.

u_i, v_i, w_i are the components of the velocity vector of O_i , and can be obtained from u, v, w using the following equations:

$$\begin{aligned} u_i &= u - ry_i + qz_i \\ v_i &= v - pz_i + rx_i \\ w_i &= w + py_i - qx_i \end{aligned} \quad (9.7)$$

where x_i, y_i, z_i are the coordinates of the point O_i in the $Oxyz$ frame. We define O_i as the point which is located at the intersection between the axis of the hub and its top. P_i can be assumed to lay on the axis of the hub, above O_i and separated from it by a distance h . Therefore:

$$\mathbf{OP}_i = \mathbf{OO}_i - h\mathbf{k} \quad (9.8)$$

h can be obtained easily as $h = r_{Gb}a_0$ (Ref 9.4) where r_{Gb} is the distance from the hinge to the centre of mass of the blade and a_0 is the coning angle (see sub-section 9.6).

To obtain (9.7) it has been taken into account that the axis of the hub is parallel to Oz .

The components of the angular velocity of the hub (not of the blade) can be expressed in the new set axes using the following relations:

$$\begin{aligned} p_w &= p \cos \beta_{ss} - q \sin \beta_{ss} \\ q_w &= -p \sin \beta_{ss} + q \cos \beta_{ss} \\ r_w &= r \end{aligned} \quad (9.9)$$

9.6 Flapping angle. Tip Path Plane

The flapping angle β will be a periodic function of the azimuthal angle ψ . When the rotor is in forward flight, ψ is arbitrarily defined in such a way that it is zero when the blade is at the rear (with the front facing the direction of flight) This is shown in the figure below. ψ is positive, increasing as the blade turns. ψ should not be confused with the yaw angle of the airframe. When the rotor is in hover or in axial flight, then the

above definition of ψ fails. However, this will not affect our theoretical results since since they will be averaged for a complete turn, thus enabling us to choose an arbitrary origin of ψ in hover or axial flight.

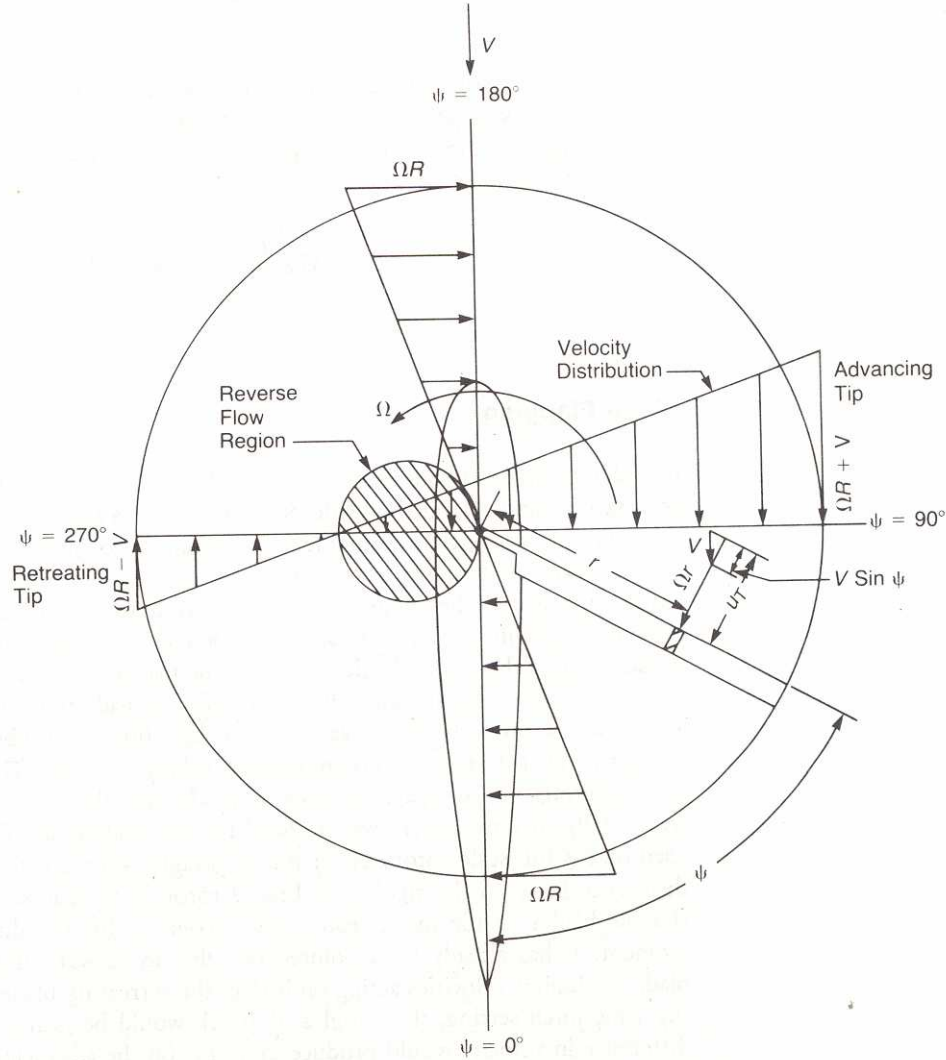


Fig 9.4. Azimuthal angle ψ in a conventional helicopter. Note that the front of the helicopter is aligned with the velocity vector (Ref 9.4).

Since β is a periodic function of ψ , it can be expressed as a series of sine and cosine terms of ψ . There is extensive evidence in the available literature to prove that a first order β is enough to represent the flapping. With the usual notation:

$$\beta = a_0 - a_{1s} \cos \psi - b_{1s} \sin \psi \quad (9.10)$$

a_0 is called the “coning angle” while a_{1s}, b_{1s} are called “flapping angles” (although strictly speaking the flapping angle is β). From now onwards we will use the term “flapping angle” to refer to a_{1s} and b_{1s} , except if stated otherwise.

One very important consequence of choosing a first order flapping is that the path followed by the tip of the blade is contained in a plane. This plane will be called “Tip Path Plane” or TPP (Ref 9.6). This plane should not be confused with the “Hub Plane” or HP (Ref 9.6). In fact, the TPP and the HP will only be the same if $a_0 = a_{1s} = b_{1s} = 0$, which usually does not happen. The TPP and the HP will be parallel if $a_{1s} = b_{1s} = 0$, which occurs when the rotor is hovering or in axial flight ($\alpha = \frac{\pi}{2}$).

The fact that in hover or in axial flight it is $a_{1s} = b_{1s} = 0$ is the logical consequence of the symmetry of that flight condition. It is also supported by empirical evidence (see Section 13). However, it does not occur if the cyclic pitch is non-zero. Nevertheless, since the quadrotor is not capable of cyclic pitch control (it lacks the swashplate) this will be zero, and so $a_{1s} = b_{1s} = 0$ in hover and axial flight.

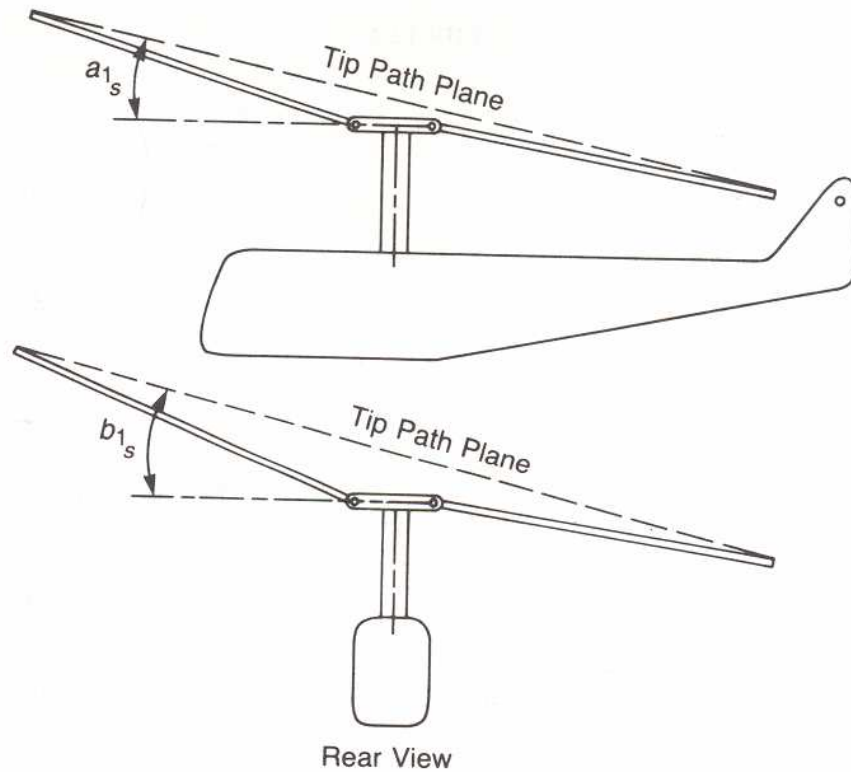


Fig 9.5. Flapping angles in a conventional helicopter where the rotor turns counter clockwise.
The coning angle a_0 has not been represented (Ref 9.4).

Usually $a_0, a_{1s}, b_{1s}, \beta$ will be small. This greatly simplifies many of the expressions which follow.

9.7 Pitch angle

The pitch angle θ (not to be confused with the pitch angle of the airframe) is defined as the angle between the zero-lift line of a blade element and the HP. Since the blade has usually a non-zero flapping angle, it is more rigorous to define it as the angle between the zero-lift line and the intersection of the HP with a plane that contains the blade element. If the blade has twist then θ will be different for each blade station. If the twist is linear:

$$\theta(r, \psi) = \theta_{root}(\psi) + \theta_1 \frac{r}{R} \quad (9.11)$$

Where r is the distance from the blade root (not from the centre of the hub) to the blade element and should not be confused with the yaw rate of the airframe. θ_{root} is the pitch angle at the blade root.

As it has been anticipated by the above expression, θ_{root} will be a periodic function of ψ , and thus it can be expressed as a series of sines and cosines. In a conventional helicopter, θ_{root} is controlled by the position of the swashplate. Since this swashplate is planar, all the sine and cosine terms are zero except for those of first order. Therefore:

$$\theta_{root} = \theta_0 - A_1 \cos \psi - B_1 \sin \psi \quad (9.12)$$

In the XPro, however, there is no swashplate to control pitch, since there is no need to do so in order to control the vehicle (contrary to what happens in conventional helicopters). The blades are attached to the hub and there is no articulated joint that enables the blade to turn around its longitudinal axis, as in conventional helicopters. But this does not mean that the pitch angle is going to be constant, because the blade is flexible around its longitudinal axis. This also happens in conventional helicopters, but in the XPro the effect is more intense because the torsional flexibility of the blade is much higher, especially at the root (where the chord and thus the cross-section are very small). However, this phenomenon (feathering) will be neglected. Therefore:

$$A_1 = B_1 = 0 \quad \theta = \theta_0 + \theta_1 \frac{r}{R}$$

Nevertheless, we will retain A_1 and B_1 in the expressions throughout this Section, because afterwards it will be useful when explaining how feathering can be introduced into the model (see sub-section 9.19).

It should be taken into account that in hover and axial flight it is $a_{1s} = b_{1s} = 0$ only if $A_1 = B_1 = 0$ (zero cyclic pitch) as indicated in the previous sub-section.

DYNAMICS

9.8 Introduction

$\left(\frac{d}{dt} \mathbf{H}_{Pi} \right)_{mean}$ appears in the equations of motion of the quadrotor (see Section 4) and therefore it needs to be calculated. However, the complexity of the kinematics of the blades makes it unadvisable to follow the same procedure which was used with other elements of the quadrotor, such as the rotor hub.

Here, on the contrary, the derivative of the angular momentum will be calculated by an indirect method, where we will consider the b-blades as an isolated system.

The total moment in the centre of mass of the b-blades system, that is P_i , will have two components, one parallel to its axis and another one contained in the plane perpendicular to this axis (hub plane-HP). We will consider them separately. We will use the term “in-plane” to refer to vectors parallel to the HP and the term “out-of-plane” for those perpendicular to the HP.

Needless to say that, as usual, we assume P_i to be fixed relative to the hub and the airframe.

The total moment at P_i is exerted on the hub.

9.9 Moments transmitted by the blades to the hub

In-plane moment

The in-plane moment at P_i is the result of the in-plane moments and the out-of-plane forces at the hinge.

According to Prouty (Ref 9.4), the in-plane moment can be assumed to be the result of only two actions: the out-of-plane component of the centrifugal force acting at the hinge offset and the in-plane components of the torque \mathbf{Q} (see sub-section 9.12). To these, we have to add the moment created by the spring k_β , because the model used by Prouty does not include a spring.

There is still another torque, that around the longitudinal axis of the blade. This torque will be non-zero and, since it is applied on an axis perpendicular to that of the hinge, it

will be transmitted to the hub. Nevertheless, this torque will be ignored. For further details about the torque around the longitudinal axis of the blade, see sub-section 9.19.

Prouty gives the following expression for the out-of-plane component of the centrifugal force acting at the hinge:

$$\Omega^2(\beta - a_0) \frac{M_b}{g} \quad (9.13)$$

Where M_b is the first static moment due to the weight force:

$$M_b = \int_0^{R-e} r g dm = m_b g r_{Gb} \quad (9.14)$$

(This r is the longitudinal coordinate of a blade element and should not be confused with the yaw rate of the airframe).

Therefore the moment produced at P_i , by the out-of-plane component of the centrifugal force:

$$e \Omega^2(\beta - a_0) \frac{M_b}{g} \quad (9.15)$$

If we consider the total effect of the b blades and project the resulting moment in $P_i x_w y_w z_w$ we get that the average in-plane moments in one turn are (after adding the contribution of \mathbf{Q} and that of the spring):

$$(m_x)_{hub} = \pm \left(\frac{1}{2} b e \Omega^2 \frac{M_b}{g} + k_\beta \right) b_{ls} + m_x \quad (9.16)$$

$$(m_y)_{hub} = \left(\frac{1}{2} b e \Omega^2 \frac{M_b}{g} + k_\beta \right) a_{ls} + m_y \quad (9.17)$$

Where m_x, m_y are the in-plane components of \mathbf{Q} , and \pm accounts for the direction of turn of the rotors (+ when counter clockwise, – if contrary).

If we want to project in body axes:

$$(M_x)_{hub} = (m_x)_{hub} \cos \beta_{ss} - (m_y)_{hub} \sin \beta_{ss} \quad (9.18)$$

$$(M_y)_{hub} = (m_y)_{hub} \cos \beta_{ss} + (m_x)_{hub} \sin \beta_{ss} \quad (9.19)$$

If the rotor is in axial flight or in hover then β_{ss} is not defined. But in this case $a_{1s} = b_{1s} = 0$. It will be seen that this implies that $m_x = m_y = 0$, according to (9.34) and (9.35). Hence, considering (9.16) and (9.17), it will be $(m_x)_{hub} = (m_y)_{hub} = 0$.

Out-of-plane moment

The out-of-plane moment at P_i is the result of the out-of-plane moments and the in-plane forces at the hinge. We will designate it $(M_z)_{hub}$.

9.10 Calculation of the derivative of the total angular momentum of the blades

The equation of moments of the b-blades system:

$$M_x \mathbf{i} + M_y \mathbf{j} + M_z \mathbf{k} - (M_x)_{hub} \mathbf{i} - (M_y)_{hub} \mathbf{j} - (M_z)_{hub} \mathbf{k} = \left(\frac{d}{dt} \mathbf{H}_{Pi} \right)_{mean} \quad (9.20)$$

Where we have seen that M_x, M_y, M_z are the moments exerted by the airflow over the b-blades system, whereas $(M_x)_{hub}, (M_y)_{hub}, (M_z)_{hub}$ are those exerted by the b-blades system over the hub.

The out-of-plane component of the derivative can be easily obtained if we neglect the flapping. This enables us to use a procedure completely analogous to that followed for the hub and the armature (see Section 4). Then:

$$\left(\frac{d}{dt} \mathbf{H}_{Pi} \right)_{mean} \cdot \mathbf{k} \approx bI_{zb} (\dot{r}_w - \dot{\Omega}) \quad (9.21)$$

And so:

$$(M_z)_{hub} = M_z - bI_{zb} (\dot{r}_w - \dot{\Omega}) \quad (9.22)$$

The in-plane components of the derivative cannot be calculated directly because in this case we cannot neglect the flapping, since its influence is now important. But we don't need to calculate them. The only thing we need, as it will be shown in Section 14, is eq (9.20), re-ordered as follows:

$$\mathbf{M}^{Pi} - \left(\frac{d}{dt} \mathbf{H}_{Pi} \right)_{mean} = (M_x)_{hub} \mathbf{i} + (M_y)_{hub} \mathbf{j} + (M_z)_{hub} \mathbf{k} \quad (9.23)$$

Where $\mathbf{M}^{Pi} = M_x \mathbf{i} + M_y \mathbf{j} + M_z \mathbf{k}$.

$(M_x)_{hub}, (M_y)_{hub}, (M_z)_{hub}$ are given by (9.18), (9.19) and (9.22), respectively.

AERODYNAMIC FORCES AND MOMENTS

9.11 Blade Element Theory

In order to model the aerodynamic forces and moments over the blade, Blade Element Theory (BET) will be used. This theory considers, as its name suggests, a blade element subjected to the following forces and moments:

$$dL = \frac{1}{2} \rho c U_R^2 c_l dr \quad (9.24) \quad \text{Lift (perpendicular to the velocity)}$$

$$dD = \frac{1}{2} \rho c U_R^2 c_d dr \quad (9.25) \quad \text{Drag (opposite to the velocity)}$$

$$dM_{ac} = \frac{1}{2} \rho c^2 U_R^2 c_{mac} dr \quad (9.26) \quad \text{Moment at the aerodynamic centre}$$

Usually, instead of dL, dD it is better to work with dT, dF_T , where:

$$\begin{aligned} dT &\approx dL \\ dF_T &\approx dD - \phi dL \end{aligned}$$

Where ϕ is the angle between the air velocity vector and the HP and is assumed to be small. ϕ should not be confused with the roll angle of the airframe.

Where U_R is the modulus of the air velocity vector seen by the blade element. This velocity can be separated into two components, U_p , and U_T .

The idea behind BET is that the total force and torque produced by the rotor can be calculated by integrating dT, dF_T, dM_{ac} across r for each blade. Although it has some important limitations compared to other theories, BET continues to be the most widely accepted method to calculate the total force and torque in a fast and easy way. Hence, it will be used here too.

It should be remembered that it has been decided to ignore the torque around the longitudinal axis of the blade (see sub-section 9.9). Therefore dM_{ac} will not be used, except in sub-section 9.19.

According to Prouty (Ref 9.4):

$$U_T = \Omega R \left(\frac{r+e}{R} + \mu \sin \psi \right) \quad (9.27)$$

$$U_p = \Omega R \left(\begin{array}{l} -\lambda_z - \lambda_{ind} \left(1 + K_c \frac{r}{R} \cos \psi \right) - \frac{r}{R} (a_{1s} \sin \psi - b_{1s} \cos \psi) - \\ -\mu (a_0 - a_{1s} \cos \psi - b_{1s} \sin \psi) \cos \psi \end{array} \right) + (r+e)(q_w \cos \psi + p_w \sin \psi) \quad (9.28)$$

$$U_R \approx U_T \quad (9.30)$$

Where:

r is the longitudinal coordinate of the blade element (not to be confused with the yaw angular rate of the airframe)

e is the hinge offset

R is the rotor radius, from the axis of the hub to the tip of the blade

$\mu = \frac{V_x}{|\Omega|R}$ is the horizontal speed to tip speed ratio

$\lambda_z = \frac{V_z}{|\Omega|R}$ is the vertical speed to tip speed ratio

$\lambda_{ind} = \frac{v_{ind}}{|\Omega|R}$, where v_{ind} is the induced velocity

It should be remembered that Ω is positive when the rotor turns counter clockwise and negative in the other case.

It should be noted that (9.28) takes into account the blade flapping and the effect of the angular rates of the hub, p_w and q_w . The induced flow (see Section 10) is represented using Glauert's model. In this model, the local induced velocity is $v_{ind} \left(1 + \frac{r}{R} K_c \cos \psi \right)$.

The nature of λ_{ind} and the way to estimate it will be the subject of an entire Section (Section 10). For the moment, it will be enough to know that it is a function of λ_z and μ .

The above model produces accurate results when the rotor is in forward flight ($V_x \neq 0$) but its application in hover or axial flight (that is, when $V_x = 0$) is problematic, because ψ is not defined in that case.

9.12 Definition of the aerodynamic forces and moments

In Section 4 \mathbf{F}_i and \mathbf{M}^{Pi} were defined. \mathbf{F}_i was the resultant of the forces exerted by the airflow on the system composed by the b blades, while \mathbf{M}^{Pi} was the resultant of the moments exerted by the airflow over the b-blades system. \mathbf{F}_i and \mathbf{M}^{Pi} were applied at P_i , that is, the centre of mass of the system composed by the b blades.

Basing on Prouty (Ref 9.4), we can model \mathbf{F}_i as the sum of two orthogonal forces (see Figure 9.6):

- The thrust \mathbf{T} , which is assumed to be perpendicular to the TPP
- A horizontal force \mathbf{H} , which is contained in the TPP

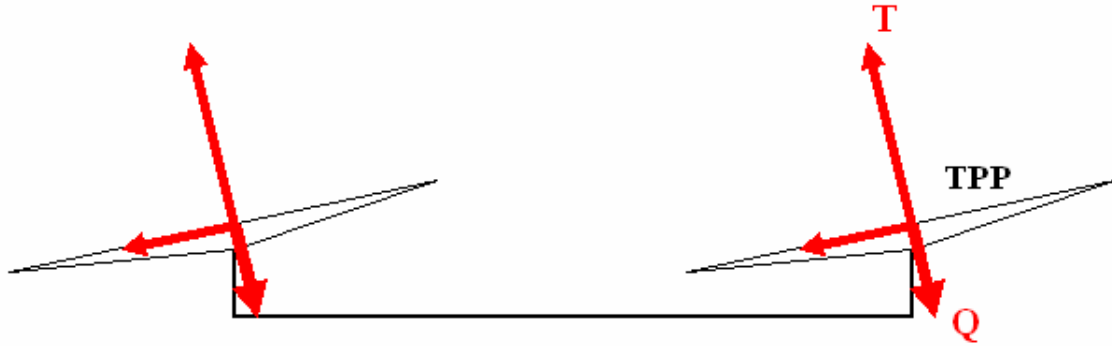


Fig 9.6 Lateral view of the quadrotor. The thrust \mathbf{T} and the torque vector \mathbf{Q} are perpendicular to the Tip Path Plane (TPP). The force \mathbf{H} is parallel to it

As for \mathbf{M}^{Pi} , and basing also on Prouty, we can model it as a torque \mathbf{Q} perpendicular to the Tip Path Plane (see Figure 9.6). It should be noted that while \mathbf{T} and \mathbf{H} have always the same orientation, regardless of the way in which the blades turn, \mathbf{Q} will point downwards if the blades turn counter clockwise and upwards in the other case.

If we want to project in the $P_i x_w y_w z_w$ axes:

$$f_x = H \cos a_{1s} + \frac{T \tan a_{1s}}{\sqrt{1 + \tan^2 a_{1s} + \tan^2(\pm b_{1s})}} \quad (9.31)$$

$$f_y = \frac{T \tan(\pm b_{1s})}{\sqrt{1 + \tan^2 a_{1s} + \tan^2(\pm b_{1s})}} \quad (9.32)$$

$$f_z = -H \sin a_{1s} + \frac{T}{\sqrt{1 + \tan^2 a_{1s} + \tan^2(\pm b_{1s})}} \quad (9.33)$$

$$m_x = -\frac{\pm Q \tan a_{1s}}{\sqrt{1 + \tan^2 a_{1s} + \tan^2(\pm b_{1s})}} \quad (9.34)$$

$$m_y = \frac{\pm Q \tan(\pm b_{1s})}{\sqrt{1 + \tan^2 a_{1s} + \tan^2(\pm b_{1s})}} \quad (9.35)$$

$$m_z = M_z = \frac{\pm Q}{\sqrt{1 + \tan^2 a_{1s} + \tan^2(\pm b_{1s})}} \quad (9.36)$$

Where $Q = |\mathbf{Q}|$, $H = |\mathbf{H}|$ and $T = |\mathbf{T}|$.

+ is chosen when the rotor turns counter clockwise, and – when it does it clockwise.

Coefficients

It is useful to define the following coefficients, following the standard notation:

$$\begin{aligned} C_T &= \frac{T}{\rho \pi R^4 \Omega^2} \\ C_H &= \frac{H}{\rho \pi R^4 \Omega^2} \\ C_Q &= \frac{Q}{\rho \pi R^5 \Omega^2} \end{aligned} \quad (9.37)$$

The coefficients C_{fx}, C_{fy}, C_{fz} and C_{mx}, C_{my}, C_{mz} are defined in a totally analogous way.

9.13 Calculation of the aerodynamic forces and moments

As it has been anticipated, BET can be used to calculate T, H, Q . This has already been done by Prouty (Ref 9.4). But before using his results we have to consider an important issue. Being rigorous, the integration of dT and dF_T has to start at the root of the blade, that is, at the first point which generates lift and drag. In the real rotor, this point can be assumed to be the joint between the blade and the hub. But the hinge, in the idealised model, is not going to be coincident with the joint. Therefore we will need to consider two different offsets, the one of the joint, e_j , and the one of the hinge, e . The problem is that the expressions obtained by Prouty for C_T, C_H, C_Q assume that both offsets are equal.

So that in order to avoid re-formulating all the expressions we will assume that $e \approx e_j$. Although this introduces some error, this will be much smaller than the one which is going to be introduced by replacing the real blade by an untapered one (see below).

The expressions given by Prouty, with some slight changes:

$$\frac{4C_T}{a\sigma} = \left(1 - \frac{e}{R}\right) \left(\left(\frac{2}{3} + \mu^2\right) \theta_0 + \frac{1}{2}(1 + \mu^2) \theta_1 - \mu B_1 - \lambda_z - \lambda_{ind} \right) \quad (9.38)$$

$$\begin{aligned} \frac{4C_H}{a\sigma} = & \frac{c_d}{a} \mu - \mu \frac{-\lambda_z - \lambda_{ind} + \mu a_{1s}}{1 + \frac{3}{2}\mu^2} \left(\theta_0 \left(-\frac{1}{3} + \frac{3}{2}\mu^2 \right) + \frac{\theta_1}{2} \left(-1 + \frac{3}{2}\mu^2 \right) + \lambda_z + \lambda_{ind} - \mu a_{1s} \right) + \\ & + \frac{\mu}{1 + \frac{1}{2}\mu^2} \left(\frac{a_0^2}{2} \left(\frac{1}{9} + \frac{\mu^2}{2} \right) + \frac{1}{3} \mu a_0 \lambda_{ind} + \frac{1}{8} \lambda_{ind}^2 \right) \end{aligned} \quad (9.39)$$

$$\begin{aligned} \frac{4C_Q}{a\sigma} = & \frac{1}{2} \frac{c_d}{a} (1 + \mu^2) - \\ & - \frac{-\lambda_z - \lambda_{ind} + \mu a_{1s}}{1 + \frac{3}{2}\mu^2} \left(\frac{\theta_0}{3} (2 - \mu^2) + \frac{\theta_1}{2} \left(1 - \frac{\mu^2}{2} \right) + \left(1 + \frac{\mu^2}{2} \right) (-\lambda_z - \lambda_{ind} + \mu a_{1s}) \right) - \\ & - \frac{\mu^2}{1 + \frac{\mu^2}{2}} \left(\frac{a_0^2}{2} \left(\frac{1}{9} + \frac{\mu^2}{2} \right) + \frac{1}{3} \mu a_0 \lambda_{ind} + \frac{1}{8} \lambda_{ind}^2 \right) \end{aligned} \quad (9.40)$$

Where σ is the rotor solidity, that is $\sigma = \frac{bc}{\pi R}$. c is the “mean” chord (see Section 13).

To arrive to the expressions above, the following hypotheses have been made:

- Lift coefficient linear with the angle of attack (slope a) and free of stall, compressibility and hysteretical effects. a identical for all the blade sections.
- Constant drag coefficient c_d
- Reverse flow region negligible (see sub-section 9.20)
- Small angle assumptions
- Constant chord (untapered blade)

It has also been considered that $e \ll R$, in order to make the expressions above more simple.

Before it was explained that in hover or in axial flight ($\mu=0$) it is $a_{1s}=b_{1s}=0$. Therefore, according to eqs (9.31) to (9.35), it will be $f_x=H$ and $f_y=m_x=m_y=0$. Besides, if we examine closely (9.39) we will see that when $\mu=0$, it is $C_H=0$ (and therefore $H=0$). Hence, f_x will also be zero in hover or axial flight.

Three term drag polar

It will be seen that the hypothesis of constant drag coefficient leads to inaccurate results, specially for C_Q when $\lambda_z < 0$. Because of this, it is convenient to eliminate this hypothesis and assume instead that the drag polar of the aerofoil can be approximated by a quadratic curve (“three term drag polar”):

$$c_d = c_{d0} + c_{d1}\alpha + c_{d2}\alpha^2 \quad (9.41)$$

The expressions of C_H and C_Q are now, according to Prouty (Ref 9.4):

$$\begin{aligned} \frac{4C_Q}{a\sigma} &= \frac{1}{2} \frac{c_{d0}}{a} (1 + \mu^2) + \\ &+ \frac{1}{1 + \frac{3}{2}\mu^2} \frac{c_{d1}}{a} \left[\theta_0 \left(\frac{1}{2} - \frac{19}{36}\mu^2 + \frac{3}{4}\mu^4 \right) + \theta_1 \left(\frac{2}{5} - \frac{2}{5}\mu^2 + \frac{\mu^4}{2} \right) + (-\lambda_z + \mu a_{1s} - \lambda_{ind}) \left(\frac{2}{3} - \frac{\mu^2}{3} \right) \right] + \\ &+ \frac{1}{\left(1 + \frac{3}{2}\mu^2 \right)^2} \frac{c_{d2}}{a} \left[\theta_0^2 \left(\frac{1}{2} + \frac{2}{9}\mu^2 - \frac{\mu^4}{24} + \frac{9}{8}\mu^6 \right) + \theta_1^2 \left(\frac{1}{3} + \frac{\mu^2}{4} + \frac{9}{16}\mu^6 \right) + \right. \\ &\quad \left. + (-\lambda_z + \mu a_{1s} - \lambda_{ind})^2 \left(1 + 2\mu^2 + \frac{3}{4}\mu^4 \right) + \right. \\ &\quad \left. + \theta_0 \theta_1 \left(\frac{4}{5} + \frac{2}{5}\mu^2 - \frac{\mu^4}{5} + \frac{3}{2}\mu^6 \right) + \right. \\ &\quad \left. + \theta_0 (-\lambda_z + \mu a_{1s} - \lambda_{ind}) \left(\frac{4}{3} + \frac{4}{3}\mu^2 - \mu^4 \right) + \right. \\ &\quad \left. + \theta_1 (-\lambda_z + \mu a_{1s} - \lambda_{ind}) \left(1 + \mu^2 - \frac{3}{4}\mu^4 \right) \right] + \\ &+ \frac{\mu^2}{\left(1 + \frac{1}{2}\mu^2 \right)^2} \frac{c_{d2}}{a} \left[a_0^2 \left(\frac{1}{18} + \frac{\mu^2}{6} - \frac{\mu^4}{8} \right) + \lambda_{ind}^2 \left(\frac{1}{8} + \frac{\mu^2}{16} \right) + a_0 \lambda_{ind} \left(\frac{\mu}{3} + \frac{\mu^3}{6} \right) \right] \end{aligned} \quad (9.42)$$

$$\begin{aligned}
\frac{4C_H}{a\sigma} = & \frac{c_{d0}}{a} \mu + \frac{\mu}{1 + \frac{3}{2}\mu^2} \frac{c_{d1}}{a} \left(\theta_0 \left(\frac{1}{9} - \frac{\mu^2}{2} \right) - \frac{1}{2} \theta_1 \mu^2 + \frac{1}{3} (-\lambda_z + \mu a_{1s} - \lambda_{ind}) \right) + \\
& + \frac{\mu}{\left(1 + \frac{3}{2}\mu^2 \right)^2} \frac{c_{d2}}{a} \left(\theta_0^2 \left(-\frac{7}{9} + \frac{5}{3}\mu^2 - \frac{15}{4}\mu^4 \right) + \theta_1^2 \left(-\frac{1}{2} + \frac{3}{2}\mu^2 - \frac{9}{8}\mu^4 \right) - \right. \\
& \left. - 2(-\lambda_z + \mu a_{1s} - \lambda_{ind})^2 + \theta_0 \theta_1 \left(-\frac{4}{3} + 3\mu^2 - \frac{9}{2}\mu^4 \right) + \right. \\
& \left. + \theta_0 (-\lambda_z + \mu a_{1s} - \lambda_{ind}) (-2 + 5\mu^2) + \right. \\
& \left. + \theta_1 (-\lambda_z + \mu a_{1s} - \lambda_{ind}) (-2 + 3\mu^2) \right) - \\
& - \frac{\mu^3}{\left(1 + \frac{1}{2}\mu^2 \right)^2} \frac{c_{d2}}{a} \left(\left(\frac{2}{9}\mu + \frac{\mu^3}{3} \right) a_0^2 + \frac{\mu}{8} \lambda_{ind}^2 + \left(\frac{1}{6} + \frac{5}{12}\mu^2 \right) a_0 \lambda_{ind} \right)
\end{aligned}
\tag{9.43}$$

Where it has been considered that $e \ll R$, in order to make the expressions above more simple.

9.14 Calculation of the coning and flapping angles

The expressions for C_T , C_H and C_Q cannot be evaluated without the values of a_0, a_{1s}, b_{1s} . Besides, the flapping angles (a_{1s} and b_{1s}) are needed to obtain f_x, f_y, f_z and m_x, m_y, m_z from T and H . And h , the distance between O_i and P_i , cannot be calculated without the coning angle (a_0). Therefore it is essential to obtain these angles. In order to do so we just have to consider that these angles are the result of the balance of torques around the hinge.

These torques are those exerted on the blade, as seen from a frame of reference attached to it. Since this frame is non-inertial, “inertial” torques will have to be considered (e.g. gyroscopic torques or those resulting from the centrifugal forces).

Balance of torques around the hinge

As before, we will assume $e \approx e_j$, so that I_{yb} and M_b are calculated at the joint between the blade and the hub.

According to Prouty (Ref 9.4), the torques around the hinge that have to be considered are the result of the aerodynamic, centrifugal and weight forces. The gyroscopic moments also have to be included.

The moment at the hinge due to the aerodynamic forces is $\int_0^{R-e} r dT$. When evaluating dT , Prouty includes the influence of the hub angular rates p_w and q_w through U_R , as shown in (9.28).

The moment due to the weight force is $M_b = \int_0^{R-e} r g dm$, which has already appeared in sub-section 9.9. However, this will not be included in our balance of torques since we define β so that it is zero when the blade is stopped. Therefore that moment gets cancelled with that created by the spring.

Each blade station (b.s.) is subjected to an inertial force $d\mathbf{F}_{\text{inertia}} = -dm\mathbf{a}_{\text{bs}}$ which will produce a torque at the hinge. The exact expression that governs \mathbf{a}_{bs} is very complex due to the complex kinematics of the blade (even if feathering and lagging are ignored) and the fact that the hub to which the blade is attached has its own linear and angular velocity relative to the ground. Padfield (Ref 9.2) gives a simplified expression for \mathbf{a}_{bs} which is still fairly complex. On the other hand, Prouty considers that the moment at the hinge due to the inertial forces is the sum of a gyroscopic moment and an additional moment produced by the component of the centrifugal force parallel to the HP. This implies ignoring many of the terms included in Padfield's expression of \mathbf{a}_{bs} . Notably, it implies neglecting the terms with \dot{p}_w, \dot{q}_w and those with $\dot{\Omega}$ or, in other words, it implies assuming that both Ω and the angular rates p_w and q_w are constant.

However, it is arguable that those ignored terms will have a great influence on the final values of a_0, a_{1s}, b_{1s} that emerge from the balance of torques. Therefore here we will accept as valid the simplifications made by Prouty.

Expressions for the coning and flapping angles

The balance of torques around the hinge will be represented by an equation with constant, sine and cosine terms (in ψ). This equation can then be broken down into three different equations. Using matrix notation:

$$(\mathbf{M} + \mathbf{M}_{\text{pq}}) \cdot \begin{bmatrix} a_0 \\ a_{1s} \\ b_{1s} \end{bmatrix} = \mathbf{F} + \mathbf{F}_{\text{pq}} \quad (9.44)$$

Where \mathbf{M} , \mathbf{M}_{pq} , \mathbf{F} and \mathbf{F}_{pq} are shown in pages 98 and 99.

The term k_β does not appear in the equations obtained by Prouty, since he did not include a spring.

As when calculating C_T , the following has been assumed:

- Lift coefficient linear with the angle of attack (slope a) and free of stall, compressibility and hysteretical effects. a identical for all the blade sections.
- Reverse flow region negligible (see sub-section 9.20)
- Small angle assumptions
- Constant chord (untapered blade)

It should be noted that the term K_c does not appear explicitly in the formula developed by Prouty, because he directly assumes $K_c = 1$. It will be seen immediately that K_c has an important influence on the flapping angles, particularly on b_{1s} .

While p_w and q_w have been considered when calculating $\int_0^{R-e} r dT$, they were ignored when calculating C_T, C_H, C_Q . This is an important inconsistency that should not be very difficult to eliminate. Nevertheless, it will be left as it is, among other reasons because an expression of C_T which includes p_w and q_w will complicate the task of obtaining the induced velocity (see Sections 10 and 14).

$$\mathbf{M} = \begin{bmatrix} -\Omega^2 \left(I_{yb} + e \frac{M_b}{g} \right) - k_\beta & \frac{1}{2} \mathcal{H}_{yb} \Omega^2 \left(1 - \frac{e}{R} \right)^2 \frac{\mu e}{4 R} & 0 \\ 0 & -\frac{1}{2} \mathcal{H}_{yb} \Omega^2 \left(1 - \frac{e}{R} \right)^2 \left[\frac{1}{4} - \frac{\mu^2}{8} - \frac{1}{6} \frac{e}{R} - \frac{1}{12} \left(\frac{e}{R} \right)^2 \right] & \Omega^2 e \frac{M_b}{g} + k_\beta \\ -\frac{1}{2} \mathcal{H}_{yb} \Omega^2 \left(1 - \frac{e}{R} \right)^2 \left[\frac{1}{3} + \frac{1}{6} \frac{e}{R} \right] \mu & \Omega^2 e \frac{M_b}{g} + k_\beta & \frac{1}{2} \mathcal{H}_{yb} \Omega^2 \left(1 - \frac{e}{R} \right)^2 \left[\frac{1}{4} + \frac{\mu^2}{8} - \frac{1}{6} \frac{e}{R} - \frac{1}{12} \left(\frac{e}{R} \right)^2 \right] \end{bmatrix} \quad (9.45)$$

$$\mathbf{F} = \begin{bmatrix} -\frac{1}{2} \mathcal{H}_{yb} \Omega^2 \left(1 - \frac{e}{R} \right)^2 \left\{ \frac{\theta_0}{4} \left[1 + \mu^2 + \frac{2}{3} \frac{e}{R} + \frac{1}{3} \left(\frac{e}{R} \right)^2 \right] + \theta_1 \left[\frac{1}{5} + \frac{\mu^2}{6} \left(1 - \frac{e}{R} \right) - \frac{1}{10} \frac{e}{R} - \frac{1}{15} \left(\frac{e}{R} \right)^2 - \frac{1}{30} \left(\frac{e}{R} \right)^3 \right] - (\lambda_z + \lambda_{ind}) \left(\frac{1}{3} + \frac{1}{6} \frac{e}{R} \right) - B_1 \mu \left(\frac{1}{3} + \frac{1}{6} \frac{e}{R} \right) \right\} \\ -\frac{1}{2} \mathcal{H}_{yb} \Omega^2 \left(1 - \frac{e}{R} \right)^2 \left\{ 2\theta_0 \mu \left[\frac{1}{3} + \frac{1}{6} \frac{e}{R} \right] + 2\theta_1 \mu \left[\frac{1}{4} - \frac{1}{6} \frac{e}{R} - \frac{1}{12} \left(\frac{e}{R} \right)^2 \right] - B_1 \left[\frac{1}{4} + \frac{3}{8} \mu^2 + \frac{1}{6} \frac{e}{R} + \frac{1}{12} \left(\frac{e}{R} \right)^2 \right] - \frac{\mu}{2} (\lambda_z + \lambda_{ind}) \right\} \\ -\frac{1}{2} \mathcal{H}_{yb} \Omega^2 \left(1 - \frac{e}{R} \right)^2 \left\{ -A_1 \left[\frac{1}{4} + \frac{\mu^2}{8} + \frac{1}{6} \frac{e}{R} + \frac{1}{12} \left(\frac{e}{R} \right)^2 \right] - K_c \lambda_{ind} \left[\frac{1}{4} - \frac{1}{6} \frac{e}{R} - \frac{1}{12} \left(\frac{e}{R} \right)^2 \right] \right\} \end{bmatrix} \quad (9.46)$$

$$\mathbf{M}_{pq} = \begin{bmatrix} 0 & 0 & 0 \\ 0 & -\frac{1}{8}\mathcal{I}_{yb}\Omega^2\left(1-\frac{e}{R}\right)^2\left(1-\frac{\mu^2}{2}\right) & \Omega^2 e \frac{M_b}{g} + k_\beta \\ 0 & \Omega^2 e \frac{M_b}{g} + k_\beta & \frac{1}{8}\mathcal{I}_{yb}\Omega^2\left(1-\frac{e}{R}\right)^2\left(1+\frac{\mu^2}{2}\right) \end{bmatrix} \quad (9.47)$$

$$\mathbf{F}_{pq} = \begin{bmatrix} 0 \\ -\frac{1}{8}\mathcal{I}_{yb}\Omega^2\left(1-\frac{e}{R}\right)^2 \frac{p_w}{\Omega} + 2q_w\Omega I_{yb} \\ -\frac{1}{8}\mathcal{I}_{yb}\Omega^2\left(1-\frac{e}{R}\right)^2 \frac{q_w}{\Omega} - 2p_w\Omega I_{yb} \end{bmatrix} \quad (9.48)$$

Where:

I_{yb} is the inertia of the blade around the hinge

$\gamma = \frac{\rho ac R^4}{I_{yb}}$ is the Lock number.

\mathbf{M}_{pq} and \mathbf{F}_{pq} are the extra terms that appear when the pitch and roll velocities are considered.

Comparison between the theoretical and experimental results

It has been indicated that when $\mu=0$ (that is, in hover and in axial flight) it is $a_{1s}=b_{1s}=0$. This is obvious if we consider the axial-symmetry of the airflow and is supported by empirical evidence (see Section 13). However, if we carefully examine expressions (9.44) to (9.48) we will see that, due to the presence of the term $K_c \lambda_i$, a_{1s} and b_{1s} are not zero when $\mu=0$. The term $K_c \lambda_i$ appears as a result of considering a non-uniform induced flow (see sub-section 9.11). If $K_c=0$ then the induced flow is uniform and $a_{1s}=b_{1s}=0$ for $\mu=0$. The disadvantage is that for $\mu>0$ we will have a large error in b_{1s} . The error will be much smaller for a_{1s} though, since in this case the term $K_c \lambda_i$ is multiplied by $\frac{e}{R}$ which is much smaller than 1.

According to Prouty (Ref 9.4) the uniform inflow assumption ($K_c=0$) fails to predict the real b_{1s} when μ is different from zero. For very low values of μ , though, this error is small. On the other hand, the $K_c=1$ assumption is good for high values of μ (especially above 0.2), but incorrect for $\mu=0$ as we have said.

The most obvious solution is to make K_c vary with μ , so that for $\mu=0$ it is $K_c=0$ whereas for $\mu>0$ it tends to 1 (or a similar value that provides a better correlation with experimental results). This was pioneered by Harris (Ref 9.7).

In Section 13 it will be seen that, finally, it was decided to assume $K_c=0$ when calculating a_{1s}, b_{1s} and $K_c=1$ when calculating C_T, C_H, C_Q . Although this approach is theoretically inconsistent, in practice it leads to acceptable results both for a_{1s}, b_{1s} and C_T, C_H, C_Q .

Influence of the direction of turn of the blades

The mathematical formulation used by Prouty for C_T, C_H, C_Q and a_0, a_{1s}, b_{1s} was developed for a rotor turning counter clockwise. However, provided that the direction of the azimuthal angle ψ is the same as the direction of rotation of the blade, the formulation is perfectly valid for clockwise rotors too. We only have to be careful when obtaining the forces and moments in Px_w, y_w, z_w axes. This is shown in expressions (9.16), (9.17) and (9.31) to (9.36), where the sign of each magnitude is carefully chosen so that the forces and torques have the appropriate direction.

9.15 Justification of the need for wind tunnel testing

Although the rotor model that has been developed here is entirely theoretical, experimental data are still required, for two reasons. Firstly, the model uses some

parameters whose value can only be inferred from experimental data. These are: $a, c_{d0}, c_{d1}, c_{d2}$. Secondly, the rotor model needs to be validated, and this can only be done by comparing simulation results with the real ones. In Section 13 it will be seen that, in fact, to improve the correlation between the simulation results and the experimental data, we can multiply the induced velocity ratio λ_{ind} by a corrective factor $\kappa(\lambda_z)$.

The experimental data can only be obtained in the wind tunnel; therefore it is necessary to carry out a well-planned sequence of wind tunnel tests. Section 12 will explain how these tests were conducted and Section 13 will be devoted to the analysis of the data which were obtained.

ESTIMATION OF THE EFFECTIVE HINGE OFFSET

9.16 Estimation of the flapping frequency ratio

Until now, we have referred in many occasions to the hinge offset e of our idealized model of the rotor, but without explaining how to calculate it. This will be the purpose of this sub-sections. We will refer to the hinge offset of our idealized model as the “effective hinge offset”.

Before we continue, it is important to define the frequency ratio λ .

The flapping motion of a real blade is governed by a partial differential equation (PDE) which results from the equilibrium of forces and moments in a differential element of the blade (Ref 9.2, page 239). There are infinite solutions to this equation called “modes”. Each mode represents a different shape in which the blade bends. There is a frequency associated to each of these modes. The frequency ratio λ results from dividing this frequency by Ω .

If there is a hinge and it has no offset ($e = 0$), then the first mode frequency ratio is $\lambda_1 = 1$ and the blade shape is a straight line. $\lambda_1 = 1$ means that the rotor is in resonance, because the flapping frequency and the rotational frequency are equal. If $e \neq 0$ or if there is no hinge, λ_1 will be slightly bigger than 1.

Bramwell (Ref 9.2) suggest using the “equation of Southwell” to estimate λ_1 in terms of the non-rotating natural frequency ω_{nr} of the blade:

$$\lambda_1^2 = \alpha_1 + \left(\frac{\omega_{nr}}{\Omega} \right)^2 \quad (9.49)$$

Where α_1 is the first Southwell’s coefficient. This coefficient can be calculated using the following formula (Ref 9.8):

$$\alpha_1 = k_{0,1} + \frac{\tilde{e}}{R} k_{1,1} \quad (9.50)$$

According to Ref 9.8, in a hingeless blade:

$$k_{0,1} = 1.19 \quad k_{1,1} = 1.57$$

According to Ref 9.8, \tilde{e} is the offset of the hinge or, in a hingeless blade, the offset of the “point of fixity”. In the blade of the XPro the point of fixity is at the joint between the blade and the hub. The offset of this joint was e_j . Therefore, entering with $e_j = 0.026m$ in (9.50) we obtain:

$$\alpha_1 = 1.35$$

There are several ways to estimate ω_{nr} , as it will be shown later.

9.17 Estimation of the hinge offset

According to Ref 9.3, and using the notation of this Section:

$$\lambda_1 = \sqrt{1 + \frac{m_b r_{Gb} e}{I_{yb}} + \frac{k_\beta}{I_{yb} \Omega^2}} \quad (9.51)$$

Taking into account that $M_b = m_b g r_{Gb}$, we finally obtain:

$$\frac{e}{R} = \frac{\lambda_1^2 - 1 - \frac{k_\beta}{I_{yb} \Omega^2}}{\frac{M_b R}{g I_{yb}}} \quad (9.52)$$

I_{yb} and M_b will depend on e . As before, we may assume $e \approx e_j$ so that they both are calculated at the joint between the blade and the hub. This way we avoid having to calculate I_{yb} and M_b at e , which is not trivial because e has not been determined yet.

We can also assume that:

$$k_\beta = I_{yb} \omega_{nr}^2 \quad (9.53)$$

If we do so, (9.52) turns into:

$$\frac{e}{R} = \frac{\alpha_1 - 1}{\frac{M_b R}{g I_{yb}}} \quad (9.54)$$

Where (9.49) has been taken into account.

It can be seen that, provided that (9.53) is valid, e will be fixed, it will not depend on Ω . This is a great advantage because it simplifies the mathematical formulation and, more important, because large variations of Ω now do not lead to large, unrealistic, variations of the effective hinge offset.

9.18 Experimental results

(9.49) and (9.52) require a series of parameters to be estimated.

To estimate k_β , several vertical loads were applied at the tip of the blade and the resulting tip deflection for each load was measured. If we define the ratio between the tip deflection and the length of the blade as $\sin \delta$ then we can obtain k_β by dividing the moment at the root by δ . This way:

$$k_\beta = 2.524 Nm$$

To estimate M_b it was taken into account that $M_b = m_b g r_{Gb}$. The mass of the blade m_b had already been measured and the position of its centre of mass $r_{Gb} = 0.111m$ was obtained from the CAD model. It should be noted that the CAD version of the blade had a simplified geometry: the planform was identical to the real one but the blade was planar instead of having camber and twist. However, it was assumed that the camber and twist would not modify r_{Gb} . With $r_{Gb} = 0.111m$:

$$M_b = 14.156 mNm$$

It is interesting to compare this value with the one that results from assuming uniform mass distribution:

$$M_b = 14.793 mNm$$

The CAD model was also used to obtain I_{yb} . Again, it was assumed that the camber and the twist would not affect its value. Hence:

$$I_{yb} = 0.211 mNm^2$$

Again, it is interesting to compare this value with the one obtained assuming uniform mass distribution:

$$I_{yb} = 0.233mNm^2$$

It can be seen that the hypothesis of uniform mass distribution is acceptable for the calculation of M_b and I_{yb} .

ω_{nr} can be obtained by taking into account that $k_\beta = I_{yb}\omega_{nr}^2$ and using the I_{yb} previously calculated. In this case we get:

$$\omega_{nr} = 109 \text{ rad/s}$$

It would be interesting to measure ω_{nr} directly. To do so, the blade would be bent and then released. The frequency of the resulting oscillations would be measured somehow, for example by filming the blade with a low speed camera and then analyzing the recorded images. Another proposed method was to measure the frequency of the fluctuations of the in-plane force and/or in-plane moment, and assume it to be equal to ω_{nr} . However, it is not clear whether this is exact.

REFINEMENTS OF THE MODEL

9.19 Feathering

The model described in this Section has considered that the pitch angle is constant. However, this does not occur in reality. Due to the blade torsional flexibility, the pitch angle will be able to vary cyclically. These cyclic variations are produced by the torques acting around the elastic axis of the blade (the elastic axis needs not be perfectly parallel to the longitudinal axis of the blade).

The importance of these cyclic variations lies in the fact that they are going to modify the coning and flapping angles, thus altering the system of forces and moments exerted on the hub.

Although it is not completely right, these cyclic variations can be assumed to be governed by the same first order trigonometric expression valid for conventional helicopters with swashplate (Ref 9.2), that is:

$$\theta = \theta_0 + \theta_1 \frac{r}{R} - A_1 \cos \psi - B_1 \sin \psi \quad (9.55)$$

This implies, among other things, that the cyclic pitch will be the same in every blade station $(-A_1 \cos \psi - B_1 \sin \psi)$.

Among the torques that act around the elastic axis are the aerodynamic and gyroscopic torques. The pitch variation due the gyroscopic torque alone can be of more than a degree (Ref 9.2). On the other hand, the cyclic pitch due to the aerodynamic torque will greatly depend on the distance between the elastic axis and the line of aerodynamic centres. This is clearer if we consider that, for each blade element, the moment dM_{ec} around the elastic centre (the intersection between the elastic axis and the blade element) is given by:

$$dM_{ec} = dM_{ac} - l dL \quad (9.56)$$

Where l is the distance between the aerodynamic centre and the elastic centre, and where dM_{ac} is the moment around the aerodynamic centre. The above expression assumes that the elastic centre is further from the leading edge than the aerodynamic centre. In fact, if the flow is incompressible the aerodynamic centre will be situated at approximately the 25% of the chord (from the leading edge). On the other hand, we can expect the elastic centre to be close to the 50% of the chord (in the vicinity of the centre of mass).

dM_{ac} has the property of being independent of the local angle of attack and so it will remain constant during each revolution of the rotor. If $l \approx 0$, then dM_{ec} will also be constant and thus it will not produce any cyclic pitch.

If dM_{ac}, dM_{ec}, l and the torsional stiffness of the blade were known, it would be possible to obtain θ_0, A_1, B_1 from the balance of torques around the elastic axis in an analogous way as when we obtained a_0, a_{1s}, b_{1s} from the balance of torques around the hinge. Moreover, the author suspects that it would be possible to simulate the effect of the torsional stiffness by giving a certain “offset” to the elastic centre and/or adding a torsional spring, in very much the same manner as it was done with the effective hinge offset and the spring of the blade.

Once θ_0, A_1, B_1 had been calculated, they could be included in the expressions that have been seen in this Section.

However, this procedure has two important problems. Firstly, it might not be possible to uncouple the problem of finding θ_0, A_1, B_1 from the problem of finding a_0, a_{1s}, b_{1s} . However, this problem could be overcome. But what represents a much more serious difficulty is how to determine dM_{ac}, l and the torsional stiffness of the blade. In fact, it is unlikely that these can be estimated theoretically, especially in the case of dM_{ac} .

Since no accurate experimental results are available, the feathering will have to be ignored in our model. Therefore A_1, B_1 will remain zero. As for θ_0 , it will be assumed to be equal to the static pitch angle at the root.

9.20 Reverse Flow Region

The reverse flow region is the part of the rotor disc where $U_T < 0$. In order for this to happen, V_x has to be non-zero (see eq 9.27) Inside this region, the lift force over the blade element is entirely different from outside. A usual approximation is to consider that it has opposite sign, as suggested by Prouty (Ref 9.4). The expressions for $a_0, a_{1s}, b_{1s}, C_T, C_H, C_Q$ have been obtained ignoring the reverse flow region and so they are, to a certain extent, incorrect.

Including the effect of the reverse flow region in a simplified way, as Prouty recommends, is certainly possible, although it complicates significantly the expressions. This additional complexity may not be justified by the improvement in the accuracy of the results, although it would be desirable to check this assertion.

In any case, the reverse flow region will be kept out of our model.

9.21 Tip losses and blade taper

A simple way to model tip losses is to reduce the length of the blade (Ref 9.4). However, determining the adequate length reduction is not straightforward, because it depends on many factors.

On the other hand, it is likely that the effect of blade taper will be of the same order of magnitude as the effect of the tip losses. Therefore, if the latter is modelled the former should be modelled too. Modifying the analytical expressions derived here to include blade taper is possible, although impractical. Probably, it would be better to use other methods based on numerical integration of lift and drag forces across the blade.

Compressibility effects at the tip need not be modelled, contrary to what happens in conventional, full-scale helicopters. With a maximum rotor speed of about 200 rad/s , the highest expected tip speed in the XPro is 50 m/s , or Mach 0.14.

10. INDUCED FLOW MODEL

10.1. Introduction

In order to complete the model of the rotor it is necessary to determine the induced velocity, because it is needed for the expressions derived in the previous Section. These expressions were obtained using Blade Element Theory (BET). However, BET does not give any information about the induced velocity, it is therefore necessary to turn into other theories to determine it.

Johnson (Ref 10.1) gives an excellent summary on the physical explanation of the link between MT and BET or, more exactly, on how the blades generate induced velocity. On the other hand, R.T.N.Chen (Ref 10.2) examines different induced flow models from a historical perspective.

Here will use the model developed by Glauert (Ref 10.3).

10.2 Glauert's inflow model

The expressions for $a_0, a_{1s}, b_{1s}, C_T, C_H, C_Q$ that appear in the previous Section were derived by Prouty using Glauert's Inflow Model (Ref 10.3). A different model could have been used in this Report but that would have required deriving again those expressions. Since Glauert's Model is reasonably accurate, it was decided to keep this model and thus use directly the expressions derived by Prouty. According to this model:

$$(v_{ind})_{local} = v_{ind} \left(1 + \frac{r}{R} K_c \cos \psi \right) \quad (10.1)$$

Where ψ is the azimuthal angle and r is the distance from the blade root to the blade element. v_{ind} is the “average” or “reference” induced velocity, but for the sake of simplicity we will just call it “induced velocity”. K_c is a constant which remains unspecified in the original work by Glauert. According to Coleman *et al* (Ref 10.4), K_c will depend on the wake skew angle. Other authors have proposed different methods of determining it (see Ref 10.2).

According to what was said in Section 9, K_c will have to vary with μ in order to obtain satisfactory predictions of the lateral flapping angle b_{1s} . For relatively high values of μ , above 0.2 (around 100 knots in a conventional, manned helicopter), $K_c = 1$ is a good approximation, according to Prouty (Ref 10.5). But for lower values K_c might even reach 2. Finally, when $\mu = 0$ we have seen that K_c has to be zero in order to obtain $b_{1s} = 0$ (b_{1s} is calculated with eq 9.44).

v_{ind} will usually be assumed to be equal to the induced velocity predicted by one of the several versions of the Momentum Theory. It should be noted that these consider the induced velocity to be uniform in the entire rotor disk, contrary to Glauert's model. However, using the induced velocity from MT as the v_{ind} of Glauert's model has proven to be an acceptable procedure (see Ref 10.5, for example).

10.3 Momentum Theory

This theory has the advantage of its simplicity and produces reasonably accurate results when combined with Glauert's model and BET. It is therefore very suitable for real-time simulations such as the one we are developing here.

We will not discuss here on the physical justification of this theory or on how to arrive to the main equations. The reader interested in these topics can find extensive information on the existing literature (for example, Refs 10.1 and 10.6).

"Classical" Momentum Theory

Momentum Theory (MT) yields the following expression for thrust (Ref 10.6):

$$T = 2\rho\pi R^2 v_{ind} \sqrt{V_x^2 + (V_z + v_{ind})^2} \quad (10.2)$$

Where R is, as usual, the rotor radius (from the axis of the hub to the tip of the blade). V_x is the component of the free stream velocity parallel to rotor disk and V_z is the component perpendicular to the rotor disk. Finally, T is the thrust, perpendicular to the rotor disk. Following Leishman (Ref 10.6) we will assume the rotor disk to be parallel to the Tip Path Plane (TTP), so that the thrust T of the previous Section is the same as the one here. In the previous Section V_x, V_z where respectively parallel and perpendicular to the Hub Plane (HP). However, since the flapping angles are small, we can also assume that the V_x, V_z of the previous Section are the same as the ones here.

Replacing T by C_T :

$$C_T = 2\lambda_{ind} \sqrt{\lambda_x^2 + (\lambda_z + \lambda_{ind})^2} \quad (10.3)$$

In the previous Section an expression for C_T was derived using BET (eqn 9.38). According to it $C_T = C_T(\lambda_z, \mu, \lambda_{ind})$. Therefore entering with (9.38) in (10.3) we arrive to an equation that yields λ_{ind} and, with it, v_{ind} . This equation will have to be solved numerically.

Once λ_{ind} is known, we can re-enter in (9.38) to obtain C_T . It is then possible, for example, to plot C_T against λ_z for several discrete values of λ_z .

As it can be seen, MT provides a simple way of calculating v_{ind} and it is therefore ideally suited for real-time simulation applications. However, MT as it has been presented here has a very serious flaw: it is only valid when the rotor is: (a) at hover, (b) climbing or (c) descending at high speed. In order to understand this better we have to briefly explain the different working regimes of a rotor. These are, after Leishman (ref 10.6):

- “Normal” or “Helicopter” working state, when $\bar{V}_z \geq 0$ (it should be remembered that V_z was positive when the free stream was blowing from above or, in other words, when the rotor was climbing)
- Vortex Ring State (VRS) when \bar{V}_z negative
- Turbulent Wake State (TWS) when \bar{V}_z more negative than in VRS
- Windmill Brake State (WBS) , approximately when $\bar{V}_z < -2\bar{v}_{ind}$

The hat symbol means that the variables have been non-dimensionalized with $v_0 = \sqrt{\frac{T}{2\rho\pi R^2}}$, where T is the thrust delivered by the rotor in each working point.

When we non-dimensionalize (10.2) as indicated above, it turns into:

$$1 = \bar{v}_{ind} \sqrt{\bar{V}_x^2 + (\bar{V}_z + \bar{v}_{ind})^2} \quad (10.4)$$

In axial flight:

$$\pm 1 = \bar{v}_{ind} (\bar{V}_z + \bar{v}_{ind}) \quad (10.5)$$

Where the \pm symbol indicates that the equation has two “branches”.

The figure on next page shows the approximate boundaries of the different working states, *in axial flight*.

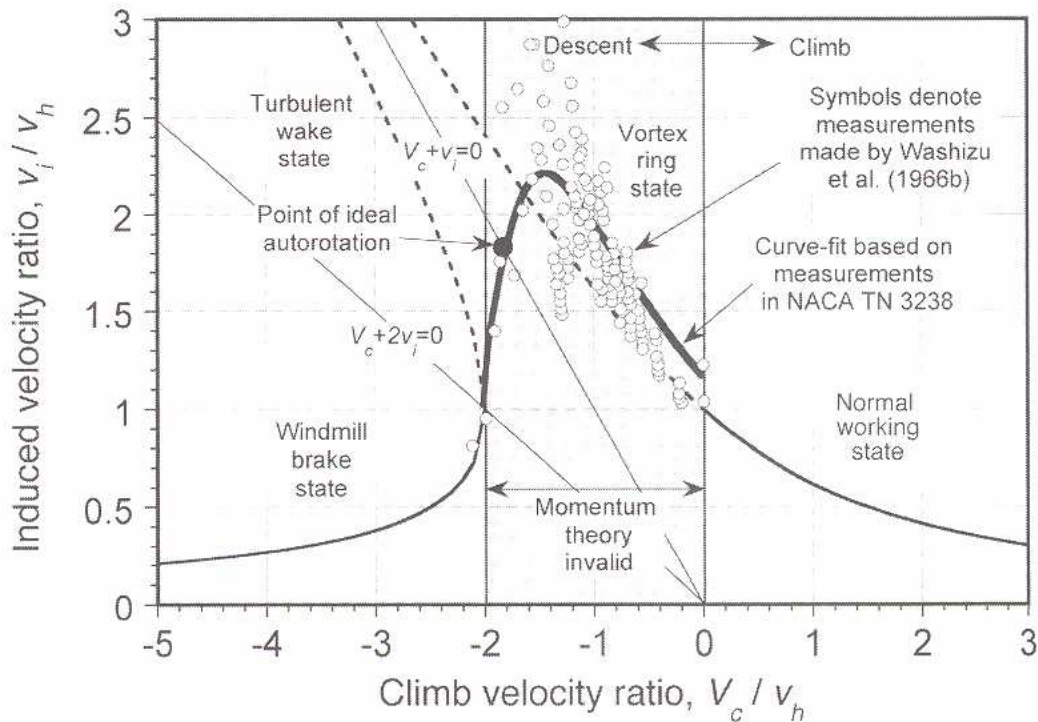


Fig 10.1. Induced Velocity Ratio vs Climb Velocity Ratio in axial flight. The two “branches” of the MT solution are shown. Solid lines have been used where those “branches” are valid (Ref 10.6).

MT will be valid for the “Normal” state and for WBS, but not for VRS and TWS, according to Leishman. This is because the hypotheses in which MT is based are not applicable in the VRS and TWS regions. However, determining the boundaries of these regions, which is equivalent to determining where MT ceases to be valid, is a difficult task. Wolkovitch (Ref 10.7), and later Peters and Chen (Ref 10.8), used a *dynamic* inflow model to estimate the upper limit $\bar{V}_z = -\eta$ of the VRS. According to Wolkovitch:

$$\eta \approx 0.7 \bar{v}_{ind}$$

It would be interesting to know if the rotors of the quadrotor can reach this limit under normal conditions (that is, those simulated in the model). Some examples of situations when one or more rotors might enter in the VRS/TWS region are:

- 1) A pitch up manoeuvre (the rear rotor sees a negative V_z)
- 2) A fast axial descent (in this case all the rotors see the same negative V_z)

For 1), with a thrust in the rear rotor of approximately 0.5kgf (close to the thrust corresponding to hover) and a pitch up rate of, for instance, 1.5 rad/s (which seems

within the normal range), we obtain $\bar{V}_z = -0.68$ in the rear rotor. Then, with (10.5) (choosing the appropriate “branch” of the equation), $\bar{v}_{ind} = 1.40$. Therefore $\bar{V}_z = -0.5\bar{v}_{ind}$, which is close to the limit but does not reach it.

For 2), with a thrust of about 0.7kgf and a descent speed of 5m/s, we obtain $\bar{V}_z = -4.28$, $\bar{v}_{ind} = 4.5$ and thus $\bar{V}_z = -0.95\bar{v}_{ind}$, which is now clearly in the VRS region according to Wolkovitch.

Therefore it is clear that the rotors might enter the VRS region under normal operation. Some helicopter simulators simply assume that the MT is going to be valid in all the operating envelope (Ref 10.9) but here we have just shown that this is not the case of the XPro. It is necessary to find another model that is valid also in the VRS and TWS region.

This is not an easy task. C.Chen (Ref 10.10) provides a comprehensive list of the different attempts that have been made to obtain a method to predict the induced velocity in the VRS and TWS. Basically, there are two types of methods available: those based on a parametric extension of the Momentum Theory and those based on wake models (prescribed or free wake). The former have the advantage of their simplicity, although they lack a solid theoretical background. Wake models represent a radical departure from MT, basing on entirely different hypotheses. They are much more accurate, too, but this comes at the price of a higher complexity (which in turn will lead to the need of larger computational resources). Here we will choose a parametric extension method, since the wake models are too complicated for our simulation.

“Modified” Momentum Theory

To understand how a parametric extension method works, we have to re-examine (10.5):

$$\pm 1 = \bar{v}_{ind} (\bar{V}_z + \bar{v}_{ind}) \quad (10.5)$$

This equation will have two solutions. If we plot \bar{V}_z against \bar{v}_{ind} we will therefore obtain two “branches” (see Figure 10.1). Parametric extension methods consist in finding a curve that smoothly joins the two branches and that is reasonably close to the empirical curve. Figure 10.1 shows a possible curve fit, but there are several, for example, that suggested by Johnson (Ref 10.1). Here, however, we will use the solution proposed by López Ruiz (Refs 10.11 and 10.12), which is:

$$1 = \frac{\bar{v}_{ind}}{k_1} \sqrt{\left(\frac{\bar{V}_z + \bar{v}_{ind}}{k_1}\right)^2 + \left(\frac{1}{k_2^2 - k_1^2}\right) \bar{V}_z^2} \quad (10.6)$$

Where $k_1 = \left(\frac{9}{5}\right)^{\frac{1}{4}}$ and $k_2 = \left(\frac{5}{4}\right)^{\frac{1}{4}}$.

This solution has the advantage of being valid in *all* the states (“Normal”, VRS, TWS and WBS), whereas that of Johnson, for example, is valid only for VRS and TWS, so that it is still necessary to use MT for the rest of the envelope.

López Ruiz bases on his own solution to propose a more general equation that includes \bar{V}_x :

$$1 = \frac{\bar{v}_{ind}}{k_1} \sqrt{\left(\frac{\bar{V}_z + \bar{v}_{ind}}{k_1}\right)^2 + \left(\frac{1}{k_2^2 - k_1^2}\right) \bar{V}_z^2 + \left(\frac{\bar{V}_x}{k_2}\right)^2} \quad (10.7)$$

With dimensions:

$$T = 2\rho\pi R^2 \frac{v_{ind}}{k_1} \sqrt{\left(\frac{V_z + v_{ind}}{k_1}\right)^2 + \left(\frac{1}{k_2^2 - k_1^2}\right) V_z^2 + \left(\frac{V_x}{k_2}\right)^2} \quad (10.8)$$

And if we want C_T :

$$C_T = 2 \frac{\lambda_{ind}}{k_1} \sqrt{\left(\frac{\lambda_z + \lambda_{ind}}{k_1}\right)^2 + \left(\frac{1}{k_2^2 - k_1^2}\right) \lambda_z^2 + \left(\frac{\mu}{k_2}\right)^2} \quad (10.9)$$

This will be the equation that will be used in our model. We will not examine here how this equation is obtained nor demonstrate its validity. Nevertheless, it is possible to assure that this solution produces satisfactory predictions (Ref 10.11).

We will refer to this model as the “Modified Momentum Theory” (MMT).

An additional advantage of MMT is that it does not underestimate v_{ind} when V_z is close to zero, contrary to what happens with MT.

As explained before, entering with (9.38) in (10.9) we get λ_{ind} and with it, v_{ind} . Then, re-entering in (9.38) we can obtain C_T .

In this way, by combining BET and MMT, we have just completed our model of the rotor.

10.4 Empirical correction

It will be seen in Section 13 that the correlation between the experimental results and those obtained with BET/MMT is good. However, it would be desirable to improve it

more. If we multiply the value of λ_{ind} obtained with BET/MMT by a certain corrective function, the resulting correlation could be better when λ_z is negative. The following function was tested:

$$\kappa = 1 - \kappa_0 \lambda_z \quad (10.10)$$

Where $\kappa_0 \approx 1.2$.

This function is completely empirical and there is no physical justification for it. In fact, it is impossible to say whether it could be applicable to other rotors.

In Section 13 it will be explained that this function does improve the correlation with experimental results, but only very slightly.

11. AERODYNAMICS OF THE AIRFRAME

11.1 Introduction

In previous sections it has been explained that the air that flows around the blades exerts on these certain forces and moments. The resultant of the forces applied to the b blades of the i th rotor has been designated \mathbf{F}_i , and the resultant of the moments, \mathbf{M}^{Pi} .

The airframe is also subjected to forces and moments exerted by the airflow around it. The resultant of these forces has been called $\mathbf{F}_{\text{airframe}}$, and the resultant of the moments, $\mathbf{M}_{\text{airframe}}^O$. It would be very interesting to develop a model for $\mathbf{F}_{\text{airframe}}$ and $\mathbf{M}_{\text{airframe}}^O$ as it has been done with \mathbf{F}_i and \mathbf{M}^{Pi} . This is mainly because $\mathbf{F}_{\text{airframe}}$ and $\mathbf{M}_{\text{airframe}}^O$ may have a significant contribution to the damping of the system.

However, it will be seen that modelling these forces and moments is a very complex task.

11.2 Overview of the model

For the sake of simplicity, it is convenient to assume that the forces are always applied in the same point of the airframe, and choose the moments in accordance. This point will be O (the origin of the body axes). As it happened with the rotor, it is convenient to define a new set of axes to study the aerodynamics of the airframe. This will be $Ox_w y_w z_w$ (see Figure 11.1).

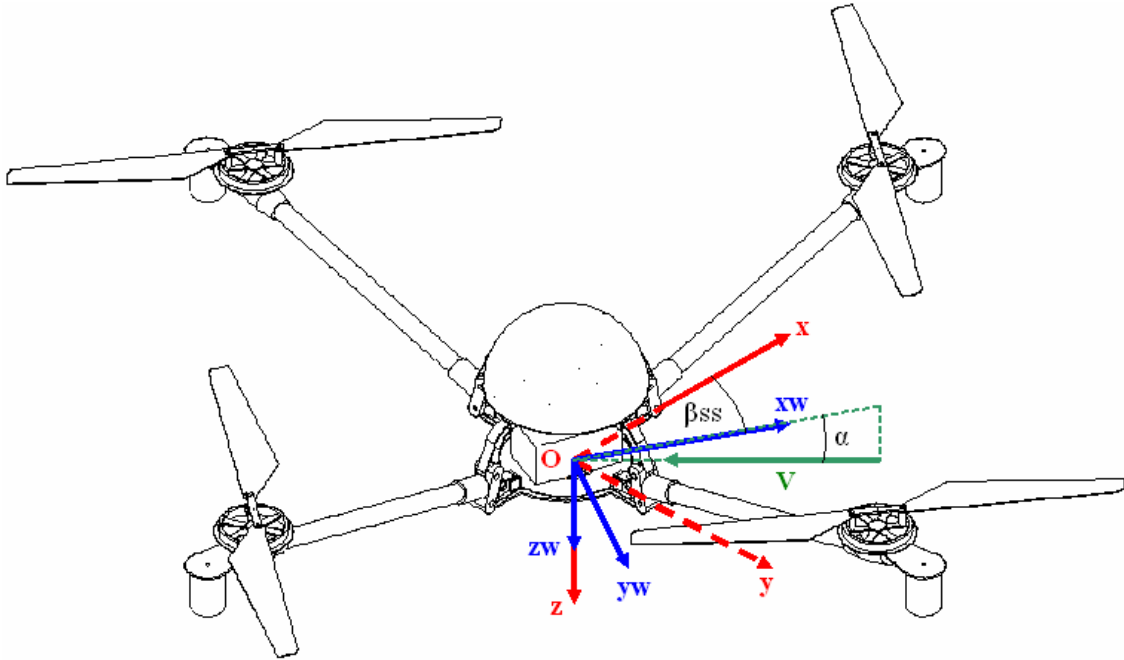


Fig 11.1. $Oxyz$ and $Ox_w y_w z_w$ axes.

In this new set of axes, the forces and moments can be defined in a totally analogous way as we did in the rotor:

$$\mathbf{F}_{\text{airframe}} = -f_{xa}\mathbf{i}_w + f_{ya}\mathbf{j}_w - f_{za}\mathbf{k}_w \quad (11.1)$$

$$\mathbf{M}_{\text{airframe}}^0 = m_{xa}\mathbf{i}_w + m_{ya}\mathbf{j}_w + m_{za}\mathbf{k}_w \quad (11.2)$$

In some occasions it will also be useful to classify the forces in terms of “lift” and “drag”.

Following Padfield (Ref 11.1), these aerodynamic forces and moments can be represented as follows:

$$\begin{aligned} f_{xa} &= \frac{1}{2} \rho V_a^2 S_{ref} C_{fxa}(\alpha_a, \beta_{SSa}) \\ f_{ya} &= \frac{1}{2} \rho V_a^2 S_{ref} C_{fya}(\alpha_a, \beta_{SSa}) \\ f_{za} &= \frac{1}{2} \rho V_a^2 S_{ref} C_{fza}(\alpha_a, \beta_{SSa}) \end{aligned} \quad (11.3)$$

$$\begin{aligned} m_{xa} &= \frac{1}{2} \rho V_a^2 S_{ref} C_{mxa}(\alpha_a, \beta_{SSa}) \\ m_{ya} &= \frac{1}{2} \rho V_a^2 S_{ref} C_{mya}(\alpha_a, \beta_{SSa}) \\ m_{za} &= \frac{1}{2} \rho V_a^2 S_{ref} C_{mza}(\alpha_a, \beta_{SSa}) \end{aligned} \quad (11.4)$$

Where α_a is the angle of attack and β_{SSa} is the sideslip angle. These are given by:

$$\beta_{SSa} = \arctg \frac{v}{u} \quad (11.5)$$

$$\alpha_a = \arctg \frac{V_{za}}{V_{xa}} \quad (11.6)$$

Where $V_{xa} = +\sqrt{u^2 + v^2}$ and $V_{za} = -w$.

S_{ref} and l_{ref} are the reference surface and the reference length, respectively. They will depend on the force or moment we are considering.

The coefficients of forces and moments can be assumed to depend only on α_a, β_{SSa} , as it is shown above. These coefficients could be obtained from a theoretical model or, more probably, from wind tunnel tests. Once this had been done, it would be possible to

calculate all the forces and moments. However, the task of determining the coefficients is not as easy as it seems.

11.3 Description of the problem

The possibility of estimating theoretically the coefficients of forces and moments is impractical unless CFD software is used. The airflow over the airframe is very complicated, with boundary layer separation in many areas. In the case of the XPro, this is worsened by the complex geometry of the airframe.

Hence, besides CFD, the only solution is to carry out wind tunnel tests. But this is also problematic. The main reason why the coefficients cannot be easily determined in the wind tunnel is the interference of the rotors. When the airframe is isolated (i.e., the rotors have been removed) these coefficients are indeed functions of α_a, β_{ss_a} only and can be obtained by testing the airframe in the wind tunnel. However, when the rotors are attached to the airframe and running the structure of the airflow is entirely different from the previous case, and so are the forces and moments.

In fact, according to Leishman (Ref 11.2), the values of these can differ in several orders of magnitude depending on whether the airframe is isolated from the rotors or not. In the first case they will be close to zero (for a wide range of velocities) but not in the second.

So if the airframe is to be tested in the wind tunnel, the rotors must be attached to it and running. The problem gets even more complicated when we consider that the airflow will be different depending on the conditions in which each rotor is operating (i.e., λ_z, μ , etc). Unfortunately, no wind tunnels large enough for the XPro were available. Above all, it was found out that the effort necessary to prepare and carry out the tests to estimate $\mathbf{F}_{\text{airframe}}$ and $\mathbf{M}_{\text{airframe}}^o$ was not worth the benefit. The reason why is that, unless the accuracy of the measures is very high, which is unlikely for tests of this complexity, the magnitude of the aerodynamic forces and moments over the airframe might be overestimated.

11.4 Order of magnitude of the aerodynamic forces and moments over the airframe

Drag

The drag D is defined as the aerodynamic force opposite to the velocity vector.

To estimate the drag over the isolated airframe a simple thought exercise can be made. An isolated airframe in free fall which keeps horizontal will accelerate until the weight force gets cancelled with the drag ($D = f_{za}$). From this point onwards it will fall at constant velocity, sometimes called “terminal velocity” V_{terminal} . Considering the reduced cross-section of the airframe, the drag will probably be small, and so this

velocity is likely to be high, at least 50 m/s. If now we consider the point of the free fall where the drag is a tenth of the weight (an order of magnitude of difference) we get that the velocity is a third of $V_{terminal}$ (where it has been taken into account that the drag is proportional to the square of the speed).

This means that for velocities which are less than 33% of $V_{terminal}$, the drag ($D = f_{za}$) is at least one order of magnitude smaller than the weight of the airframe. Or, in other words, one order of magnitude smaller than the typical value of the total thrust (which is equal to the weight).

This simple exercise can be repeated assuming that the airframe is vertical as it falls. In this case the drag will be $D = f_{xa}$ (or $D = f_{ya}$) and the terminal velocity will probably be larger, since the cross-section is now smaller (see Figure 3.1).

Considering a terminal velocity of 50m/s for both situations (which is probably much lower than the real one), we obtain that, for velocities up to 17m/s, the drag is one order of magnitude smaller than the typical total thrust.

Even if we assume that the drag over the airframe increases by a 20% when the rotors are attached to it (due to rotor interference effects) we still obtain that for low velocities (~10m/s) it is an order of magnitude smaller than the typical total thrust.

Lift

The lift is the aerodynamic force perpendicular to the velocity vector.

Since the geometry of the airframe has not been designed to generate lift, it is likely that this will be very low, at least compared to the thrust delivered by the rotors.

Moments

Looking at Figure 3.1 it is clear that, when the blades are not considered, the primary contribution to the pitch/roll/yaw moments is the moment caused by the drag force acting on each arm and on the motor casing. Some estimates of this drag were obtained in the wind tunnel but not with enough accuracy. Basing on these estimates, we may assume that, for a very low airspeed (1 m/s or less), this drag force is going to be less than 0.01N. Then, if we assume that the force is applied at the end of the arm and that it is opposite to the velocity vector at that point, we obtain a moment at O of not more than 0.005Nm. If the quadrotor pitches up, for instance, there will be two forces involved (one at each of the arms that move) which will create a pitch *down* moment of 0.01Nm ($2 \times 0.005 = 0.01\text{Nm}$). It is interesting to compare this value with those of other moments that are applied at O , which can be obtained from the simulation (see Section 16).

In a pitch up manoeuvre there are two basic contributions to the pitch moment around O , as it will be explained in Section 16. The first is the pitch up moment created by the difference in the thrust at the front and rear rotors. The second is a pitch down moment that results from adding the in-plane moments at each of the rotors. If the manoeuvre is performed at a constant angular rate of about 0.3rad/s, both moments will be of the same order of magnitude (about 0.05Nm, according to the simulation). When both moments are combined, the result will be a pitch up or pitch down moment (depending on the circumstances) of about 0.005-0.01Nm.

We can see that this moment has the same order of magnitude of the estimated pitch moment created by airflow over the airframe. Even if we have overestimated the latter (which is quite probable) it is clear that it might be influential. This will have to be borne in mind when interpreting the simulation results.

11.5 Conclusions

A model of the aerodynamic forces and moments over the airframe can only be built if experimental data are available. Ideally, these data will have been obtained in a wind tunnel with the rotors attached to the airframe and running, in order to account for the interference caused by these. Such tests were difficult if not impossible to carry out with the means available at the time this Report was written.

$\mathbf{F}_{\text{airframe}}$ is likely to have little impact on the linear acceleration of the quadrotor (or, more exactly, on that of its c.g.) because it is at least one order of magnitude smaller than the typical force acting on the vehicle (the thrust). This is true for a wide range of velocities up to at least 10m/s. Therefore, for Performance studies *at speeds confined to that range* $\mathbf{F}_{\text{airframe}}$ can be neglected:

$$\mathbf{F}_{\text{airframe}} \approx \mathbf{0}$$

$\mathbf{M}_{\text{airframe}}^O$ is important because of its contribution to the damping of the system. It will tend to oppose to the angular rotation of the airframe and therefore it is likely to increase the damping. Since the quadrotor is an inherently unstable machine, this might become very important.

Unfortunately, there is no easy way of calculating $\mathbf{M}_{\text{airframe}}^O$. A half-hearted approach to the task of measuring it accurately will likely result in it being either underestimated or overestimated. Therefore it will be assumed that:

$$\mathbf{M}_{\text{airframe}}^O \approx \mathbf{0}$$

This may become one serious limitation of the model and should be kept in mind when interpreting the results of a simulation. In those cases when the sum of the other moments acting at O is small, the influence of $\mathbf{M}_{\text{airframe}}^O$ might be important.

It is worth noting that, to the best of the knowledge of the author, no serious attempts have yet been made in the research community (Refs 1.1 to 1.11) to model the aerodynamic forces and moments over the airframe of the quadrotor.

12. WIND TUNNEL TESTS

INTRODUCTION

12.1 Overview of the aim of the tests

The aim of these tests is to obtain some experimental data which are needed to complete the quadrotor model. The information required is of two types:

- About the performance of the motor
- About the aerodynamic forces and moments in the rotor

This information is very important as explained below.

Performance of the motor

In Section 6 it was explained that, to model the dynamics of the D.C. motor, it was necessary to know the constants R_a, K, F, L . In the following section, 7, the issue of how to obtain these constants was addressed, and it was concluded that:

- R_a, K, F could be obtained from the data provided by the manufacturer of the motor (see Appendix C) or from experimental tests.
- L could only be obtained experimentally.

R_a, K, F were calculated using the data from the manufacturer. However, it was decided to estimate them by performing experimental tests too, so that afterwards it would be possible to compare the results obtained in both ways. Besides, the testing of the motor could easily be done using the same installation that was required for the rotor tests without any need for additional equipment.

As for L , a method to calculate it was proposed in Section 7. However, it was decided that it would be enough to estimate it. To do so, the values of L for motors similar to the Mabuchi RS-545SH were compared, and finally a value of 1mH was adopted. In Section 16 it will be seen that the effect of L in the transient response of the motors is indeed very small. Therefore the impact in the model of any errors in the estimation of L will also be small.

Aerodynamic forces and moments in the rotor

In Section 9 it was explained that to model the aerodynamics of the rotor it was necessary to have experimental data from the wind tunnel. In that Section we also defined the aerodynamic forces and moments as follows:

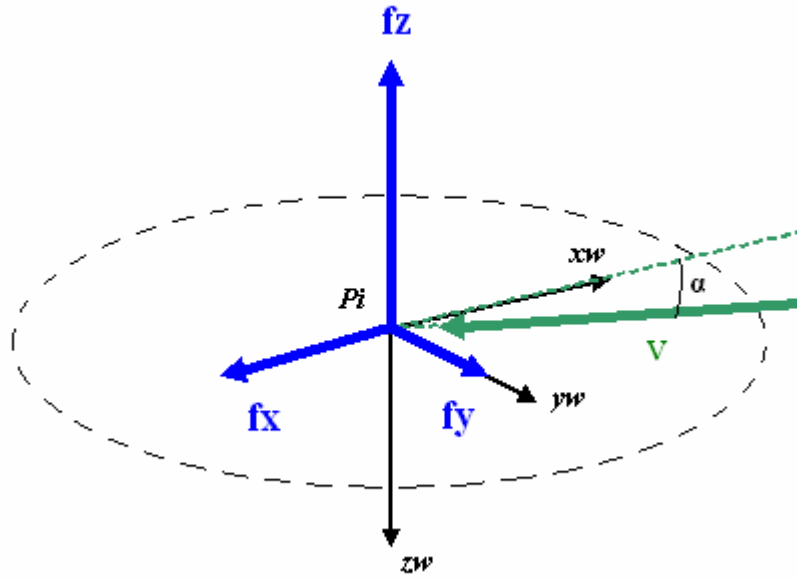


Fig 9.3b. Forces on the rotor (quantities positive as shown).

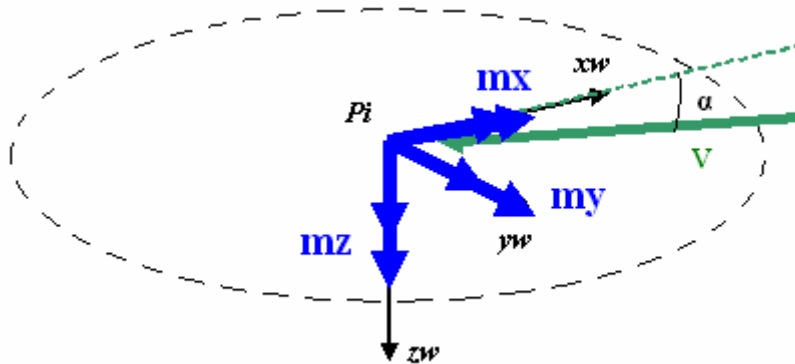


Fig 9.3c. Moments on the rotor (quantities positive as shown).

It should also be remembered that:

$$\lambda_z = \frac{V_z}{|\Omega|R} \quad \mu = \frac{V_z}{|\Omega|R}$$

Where the reason for taking the absolute value is that Ω is negative when the rotor turns clockwise (as explained in Section 4). In fact, it will be seen that the rotor used in the wind tunnel tests rotated clockwise.

Regarding the in-plane moments, it is important to realise that what will actually be measured in the rotor tests is $(m_x)_{hub}$ and $(m_y)_{hub}$, not m_x and m_y .

The aim of the rotor tests is double:

- To gather enough data to estimate some of the parameters required by our theoretical model of the rotor, which cannot be obtained otherwise. The parameters needed are $a, c_{d0}, c_{d1}, c_{d2}$. The corrective function $\kappa(\lambda_z)$ will also be selected using the results from the wind tunnel.
- To validate the results of the rotor model developed in Sections 9 and 10.

12.2 Brief description of the test installation

The rotor used in the tests turned clockwise. This implies that, according to Figure 9.3c, m_z will be negative.

To measure the forces and moments a 5-component strain balance was used. The rotor-motor assembly was attached to it by means of a custom-made metal support. This support could rotate around the axis of the balance (see Fig 12.1).



Fig 12.1. Picture of the test installation showing how the support of the rotor can rotate around the axis of the balance.

The balance itself was fitted into an arm which in turn was attached to the test bench. (see Fig 12.1).

The facility for the tests was the Weybridge wind tunnel, owned and operated by Cranfield University. This was a low speed, open test section wind tunnel, capable of producing airflows of up to 30 m/s.

Airflow speed at the contraction section of the tunnel was measured by comparing the pressure at this section and the pressure in a section upstream (see Fig 12.2).



Fig 12.2. Measuring equipment. In the background, the contraction section can be seen in the left. The section upstream where the pressure was also measured is just behind the computer screen.

The electrical current to the motor was provided by a D.C. power supply unit. This unit allowed setting either the voltage or the current, but not both at the same time (because when one of them is set, the other becomes an output variable of the physical system). Since the variable used to control the motor is the voltage v_a , as explained in Section 6, the voltage would be the variable set, and the current would then be an output. Attention had to be paid to the losses at the cable which connected the power unit with the motor. This cable had a resistance of 0.3 ohm.

To measure the rpm of the rotor, two methods were considered: either attaching a tachometer-generator to the hub or using an infrared transmitter-receiver that detected the passing of the blade. Finally, the second was adopted because it had two big advantages. Firstly, the IR transmitter-receiver was much cheaper than the tachometer. Secondly, with this method there was no mechanical linkage with the rotor, thus avoiding vibration problems that would have occurred had the tachometer been used. The figure on next page shows the IR transmitter-receiver already installed.

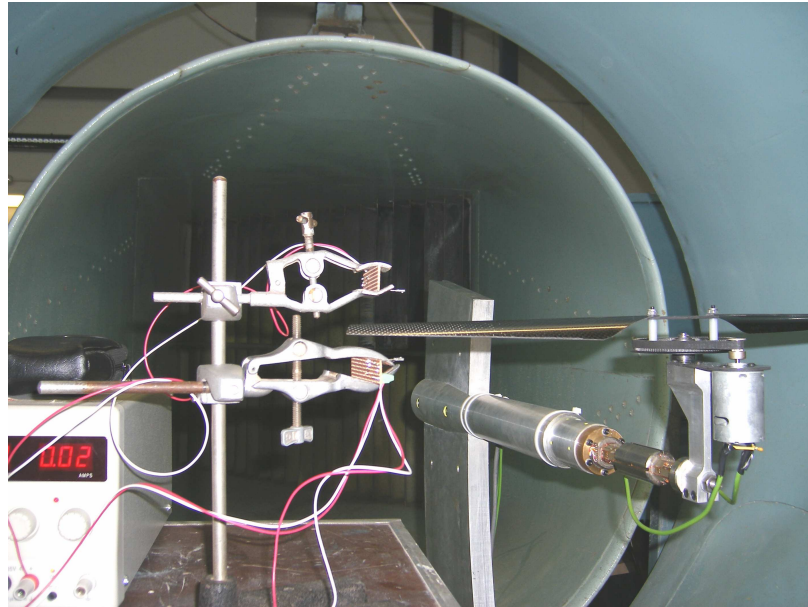


Fig 12.3. IR transmitter-receiver already installed. Note how the installation blocks completely the wind tunnel, thus making it impossible to use the IR transmitter-receiver while the wind tunnel was operating.

The main problem of the IR transmitter-receiver installation was its size, which prevented it from being used while the wind tunnel was working, because it would have substantially modified the airflow. It had to be accepted that no rpm measures would be obtained with the wind tunnel working.

The electric signals from the balance and the IR transmitter-receiver were fed into a PC. The measures were organized and viewed in the PC using LabView software.

In order to estimate the flapping and coning angles, a camera was used. This camera was fixed so that all the pictures were taken from the same position and angle.

EMI shielding

It was found out that the motor was a strong source of Electromagnetic Interference (EMI) and that this was significantly increasing the error in the measures of the balance. Therefore, it was decided to “shield” the balance by covering it with a thick aluminium plate. Besides, all the cables were also protected with aluminium foil. In this way it was possible to minimize the interference caused on the electronic circuits of the balance.

Translation and rotation of axes

The balance measured the moments and forces around a certain point of its geometry that was given in the calibration instructions document. But the position of this point was not the same as that of P_i , which was the point where the aerodynamic forces

and moments had been defined (see Section 9). In addition, the rotor-motor assembly was attached to a support that rotated around the axis of the balance. Hence, to obtain the forces moments at P_i from those measured by the balance it was necessary to translate and rotate the axes.

In Section 9 it was explained that P_i was the centre of mass of the system composed by the b blades (2 blades in the tests). Another point, called O_i , was defined as the intersection between the axis of the hub and the top of it (see Figure 12.4). P_i was assumed to be on the same axis, above O_i and separated of it by a distance $h = r_G a_0$. This poses a problem because a_0 is not known (unless it is measured directly). It could be estimated with (9.44), but since determining the parameters that appear in that formula is precisely one of the aims of these tests, we cannot use this formula before having found the values of those parameters, and to do so we need the forces and moments at P_i . However, it can be demonstrated that, due to the geometry of the system, h is only going to affect the measurements of the in-plane moments. The moment around the hub m_z will be insensitive to h , as well as all the forces. Therefore, for the sake of simplicity, we will assume $P_i \equiv O_i$.

It is important to remember that, according to expressions (9.44) to (9.48), a_0 will depend on V, α, Ω (speed of the free stream, angle of attack and speed of the rotor, respectively). Hence, it will be different for each test of the sequence. Since h depends on a_0 , the same will be applicable to this parameter.

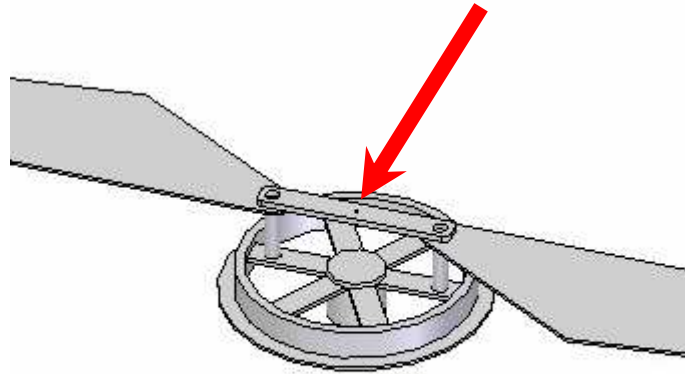


Fig 12.4. Detail of the position of the point O_i .

Description of the sequence of tests

It has previously been mentioned that it was decided to use the installation to test the performance of the motor as well. Hence, the sequence of tests can be divided in two different parts. Firstly, a set of measures with no free stream, to obtain the constants of the motor and to measure rotor forces and moments in the hover condition. Secondly, another sequence of tests with the wind tunnel working, to measure those forces and moments in the rest of the flight conditions.

However, this Section will be organized in a slightly different way. The first part will be devoted to the motor and the second one, to the rotor. For the first one we will use the results obtained without free stream, whereas for the second we will use the results obtained with and without free stream.

MOTOR PERFORMANCE

12.3 Overview

It was explained in Section 3.4 that to obtain R_a, K, F it was necessary to know the voltage v_a , the current i_a , the rotational speed of the motor and the load torque τ_{load} in two different operating points. These points were in the steady state regime, so that the equations to be used were:

$$v_a = K g_r \Omega + R_a i_a \quad (7.2)$$

$$K i_a = \tau_{load} + F g_r \Omega \quad (7.5)$$

Where it has been taken into account that the rotational speed of the motor is equal to the product of the ratio $g_r = 10$ by the rotational speed of the rotor Ω (where the subscript i has been omitted for the sake of clarity). It should also be remembered that the load torque τ_{load} , in a steady state condition, is equal to the absolute value of the torque m_z divided by the gear ratio (in a non-steady condition the relation is more complex, as shown by eq 4.50).

The ideal sequence of tests would have consisted in running the motor without removing the rotor and without any airflow in the tunnel. This would have been done for different voltages. τ_{load} would have been measured with the balance, Ω by means of the IR transmitter-receiver and v_a, i_a with the power generator unit.

However, due to practical reasons, it was decided not to take measures from the IR transmitter-receiver and the balance simultaneously. Hence, the sequence of tests was the following: firstly, Ω was measured for different voltages; secondly, the IR transmitter-receiver was removed and the balance was used to measure the forces and

moments, including τ_{load} , for those very same voltages. Since the voltages were the same, it could be assumed that Ω would also be the same.

The Ω measurements can be seen in Appendix D, whereas the measures of forces and moments are in Appendix E.

12.4 Analysis of the results

Each set of values of $v_a, i_a, \Omega, \tau_{load}$ represents a working point of the motor. With the previous tests, several of these working points were obtained. As it has been said above, with two of these points it is possible to obtain an estimate of R_a, K, F . In particular, using (7.2) R_a, K can be obtained, whereas using (7.5) F and a different estimation of K can be obtained.

Grouping the operating points by pairs and using (7.2) up to nine values of R_a, K were obtained. The figures below show some estimated working points, compared to the “smoothed” experimental curve. The estimated points were obtained with R_a, K taken as (a) the average of the nine values or (b) the last value, corresponding to the two highest voltages:

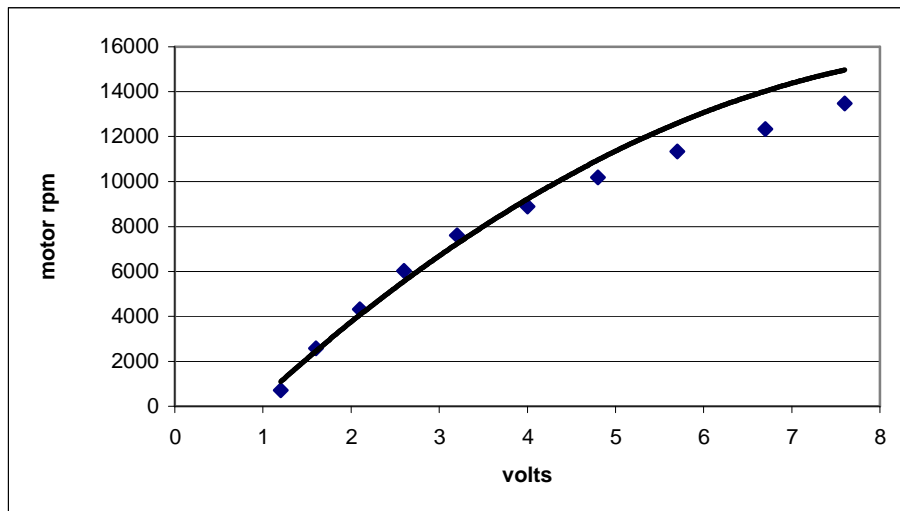


Fig 12.5(a). Motor-rotor performance: comparison between the “smoothed” experimental curve (solid line) and the results estimated. R_a, K were taken as the average of the nine obtained values.

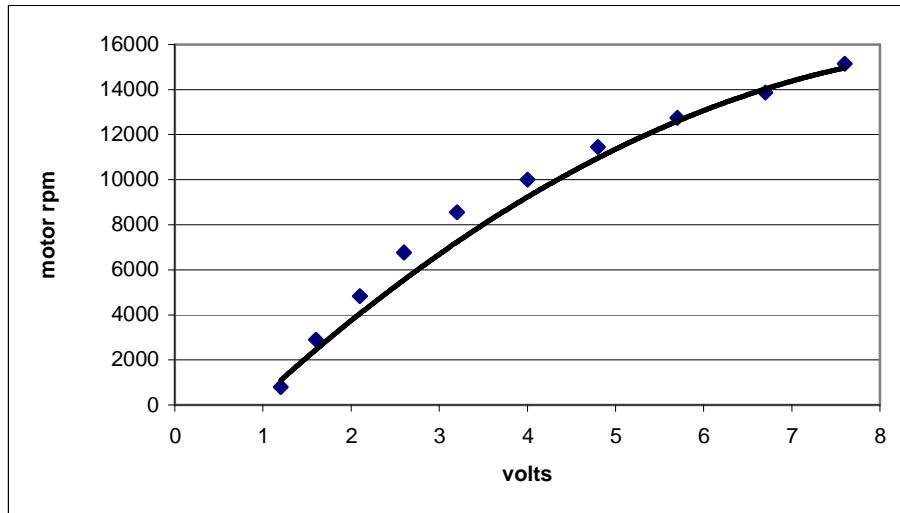


Fig 12.5(b). Motor-rotor performance: comparison between the “smoothed” experimental curve (solid line) and the results estimated. R_a, K were taken as the average of the two last obtained values.

It is important to remember that Ω is the rotational speed of the rotor, which is ten times smaller than that of the motor.

It can be seen that with (b) the prediction is better for the highest voltages, which is interesting because the motor will be normally operating in that region. Therefore it was decided to use the values of R_a, K corresponding to (b). These are:

$$R_a = 0.291 \text{ ohm} \quad K = 0.00347 \text{ volts} \cdot \text{s} \cdot \text{rad}^{-1}$$

It is interesting to compare these values to those obtained in Section 7 using the data provided by the manufacturer, which were:

$$R_a = 0.267 \text{ ohm} \quad K = 0.00464 \text{ volts} \cdot \text{s} \cdot \text{rad}^{-1}$$

From this point onwards, unless it is said otherwise, the values of R_a, K used will be the experimental ones, since they model more accurately the performance of the motor.

As for F , the procedure is similar. F (and K too) can be obtained using two different operating points and eq (7.5). However, it was suspected that the balance would not be capable of measuring τ_{load} with the precision which was needed for estimating F .

Hence, it was preferred to keep the value of F obtained in Section 7, which was:

$$F = 2.035 \text{E} - 06 \text{ N} \cdot \text{m} \cdot \text{s} \cdot \text{rad}^{-1}$$

AERODYNAMICS OF THE ROTOR

12.5 No free stream test

This condition corresponds to the case in which the quadrotor is hovering over a fixed point, and so all the components of the velocity are zero. The same sequence of tests that was done to study the steady state performance of the motor was used to measure the aerodynamic forces and moments in this condition.

It is worth noting that, since the mass of the quadrotor is fixed, there will only be one value of thrust which makes it possible to hover at constant altitude. Because the thrust, in this condition, is a function of Ω only (see Section 13), there will only be one value of Ω , that is, one voltage, for which hovering is possible. For any other Ω the quadrotor will either ascend or descend, and thus there will be a free stream blowing through the rotor.

12.6 Tests with free stream

The priority is to obtain data corresponding to flight conditions *within* the normal operating envelope. Since the XPro does not achieve high linear speeds under normal operation it will not be necessary to consider a very wide range of speeds for the tests.

In any case, the number of cases to study is much larger than when there is no free stream. This is because the degrees of freedom are 3: the airspeed V , the rpm (i.e., the voltage) and the angle of attack α . Besides, since the balance can only measure two of the three components of the aerodynamic force, it is necessary to do all the tests in two different configurations: with the axis of the balance perpendicular to the stream and with the axis parallel to the stream. This is the only way how the three components of the force can be obtained.

It is likely that the coefficients of forces and moments will strongly depend on λ_z, μ but will be basically insensitive to Ω , because they do not depend explicitly on it (only implicitly, through the coning and flapping angles). This would allow us to substantially reduce the number of cases to study, because we could keep V (or Ω) constant.

However, since one of the purposes of the test is precisely to validate the theoretical model of the rotor, it seems unwise to use the conclusions obtained from this model when designing the test sequence. The fact that the coefficients of forces and moments do not depend on Ω should not be assumed *a priori*. On the other hand, the time available for the tests is limited and therefore any reduction on the number of cases to study is welcome.

Finally, a compromise had to be achieved: neither V nor Ω were kept fixed, but the number of values of V to be used was reduced in the confidence that the coefficients would finally depend on λ_z, μ but not on Ω .

Selection of the points to investigate*Values of α to be investigated:*

An adequate selection of the values of α to be covered is essential since, due to the characteristics of the test installation, the task of changing its value is very time-consuming. Since the time available for the experiments is always limited, it is necessary to limit the number of cases to the most representative ones.

There are two limit cases that need to be studied, which are $\alpha = \pm 90^\circ$ and $\alpha = 0^\circ$. The first corresponds to axial flight, that is, when the quadrotor is descending or ascending without any lateral movement. The second corresponds to the case in which the vertical component of the velocity in body axes is zero but at least one of the other two is not. It should be noted that this second case *does not* correspond to the horizontal flight condition. It was explained in Section 2 that in a steady, horizontal flight situation the pitch angle of the quadrotor has to be non-zero so that there is a horizontal component of the thrust.

Apart from those two limit cases, it would be interesting to study the intermediate case, that is, $\alpha = \pm 45^\circ$. Alternatively, $\alpha = \pm 30^\circ, \pm 60^\circ$ could be investigated.

Finally, when the wind tunnel tests were being planned, it was decided to cover the following points: $\alpha = 0^\circ, \pm 5^\circ, \pm 15^\circ, \pm 30^\circ, \pm 45^\circ, \pm 60^\circ, \pm 75^\circ, \pm 90^\circ$.

Values of V to be investigated:

As it has been said, there is a great interest in studying those situations where the linear velocities are low, in part because during normal operation the quadrotor does not fly very fast, but also because in Section 11 it was decided to neglect the aerodynamic forces over the airframe (and this can only be done if the linear velocity is not too high). Hence, in the wind tunnel tests, it is enough to use small values of V . However, for axial flight, it might be interesting to use higher values of V too, because this is the flight condition that we will study in more detail (see Section 13). Finally, it was decided to use five speed settings for axial flight (from 1.5m/s to 15m/s, approximately) and, as a general rule, three speed settings for the rest of the tests (covering between 2.5 and 8m/s).

Values of Ω to be investigated:

It is not necessary to cover all the voltages (ie, values of Ω) from zero to the maximum (12 volts) because we are interested only in the normal flying conditions. In those cases, Ω is between 90 and 200 rad/s, and the armature voltage is between 4 and 10 volts. Therefore, it would be adequate to cover some equidistant points within this range. Additionally, some more points close to the trim hover condition (which is the one in which we are more interested) could be included.

This poses the problem of knowing beforehand which is going to be the value of Ω for the trim hover condition. But the thrust delivered by each rotor in this condition is known, because it is a fourth of the weight of the vehicle. From the tests with no free stream, the value of Ω associated to this thrust can be obtained. This was done and the result was a value of around 160 rad/s or 7.5 volts at the armature.

In any case, the selection of the values of Ω is not very critical since this is the easiest parameter to modify (just by varying the voltage).

Finally, it was decided to study the following points: 5, 6, 7, 8, 9, 10, 11, 12 volts. It should be noted that these were the voltages produced by the D.C. power supply unit. The actual armature voltages would actually be smaller because of the losses at the cable. It was considered unadvisable to go beyond 12 volts because of the risk of structural failure. On the other hand, it was not considered interesting to study voltages below 5 because the motor would rarely operate in that region.

Measures corresponding to 11 and 12 volts should be treated very cautiously, though, because it was found that the error of the balance in those cases was higher than in the rest (probably because of the EM interference of the motor).

In-plane forces

However, there was still one important consideration to be made; this had to do with the balance. As it has been indicated above, this was a five component balance, which means that there was one component that could not be measured, and this component was the force parallel to its axis. This implied that it would be possible to measure only one of the two components of the force in the plane of the rotor. So, if both components were to be measured, it would be necessary to go through all the test cases in two different configurations: one with the balance perpendicular to the free stream and the other with it parallel.

However, the benefit of measuring both forces did not compensate for the extra time required to do so, especially if we consider that, as it will be seen, measures of the in-plane forces (and moments) were not reliable because of the error of the balance.

Therefore, it was decided to carry out all the tests in only one configuration: that where the axis of the balance is perpendicular to the free stream. Hence, the lateral force at O_i was not measured. Another consequence of using this configuration is that the contribution of the lateral force to the roll moment at O_i could not be obtained too. This will have to be borne in mind when the analysis of the experimental data is carried out (see next Section).

12.7 Some important considerations

Airspeed measurements

Anytime the rotor is running, no matter in what condition, it generates a downward induced velocity, as it has already been mentioned. When the tests were being conducted, the dynamic pressure was measured at the contraction section of the tunnel, which was about 1m away from the rotor. It was soon found out that, when the rotor was opposed to the wind direction ($\alpha = 90^\circ$), the induced flow was intense enough to greatly affect these pressure measurements. In fact, this was corroborated when some smoke tests were conducted, with the smoke pipe placed at the contraction section. In those tests it could be seen how the rotor was able to reverse the airflow in the wind tunnel, provided that the speed of the free stream was small enough.

As a result, eventually what was measured was not V_z but $V_z + (v_{ind})_{averaged}$, where $(v_{ind})_{averaged}$ is the average induced velocity in the rotor disc. Since there is no easy way of estimating it, it is not possible to know the error made.

Rotor instabilities

When the wind tunnel tests were carried out, it was discovered that in certain situations the rotor Tip Path Plane (TPP) oscillated intensely. One of the reasons could be the unsteady nature of the airflow when the rotor is in the Vortex Ring State (VRS) or the Turbulent Wake State (TWS). This would be consistent with the fact that in many cases the oscillations were observed when the rotor was likely to be working in one of those regimes. However, other explanations should not be ruled out (resonances, for example).

Rotor instabilities should be investigated further. In particular, it would be necessary to identify accurately in which situations they are likely to appear. This is a very important issue because, as we will see in Section 16, rotor instabilities can have significant effect on quadrotor flight dynamics.

13. ANALYSIS OF THE EXPERIMENTAL DATA. ROTOR MODEL VALIDATION

INTRODUCTION

13.1 About the need for experimental data

As it was explained in the previous section, there were two reasons why it was necessary to have data from wind tunnel tests. Firstly, these data were to be used to estimate some of the parameters of the rotor model. Then, after the model was completed with the introduction of the values of these parameters, the results from the wind tunnel were to be used to validate the rotor model. This Section will deal with these two tasks. Since both are clearly interrelated, they will be done simultaneously.

The rotor model will be the only element of the quadrotor simulation that will be validated, since no flight test data are available to validate the model of the complete vehicle. Therefore it is essential to carry out this task carefully, since it will be our only opportunity to validate at least part of the quadrotor simulation.

Since the rotors are the elements that have the greatest influence on quadrotor flight dynamics, the validation of the rotor model is even more important. Success in producing a realistic model of the rotor will ensure that we are on the right way to obtaining a realistic simulator of the quadrotor.

In order to validate the rotor model, a Simulink version of it was built. Thanks to the modular structure of Simulink, this could be later integrated as a part of the simulation of the complete vehicle. In Section 14 more details are given about the Simulink model of the rotor.

The whole set of data from the wind tunnel tests can be found in Appendix E.

13.2 Estimated aerodynamic properties of the blade

The physical model developed in Section 9 requires knowing several parameters which are related to the geometric and aerodynamic properties of the blade. These are listed on the table on next page.

Symbol	Name
θ_0	Collective Pitch
θ_1	Twist
a	Slope of the lift coefficient of the aerofoil
c_{d0}	1 st term of the drag polar
c_{d1}	2 nd term of the drag polar
c_{d2}	3 rd term of the drag polar
c	Mean chord

Table 13.1. Parameters required by the rotor model.

Apart from these, there are some other parameters which have been measured directly, such as the mass of the blade m_b , the radius R , etc. Another important parameter, the non-rotating flap frequency ω_{nr} was estimated in Section 9.

From the parameters listed on Table 13.1, θ_0, θ_1 can be measured directly on a sample blade:

$$\theta_0 = 0.37 \text{ rad } (21^\circ) \quad \theta_1 = -0.09 \text{ rad } (\approx -5^\circ)$$

It is very important to bear in mind that, due to the high degree of simplification introduced by our theoretical model, the values of θ_0, θ_1 that provide a better correlation with the experimental results need not be the real ones, that is, the ones measured on the blade. However, the more accurate our model is, the less discrepancy there will be.

As for $a, c_{d0}, c_{d1}, c_{d2}$ they cannot be easily estimated, unless specific wind tunnel tests are carried out. It should be remembered that our model assumes that $a, c_{d0}, c_{d1}, c_{d2}$ are identical for every blade element. For this to be true, all the aerofoils must have an identical shape (identical camber and relative thickness). The blades of the Xpro have constant thickness, and the radius of curvature is constant both chordwise and spanwise. Since they are tapered, the relative thickness will not be identical for every blade element. However, since the thickness is very small ($\approx 1 \text{ mm}$), this can be ignored. Hence, the hypothesis of identical $a, c_{d0}, c_{d1}, c_{d2}$ throughout the blade seems plausible.

Most of the books about helicopter theory (see Refs 13.1 to 13.3) provide estimates for $a, c_{d0}, c_{d1}, c_{d2}$. Unfortunately, most of these estimates refer to blades of conventional, full-sized helicopters, which are quite different from those of the XPro. The best solution to estimate $a, c_{d0}, c_{d1}, c_{d2}$ is probably to infer them from the results of the rotor tests, which is equivalent to choosing them (within reasonable limits) so that the correlation between the results of the model and the experimental data is good.

Finally, as for the mean chord c , its value will depend greatly on how we define it. In conventional helicopters the blades are usually untapered and thus the mean chord is simply the chord of every section of the blade. However, as we have said before, the blades of the XPro are tapered. When the blades are tapered, a usual practice is to assume that the mean chord is the one of the blade element situated at 70% of the blade span. The reason why this blade element is chosen is because it usually leads to accurate results, since it is quite representative of the whole blade. Following this convention, we obtain a mean chord $c = 0.032m$. Since there is no formal justification for the need to choose the chord at 70% of the span, we could alter this value to provide a better correlation with the experimental results. This is in fact what we will do.

Therefore we have five parameters $c, a, c_{d0}, c_{d1}, c_{d2}$ which we have to carefully choose to obtain the best correlation with experimental results. However, a closer look at the expressions derived in Section 9 reveals that we do not need to know the five. It is enough to know the values of ac (or $a\sigma$, which is equivalent) and $\frac{c_{d0}}{a}, \frac{c_{d1}}{a}, \frac{c_{d2}}{a}$. This is an important advantage because it reduces from five to four the number of parameters to be estimated. In other words, we can arbitrarily choose one of the five parameters $c, a, c_{d0}, c_{d1}, c_{d2}$ and the results will be the same as if we have chosen a different one, provided that ac and $\frac{c_{d0}}{a}, \frac{c_{d1}}{a}, \frac{c_{d2}}{a}$ remain constant.

Therefore we will proceed as follows: c will be assumed to be that of the blade element at $\approx 60\%$ of the span ($0.04m$), and will not be further modified. Then, a and c_{d0}, c_{d1}, c_{d2} will be chosen so that we get the best correlation with empirical data. The reason why the chord at 60% of the span is used instead of the one at 70% is because it appears to give a better correlation with the experimental data. And as we have said before, there is no strict obligation to use the chord at 70% of the span.

13.3 Empirical λ_{ind}

As it was explained in Section 10, an empirical correction of the λ_{ind} predicted by MMT can be required. Arbitrarily, we decided that this correction would consist in multiplying that value by a function of λ_z which we called $\kappa(\lambda_z)$.

$$(\lambda_{ind})_{corrected} = \kappa \lambda_{ind} \quad (13.1)$$

We will choose this function so that $\kappa(\lambda_z = 0) = 1$, because doing so has some advantages, as it will be shown afterwards.

AXIAL FLIGHT

13.4 Introduction

We will start our analysis with the axial flight case ($\alpha = \pm \frac{\pi}{2}$), which is simpler to study because there is only one variable, λ_z , rather than two (λ_z and μ).

When the wind tunnel tests were conducted in axial flight conditions, it was observed that, as expected, there was no tilt of the Tip Path Plane ($a_{1s} = b_{1s} = 0$). Therefore, $C_{fz} = C_T$ and $|C_{mz}| = C_Q$ (the absolute value due to the fact that the sign of C_{mz} depends on the direction of rotation). Because of this, while we study the axial flight situation we will use C_T and C_Q and the terms “thrust” and “torque”. But it should not be forgotten at any moment that what we actually measure in the wind tunnel is C_{fz} and C_{mz} , and that what the rotor simulation provides are these coefficients too.

Both for the thrust and the torque we will be primarily interested in the curves of C_{fz} against λ_z and $-C_{mz}$ against λ_z .

The reason why we plot $-C_{mz}$ instead of C_{mz} is simply because the rotor we used in the wind tunnel tests rotated clockwise and thus C_{mz} is negative.

13.5 Thrust

If we take expression (9.38) and particularize it for axial flight ($\mu = 0$):

$$\frac{4C_T}{a\sigma} = \left(1 - \frac{e}{R}\right) \left(\frac{2}{3}\theta_0 + \frac{1}{2}\theta_1 - \lambda_z - \lambda_{ind}\right) \quad (13.2)$$

Since the thrust coefficient depends on a but not on c_{d0}, c_{d1}, c_{d2} , we can use C_T to estimate a . Later, we will use the torque coefficient to estimate c_{d0}, c_{d1}, c_{d2} . It should be remembered that the effective hinge offset e need not be estimated since it is perfectly defined once ω_{nr} is known.

As for the effect of a on C_T , a quick examination of expression (13.2) reveals that a is a factor affecting all the terms involved in that expression. Therefore a will not affect the “shape” of the curve of C_T against λ_z .

The main influence on the “shape” will come from λ_{ind} , that is, from the induced flow. And λ_{ind} will depend on the corrective function κ that we have chosen, as explained

before. If we assume κ to be 1 for $\lambda_z = 0$ (hover), then the value of λ_{ind} at that point will not depend on the function. Hence, it is possible to use the “hover” point to find a and then use the corrective function to adjust the shape.

Taking the “hover” point as a reference we find $a = 5.5$, which is equal to the typical value given by Bramwell in Ref 13.1. This is indeed an encouraging signal that shows that the rotor model is well conceived and that the value of c was well chosen too.

Once this is done we can test different κ until we find the one which produces the best fit between the theoretical and empirical values of C_T . Ideally, κ should be chosen to produce the best correlation between the theoretical and empirical values of λ_{ind} , not C_T . It should be remembered that the true meaning of λ_{ind} was given by Glauert’s formula (see Section 10). According to this formula, λ_{ind} was the local induced velocity at $\psi = \pm \frac{\pi}{2}$, non-dimensionalized with ΩR . But Glauert’s formula is not valid in axial flight. Therefore it is much more convenient to choose κ so that the theoretical C_T is well correlated to the experimental one.

After testing several κ , it was decided to use the following:

$$\kappa = 1 - \kappa_0 \lambda_z \quad (13.3)$$

With $\kappa_0 = 1.2$.

The figure on next page shows the experimental values of C_T , together with the solutions predicted by the Simulink model with the correction $\kappa = 1 - 1.2\lambda_z$ already included. It also shows the solution predicted by “classic” Momentum Theory (see Section 10).

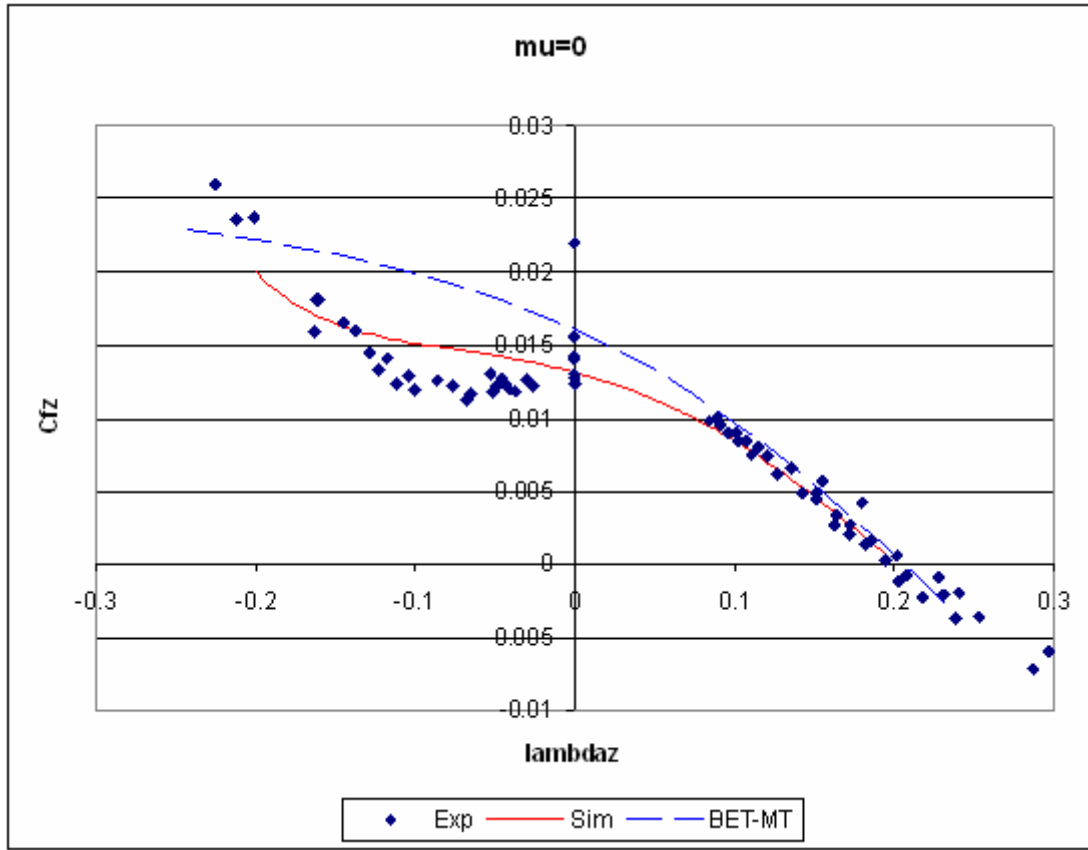


Fig 13.1. Thrust coefficient C_T (or C_{fz}) plotted against λ_z , in axial flight ($\mu = 0$).

The reason why κ was introduced was to try to represent the “pit” in the C_T curve, on the left, which might play an important role in some situations. In particular, this “pit” modifies the total damping introduced by C_T during certain manoeuvres. By introducing κ , which is bigger than 1 in the $\lambda_z < 0$ region, λ_{ind} is increased. If we look at (13.2), it is clear that increasing λ_{ind} will decrease C_T , thus reproducing the “pit” which is shown in the figure above.

However, it can be seen that $\kappa_0 = 1.2$ is not sufficient to adequately reproduce this “pit” in the C_T curve. In fact, it was found out that the effect of $\kappa = 1 - 1.2\lambda_z$ was almost negligible in the entire curve. It would be necessary to use a value higher than 1.2, but this in turn can deteriorate the correlation in other regions of the plot. This issue should be further investigated. Other corrective functions could be tested too.

There is another important phenomenon that can be observed in Figure 13.1, which is the dispersion of the experimental points for $\lambda_z = 0$ (hover condition). It is necessary to know that those points correspond to different regimes of the rotor (different values of Ω). According to our theoretical model, C_T does not depend on Ω . Therefore all the experimental points for $\lambda_z = 0$ should collapse into a single point. It can be seen that

some of the points are indeed very close to each other, while others are very far. The figure below identifies the spinning speeds associated to each of these points:

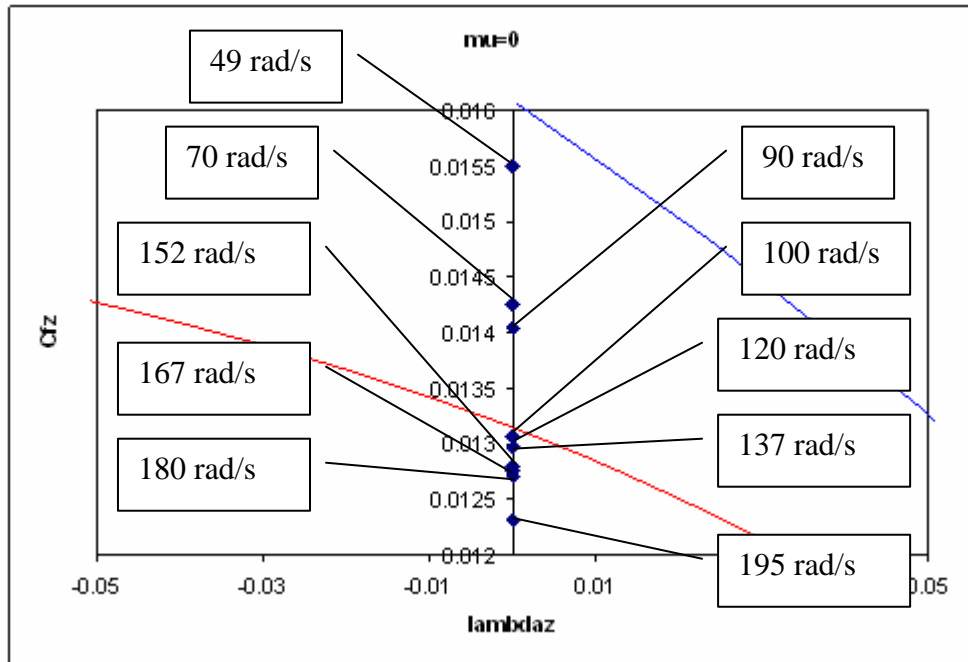


Fig 13.2. Dependence of the measured C_T on the spinning speed.

It can be seen that as Ω increases, the points tend to get concentrated. In fact, for values of Ω above 100 rad/s the points practically collapse into a single one, as expected. But below 100 rad/s there is indeed a great dispersion. At the beginning it was thought that this might have to do with the “ground effect”. The tests with no free stream ($\lambda_z = 0$) were carried out with the rotor horizontal and about 1.5m above the ground. This led to thinking that there might be some air recirculation which was causing the dispersion of the points. To investigate this issue the tests were repeated with the rotor vertical, so that downstream the airflow would not encounter the ground and thus would not be forced to move backwards. However, the result was the same: the dispersion of the points was still there. This led to the conclusion that this dispersion was correct, and that what was failing was the model. Later the fact that the dispersion of the points was correct was confirmed by the results of Felker and McKillip (see below).

The model we have developed is based on Blade Element Theory (BET) and “Modified” Momentum Theory (MMT). According to what we have just said, this model fails when the spinning speed of the rotor is too low, probably because the blades are not producing the predicted induced flow. It would be interesting to have a more accurate model based on wake methods (see Section 8) to confirm this.

Hence, we have found the first of several limitations of our model. All these limitations will be summarized in Section 15.

Anyway, since the rotors of the XPro will be rarely operating below 100rad/s (the value for hover is about 160rad/s) it can be assumed that C_T does not depend on Ω when $\lambda_z = 0$. It is important to comment that the estimate of a was obtained looking at the “hover” points corresponding to Ω higher than 100rad/s.

As for the rest of the experimental points, that is, those obtained for non-zero values of λ_z , it can be seen in Figure 13.1 that they fall over the same curve, which implies that they do not depend on Ω . Taking into account that these points were obtained at speeds higher than 100rad/s, this is consistent with what has been previously said, i.e., that above 100rad/s it can be assumed that C_T does not depend on Ω , as predicted by our model.

Comparison with the results by Felker and McKillip

Felker and McKillip (Ref 13.4) conducted a series of tests to study the behaviour of rotors in axial flight. Rather than installing the rotor in a wind tunnel and blowing air through it, they placed the rotor over rails and moved it at different speeds on a track which was 200 meters long.

Figure 13.3 (next page) shows the measured C_T for constant pitch, plotted against the non-dimensionalized vertical speed. It should be noted that this speed was non-dimensionalized with the hover induced velocity rather than with ΩR , as we have done. But the qualitative results are identical to those shown in Figure 13.1. The dispersion of the points for $V_z = 0$ can be seen clearly, and the right side of the “pit” is also present. It is important to realise that the range of values of V_z tested by Felker and McKillip is smaller than the one which has been covered here. The solid line represents the results obtained with BET combined with “classic” Momentum Theory (MT), and assuming uniform induced flow (as we have done). It can be seen that BET-MT fails to reproduce C_T for negative λ_z , just as was shown in Figure 13.1.

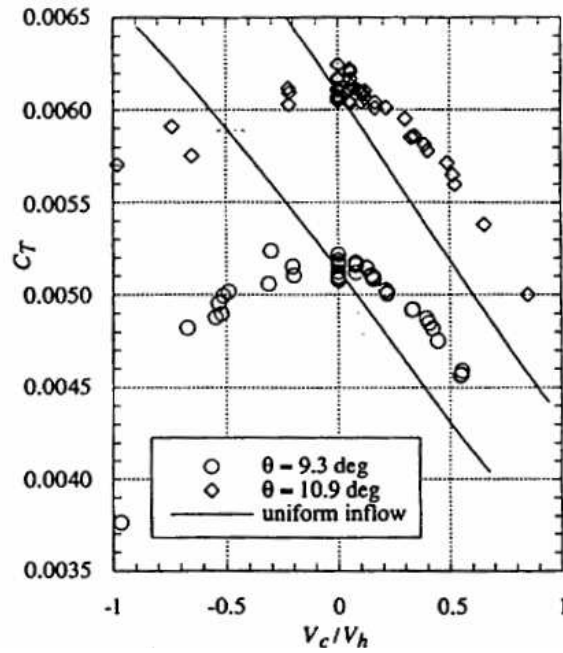


Fig 13.3. C_T values measured by Felker and McKillip. Two different pitch angles were used.

13.6 Torque

As it was said before, we can estimate c_d from the experimental measures of C_Q in axial flight. According to (9.42), when $\mu = 0$ it is:

$$\begin{aligned} \frac{4C_Q}{a\sigma} = & \frac{1}{2} \frac{c_{d0}}{a} + \frac{c_{d1}}{a} \left[\frac{1}{2} \theta_0 + \frac{2}{5} \theta_1 + \frac{2}{3} (-\lambda_z - \lambda_{ind}) \right] + \\ & + \frac{c_{d2}}{a} \left[\frac{1}{2} \theta_0^2 + \frac{1}{3} \theta_1^2 + (-\lambda_z - \lambda_{ind})^2 + \frac{4}{5} \theta_0 \theta_1 + \frac{4}{3} \theta_0 (-\lambda_z - \lambda_{ind}) + \theta_1 (-\lambda_z - \lambda_{ind}) \right] \end{aligned} \quad (13.4)$$

It can be seen that the effect of c_{d0} will be just to move vertically the curve “ C_Q against λ_z ”. Hence, we can use c_{d1} and c_{d2} to adjust the “shape” of the curve and then choose c_{d0} so that the curve passes through the point corresponding to $\lambda_z = 0$. Actually, there are several experimental points corresponding to $\lambda_z = 0$, just as it happened with C_T , and for the same reasons. However, the values of C_Q associated with moderate to high values of Ω collapse into a single point, as it also happened with C_T . It will be that point that we will use as a reference to obtain c_{d0} .

One simple way to adjust the “shape” of the curve with c_{d1} and c_{d2} is as follows. Firstly, we neglect the third term of (13.4). Since $\theta_0, \theta_1, \lambda_z, \lambda_{ind}$ are smaller than 1, this is

licit as a first approach. Then, assuming that for $\lambda_z > 0.15$ (approximately) it is $\frac{d\lambda_{ind}}{d\lambda_z} \approx 0$, we can derive (13.4) to obtain:

$$\frac{dC_Q}{d\lambda_z} \approx -\frac{2}{3} \frac{\sigma}{4} c_{d1} \quad (13.5)$$

Now, we take advantage of the fact that the experimental values of C_Q fall over the same imaginary line for $\lambda_z > 0.15$ (see Figure 13.4). Using the least squares method we can calculate this slope. Then we choose c_{d1} so that the slope is equal to (13.5). By doing so we obtain $c_{d1} \approx 0.7$.

To estimate c_{d2} we first derive C_Q using expression (13.4), but without neglecting any terms:

$$\frac{dC_Q}{d\lambda_z} = \frac{\sigma}{4} \left\{ -c_{d1} \frac{2}{3} \left(1 + \frac{d\lambda_{ind}}{d\lambda_z} \right) + c_{d2} \left[2(\lambda_z + \lambda_{ind}) \left(1 + \frac{d\lambda_{ind}}{d\lambda_z} \right) - \left(\frac{4}{3} \theta_0 + \theta_1 \right) \left(1 + \frac{d\lambda_{ind}}{d\lambda_z} \right) \right] \right\} \quad (13.6)$$

$$\frac{d^2 C_Q}{d\lambda_z^2} = \frac{\sigma}{4} \left(-c_{d1} \frac{2}{3} \frac{d^2 \lambda_{ind}}{d\lambda_z^2} + c_{d2} \left[2 \left(1 + \frac{d\lambda_{ind}}{d\lambda_z} \right)^2 - \left(\frac{4}{3} \theta_0 + \theta_1 \right) \frac{d^2 \lambda_{ind}}{d\lambda_z^2} \right] \right) \quad (13.7)$$

Afterwards, we take into account that in $\lambda_z = 0$ the slope of the curve of the induced velocity against the vertical speed is approximately $-\frac{1}{2}$ (see Figure 10.1) and so

$\frac{d\lambda_{ind}}{d\lambda_z} \approx -\frac{1}{2}$. In the vicinity of $\lambda_z = 0$, it can also be assumed that the rate of change of

this slope is zero. Therefore $\frac{d^2 \lambda_{ind}}{d\lambda_z^2} \approx 0$ for $\lambda_z = 0$. Besides, we can calculate λ_{ind} when

$\lambda_z = 0$ using BET-MMT. Looking at the experimental points in Figure 13.4, it seems plausible that there will be a inflection point at $\lambda_z \approx 0$. Therefore $\frac{d^2 C_Q}{d\lambda_z^2} \approx 0$ there.

Taking all this into account we enter in (13.7) and we obtain $c_{d2} \approx 0$. This is obviously a rough approximation but it will be seen later that it leads to good results.

Finally, we can select c_{d0} so that the theoretical C_Q is equal to the experimental one when $\lambda_z = 0$, thus obtaining $c_{d0} = 0.042$. However, it was found out that using this value C_Q was slightly underestimated for positive values of λ_z . Preferring to have

conservative results, it was decided to rise the value of c_{d0} so that it correlated better with those values, even if that meant overestimating C_Q in other ranges of λ_z . The final value adopted was then $c_{d0} = 0.05$.

The figure below compares the experimental data with the results obtained by Simulink using $c_d = 0.05 + 0.7\alpha$. It also shows the results when a constant drag coefficient $c_d = 0.08$ is used. It should be noted that $\kappa = 1 - 1.2\lambda_z$ was assumed.

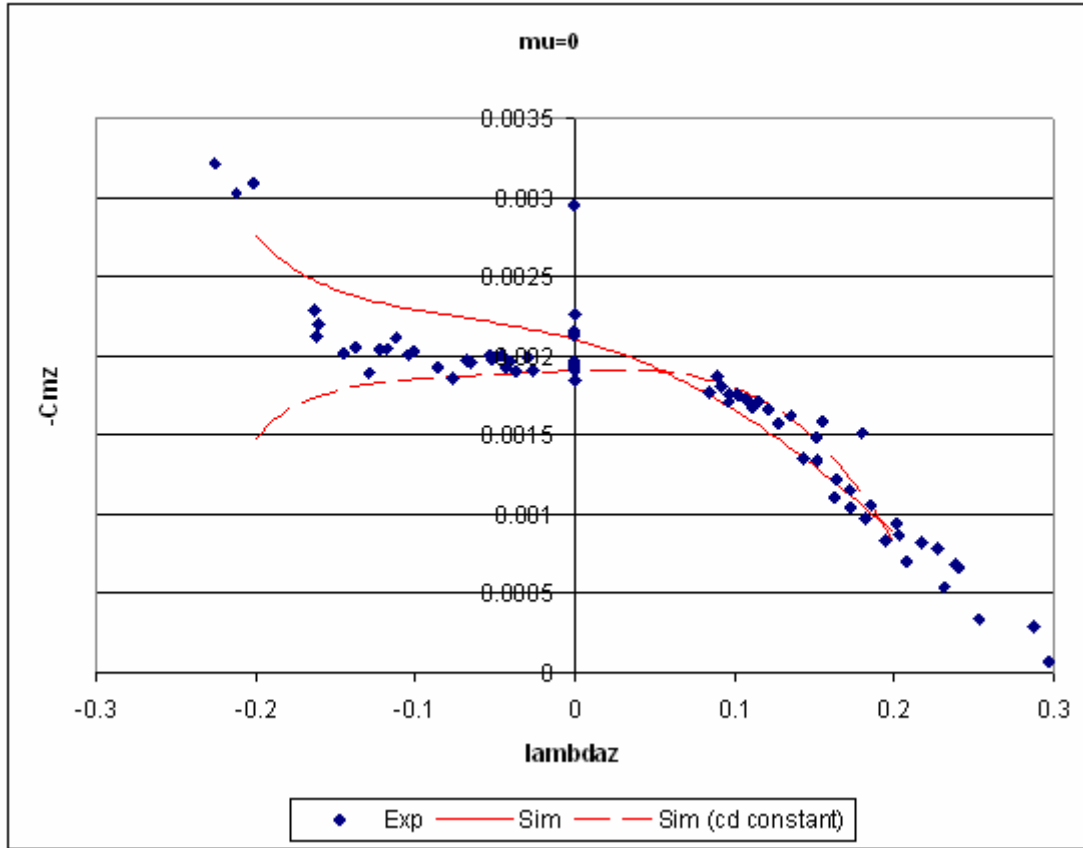


Fig 13.4. $-C_Q$ (or $-C_{mz}$) plotted against λ_z .

It can be seen that when a constant c_d is used there correlation is good for positive λ_z but the trend is wrong when λ_z is negative. This is the reason why the drag polar was introduced. When we use $c_d = 0.05 + 0.7\alpha$ the correlation for negative λ_z is much better. This issue is worth explaining in more detail.

As it was discussed in Section 10, there are four working states for every rotor: “Normal”, Vortex Ring, Turbulent Wake and Windmill Brake. The first corresponds to positive λ_z whereas the other three correspond to negative λ_z . From these three, Windmill Brake State is the regime associated with the most negative λ_z (highest

descent speeds). Figure 10.1 shows the induced velocity against the vertical speed (both non-dimensionalized with the hover induced velocity). In this figure the regions corresponding to each state are marked. It can be seen that as the vertical speed becomes more negative (higher rate of descent) the induced velocity decreases. Since the drag over the blade, and therefore the torque, are proportional to this induced velocity, we can expect that the torque will decrease as we move to the left. In fact, there will be a point, the “autorotation” point, where the torque will be zero (in the limit between TWS and WBS, if the drag due to friction is neglected). From there to the left the aerodynamic torque will be negative, that is, it will be *driving* the rotor rather than opposing to its movement.

This raises the question of why this does not happen in the case of the XPro. In Figure 13.4 it can be seen that, rather than decreasing with negative λ_z , the torque increases. The explanation lies in the fact that the curve of induced velocity against vertical velocity has been obtained for *constant* thrust. And this implies that the blade pitch is different at each point of the curve. However, in the XPro it is the contrary. The pitch is fixed, but not the thrust. In Figure 10.1 when the rotor approaches the autorotation point, the pitch decreases. From a physical point of view, the blade pitch has to be decreased to prevent the aerofoil drag from rising. In the XPro, since the pitch cannot be reduced, the drag rises dramatically thus preventing the rotor from entering autorotation. Instead, the torque keeps increasing as shown in Figure 13.4.

If we use a constant c_d , this effect will be hidden since the aerofoil drag will be highly independent from the blade pitch. The result is that the predicted C_Q will decrease instead of rising, as shown in Figure 13.4. That is why a more complex c_d is needed. The three-term polar provides a good approximation, according to most of the literature (see Refs 13.2 and 13.3, for example) and so it is the one used here.

The reader might be tempted to ask why so much effort is put in modelling accurately C_Q when it has been shown that C_T is already quite accurate. If C_T is good, wouldn't that be enough? The answer is that the thrust is implicitly related to the torque through Ω . If C_Q is badly predicted, then the calculated Ω will be wrong too, and therefore the thrust $T = \rho \pi R^4 \Omega^2 C_T$ will be wrong, even if C_T is right. That is why an accurate prediction for C_Q is as important as that for C_T .

13.7 Coning angles

Once $a, c_{d0}, c_{d1}, c_{d2}$ and κ have been determined, there are no more parameters of the rotor model that need to be estimated using the results from the wind tunnel. If before the tasks of estimating parameters and validating the model had been done simultaneously, from now on we will only deal with model validation.

While the tests of the rotor in hover were being carried out, a series of pictures were taken in order to estimate the coning angle a_0 . It should be remembered that in this situation (as well as when $\alpha = \pm \frac{\pi}{2}$) the flapping angles a_{1s} and b_{1s} are zero.

The photos were analyzed with specific software in order to measure accurately the coning angle. The figure below compares these measurements with the results predicted by Simulink (solid line).

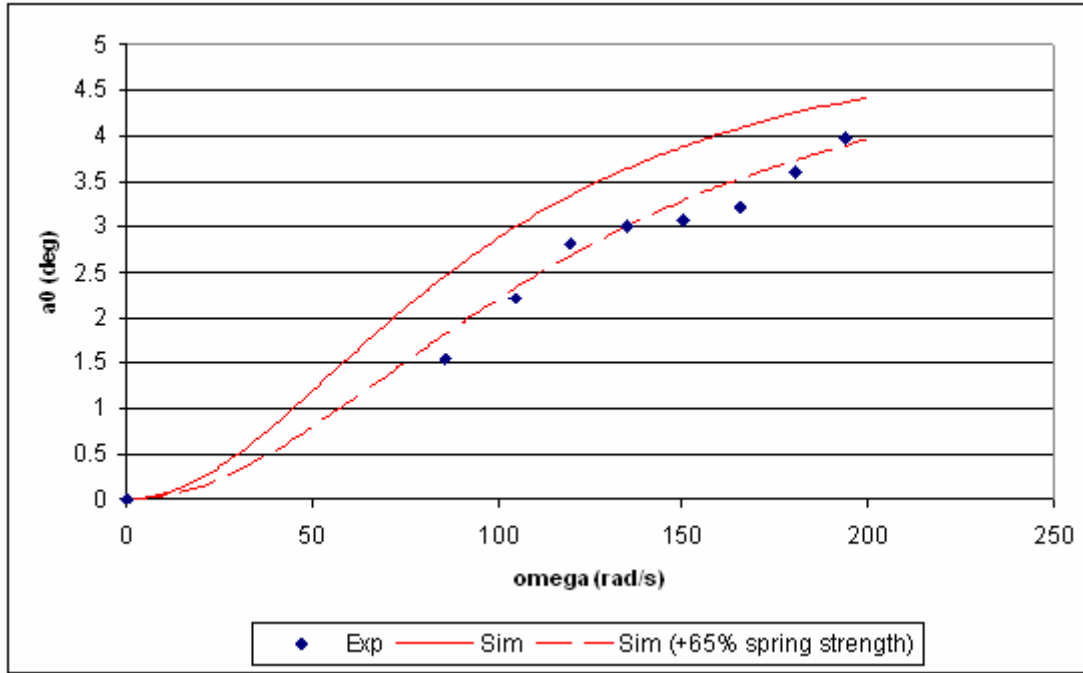


Fig 13.5. Coning angle a_0 in hover.

It can be seen that the model reproduces the trend for the real values of a_0 . However, the values predicted by the model are overestimated by approximately a 20%. This implies that the stiffness of the blade has been underestimated. In fact, if we increase by a 65% the strength k_β of the torsional spring in the idealized model (and we also modify ω_{nr} in accordance, as dictated by eq 9.53), the new predictions are much better (segmented line), the error being almost negligible.

It would have been interesting to measure the coning angles with the free stream blowing parallel to the axis of the hub (axial flight). It is likely that the model would have also predicted satisfactorily the trend for the values of a_0 .

Anyway, according to Bramwell (Ref 13.1), a_0 plays a very little part in flight dynamics compared to a_{1s} and b_{1s} . There is much more need to get right the flapping angles than a_0 , since they have a great influence on the in-plane forces and moments.

13.8 Ground effect

It is accepted in the specialized literature (see Refs 13.2 and 13.3, for example) that the ground effect in hover becomes noticeable when the altitude of the rotor above the ground is less than one rotor diameter. This also applies for axial flight, although in this case the problem is purely academic since a rotor moving vertically will soon be far from the ground!

For the XPro, an altitude of one rotor diameter is very low in absolute terms, just half a metre (about 1.6 feet). It seems probable that the XPro will rarely fly so close to the ground, except when taking off or landing. This is the main reason why no tests were done to assess the ground effect, the priority given to study more usual flight conditions. In any case, it will be seen in Section 14 that provisions have been made to include in the future a detailed model of the ground effect in the XPro simulation.

FORWARD FLIGHT

13.9 Introduction

The study of forward flight is more complex because there is a new variable, μ . However, this is not really a problem once we know how it will influence the different magnitudes. And this we know thanks to the rotor model that we have developed.

Since the TPP is tilted in forward flight, it is now necessary to make the difference between C_T and C_{fz} , and between C_Q and C_{mz} . We will refer to f_z and m_z as the “out-of-plane” force and moment, respectively.

13.10 Out-of-plane force

We can plot the $C_{fz}(\lambda_z, \mu)$ surface using our theoretical model:

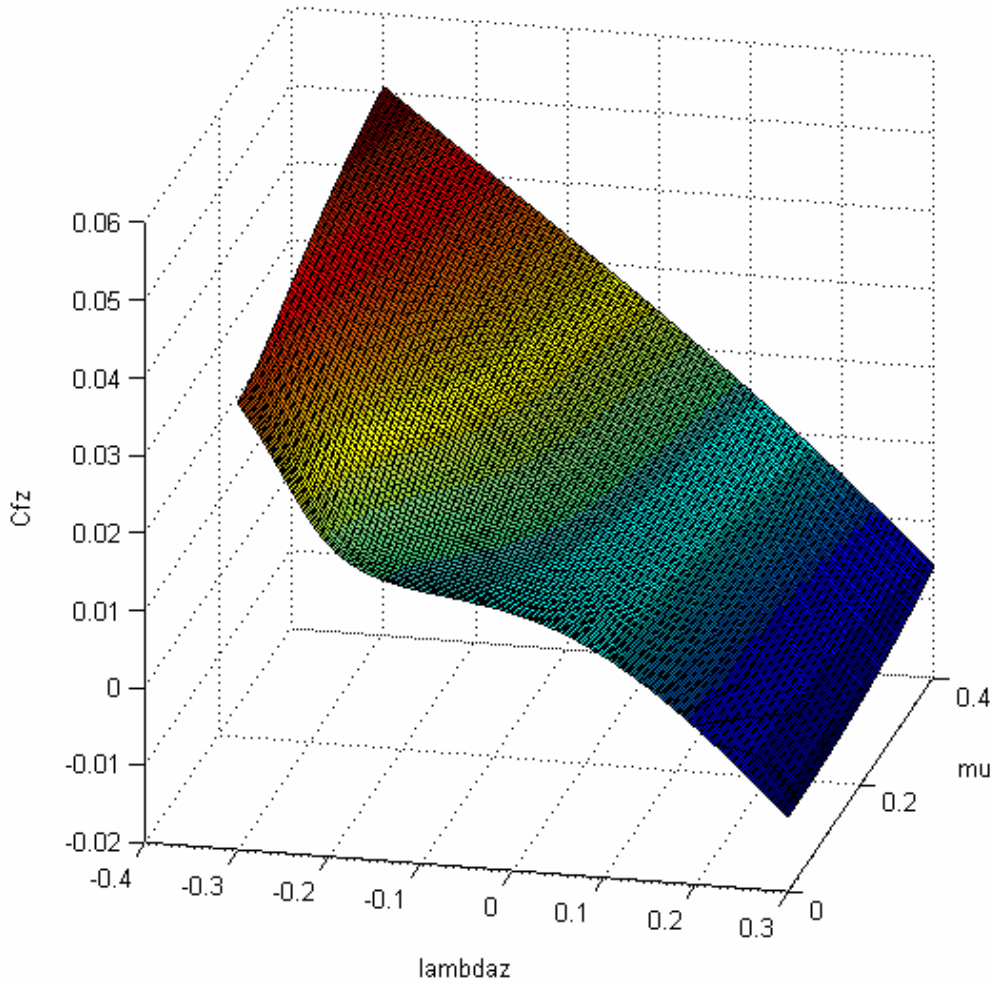


Fig 13.6. $C_{fz}(\lambda_z, \mu)$ surface.

Alternatively, we can plot C_{fz} against λ_z for discrete values of μ . This is what is shown in the figures of Appendix F:

When looking at those figures, it can be seen that the agreement between the Simulink model and the experimental results is good. The predicted values of C_{fz} are close to the real ones even in the region where λ_z is negative, which is the most complicated to model, as we have seen (Section 10). There is, of course, room for improvement, but the author believes that with the current rotor model, based on BET and MMT, it will be difficult to obtain much better predictions. A substantial increase in the accuracy of these predictions will only come with the use of more complex theories (free wake, prescribed wake...) or by replacing the theoretical model with an empirical one (which, however, will be less flexible).

13.11 Out-of-plane moment

The figure below shows the $-C_{mz}(\lambda_z, \mu)$ surface as calculated with the Simulink model of the rotor:

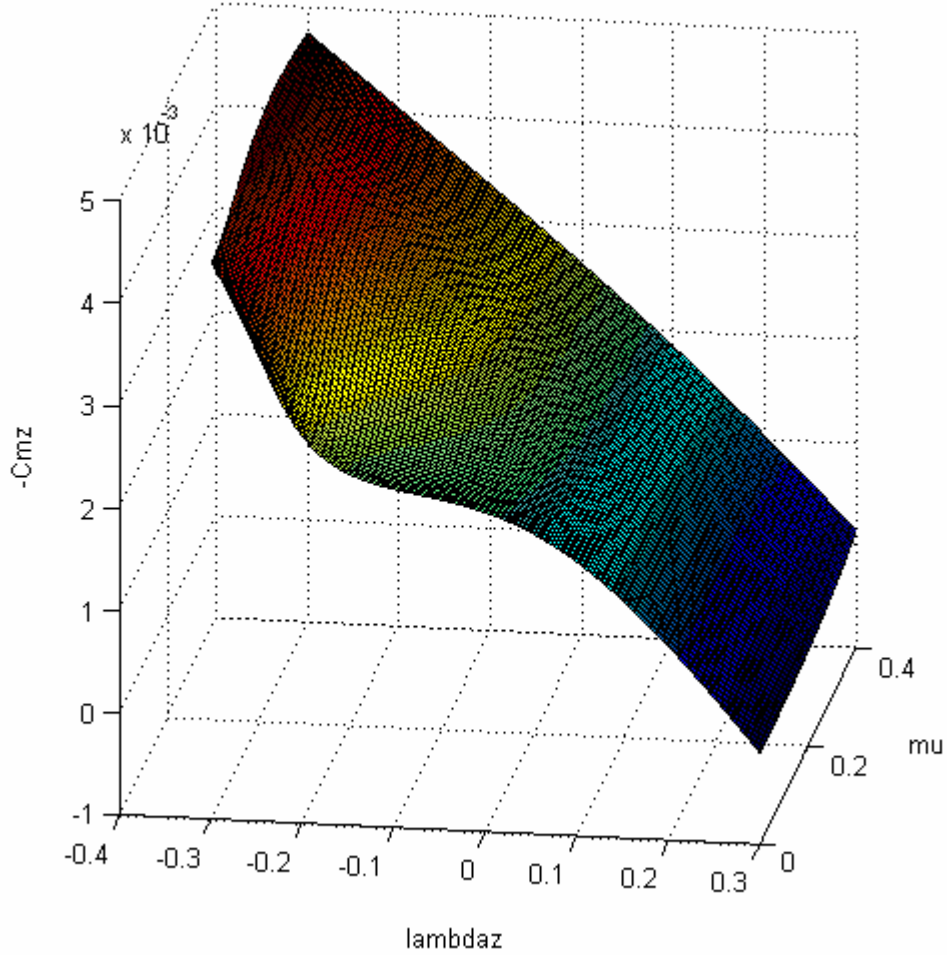


Fig 13.7. $-C_{mz}(\lambda_z, \mu)$ surface

The figures of Appendix F show $-C_{mz}$ against λ_z for discrete values of μ :

It can be seen that, as it happened with C_{fz} , the agreement with the experimental results is good, even in the region where λ_z is negative. The use of $c_d = c_{d0} + c_{d1}\alpha + c_{d2}\alpha^2$ is definitely contributing to improve the correlation in this region.

Again, it is felt that significant improvements in the predicted $-C_{mz}$ can only be achieved by using more sophisticated theories.

13.12 Flapping angles

As it was explained in Section 9, the flapping angles a_{1s}, b_{1s} are expected to be zero in hover and axial flight. This was confirmed during the wind tunnel tests. However, when $\mu \neq 0$, that is, in the rest of the flight conditions, a_{1s}, b_{1s} become quite important. These two angles affect the flight dynamics of the vehicle in three ways, as it was explained in Section 9:

- They determine the tilt of the Tip Path Plane (TPP) and so the tilt of the thrust vector \mathbf{T} and the torque vector \mathbf{Q}
- They determine the magnitude of the hub moments produced by the out-of-plane component of the centrifugal force applied at the hinge
- They determine the magnitude of the torque produced by the torsional spring

As a result, a_{1s}, b_{1s} are the main variables that determine the in-plane forces and moments, that is, the forces and moments parallel to the Hub Plane HP (it is true, though, that there is a force H which has an in-plane component and which is non-zero even if $a_{1s} = b_{1s} = 0$).

Since the in-plane forces and moments play an essential role in the Stability and Control of the quadrotor (the other element that plays a key role is the damping introduced by the thrust, see Section 16), it is very important to predict accurately a_{1s} and b_{1s} .

In Section 9 it was explained that the expressions derived for a_{1s} and b_{1s} had some disagreements with empirical results. The main problem was with b_{1s} , because it strongly depended on the longitudinal distribution of induced velocity (through K_c). It was seen that, in order to get b_{1s} right, K_c had to tend to zero when μ did. But, on the other hand, above $\mu = 0.1$, K_c had to tend to 1 as μ increased. This is an important issue if we consider that during normal operation μ will be precisely between 0 and 0.1.

Nevertheless, it was decided to assume $K_c = 0$, which implied assuming uniform induced flow in all the flight conditions. Although we have seen that this leads to significant errors in b_{1s} , particularly between $\mu = 0.02$ and $\mu = 0.2$, it was concluded that there was no other practical solution. $K_c = 1$ was rejected because it led to non-zero values of b_{1s} in axial flight, and this was considered unacceptable taking into account that the XPro would probably be flying in that regime very often.

However, $K_c = 1$ had already been used to integrate C_T, C_H, C_Q . In this case, though, it was decided to leave it like that, because $K_c = 1$ gives better results starting from very

low values of μ , and because when $\mu = 0$ (when $K_c = 1$ is incorrect) the error is very small.

To assess the ability of the model to predict the flapping angles, several experimental measures were available. These had been obtained in the same way as with the coning angles in axial flight, that is, analyzing several pictures that had been taken while the rotor was running at the wind tunnel. Unfortunately, all the images available had been taken from the side, so that $\beta(\psi = \pi)$ could be measured but not $\beta\left(\psi = \frac{3\pi}{2}\right)$.

Considering that:

$$\beta(\psi = \pi) = a_0 + a_{1s}$$

$$\beta\left(\psi = \frac{3\pi}{2}\right) = a_0 + b_{1s}$$

This meant that no information could be obtained about b_{1s} . In retrospective, it would have been more interesting to know $a_0 + b_{1s}$ rather than $a_0 + a_{1s}$, because we have seen that there are more problems to estimate b_{1s} than a_{1s} , but this was not clear when the tests were done.

The figures on next page compare the predicted and the real values of $a_0 + a_{1s}$ (solid line). The latter were taken with a constant airspeed of 15.5m/s which, when combined with the different rpm settings, gave higher μ than those which are more frequent during normal operation of the XPro.

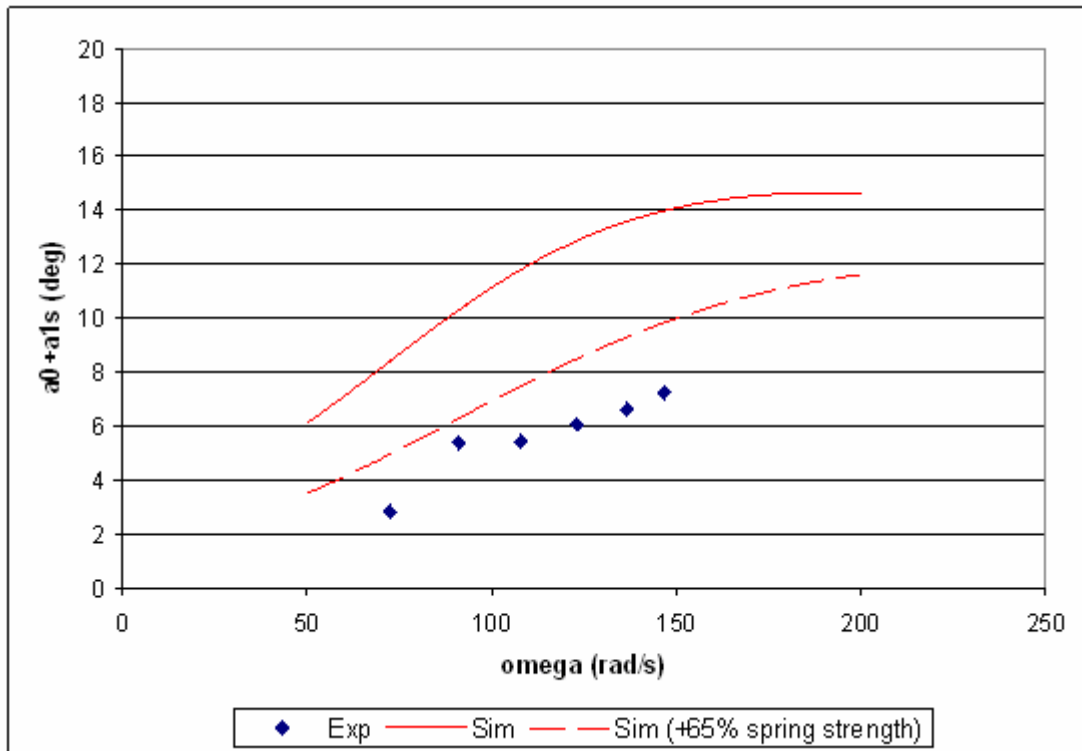


Fig 13.8. $a_0 + a_{1s}$, against Ω (rotor horizontal, free stream velocity of 15.5m/s)

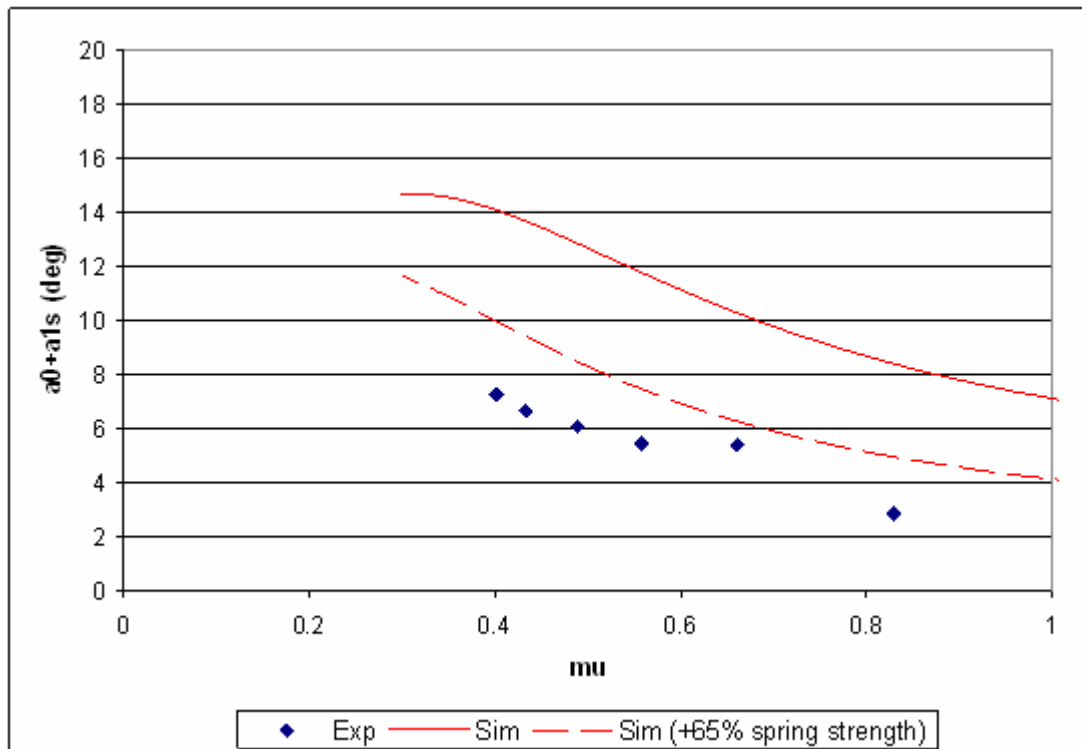


Fig 13.9. $a_0 + a_{1s}$ against μ (rotor horizontal, free stream velocity of 15.5m/s)

As it happened with the coning angle, the model represents satisfactorily the trend for the values of the flapping angles, but it overestimates them, in this case by a larger percentage, around a 100%. Again, this is because the real stiffness of the blade has been underestimated. If we increase the spring strength k_β by a 65% (and we also modify ω_{nr} in accordance, as dictated by eq 9.53), the error is reduced to a 30% (segmented line).

On the other hand, modifying the coefficient of Southwell, α_1 (see sub-section 9.16), does not seem to improve the correlation.

It should be remembered that k_β had been inferred from a set of tests in which the blade was bent as a result of applying a vertical load (see sub-section 9.18). It is not clear why the value of k_β thus obtained leads to overestimating the coning and flapping angles, and therefore this issue should be investigated further.

Some additional comments about the lateral flapping angle

According to Prouty (Ref 13.3), b_{1s} is usually positive. However, this is not true in every case. There are rotors in which it is the contrary, and those of the XPro are one example.

In a fully articulated rotor with no hinge offset ($k_\beta = 0, e = 0$) the lateral flapping angle b_{1s} will be positive. But if $k_\beta \neq 0$ and/or $e \neq 0$, then it might occur that b_{1s} becomes negative. This is what happens in the XPro rotor in forward flight, at moderate to high speeds.

From a physical point of view, a negative b_{1s} means that a clockwise rotor will tilt to right instead of doing it to left (as seen from behind). This was confirmed in the wind tunnel.

13.13 In-plane forces

Unfortunately, the error of the balance used in the wind tunnel tests was of the same order of magnitude as the in-plane forces. This limitation, which was already commented in the previous section, effectively prevents us from getting any reliable information about these forces. Moreover, the balance could only measure the in-plane forces in one direction (that contained in a plane which was parallel to the free stream) and as a result no measures of f_y are available. If b_{1s} was zero in forward flight, then this would not be a problem because it would be $f_y = 0$. But we have shown that b_{1s} is not zero (the TPP tilts laterally apart from longitudinally).

Appendix F contains a set of figures that compare the measured and the estimated C_{fx} for different values of μ . Both the model and the measures agree in the order of magnitude of C_{fx} . They also agree in the fact that C_{fx} increases with μ . However, it can be seen that, for a given μ , the experimental points are very scattered, which makes it very difficult to identify any trend. This dispersion might be indicating that the random error due to the balance is very high as we were suspecting.

Hence, because of this error, no solid conclusions can be established.

13.14 In-plane moments

As it happened with the in-plane forces, the error of the balance is of the same order of magnitude (or higher) than the in-plane moments we intend to measure. This is probably the reason why the experimental points have so much dispersion (see the relevant figures in Appendix F).

Pitch moment

The $(C_{my})_{hub}$ given by Simulink is of the same order of magnitude as the measured one. It also has the same sign, which means that the direction of the moment is well predicted. The theoretical $(C_{my})_{hub}$ is fairly insensitive to μ , although a closer look at the curves reveals that it slightly increases with μ . As for the measured $(C_{my})_{hub}$, the points are so scattered that it is difficult to identify any trend with μ or λ_z .

Roll moment

Most of what has been said regarding $(C_{my})_{hub}$ can also be applied to $(C_{mx})_{hub}$. The theoretical $(C_{mx})_{hub}$ has the same order of magnitude as the experimental one. Besides, they both have the same sign (except for very low values of μ). The predicted $(C_{mx})_{hub}$ increases with μ , as it happened with the theoretical $(C_{my})_{hub}$.

Again, the experimental points are very scattered and it is difficult to identify any trend. This dispersion of the points might be an indicator of the error of the balance.

Apart from the error of the balance, there is another reason for the lack of accuracy in the measures of $(C_{mx})_{hub}$. This is the fact that the balance could only measure forces in two of the three axes (see Section 12). Hence, there is a missing force, whose contribution to the roll moment is unknown.

13.15 Ground effect

Ground effect in forward flight will be very rare for a quadrotor, because of the risk of collision with the ground or with obstacles when moving at moderate speeds at very low

altitude. Besides, the study of ground effect in this flight condition is much more complex than in hover. For all these reasons, ground effect in forward flight is just ignored.

13.16 “No blades”

Some wind tunnel tests were made without the blades. But again, the results are not reliable due to the error of the balance.

CONCLUSIONS

It should be remembered that the two aims of this Section were to estimate the parameters required by the rotor model and to validate it.

The parameters $a, c_{d0}, c_{d1}, c_{d2}$ have been inferred from the curves of C_T and C_Q against λ_z in axial flight. It has been found that a was equal to the typical value given by Bramwell (Ref 13.1), and that a linear drag polar ($c_{d2} = 0$) produced good predictions of C_Q . On the other hand, it has been confirmed that a constant c_d is inadequate to model C_Q . A corrective factor κ for λ_{ind} has also been obtained, but has been found to be almost irrelevant.

Overall, the predictions of C_T and C_Q have been found to be satisfactory. However, there is a high disagreement between the calculated and the experimental C_T and C_Q when the spinning speed Ω is very low (below $80-100 \text{ rad/s}$). This is likely to be caused by the intrinsic limitations of the BET-MMT theory that has been used as the basis for the model.

The predicted values of the coning angle a_0 are well correlated with the experimental measures. The predicted $a_0 + a_{1s}$ was overestimated, probably because k_β was underestimated. But at least the model was able to predict correctly the trend for $a_0 + a_{1s}$. On the other hand, no experimental data was available to assess the quality of the predictions of the lateral flapping angle b_{1s} . In fact, it is now clear that it is more complex to estimate b_{1s} than a_{1s} , because of its high sensitivity to small changes in μ .

C_{fz} and C_{mz} have been plotted against λ_z for different values of μ . In both cases the correlation with experimental data was satisfactory. On the other hand, it has been impossible to establish decisive conclusions about the quality of the predictions of C_{fx} , $(C_{mx})_{hub}$ and $(C_{my})_{hub}$, because of the error in the measures of the in-plane forces and

moments. But it has been found that the predicted $C_{fx}, (C_{mx})_{hub}, (C_{my})_{hub}$ have the same sign and order of magnitude as the measured ones.

All in all, it can be said that rotor model validation has been successful, but incomplete. Successful, because the variations of thrust and torque with λ_z, μ and Ω are well modelled for a large range of values of those variables. Incomplete, because it has not been possible to reach similar conclusions for the in-plane forces and moments. This is not due to flaws of the model but to the lack of reliable experimental data.

It is likely that further refinements of the model based on BET-MMT (see Section 9) will improve the accuracy of the results. However, these improvements will probably be limited. To really improve the results it will be necessary to move to more sophisticated aerodynamic models, such as prescribed and free wake methods.

Another possibility to improve the predictions would be to apply system identification methods to the rotor (see Section 8). Nevertheless, this would require a great amount of reliable experimental data.

14. THE MATLAB/SIMULINK MODEL OF THE QUADROTOR

INTRODUCTION

14.1 Overview of the previous work and its importance

As it was stated in the Summary and in the Introduction of this Report, the main purpose of this Project is to develop a Matlab/Simulink model of the Draganfly XPro, which will serve to predict its flight dynamics. All the work which has been described in the previous sections was done in order to obtain the information that was required by the Matlab/Simulink model. It will be remembered that this information comprised the following:

- Equations of Motion
- Electric equations of the DC motors
- Modelling of the rotor
- Modelling of the induced flow
- Modelling of the aerodynamic forces and moments over the airframe
- Mass and inertial properties

Now that this information has been gathered, it is possible to build the Simulink model.

As for the numerical data, such as the masses, the moments of inertia, the parameters of the motors, etc, it has been previously shown how they were obtained and in which equations they appeared. Therefore no additional comments about them will be made in this Section.

As for the equations of motion, the electric equations of the motors and the model of the aerodynamic forces and moments, some comments will be made if necessary. In any case, the reader is strongly advised to go slowly through the sections related to these topics before starting with this one.

14.2 Brief description of the model

The physical model which has been developed in the previous sections will be contained in a single Simulink block called “Quadrotor” whose inputs are the four motor voltages $v_{a1}, v_{a2}, v_{a3}, v_{a4}$ and the three components of the gust velocity V_{gx}, V_{gy}, V_{gz} . The outputs can be selected at will from all the variables available, but default ones will be $x_e, y_e, z_e, u_e, v_e, w_e, \phi, \theta, \psi, u, v, w, p, q, r$.

There will be an external block in charge of providing the voltage signals and another one which generates the gust velocity vector (“Signal” and “Gusts” blocks, respectively).

14.3 Summary of the equations available

It is convenient to remember the basic equations and formulae that define the physical model of the quadrotor. The reader is advised to refer to the relevant sections in order to revise the notation used.

Eq. of Forces:

$$\sum_i \mathbf{F}_i + m_T \mathbf{g} + \mathbf{F}_{\text{airframe}} = m_T \left(\mathbf{a}_o + \frac{d\boldsymbol{\omega}}{dt} \times \mathbf{OG}_T + \boldsymbol{\omega} \times (\boldsymbol{\omega} \times \mathbf{OG}_T) \right) \quad (4.36)$$

Eq. of Moments:

$$\begin{aligned} & \sum_i (\mathbf{M}^{\text{Pi}} + \mathbf{OP}_i \times \mathbf{F}_i) + \mathbf{M}_{\text{airframe}}^o - \mathbf{OG}_T \times \left(\sum_i \mathbf{F}_i + \mathbf{F}_{\text{airframe}} \right) = \sum_i \left(\frac{d}{dt} \mathbf{H}_{\text{Pi}} \right)_{\text{mean}} + \\ & + \left(\sum_i \mathbf{I}_{\text{OPi}} + \sum_i \mathbf{I}_{\text{Gi}} + \sum_i \mathbf{I}_{\text{OGi}} + \sum_j \mathbf{I}_{\text{Gj}} + \sum_j \mathbf{I}_{\text{OGj}} + \mathbf{I}_G + \mathbf{I}_{\text{OG}} - \mathbf{I}_{\text{OG}_T} \right) \cdot \frac{d\boldsymbol{\omega}}{dt} + \\ & + \boldsymbol{\omega} \times \left(\sum_i \mathbf{I}_{\text{OPi}} + \sum_i \mathbf{I}_{\text{Gi}} + \sum_i \mathbf{I}_{\text{OGi}} + \sum_j \mathbf{I}_{\text{Gj}} + \sum_j \mathbf{I}_{\text{OGj}} + \mathbf{I}_G + \mathbf{I}_{\text{OG}} - \mathbf{I}_{\text{OG}_T} \right) \cdot \boldsymbol{\omega} - \\ & - \sum_i \mathbf{I}_{\text{Gi}} \cdot \dot{\Omega}_i \mathbf{k} - \boldsymbol{\omega} \times \sum_i \mathbf{I}_{\text{Gi}} \cdot \Omega_i \mathbf{k} - \sum_j \mathbf{I}_{\text{Gj}} \cdot g_r \dot{\Omega}_i \mathbf{k} - \boldsymbol{\omega} \times \sum_j \mathbf{I}_{\text{Gj}} \cdot g_r \Omega_i \mathbf{k} \end{aligned} \quad (4.45)$$

Balance of torques:

$$\frac{M_{zi}}{g_r} - \tau_j + F g_r \Omega_i = \frac{b I_{zb} + I_{zi}}{g_r} (\dot{r} - \dot{\Omega}_i) + I_{zj} (\dot{r} - g_r \dot{\Omega}_i) \quad (4.50)$$

Electric equation of the motor:

$$\pm v_{aj} = K g_r \Omega_i + \frac{R_a}{K} \tau_j + \frac{L_a}{K} \dot{\tau}_j \quad (6.7)$$

“Kinematic” relations:

$$\begin{aligned} \dot{\phi} &= p + (q \sin \phi + r \cos \phi) \tan \theta \\ \dot{\theta} &= q \cos \phi - r \sin \phi \\ \dot{\psi} &= (q \sin \phi + r \cos \phi) \sec \theta \end{aligned} \quad (4.38)$$

“Navigation” equations:

$$(\mathbf{v}_o)_e = \mathbf{M}_{DC}^T \cdot \mathbf{v}_o \quad (4.52)$$

Modelling of the rotor:

$$\mathbf{M}^{Pi} - \left(\frac{d}{dt} \mathbf{H}_{Pi} \right)_{mean} = (M_{xi})_{hub} \mathbf{i} + (M_{yi})_{hub} \mathbf{j} + (M_{zi})_{hub} \mathbf{k} \quad (9.23)$$

Aerodynamics of the airframe:

$$\mathbf{F}_{airframe} \approx \mathbf{0} \quad \mathbf{M}_{airframe}^o \approx \mathbf{0}$$

14.4 Basic requirements for the solving algorithm

When designing the Simulink model, one of the key constraints is to avoid algebraic loops. These slow down the simulation and might even cause the simulation to stop. Besides, if there are any algebraic loops in the model it is not possible to use Real Time Workshop, which is an interesting tool that might be needed for future work with the model.

Any system with algebraic loops can be expressed as $\dot{\mathbf{x}} = \mathbf{F}(\mathbf{x}, \dot{\mathbf{x}}, \mathbf{t})$, where \mathbf{x} is the state-space vector. To get rid of the algebraic loops, the system has to be re-formulated as $\dot{\mathbf{x}} = \mathbf{F}(\mathbf{x}, \mathbf{t})$.

Apart from avoiding algebraic loops, which is compulsory, it would be advisable to uncouple the equations as much as possible, in order to simplify the model (which is always convenient).

Many Matlab/Simulink models include S-Functions. These are useful especially for calculations that otherwise would require a complex grouping of blocks. However, S-Functions slow down the simulation (because each time that an S-Function is to be executed, Matlab calls the interpreter, and this consumes time). Therefore, the number of S-Functions should be kept to a minimum.

“DYNAMICS” BLOCK

14.5 Introduction

The function of the “Dynamics” block is to integrate the state-space vector $\mathbf{x} = (p, q, r, \phi, \theta, \psi, u, v, w, x_e, y_e, z_e, \Omega_1, \tau_1, \Omega_2, \tau_2, \Omega_3, \tau_3, \Omega_4, \tau_4)$. We will see that to do so, it requires $F_{xi}, F_{yi}, F_{zi}, (M_{xi})_{hub}, (M_{yi})_{hub}, M_{zi}$ and the voltages $v_{a1}, v_{a2}, v_{a3}, v_{a4}$. While the voltages are the control parameters and thus are set externally, the forces and moments

need to be calculated using the model seen in Sections 9 and 10. This will be done in a specific block called “Rotors”. Since $F_{xi}, F_{yi}, F_{zi}, (M_{xi})_{hub}, (M_{yi})_{hub}, M_{zi}$ depend on $p, q, r, u, v, w, \Omega_1, \Omega_2, \Omega_3, \Omega_4$ but not on their derivatives, no algebraic loops will be created.

For the moment it will be assumed that $F_{xi}, F_{yi}, F_{zi}, (M_{xi})_{hub}, (M_{yi})_{hub}, M_{zi}$ have already been calculated.

14.6 Calculation of the rotating speed of the rotors and the EM torque

Care has to be taken to avoid algebraic loops.

The easiest way to proceed is probably the one which is now described. First, we merge equations (4.50) and (6.7) into a single system. Using matrix notation:

$$\begin{bmatrix} \dot{\Omega}_i \\ \dot{\tau}_j \end{bmatrix} = \begin{bmatrix} \frac{-Fg_r}{g_r} & \frac{1}{g_r} \\ \frac{bI_{zb} + I_{zi} + g_r I_{zj}}{g_r} & \frac{bI_{zb} + I_{zi} + g_r I_{zj}}{g_r} \\ -\frac{K^2 g_r}{L} & -\frac{R_a}{L} \end{bmatrix} \begin{bmatrix} \Omega_i \\ \tau_j \end{bmatrix} + \begin{bmatrix} \left(\frac{bI_{zb} + I_{zi} + I_{zj}}{g_r} \right) \dot{r} - \frac{M_{zi}}{g_r} \\ \frac{bI_{zb} + I_{zi} + g_r I_{zj}}{g_r} \\ \pm \frac{K}{L} v_{aj} \end{bmatrix} \quad (14.1)$$

The term with \dot{r} can be neglected. This is convenient in order to simplify the problem.

From (14.1) we obtain $\dot{\Omega}_i$ and $\dot{\tau}_j$ and, integrating, Ω_i and τ_j . This is done in the block “Motor” whose content is shown in the figure below:

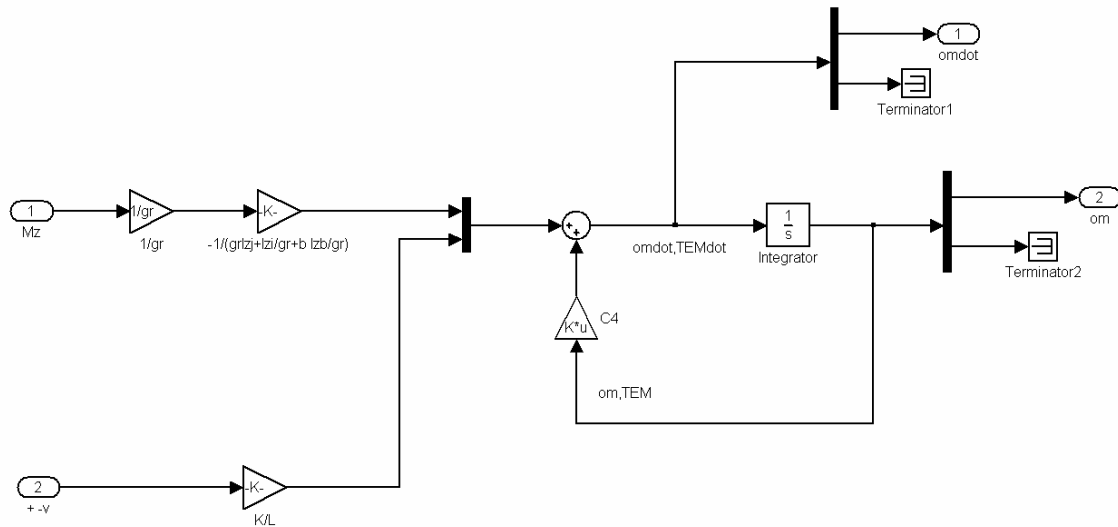


Fig 14.1. Interior of block “Motor”

14.7 Calculation of the body angular rates

To calculate these angular rates we need equations (4.45) and (9.23). We also need:

$$(M_{zi})_{hub} = M_{zi} - bI_{zb}(\dot{r} - \dot{\Omega}_i) \quad (9.22)$$

$$\mathbf{M}^{Pi} - \left(\frac{d}{dt} \mathbf{H}_{Pi} \right)_{mean} = (M_{xi})_{hub} \mathbf{i} + (M_{yi})_{hub} \mathbf{j} + (M_{zi})_{hub} \mathbf{k}$$

With (4.45), (9.22) and (9.23):

$$\begin{aligned} & \sum_i \left((M_{xi})_{hub} \mathbf{i} + (M_{yi})_{hub} \mathbf{j} + M_{zi} \mathbf{k} + \mathbf{OP}_i \times \mathbf{F}_i \right) + \mathbf{M}_{airframe}^O - \mathbf{OG}_T \times \left(\sum_i \mathbf{F}_i + \mathbf{F}_{airframe} \right) = \\ & = \left(\sum_i \begin{bmatrix} 0 & 0 & 0 \\ 0 & 0 & 0 \\ 0 & 0 & bI_{zb} \end{bmatrix} + \sum_i \mathbf{I}_{OPi} + \sum_i \mathbf{I}_{Gi} + \sum_i \mathbf{I}_{OGi} + \sum_j \mathbf{I}_{Gj} + \sum_j \mathbf{I}_{OGj} + \mathbf{I}_G + \mathbf{I}_{OG} - \mathbf{I}_{OG_T} \right) \cdot \frac{d\boldsymbol{\omega}}{dt} + \\ & + \boldsymbol{\omega} \times \left(\sum_i \mathbf{I}_{OPi} + \sum_i \mathbf{I}_{Gi} + \sum_i \mathbf{I}_{OGi} + \sum_j \mathbf{I}_{Gj} + \sum_j \mathbf{I}_{OGj} + \mathbf{I}_G + \mathbf{I}_{OG} - \mathbf{I}_{OG_T} \right) \cdot \boldsymbol{\omega} - \\ & - \sum_i \begin{bmatrix} 0 & 0 & 0 \\ 0 & 0 & 0 \\ 0 & 0 & bI_{zb} \end{bmatrix} \dot{\Omega}_i \mathbf{k} - \sum_i \mathbf{I}_{Gi} \cdot \dot{\Omega}_i \mathbf{k} - \boldsymbol{\omega} \times \sum_i \mathbf{I}_{Gi} \cdot \Omega_i \mathbf{k} - \sum_j \mathbf{I}_{Gj} \cdot g_r \dot{\Omega}_i \mathbf{k} - \boldsymbol{\omega} \times \sum_j \mathbf{I}_{Gj} \cdot g_r \Omega_i \mathbf{k} \end{aligned} \quad (14.2)$$

It should be noted that, to evaluate \mathbf{I}_{OPi} , it will be assumed that $O_i \approx P_i$.

Entering with $\dot{\Omega}_i$ and Ω_i in (14.2) we can obtain $\dot{p}, \dot{q}, \dot{r}$. This is done in Block “Dynamics” (see Figure 14.2, on next page). Once $\frac{d\boldsymbol{\omega}}{dt} = \dot{p}\mathbf{i} + \dot{q}\mathbf{j} + \dot{r}\mathbf{k}$ has been calculated, Block “Dynamics” also integrates it to get $\boldsymbol{\omega} = p\mathbf{i} + q\mathbf{j} + r\mathbf{k}$.

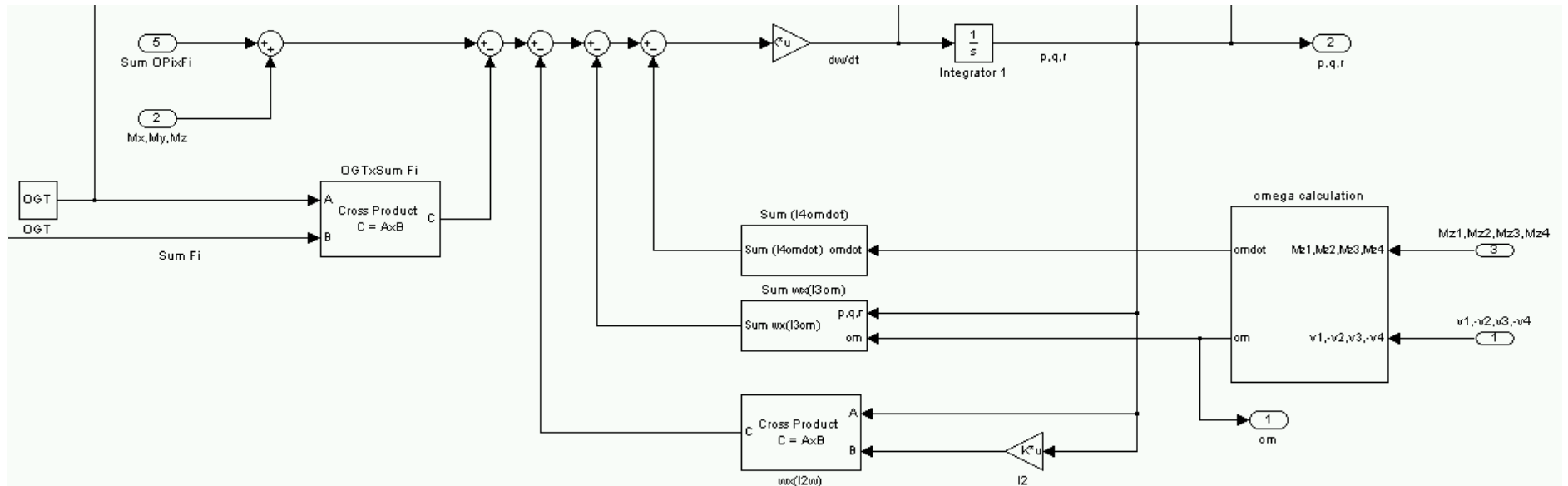


Fig 14.2. Detail of Block “Dynamics” showing how the angular rates are calculated.

14.8 Calculation of the velocity and position of O

Entering with p, q, r in (4.38) we can obtain $\dot{\phi}, \dot{\theta}, \dot{\psi}$ and then integrate to get ϕ, θ, ψ . This is done in Block “Euler”.

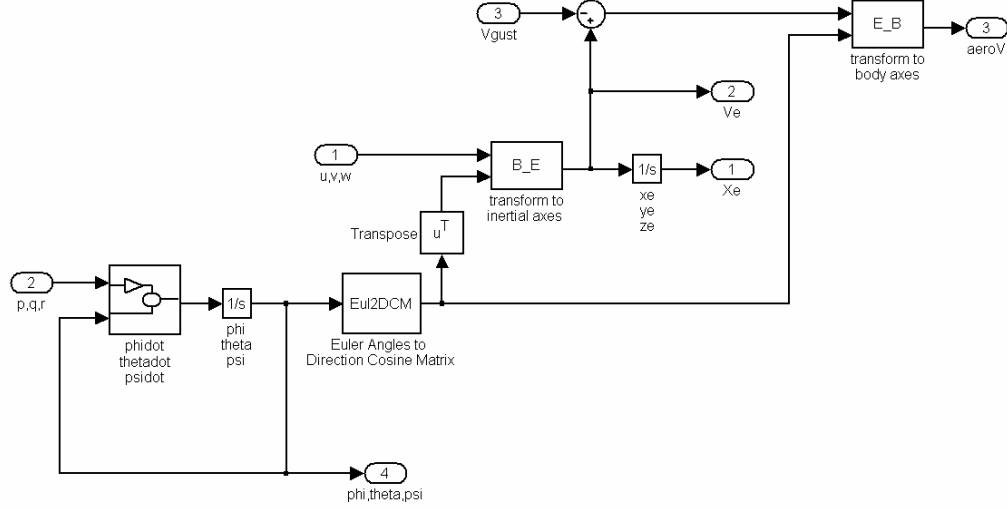


Fig 14.3. Interior of Block “Euler”

With ϕ, θ, ψ we can calculate \mathbf{g} by using $\mathbf{g} = -\sin \theta \mathbf{i} + \sin \phi \cos \theta \mathbf{j} + \cos \phi \cos \theta \mathbf{k}$.

Then, with \mathbf{g} , $\boldsymbol{\omega}$ and $\frac{d\boldsymbol{\omega}}{dt}$ in (4.36) it is immediate to obtain \mathbf{a}_O and, by integration, $\mathbf{v}_O = u\mathbf{i} + v\mathbf{j} + w\mathbf{k}$. This is done in the “Dynamics” block.

Using (4.52) $(\mathbf{v}_O)_e$ is then calculated. Finally, the coordinates of O in $O_e x_e y_e z_e$ are found by integration. This is done in Block “Euler” (see Figure 14.3).

14.9 State-space vector

Following the method described in sub-sections 14.6 to 14.8 we have been able to calculate all the components of the state-space vector of the system.

According to the solving sequence described above, the order in which the variables are integrated is: $p, q, r, \phi, \theta, \psi, u, v, w, x_e, y_e, z_e, \Omega_1, \tau_1, \Omega_2, \tau_2, \Omega_3, \tau_3, \Omega_4, \tau_4$

Therefore Matlab/Simulink will define the state-space vector as:

$$\mathbf{x} = (p, q, r, \phi, \theta, \psi, u, v, w, x_e, y_e, z_e, \Omega_1, \tau_1, \Omega_2, \tau_2, \Omega_3, \tau_3, \Omega_4, \tau_4) \quad (14.3)$$

“ROTORS” BLOCK

14.10 Introduction

As it was explained before, this block calculates $F_{xi}, F_{yi}, F_{zi}, (M_{xi})_{hub}, (M_{yi})_{hub}, M_{zi}$ using the model that has been described in Sections 9 and 10. The input is $p, q, r, u, v, w, \Omega_1, \Omega_2, \Omega_3, \Omega_4$, as well as the coordinate z_e (which is needed to estimate the k_{GE} factor that accounts for the ground effect). The outputs are $(M_{xi})_{hub}, (M_{yi})_{hub}, M_{zi}$ together with $\sum_i \mathbf{F}_i$ and $\sum_i (\mathbf{OG}_i \times \mathbf{F}_i)$, which are the specific results required by block “Dynamics”.

14.11 Preliminary calculations

The core of block “Rotors” is another block called “Model of the Rotor” where $F_{xi}, F_{yi}, F_{zi}, (M_{xi})_{hub}, (M_{yi})_{hub}, M_{zi}$ are determined. But before these are calculated, it is necessary to obtain λ_z, μ and β_{ss} for each rotor. In order to do so, the first step is to determine the components of the linear velocity of the point O_i (the intersection between the axis of the hub and the top of it). Once this has been done it is immediate to obtain λ_z and μ . As for the sideslip angle β_{ss} , it can be determined using (9.5). However, before doing so we have to consider that β_{ss} varies from $-\pi$ to π , while the “arctan” function (see eq 9.5) ranges from $-\frac{\pi}{2}$ to $\frac{\pi}{2}$. Hence, it is necessary to carefully define an algorithm that assigns the correct value to β_{ss} for each situation. This algorithm is included in a sub-block contained in “Model of the Rotor”.

It is also necessary to make the transformation from p, q, r into p_w, q_w, r_w . This is done using the previous value of β_{ss} and eqs (9.9).

In addition, we have to consider separately the axial flight case (when β_{ss} is not defined) from the rest of the flying conditions. S-Function “blades” accounts for this, as we will see later.

14.12 Calculation of the induced velocity

In Section 10 it was explained that λ_{ind} can be obtained by numerically solving the equation which results from equating the C_T predicted by BET (9.38) and the C_T predicted by MMT (10.9). As a result:

$$\begin{aligned}
& \frac{a\sigma}{4} \left(1 - \frac{e}{R}\right) \left(\left(\frac{2}{3} + \mu^2\right) \theta_0 + \frac{1}{2} (1 + \mu^2) \theta_1 - \lambda_z - \mu B_1 - \lambda_{ind} \right) = \\
& = 2 \frac{\lambda_{ind}}{k_1} \sqrt{\left(\frac{\lambda_z + \lambda_{ind}}{k_1} \right)^2 + \left(\frac{1}{k_2^2 - k_1^2} \right) \lambda_z^2 + \left(\frac{\mu}{k_2} \right)^2}
\end{aligned} \tag{14.4}$$

It should be remembered that the effect of p_w, q_w was not considered when obtaining expression (9.38).

It will be later seen that the effective hinge offset e can be assumed to be fixed. Hence, (14.4) has two parameters that depend on the flight conditions, λ_z and μ .

As we have said, (14.4) needs to be solved numerically. In order to save computing time during the simulation, it is advisable to do that off-line. Matlab has several commands to solve numerical equations (Ref 14.1). The procedure would be as follows: the equation is solved for a set of discrete values of λ_z, μ , chosen in such a way that they cover all the range of values that can appear in normal flight conditions (± 1 for λ_z and $0-2$ for μ). Then, while the simulation is running, λ_z, μ are calculated and then a lookup table is used to determine λ_{ind} by 2D interpolation.

One of the reasons for not including the effect of p_w, q_w in the expression of C_T from BET is that it would make more difficult to use the method that has been described here (a 4D interpolation would be required).

When (14.4) is solved four roots are obtained. Two are complex and the other two, real. The appropriate real root has to be chosen.

As explained in Sections 10 and 13, it was decided to multiply the obtained λ_{ind} by a corrective factor to improve the correlation between the theoretical and the real value. This factor was $\kappa = 1 - 1.2\lambda_z$.

In order to account for the ground effect, the previous λ_{ind} has to be multiplied by the k_{GE} factor. Ground effect, though, was finally not included in the model, as seen in Section 13.

14.13 Calculation of the coning and flapping angles and the forces and moments

Once λ_{ind} has been obtained, it is possible to enter in (9.38) to calculate C_T , which is in turn required to determine a_0, a_{1s}, b_{1s} using (9.44). Then, with a_0, a_{1s} in (9.42) and (9.43) we obtain C_H and C_Q , respectively.

Since all these expressions are quite complex, it is worth using an S-Function block to calculate them rather than trying to code them using Simulink's default blocks. As we saw before, adding S-Functions will slow down the simulation. However, since we only add one (actually, four, one for each rotor) the loss of computational performance is minimal.

The S-Function will be called “blades” and it will calculate $C_T, a_0, a_{1s}, b_{1s}, C_H, C_Q$ using the procedure which has just been described. It will also determine $f_{xi}, f_{yi}, f_{zi}, (m_{xi})_{hub}, (m_{yi})_{hub}, m_{zi}$ and $F_{xi}, F_{yi}, F_{zi}, (M_{xi})_{hub}, (M_{yi})_{hub}, M_{zi}$ using eqs (9.3) and (9.4), (9.16) to (9.19) and (9.31) to (9.36). Appendix G contains the code of the S-Function.

This S-Function, as indicated before, considers the axial flight case separately from the rest.

TRIM AND INITIALIZATION

14.14 Data Loading

In order to easily modify all the parameters of the model, their values are stored in a single m.file (a Matlab file) call “DATA” (see Appendix G). When the Simulink model is initialized, these values are loaded into the Workspace and, from there, they are retrieved by Simulink. Among the parameters stored are the air density ρ , the coordinates of several relevant points (G_T, G_i, G_j, O_i, P_i), masses, moments of inertia, motor constants, etc.

The parameters of the motors (R_a, L_a , etc) can be selected independently for each of them. The same applies to the masses of the armatures (m_j) and the hubs (m_i). This way it will be possible to study the effect on flight dynamics of small variations of these parameters from one motor to another, or from one rotor to another.

$\mathbf{I}_{OPI}, \mathbf{I}_{OGi}, \mathbf{I}_{OGj}, \mathbf{I}_{OG}, \mathbf{I}_{OG_T}$ are calculated in a different m.file called “calc” (see Appendix G). This file is also used to make some minor calculations that are required for the Simulink model.

14.15 Locating the points of equilibrium of the dynamical system

The physical model of the quadrotor that has been developed can be reduced to the expression below:

$$\dot{\mathbf{x}} = \mathbf{F}(\mathbf{x}, \mathbf{u})$$

where:

$\mathbf{x} = (p, q, r, \phi, \theta, \psi, u, v, w, x_e, y_e, z_e, \Omega_1, \tau_1, \Omega_2, \tau_2, \Omega_3, \tau_3, \Omega_4, \tau_4)$ is the state-space vector

$\mathbf{u} = (V_{gx}, V_{gy}, V_{gz}, v_{a1}, v_{a2}, v_{a3}, v_{a4})$ is the input vector

The points of equilibria of the system are those points $\mathbf{x}_0, \mathbf{u}_0$ where $\dot{\mathbf{x}} = 0$ for every t . According to this strict definition, only hover is a point of equilibrium, because in any other flight condition x_e, y_e, z_e will vary with time and so $\dot{x}_e, \dot{y}_e, \dot{z}_e$ will be non-zero. However, here we will relax the definition by considering that points of equilibrium are those where $\dot{x}_e, \dot{y}_e, \dot{z}_e$ are constant (but not necessarily zero) and the rest of the components of $\dot{\mathbf{x}}$ are zero.

Physically, these points represent flight conditions in which the balances of external forces and moments over the whole quadrotor are zero.

One of the reasons why the points of equilibrium are important is because they are needed to linearize the model. Another reason is that they are useful as starting points for the simulation.

The most obvious of these points of equilibrium is hover, as we have said. In Section 16 we will study the possibility of having an equilibrium point in horizontal flight. It will be seen that maintaining equilibrium in horizontal flight is more complicated than expected.

The default starting condition will be hover. However, the region where the physical model is valid is very ample and covers many other points apart from hover. The boundaries of this region will be studied in detail in Section 15.

14.16 Initialization

In Section 16 it will be explained how to determine the exact value of \mathbf{x} in hover using the *trim* command (Ref 14.2). Once it has been calculated, the simulation can be started

SIMULATION PARAMETERS. OTHER FEATURES

14.17 Simulation parameters

Variable step size vs Fixed step size

Variable step size solvers are usually more efficient both in terms of precision and computational resources, because they adjust the step size according to the rate of change of \mathbf{x} . Hence, in the proximities of singularities the discretization is very fine while in those zones where \mathbf{x} changes very slowly the step size is much larger.

The inclusion of the term $\frac{L}{K}\dot{\tau}$ in the model makes the system become fairly “stiff”. It was found out that fixed-step solvers had many difficulties to integrate \mathbf{x} . Therefore, it became clear that a variable-step solver would have to be used.

Choice of the numerical solver

Since the system is quite “stiff”, it was decided to use the “ode23t” solver. This is a one-step solver based on trapezoidal integration (Ref 14.2), with a very good performance compared to other solvers which are not optimized for stiff systems (such as Runge-Kutta variants.)

14.18 Other features

Saturation voltages

The motor voltage v_{aj} has to be within a determined range for the motor to work. Outside this range the model of Section 6 is not valid. In addition, the real motor may not work or, worse, it might get damaged.

The manufacturer defines an operational range which goes from 4.5 to 12 volts (see Appendix C). Motor tests (see Section 12) have shown, however, that the motor is capable of driving the rotor with voltages as low as 1 volt. The upper limit has not been reached during these tests because of the risk of motor damage.

The lower and upper limits of the voltage have been included in the simulation. For the lower limit, a conservative value of 1.4 volts has been chosen. For the upper limit, the nominal 12 volts have been increased by a 10%.

It should be noted that below 80rad/s (about 4 volts, depending on the flight conditions) the aerodynamic model of the rotor is not valid (see Section 13) so it is probably useless to run the simulation at voltages lower than 4 volts.

“Signals” block

This block is in charge of providing the input signals v_{aj} that are used to control the motors. Taking into account the way in which the attitude of the quadrotor is controlled (which was explained in Section 2) the most convenient thing to do is to split v_{aj} into two different signals. The first is a constant signal whose value corresponds to the trim hover condition. With this value, the rpm of the rotors will be such that the resulting thrust will balance the weight. This first signal is fed into the four motors, and will be called “Signal 0”.

The second signal will be called “Signal 1”. The opposite of this signal will be “-Signal 1”.

Gust model

The gust model is contained in a separate block called “Gusts”. The output of this block is the gust velocity vector (V_{gx}, V_{gy}, V_{gz}) . In other words, the velocity of the mass of air relative to the ground. This velocity vector is transformed to body axes in order to find out the velocity of the rotor relative to the mass of air.

The present model, as we have seen, assumes that the whole mass of air is moving. In the future, x_e, y_e, z_e could be introduced into the “Gusts” block to calculate the local velocity at the mass of air, which would be different from one point to another.

Battery power

The Draganfly XPro manual (Ref 14.3) brings the attention to the fact that, as the battery level gets low, the vehicle requires “more throttle” to keep levelled and gets more difficult to control. What happens is that, as the battery discharges, the voltage it is able to supply slightly decreases. It should be noted that the battery takes an average of 15 minutes to discharge (depending on the payload of the quadrotor).

The impact of a reduced voltage on the response of the quadrotor can be evaluated in our model by just changing the bias of the input signal.

Wind Tunnel Model

The calculation of λ_{ind} and the execution of the S-Function is done in the block called “Rotor Aerodynamics”. We can use this block as the core of a separate model that calculates the coning and flapping angles and the forces and moments in the rotor when it is installed in a wind tunnel. This model was already used in Section 13 to make comparisons with the data from the real wind tunnel tests.

15. LIMITATIONS OF THE MODEL

15.1 Introduction

Inevitably, a model of a physical system is never complete. Time constraints, lack of experimental data, unknown effects, limited computational resources, etc prevent the engineer or the scientist from producing a model with an infinite level of detail. It is thus necessary to make simplifications, and these obviously impose certain limitations on the validity of the model. The Matlab/Simulink model that has been developed here is no exception.

The definition of the boundaries of the region where the model is valid is possibly as important as the study of the results produced by the model itself. Whenever we are trying to extract conclusions from the simulations it is necessary to bear in mind whether or not the referred boundaries were trespassed during these simulations.

What follows is a comprehensive list of the limitations that are applicable to the Matlab/Simulink model used here. However, a detailed explanation of their causes will not be done here. The reader is advised to refer to the appropriate sections to obtain more information about the reasons for the existence of each of those limits.

15.2 Motor model

The motor model developed in Section 6 is linear and this implies that the extremes of its operating range (4.5 and 12 volts, according to the manufacturer) are not well modelled. Besides, the motor constants R_a and K have been chosen so that the correlation between theory and experiment is best between 4 and 8 volts.

It has been estimated that, in flight, the motors work at between 5 and 10 volts, which is a range that falls almost entirely in the region where the accuracy of the model is better.

The link between the motor and the load (the rotor) is done by means of a strap. It has been implicitly assumed that this transmission has a 100% efficiency. In reality, the efficiency will be less than 100%. Hence, the effective gear ratio will be lower than expected, and so the torque that the motor needs to deliver will be higher. As a result, power consumptions (voltage x current) will be higher too. However, this issue is more relevant for Performance studies than for Stability and Control.

15.3 Rotor model

Rotor modelling is undoubtedly the most difficult part of quadrotor modelling (if we do not consider the aerodynamics of the airframe). Because of this complexity, it is also the part of the quadrotor model where more limitations can be encountered.

It has been found that the BET-MMT model used fails to predict the correct C_T and C_Q for values of Ω below 100rad/s (although it is likely that this lower limit can be lowered by at least a 20% for many studies where a high accuracy is not required).

Because of all this, there is no much confidence on the results predicted by the model when the spinning speed falls below $80\text{--}100\text{rad/s}$.

Another assumption of the rotor model is that $\dot{\Omega}$ is small enough so as to neglect the variation of Ω within one turn of the rotor. This assumption was made in order to be able to use the results that had been obtained for conventional helicopters, in which Ω is always kept constant. If $\dot{\Omega}$ is too high, the assumption will no longer be valid. A practical upper limit for $\dot{\Omega}$ could be $\frac{0.05}{2\pi}\Omega^2$, which is the angular acceleration required to produce a 5% change in the value of Ω in one turn. For $\Omega = 160\text{rad/s}$ (close to the hovering value) this means 200rad/s^2 , which is over the experimental maximum acceleration that can be achieved.

Values of λ_z below -0.3 or above 0.3 have not been tested in the wind tunnel. Values of μ above 0.16 have not been consistently tested neither. All the conclusions about the rotor model which were written in Section 13 apply within those boundaries. This, however, is not a great limitation since the quadrotor is unlikely to trespass them often. With $\Omega = 90\text{rad/s}$, to go beyond $\lambda_z = 0.3$ in axial flight it is necessary to reach at least 7m/s of vertical speed. But with a more realistic Ω of 150rad/s , a speed of 12m/s is necessary. In roll/pitch manoeuvres, an impossible angular rate of $15\text{--}30\text{rad/s}$ is necessary before reaching $|\lambda_z| = 0.3$. As for μ , it is more restrictive. A horizontal speed of 6m/s in forward flight can be enough to reach $\mu = 0.16$. However, model predictions can still be valid above this value, although this has to be confirmed.

The rotor model has been obtained using Blade Element Theory. For each blade element, it has been assumed that the boundary layer was adhered to the aerofoil. Strictly speaking, the model is not valid when this is not true (e.g. when the aerofoil has stalled). In practice, the model will still produce satisfactory results even if the boundary layer is not adhered in some portions of the blade.

15.4 Aerodynamics of the airframe

The forces and moments exerted by the airflow over the airframe have not been included and so the model will not be valid, strictly speaking, when they reach the order of magnitude of the other forces and moments. As for the forces, it was shown in Section 11 that this is not likely to occur for linear velocities less than $10\text{--}20\text{m/s}$. However, as for the moments, there is more uncertainty.

15.5 Simulink block design. Numerical solver

The quadrotor model is complex, with a high level of cross-coupling between the variables of the state-space vector. Besides, it is very sensitive to small disturbances. These can be of physical origin (and thus they should not be removed) but they can also be owed to numerical error in the solving algorithms (the *trim* algorithm which is used to find the initial conditions or the numerical solver which is used to calculate the state-space vector at each step).

It is not always trivial to make the difference between both types of disturbances, let alone to remove those due to numerical error. A possible way to assess the influence of the latter consists in starting the simulation in the hover condition and letting it run without introducing any signal (zero “Signal 1”) during an arbitrary time, e.g. 10 seconds. If the XPro is perfectly axial-symmetrical (there are no mass “asymmetries” or others) then all the components of the state-space vector should remain zero (initial altitude is set to zero). Should there be any oscillations in the value of these components, they can be assumed to be due to what we have called “numerical errors”. We can also assume that the order of magnitude of these errors will be the same under other flight conditions. The results obtained are summarized in the table below. It should be noted that the absolute error is given per second of simulated time:

Variable	Order of magnitude of the Absolute Error (per second)
x_e, y_e	$\pm 10^{-11} m$
z_e	$\pm 10^{-8} m$
u_e, v_e, u, v	$\pm 10^{-10} m/s$
w_e, w	$\pm 10^{-9} m/s$
ϕ, θ	$\pm 10^{-11} rad$
ψ	$\pm 10^{-13} rad$
p, q	$\pm 10^{-11} rad/s$
r	$\pm 10^{-12} rad/s$

Table 15.1.

It is important to realise that the order of magnitude of the absolute error may not be linear with time. In any case, for simulation times of up to 10 seconds it has been confirmed that it is totally negligible.

There is also a mathematical discontinuity at $\theta, \phi = \pm \frac{\pi}{2}$. A future version of the simulation may use quaternions instead of Euler formulation to solve this issue. Anyway, the existence of this discontinuity is not a great problem, since the quadrotor is not likely to reach such high pitch/roll angles. Besides, it is likely that the physical model will not be valid in those cases (as mentioned before).

15.6 “Envelope” of the model

According to all what has been said, conservative boundaries of the model’s region of validity could be the following:

$\pm 10m/s$ in axial flight

$\pm 6m/s$ in horizontal flight (probably much more)

$\Omega = 80 - 200rad/s$

$\phi, \theta = \pm \frac{\pi}{2}rad$

16. RUNNING THE MATLAB/SIMULINK MODEL OF THE QUADROTOR

16.1 Introduction

A rigorous validation of the Matlab/Simulink model of the XPro was not possible because it would have required real flight data and these were not available at the time this Report was prepared. The only experimental data available were those from the wind tunnel, which have already been used in Section 13 to validate the model of the rotor.

Hence, we will be constrained to a “limited” model validation which will consist in analyzing the results predicted by Simulink and trying to identify the physical phenomena underlying those results.

In doing so, it is expected that not only we will be able to assess the accuracy of the model but also reach some interesting conclusions about Quadrotor Flight Dynamics. These conclusions might be helpful in the future when studying Stability and Control in more depth.

In many ways, this Section is the culmination of all the work that has been described before.

The model will be run in open loop, no controller will be used.

16.2 Hover

Hover is the default initial condition of the Simulink model, as stated in Section 14. To determine the initial value of the state-space vector, the *trim* command is used. When we do so, we find that the voltage at each motor is 7.85 volts. This value can be compared with the one measured in the wind tunnel when the rotor was delivering the same thrust (i.e., a fourth of the total weight, or $5.78N$). The measured value was 7.42 volts, although there is an uncertainty of up to a 5-8% due to the error of the balance.

The constant voltage fed into the motors to maintain hover will be designated as “Signal 0”.

The hovering altitude is set to zero, which does not mean that the quadrotor is on the ground. In fact, it will be assumed that the vehicle is far enough from the ground so that there is no “ground effect”.

16.3 Heave

From an initial hovering condition, an identical signal is applied to the four motors. This signal, which we will call “Signal 1”, superimposes itself over the initial voltage (Signal 0). The resulting “Signal 0+Signal 1” has the same “shape” as Signal 1 and a bias which is given by Signal 0. When feeding the four motors simultaneously with these signals, the quadrotor will move vertically (“heave”). If “Signal 1” is a step function...

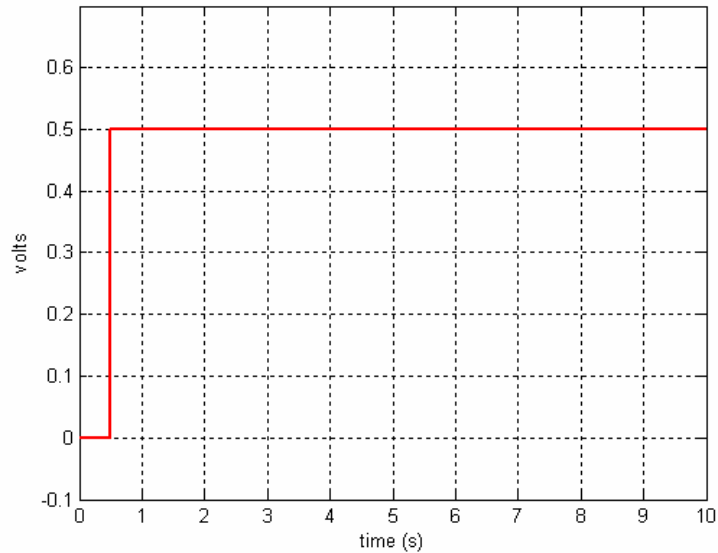


Fig 16.1. Heave: step input.

...then the vertical speed and the altitude:

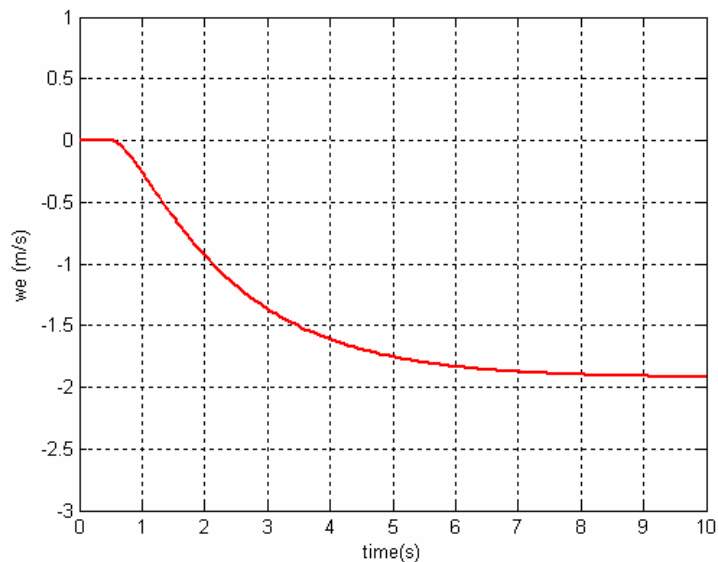


Fig 16.2. Heave: vertical speed (step input).

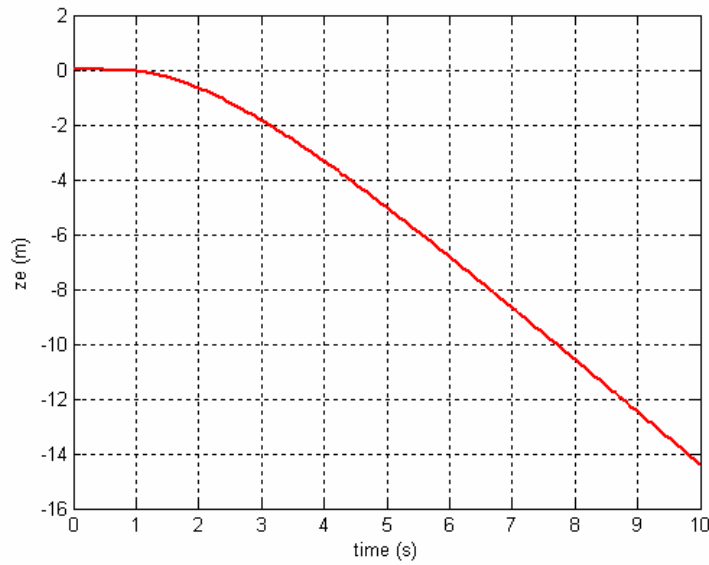


Fig 16.3. Heave: altitude (step input).

It can be seen that the vertical velocity w_e (or w) increases until it reaches a given value. It should be noted that, since $O_e z_e$ and Oz are pointing downwards, a negative velocity means that the quadrotor is ascending, and a negative altitude z_e means that it is *above* the starting level.

The fact that the climb speed tends to a constant value was expected and is caused by the dependence of C_T with λ_z . Looking at Figure 13.1 it can be seen that when the rotor is ascending (positive λ_z) C_T decreases as the climb speed becomes higher. So, from a starting hover condition, if we increase the voltage in the four motors in a given value, and then keep it constant, the initial result will be that the total thrust will become larger than the weight and so the vehicle will start to ascend. However, as the climb speed becomes larger, C_T will decrease, and so the thrust. Eventually, a new equilibrium will be reached when the total thrust equates the weight again. From that point onwards, there will be no vertical acceleration and thus the quadrotor will ascend at constant speed.

The figure on next page compares the history of w_e previously shown with that which would have been obtained with a constant C_T :

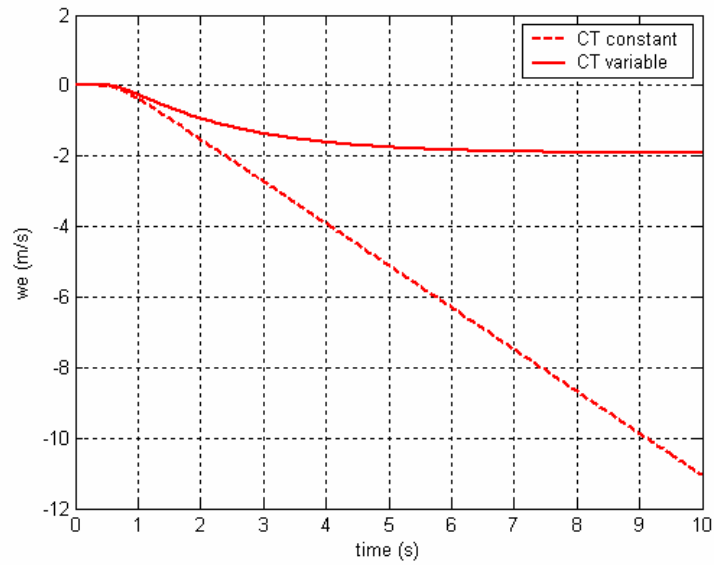


Fig 16.4. Heave: effect of C_T on the vertical speed (step input).

When C_T is constant, the quadrotor is always accelerated, there is no limit value for the speed. This speaks for the importance of modelling the dependence of C_T with λ_z .

The dependence of the thrust on the vertical speed also applies on descents, but in this case the thrust rises. Hence, if the voltages are decreased instead of being increased, the quadrotor will descend at increasing speeds until a limit value is reached.

So if we use two consecutive step signals of opposite sign and equal amplitude (that is, a pulse signal) we can expect that the quadrotor will heave and then stop.

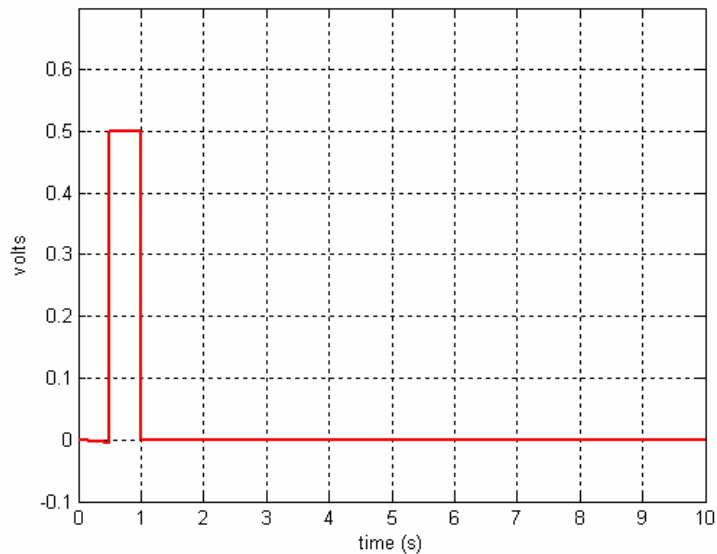


Fig 16.5. Heave: pulse input.

Using the Signal 1 shown in the Figure 16.5:

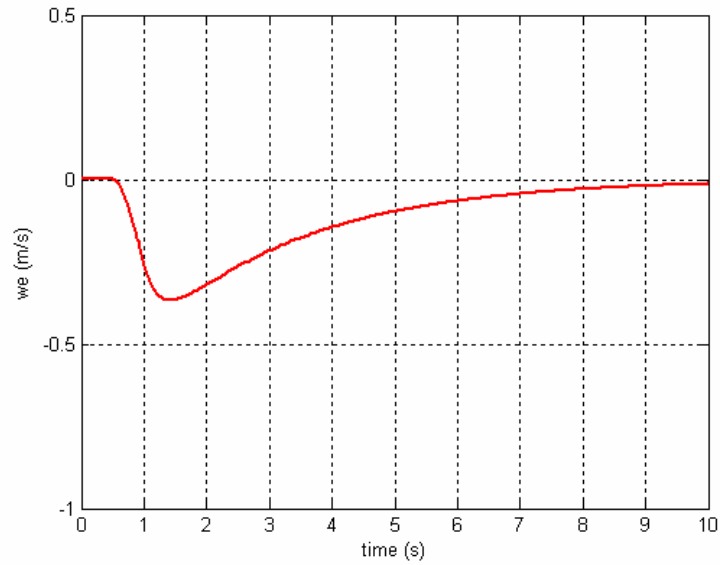


Fig 16.6. Heave: vertical speed (pulse input).

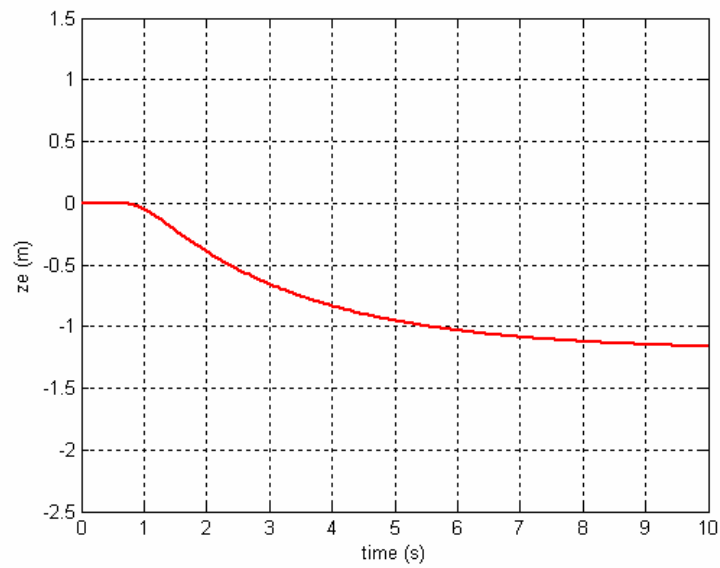


Fig 16.7. Heave: altitude (pulse input).

It was confirmed that the only effect of changing the length of the pulse is to modify the maximum climb speed. As expected, the quadrotor ascends and then stops at a new altitude.

This technique to control the altitude by means of step signals is widely accepted and provides the basis for several control laws that have been developed. In fact, the

relationship between thrust and vertical velocity is a well-known phenomenon in the quadrotor research community. G.M. Hoffmann *et al* (Ref 16.1) were among the first to describe this effect in detail as well as to study its implications for quadrotor control.

It is important to realise that altitude control in forward flight is much more complex, because there is much more cross-coupling between degrees of freedom (in forward flight, the quadrotor has a pitch down attitude).

16.4 Pitch up manoeuvre

It has been seen that axial flight is not too demanding from the Control perspective. However, attitude control is an entirely different affair. Part of the difficulty comes from the reduced size of the XPro. As explained in Section 2, this means that the moments of inertia are low and so the dynamics are very fast. Apart from this, there is another characteristic that greatly increases the difficulty of attitude control: the lack of damping when rotating around any of the three axes. This, coupled with the low inertias, makes attitude control a great challenge.

Besides, we have to consider the coupling between attitude and *altitude* control. This further complicates the problem, as it will be seen.

Pitch up manoeuvre

As it was explained in Section 2, in order to pitch up thrust has to be increased in the front rotor and decreased in the rear one, while remaining constant in the other two. To prevent yawing, the total reaction torque has to be kept equal to zero at all times. This imposes a constraint on the amount of thrust that can be increased in one rotor relative to the other. It should be noted that, since the thrust and the torque are quadratic with Ω , this constraint *does not* mean that the speeds of the front and rear rotors are increased and decreased by exactly the same amount $\Delta\Omega$. However, we can assume that if $\Delta\Omega$ is small compared to Ω .

In any case, maintaining a perfect balance of torques while the thrusts are being independently modified is almost impossible, since these torques will directly depend on other variables apart from Ω , such as the tangential velocities of the centres of the rotors or the pitch rate.

Here, however, we will ignore these effects and just try to achieve a “pseudo-balance” of torques. To do so, we will increase and decrease the voltages in the front and rear motors by the same amount, so that the same happens to Ω (again, only approximately, since the inertias of the rotors and the motors, as well as the inductances, will probably make Ω be different from the desired one).

Three different types of “Signal 1” will be used in the front motor (step, pulse, 2 opposite pulses). The rear motor will receive “-Signal 1”. Obviously, both motors will

still be fed with “Signal 0” in the same time. The following figures show “Signal 1” (left) and the corresponding pitch angle θ (right). In all the cases, the behaviour of θ is quite spectacular:

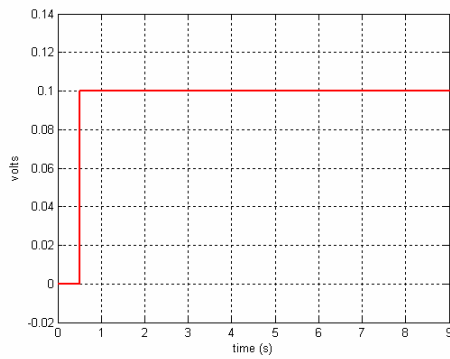


Fig 16.8(a). Pitch up: step input.

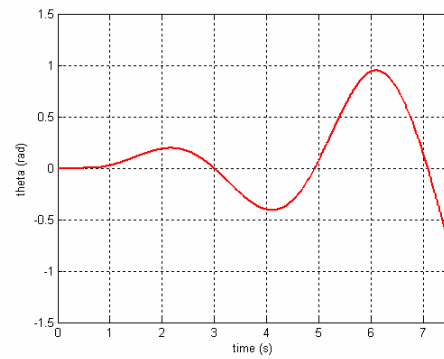
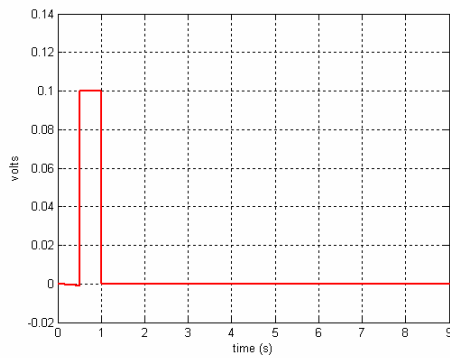
Fig 16.8(b). θ (step input).

Fig 16.9(a). Pitch up: pulse input.

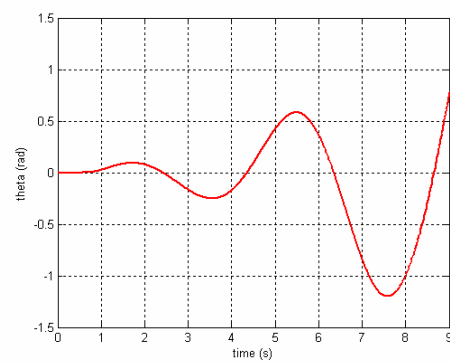
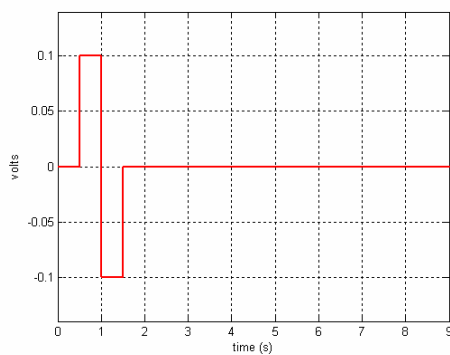
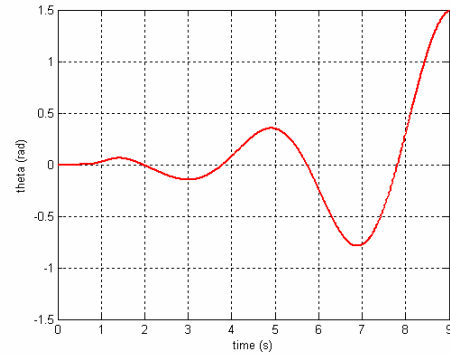
Fig 16.9(b). θ (pulse input).

Fig 16.10(a). Pitch up: double pulse input.

Fig 16.10(b). θ (double pulse input).

It can be seen the pitch angle θ heavily oscillates. Besides, the amplitude of the oscillations diverges.

Explanation of the phenomenon: attitude-altitude coupling

When the results above were first obtained, it was not immediately obvious what was going on. However, it was soon found out that there are several reasons that explained this flight behaviour.

In-plane force f_x :

When the quadrotor pitches up, the total thrust vector tilts. As a result, the vertical component of the thrust is reduced and is no longer capable of balancing the weight. Hence, the vehicle starts to fall. The arising vertical velocity will have a component parallel to the Hub Plane (HP). Since the quadrotor has a pitch up attitude, this in-plane velocity will point to the front of the vehicle, as seen by an observer situated in the centre of the rotor. According to what was explained in Sections 9 and 13, such an in-plane velocity will make the Tip Path Plane (TPP) tilt in the same direction (as well as laterally) and will create an in-plane force H in the same direction too. The in-plane component of the thrust (due to the TPP tilt) added to H is what we called f_x . This force f_x (there will be one at each rotor) will create a pitch down moment around the c.g. of the XPro, which is below the HP (see Figure 16.11).

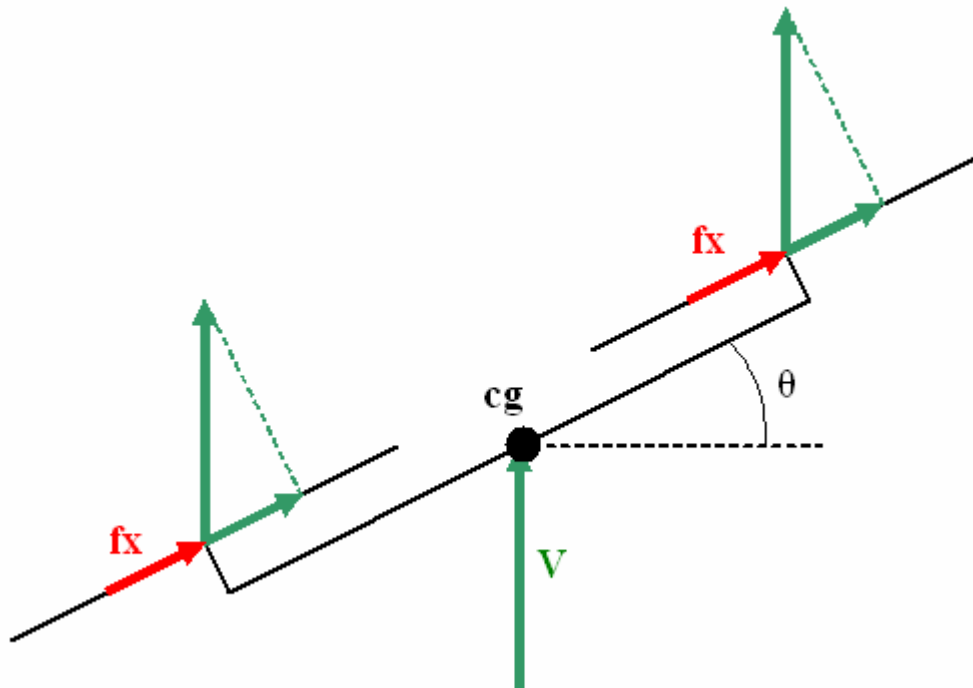


Fig 16.11. Quadrotor pitching up. There is a component of the velocity parallel to the Hub Plane (HP). As a result, there will be a force f_x which will also be parallel to the HP. This force creates a pitch down moment around the c.g. of the quadrotor.

As the falling speed increases, a point will be reached when this pitch down moment is higher than the pitch up moment created by the difference between the thrusts of the front and rear rotors. Hence, the quadrotor will pitch down.

Pitching down will then reverse the direction of the f_x force, so that a pitch up moment will be created. As a result, the quadrotor will pitch up again.

A way of reducing the intensity of these effects would be to raise the c.g. of the vehicle so that it is as close as possible to the HP. This would reduce the moment arm of f_x and thus reduce the amplitude of the oscillations in θ (although they would still be divergent). These oscillations cannot be eliminated unless the moment arm is exactly zero, and this is unlikely to happen since the actual point of application of f_x is at P_i , and the position of P_i changes with the tilt of the TPP (through h , as explained in Section 9). In any case, the benefit of raising the c.g. is obvious. Later we will see that there are other reasons why it is interesting to raise the c.g., although it is always for the same purpose, to reduce the moment arm of the in-plane forces acting at the rotors.

It is worth noting that it is very inconvenient to place the c.g. above the HP. If the c.g. is above the HP then θ will diverge faster, since the in-plane forces f_x will contribute to the pitch up moment, rather than opposing to it.

In-plane moment $(M_y)_{hub}$:

The hub in-plane moments also play a role during the pitch up manoeuvre. These moments were due to the centrifugal force at the hinge, the spring and the in-plane components of the torque vector \mathbf{Q} . If the in-plane velocity is pointing to the front (as it happens in the four rotors when the vehicle has a pitch up attitude and is falling) then these moments are, in $Oxyz$ axes:

$$(M_x)_{hub} = \mp \left(\frac{1}{2} be\Omega^2 \frac{M_b}{g} + k_\beta \right) b_{1s} + \frac{\pm Q \tan a_{1s}}{\sqrt{1 + \tan^2 a_{1s} + \tan^2 (\pm b_{1s})}} \quad (16.1)$$

$$(M_y)_{hub} = - \left(\frac{1}{2} be\Omega^2 \frac{M_b}{g} + k_\beta \right) a_{1s} - \frac{\pm Q \tan (\pm b_{1s})}{\sqrt{1 + \tan^2 a_{1s} + \tan^2 (\pm b_{1s})}} \quad (16.2)$$

\pm accounts for the direction of turn of the rotors (+ when counter clockwise, – if contrary).

As a result of the in-plane velocity that appears when the vehicle starts to fall, a_{1s} and b_{1s} will be non-zero (that was why the TPP tilted). In consequence, $(M_x)_{hub}$ and $(M_y)_{hub}$ will also be non-zero.

a_{1s}, b_{1s} will be roughly equal in the four rotors (because the in-plane velocity is equal in the four rotors). Hence, since two rotors are spinning clockwise and the other two, counter clockwise, the roll moments $(M_x)_{hub}$ are going to be cancelled according to (16.1). But that will not occur with $(M_y)_{hub}$. In fact, if we sum the four pitch moments $(M_y)_{hub}$, we obtain a negative (pitch down) moment. This moment will thus have the same direction as that created by the f_x forces around the c.g.

When the quadrotor pitches down, $(M_y)_{hub}$ reverses its sign, just as it happens with the moment created by the f_x forces.

To prove that the causes of the oscillations in θ are the f_x forces and $(M_y)_{hub}$, a simulation was made where they were both zero. The figure below compares the results with those obtained when they are not zero. In both cases, a pulse signal was used:

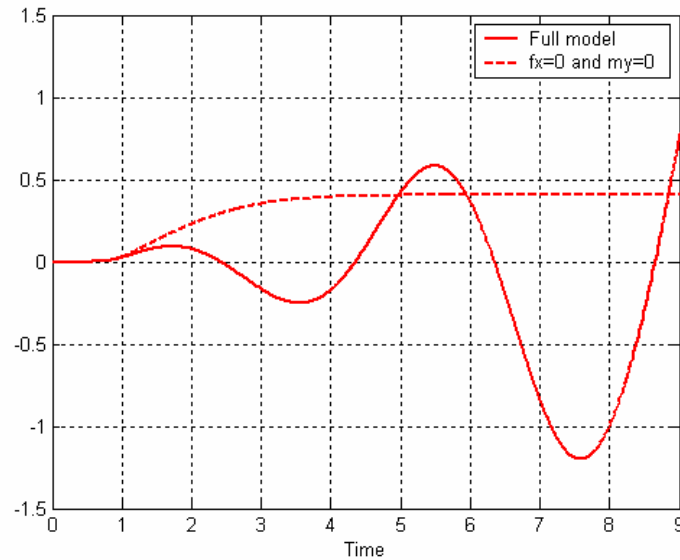


Fig 16.12. Pitch up: effect of f_x and m_y (pulse input).

Attitude-altitude coupling:

As the quadrotor starts to fall at the beginning of the pitch up manoeuvre, thrust is increased by equal in the four rotors due to the dependence of C_T on λ_z . The consequence is that the quadrotor will stop falling and start to ascend. This will reverse the direction of f_x , no matter what was it at that precise moment, leading to a change in the direction of the pitch moment. Hence, we see another effect that contributes to the oscillations in θ .

Vertical motion gets even more complex when the thrust decreases as the vehicle ascends and/or when new changes in the tilt angle of the thrust vector modify the total vertical force. The figure below illustrates this complexity by showing the typical history of w_e and z_e as the quadrotor oscillates:

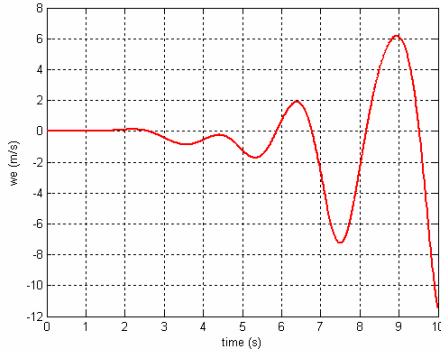


Fig 16.13(a). Pitch up: vertical speed.

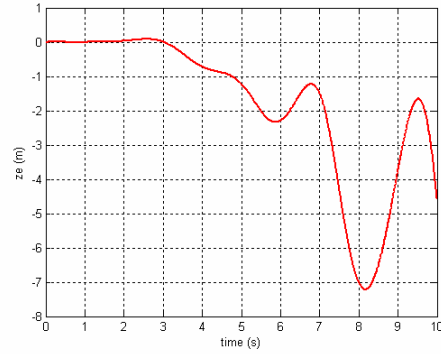
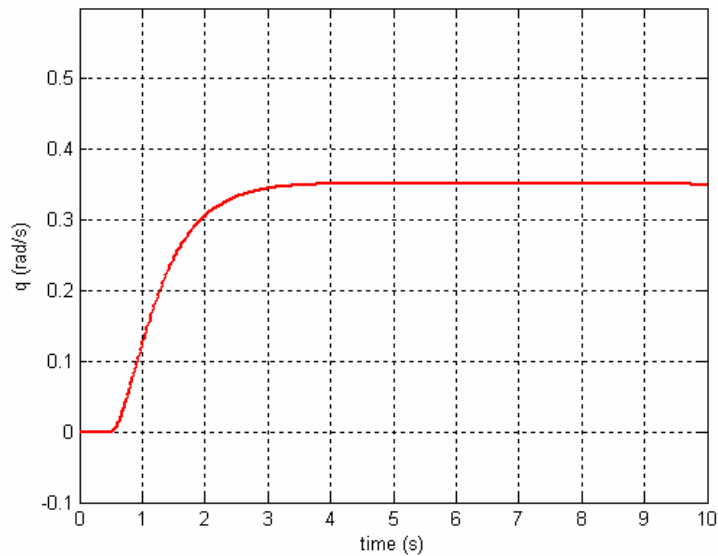


Fig 16.13(b). Pitch up: altitude.

16.5 Quadrotor with gimbal support

If the quadrotor is supported by a gimbal, there will not be divergent oscillations of θ . This was confirmed by modifying the simulation to include a gimbal support (mathematically, this is equivalent to making zero the sum of all the external forces in the equation of forces). Using a step signal as “Signal 1” we obtain the following pitch rate q and pitch angle θ :

Fig 16.14. Pitch up: q (step input, gimbal support).

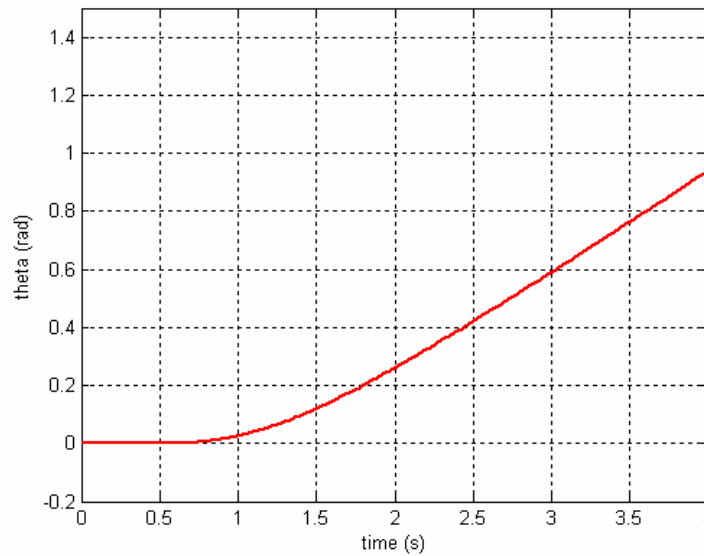


Fig 16.15. Pitch up: θ (step input, gimbal support).

Not only are there no oscillations but besides θ tends to increase linearly. This is because the pitch rate q converges to a certain value, just as it happened with w_e in axial flight. One source of damping, as in the “heave” manoeuvre, is the dependence of the thrust with the velocity of the air blowing through the rotor. In the pitching up motion, the front rotor is exposed to a flow of air blowing from above, whereas the rear rotor sees a flow of air that comes from below. As a result, the thrust will increase in the rear rotor and decrease in the front one. This produces a pitch down moment that will oppose the original pitch up moment.

But there is another source of damping that has to do with blade flapping dynamics. Even if the quadrotor does not “fall” because it is supported by a gimbal, there will be a small in-plane velocity at the rotor. This is because the vehicle is rotating around its c.g., and the c.g. is not at the same level as the Hub Plane (see Figure below). When the quadrotor pitches up the in-plane velocity will point to the front of the vehicle, as seen by an observer situated in the centre of the rotor.

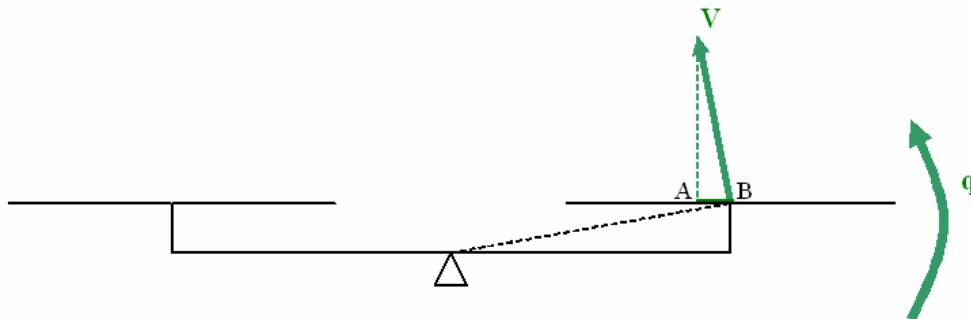


Fig 16.16. Quadrotor with gimbal support. When it pitches up there is an in-plane velocity at the rotor (AB).

Since a_{1s}, b_{1s} are non-zero, $(M_x)_{hub}$ and $(M_y)_{hub}$ will be non-zero too. As for $(M_x)_{hub}$, we have seen that when we add the values for the four rotors the net result is zero. But the total contribution from the four $(M_y)_{hub}$ will not be zero. In fact, it will be negative (pitch down moment) when the in-plane velocity points to the front.

In brief, there are two restoring moments: that which is caused by the variation of C_T with λ_z and that which is caused by $(M_y)_{hub}$.

To prove this, a simulation was made where C_T was constant and $(M_y)_{hub} = 0$. The figure below compares the results with those obtained in the complete model. A step signal was used in both cases.

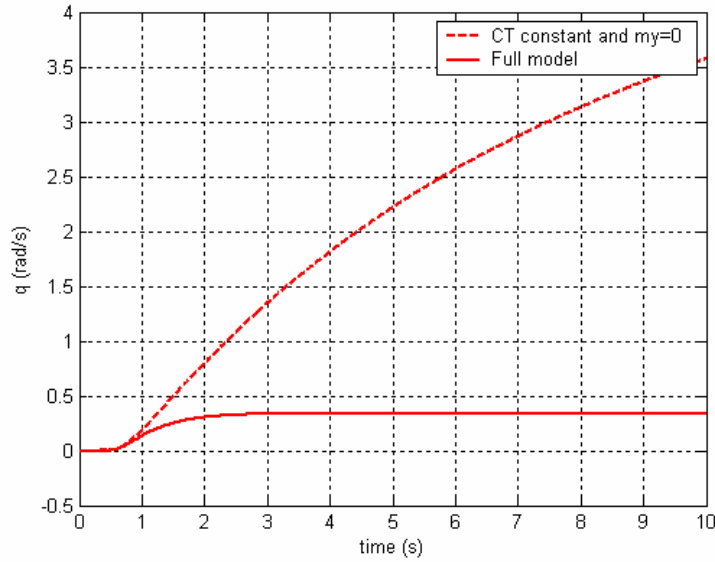


Fig 16.17. Pitch up: effect of C_T and m_y on q (step input, gimbal support).

It can be seen that if C_T is constant and $(M_y)_{hub} = 0$ there are no restoring moments and so q increases continuously, whereas in the other case the presence of the restoring moment leads to a constant q .

If we use two out-of-phase, opposed step functions (that is, a pulse function) we are likely to obtain a θ that converges to a certain value, just as it occurred with z_e in the “heave” manoeuvre”. This is confirmed in Figures 16.18 and 16.19:

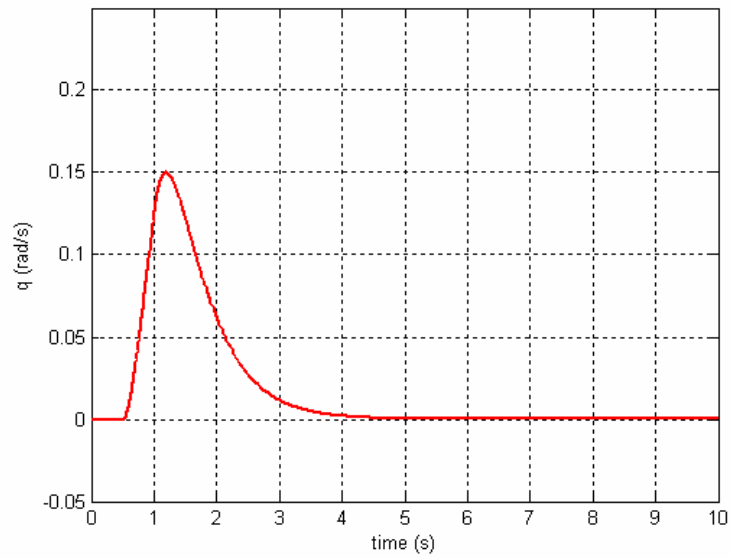


Fig 16.18. Pitch up: q (pulse input, gimbal support).

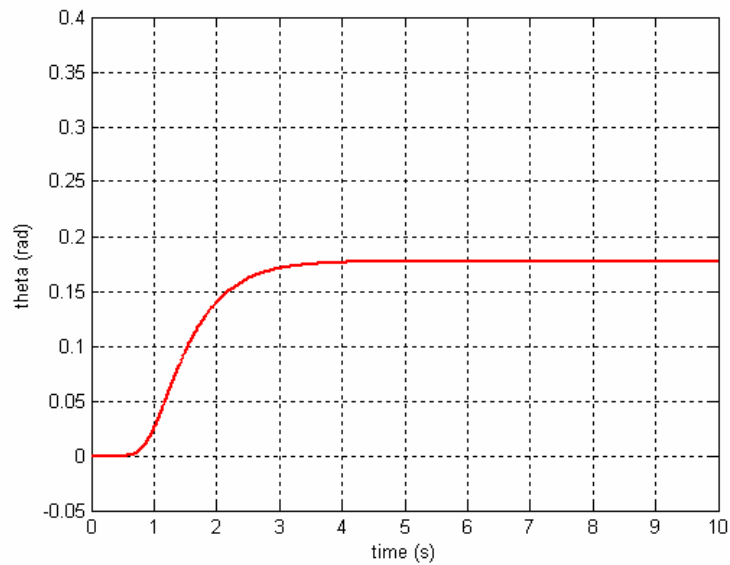


Fig 16.19. Pitch up: θ (pulse input, gimbal support).

Hence, in a gimballed quadrotor, pitch control is possible by means of step signals, just as altitude control and, it will be seen, yaw control.

The importance of the “gimbal support” case is that it enables us to study the longitudinal dynamics of the vehicle when they are uncoupled from the vertical motion. Some controllers have been tested in gimballed or tethered quadrotors (see Refs 16.1 and 16.2). But we cannot forget that this is just a laboratory experiment. In real flight the quadrotor will be free to move vertically and thus the cross coupling between altitude and attitude will be present.

Influence of the spring strength

Still with the quadrotor on its imaginary gimbal support, it is interesting to study the influence of the spring strength.

In Section 9 it was explained that our model of the rotor would simulate the blade stiffness by means of an offset hinge e and a torsional spring. As suggested by Young (Ref 9.5), the spring strength k_β was made to match the non-rotating flap frequency of the blade, and the hinge offset e was made to match the rotating flap frequency. This was done in sub-sections 9.16 and 9.17.

The figure below shows the history of θ with a pulse signal and with different values of spring strength: k_β , $2.5k_\beta$ and $5k_\beta$ (ω_{nr} was changed accordingly, too). k_β is the actual spring strength ($2.524Nm$), which was obtained in sub-section 9.18. The solid line corresponds to k_β and the dashed lines to the other values of the spring strength. The arrow indicates rising values of the spring strength:

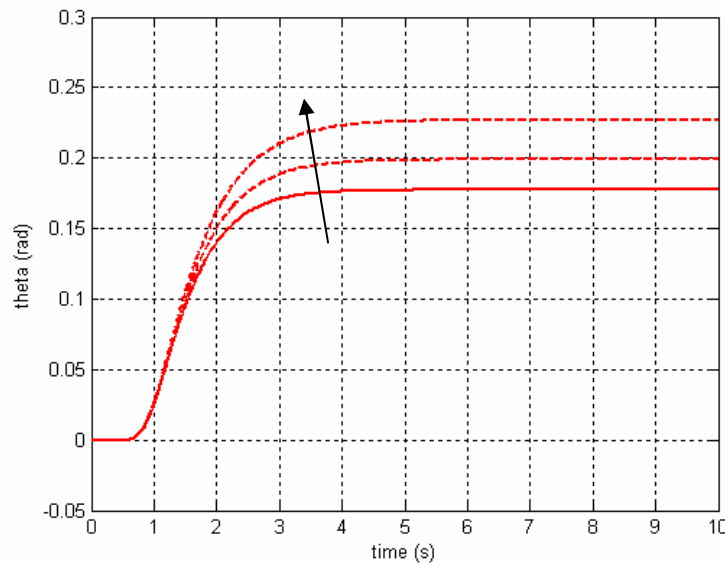


Fig 16.20. Pitch up: effect of the spring strength on θ (pulse input, gimbal support). The arrow denotes increasing strength. The solid line corresponds to the default spring strength.

We can see that, as the spring strength increases, the final value of θ increases too. This might occur because the flapping angle a_{1s} decreases as the spring strength becomes larger, and in doing so it makes $(M_y)_{hub}$ decrease too.

Other cross-coupling effects

Since the quadrotor is not perfectly axial-symmetrical, the products of inertia of the airframe are non-zero. This introduces some coupling between the three Euler angles and will eventually lead to rolling and yawing.

16.6 Roll manoeuvre

Due to the axial-symmetry of the quadrotor, all what has been explained regarding the pitch up manoeuvre is applicable to the roll manoeuvre.

Nevertheless, since this axial-symmetry is not perfect, there are slight differences in the inertia around the Ox and Oy axes. Hence, the solutions will not be exactly identical.

16.7 Yaw manoeuvre

Since the inertia of the quadrotor around the Oz axis is approximately double than around the other axes, yaw control should be easier. Besides, there is no obvious cross-coupling between yaw control and altitude control, although this is arguable, as we will see later.

As it was explained in Section 2, to yaw to the right the speed of the rotors turning counter clockwise (front and rear) has to be increased, while decreased on the other two. This increases the reaction torque in the former and reduces it in the latter. The total thrust has to remain constant and because of this there is a constraint on the amount of torque that can be increased in one couple of rotors relative to the other. We can assume that to keep the thrust constant it is enough to increase and decrease Ω by the same amount in each couple, but this is not entirely true (because the torque and the thrust are quadratic —not linear—, with Ω , and because there are other variables affecting both).

First, we will test a step function as “Signal 1”. This will be fed into the front and rear rotors, while “-Signal 1” goes into the other two:

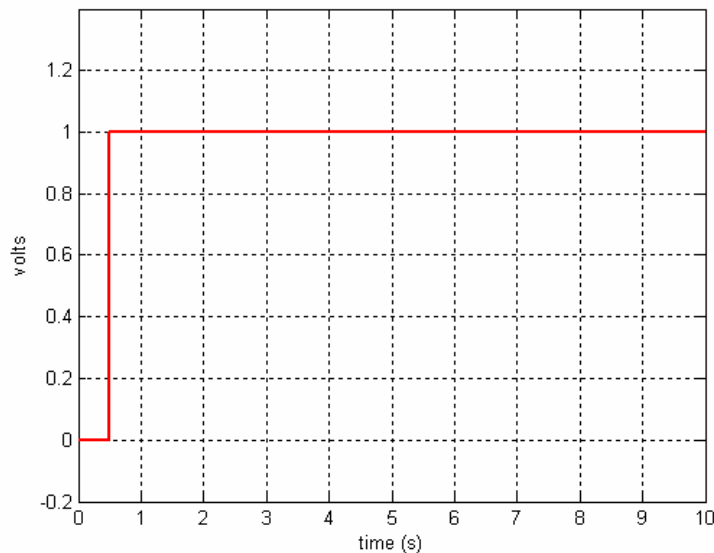


Fig 16.21. Yawing: step input (Signal 1).

Then, the yaw rate r and the yaw angle ψ :

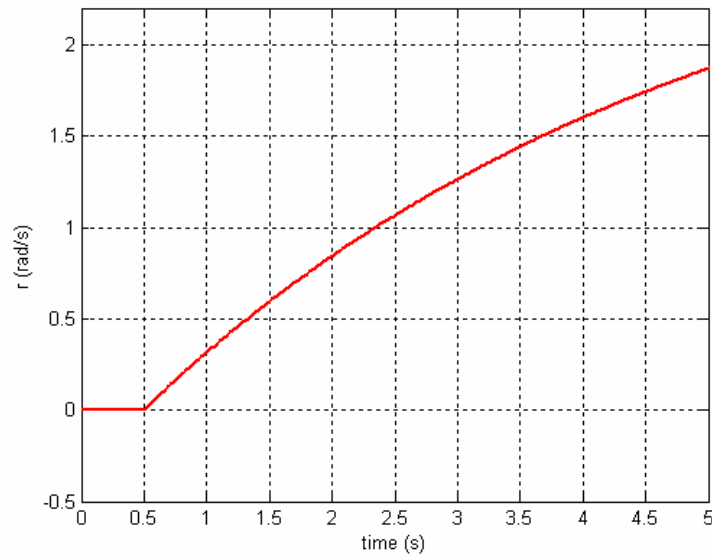


Fig 16.22. Yawing: r (step input).

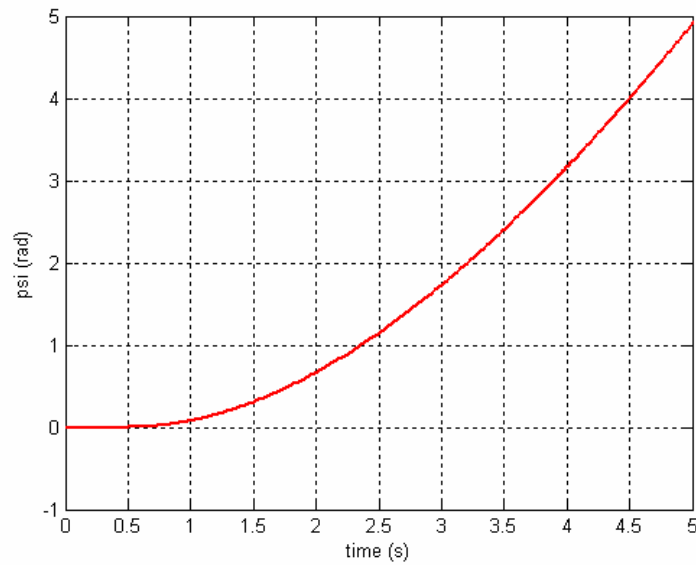


Fig 16.23. Yawing: ψ (step input).

Fig 16.22 shows that the yaw rate r *does not* tend to a constant value. As a result, ψ does not tend to increase linearly (Fig 16.23). This is different from what happened with w_e and z_e when a step signal was used. In that case, w_e tended to a constant value, and z_e tended to increase linearly. We saw that this was because of the damping effect of the thrust. In fact, in the yaw manoeuvre there is also a source of damping, as it is

revealed by the fact that the slope of the r curve (that is, \dot{r}) slowly decreases. However, this is not enough to make r converge to a constant value.

To understand the origin of this source of damping we have to bear in mind that, when the quadrotor yaws to the right, a tangential velocity appears at the centre of each rotor. This in-plane velocity, as it has been said before, leads to an in-plane force f_x which in turn creates a yawing moment (to the left) around the c.g. of the vehicle. However, this is not large enough to cancel the main yawing moment to the right.

To prove what has been said the simulation was repeated but with $f_x = 0$:

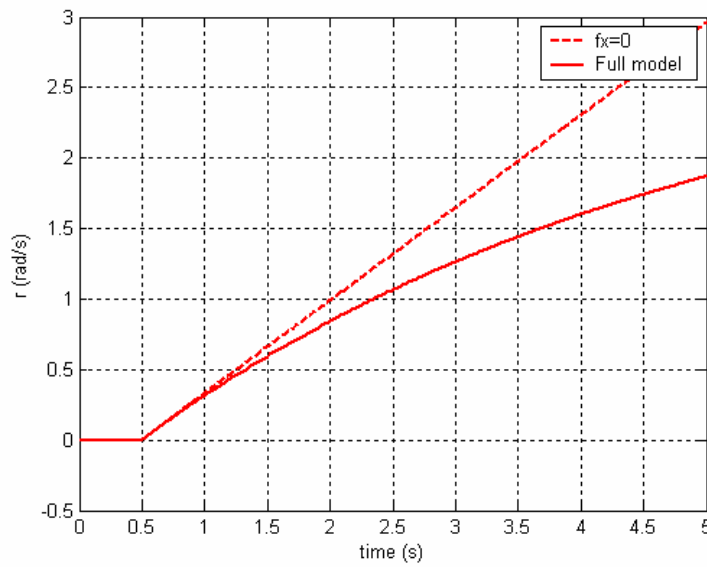


Fig 16.24. Yawing: effect of f_x on r (step input).

When $f_x = 0$ there is no moment opposed to the total reaction torque and thus r raises linearly (\dot{r} constant). On the other hand, when $f_x \neq 0$ there is a moment that opposes to the total reaction torque. In consequence, \dot{r} slowly decreases and so does the slope of r .

Again, this shows the importance of modelling the in-plane force f_x , since not doing so will leave us without an important source of damping. It should be remembered that f_x was created both by H and by the tilt of the thrust vector. It should be noted that a lateral force f_y will also appear at each rotor due to the lateral tilt of the TPP (which is coupled with the longitudinal tilt). However, this force will be perpendicular to the tangential velocity of the centre of the rotor, so that the line of application of the force vector will pass through the central axis of the quadrotor. As a result, it will not produce any yawing moment.

If we use a pulse signal (two opposed, out-of-phase step signals) instead of a step signal:

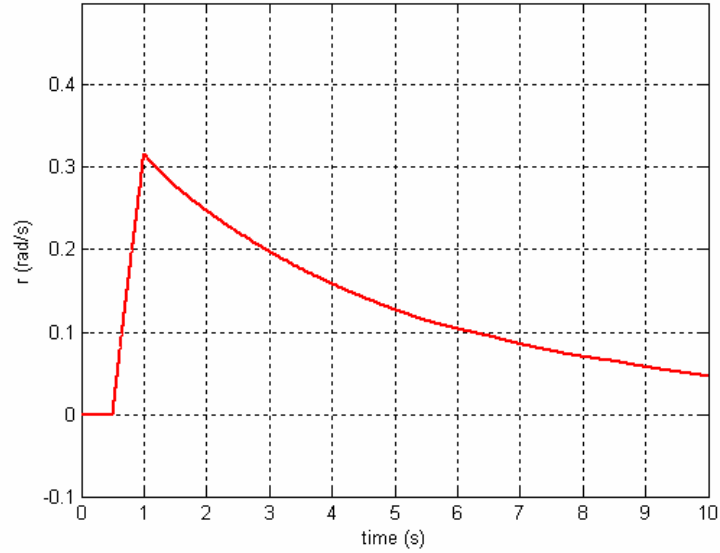


Fig 16.25. Yawing: r (pulse input).

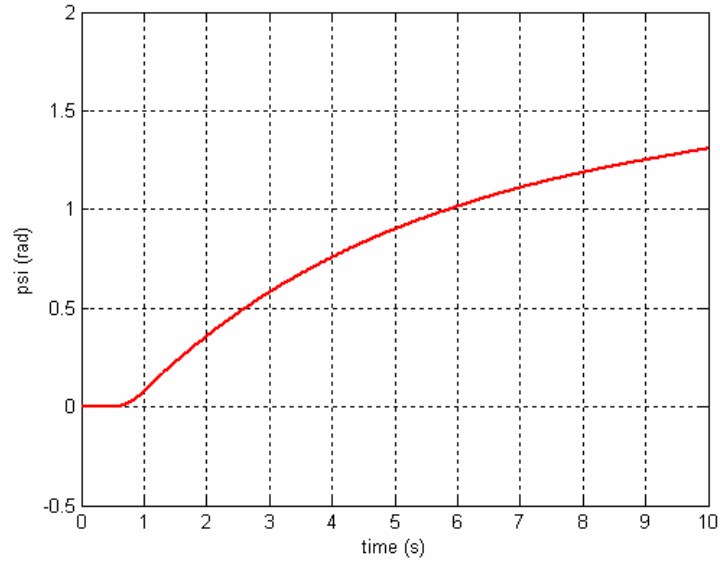


Fig 16.26. Yawing: ψ (pulse input).

We can see that now r tends to zero, but not fast enough for ψ to converge quickly to a constant value. Hence, it is clear that for yaw control a pulse signal is not as effective as it was for altitude control (or pitch control, when there is a gimbal support).

Cross-coupling effects

When the quadrotor yaws to the right, the TPP of each rotor tilts to the left because of the tangential velocity at the rotor centre, as explained. When the TPP tilts, the thrust is no longer aligned with the weight and the quadrotor will start to fall. This will lead to divergent oscillations in θ and ϕ . These oscillations will not occur if the quadrotor has a gimbal support and therefore it cannot fall.

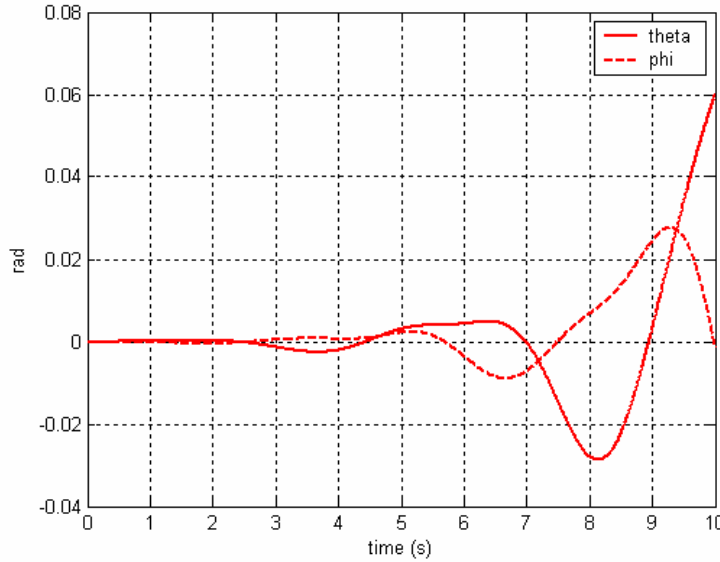


Fig 16.27. Yawing: ϕ and θ (pulse input).

16.8 Transition from hover to forward flight

In Section 2 it was explained that in forward flight the quadrotor must keep a negative pitch angle so that there is a horizontal component of the total thrust that overcomes the drag of the airframe. Therefore, the transition between hover and forward flight consists in achieving a negative pitch angle without any loss of altitude, or at least with the minimum loss.

However, we have seen that when the quadrotor pitches up or down there is a loss of altitude due to the tilt of the thrust vector, which is followed by divergent oscillations of θ . The only means of avoiding this would be to simultaneously increase the thrust in all the four rotors as soon as the vehicle starts to pitch. This would be done with a “Signal 2” that would be added to the previous.

The equation governing this increase in thrust would be: $\Delta T_2(t) = \frac{W}{4 \cos \theta(t)}$ (where W is the total weight and the “2” subscript denotes that the increase in thrust is done through “Signal 2”). The ideal $\theta(t)$ would be similar to that of Figure 16.19, but negative.

It would be interesting to test whether this technique can effectively work.

16.9 Forward flight

In horizontal flight at constant speed the quadrotor has a slight pitch down attitude so that there is a horizontal component of the thrust to overcome the drag over the airframe and the in-plane forces over the rotors.

Since the vehicle is moving forward, there will be an in-plane velocity at each rotor. As a result, there will also be a non-zero f_x force at each rotor (both due to the H force and to the tilt of the TPP). Since the c.g. of the vehicle is not in the HP (Hub Plane), these in-plane forces will create a pitch up moment. This effect was first described by Hoffmann *et al* (Ref 16.3) who wisely identified it as a source of pitch control problems.

Besides, there will also be a lateral tilt of the TPP. The TPP of the clockwise rotors will be slightly tilted to the right (as seen from behind) whereas the TPP of the other two rotors will be tilted to the left. This is just the opposite of what happens in usual helicopter rotors and had to do with blade stiffness (see Section 13). In any case, since one couple of rotors is tilted to the right and the other to the left, there will be no net lateral force.

We still have to consider the in-plane hub moments. In forward, horizontal flight, these are:

$$(M_x)_{hub} = \pm \left(\frac{1}{2} be\Omega^2 \frac{M_b}{g} + k_\beta \right) b_{1s} - \frac{\pm Q \tan a_{1s}}{\sqrt{1 + \tan^2 a_{1s} + \tan^2 (\pm b_{1s})}} \quad (16.3)$$

$$(M_y)_{hub} = \left(\frac{1}{2} be\Omega^2 \frac{M_b}{g} + k_\beta \right) a_{1s} + \frac{\pm Q \tan (\pm b_{1s})}{\sqrt{1 + \tan^2 a_{1s} + \tan^2 (\pm b_{1s})}} \quad (16.4)$$

\pm accounts for the direction of turn of the rotors (+ when counter clockwise, – if contrary), as explained before.

In forward, steady flight a_{1s} , b_{1s} and Ω will be equal in the four rotors (although maybe not rigorously equal). Hence, since two rotors are spinning clockwise and the other two, counter clockwise, the roll moments $(M_x)_{hub}$ are going to be cancelled. This was first commented by Hoffmann *et al* and led to them ignoring b_{1s} in all their analysis. However, b_{1s} might be relevant in other situations and it is not advisable to ignore it. On the other hand, if we sum the four pitch moments $(M_y)_{hub}$, the result is not zero, but positive. This means that there is a net pitch up moment around the c.g. of the

vehicle. This moment will reinforce that created by the f_x forces, which was also a pitch up moment, further complicating attitude control.

These pitch up moments has to be cancelled somehow. And the only way to do so is by having a different thrust in the front and rear rotors. However, it might occur, as Hoffmann *et al* explain, that the control moment produced by independently adjusting the thrust in the two rotors will be incapable of cancelling the unwanted pitch up moments at all times. This will definitely have to be investigated further.

We can use the *trim* command to try to trim the quadrotor in a horizontal flight condition. However, although *trim* does find a possible solution, when this is used as the initial condition for the Simulink model, the quadrotor soon departs from it and control is lost. This might be caused by an inadequate setup of the options of the *trim* command or just because the algorithms that it uses to find the point of equilibrium are not suitable for a system of the complexity of the quadrotor. It could also happen that the equilibrium solution is correct but that imperceptible variations of one or more variables of the state-space vector (due to the numerical error of the solver, for instance) make the system depart from this equilibrium. This issue should be investigated further.

In any case, it is clear that the problem of pitch control in horizontal, steady flight is one of the challenges to be faced when designing a controller for the quadrotor. Another challenge, which has already been described, is the attitude-altitude cross-coupling.

16.10 Control power

From the wind tunnel tests it is known that $\frac{\Delta C_T}{\Delta C_Q} \sim 5-10$. In the pitch up manoeuvre, the

control moment is approximately $2L\Delta T$, where ΔT is the amount by which the thrust is increased in the front rotor (decreased in the rear one) and $L = 0.453m$ is the moment arm. In the yaw manoeuvre, the control moment can be estimated as $4\Delta Q$, (where ΔQ is the amount by which the reaction torque is increased/decreased at each rotor). If we compare both moments:

$$\frac{M}{N} = \frac{2L\Delta T}{4\Delta Q} = \frac{L\Delta C_T}{2R\Delta C_Q} \sim \frac{\Delta C_T}{\Delta C_Q} \sim 5-10$$

Where it has been taken into account that $R = 0.258m$.

Hence, pitch control power should be 5 to 10 times larger than yaw control power. However, when we run the simulation we find that the former is only 3 times larger than the latter (approximately). This is probably because the *effective* pitch control power is smaller as a result of the damping introduced by C_T (see sub-section 16.5). On the other hand, there is much less damping on the yaw manoeuvre (see sub-section 16.7).

16.11 Gusts

In Section 14 it was explained that a simple gust model had been included in the simulation of the XPro. This model is fairly simple, although provisions have been made to include much more complex models in the future. It simulates the gust as a sudden movement of the whole mass of air relative to the ground. This is a simplification and as such has several implications. The gust velocity is usually not uniform, it depends on the coordinates in Earth axes. For example, gusts might be generated in the vicinity of obstacles. Since the gust velocity is not uniform (i.e., not all the mass of air moves at the same speed relative to the ground), it will neither be uniform across the vehicle body. This will lead to extra aerodynamic moments over the airframe. Besides, this non-uniformity will imply that each of the rotors will be working under different conditions. Of course, these effects will be proportional to the gradient of velocities. But in any case, they have not been modelled here.

Hence, our study of quadrotor response to gusts will be quite limited. However, this will not prevent us from reaching some interesting conclusions.

Vertical gust

Starting from a hovering condition, we expose the quadrotor to a vertical gust blowing from below:

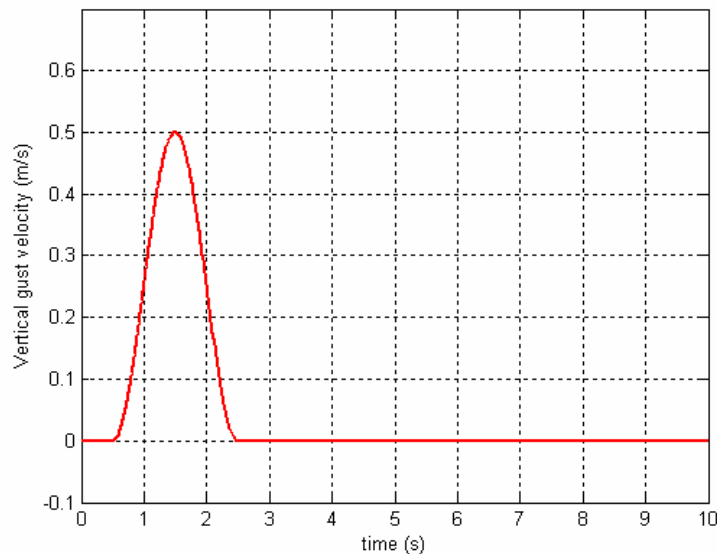


Fig 16.28. Vertical gust velocity, relative to the ground.

Since the gust comes from below, the air passing through the rotors will increase the thrust as seen in Section 13, and the quadrotor will ascend. As it starts to ascend, the velocity of the air that passes through the air will tend to decrease (and so the thrust)

unless the gust velocity keeps increasing and compensates for this. Figure below shows the history of w_e and z_e .

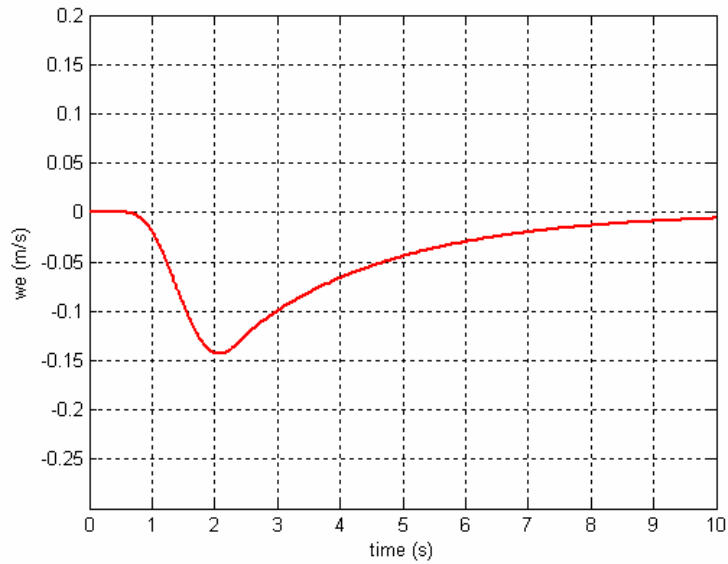


Fig 16.29. Vertical gust: quadrotor vertical velocity.

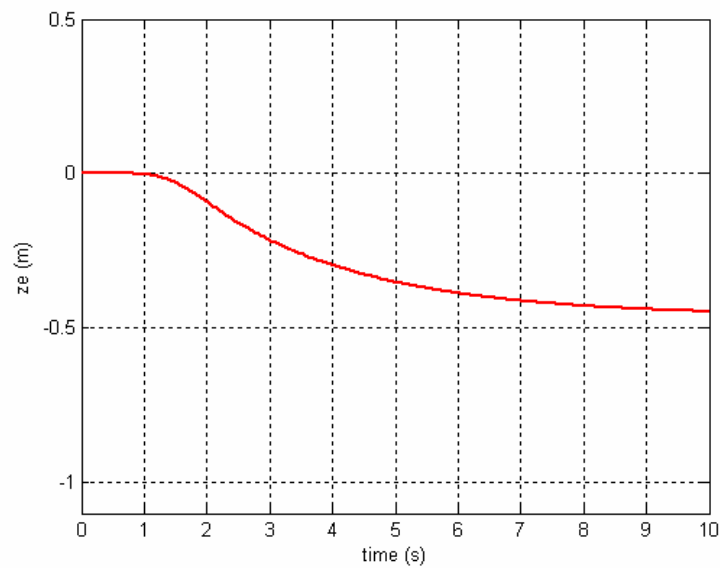


Fig 16.30. Vertical gust: altitude.

It can be seen that the response of the quadrotor in w_e and z_e is analogous to that of Figures 16.6 and 16.7, respectively. We can say that the quadrotor response is “stable”.

If the gust comes from above, the only thing that changes is that the quadrotor descends instead of ascending (this might be a problem if the vehicle is too close to the ground!).

Horizontal gust

We will now expose the quadrotor to a horizontal gust blowing from the front:

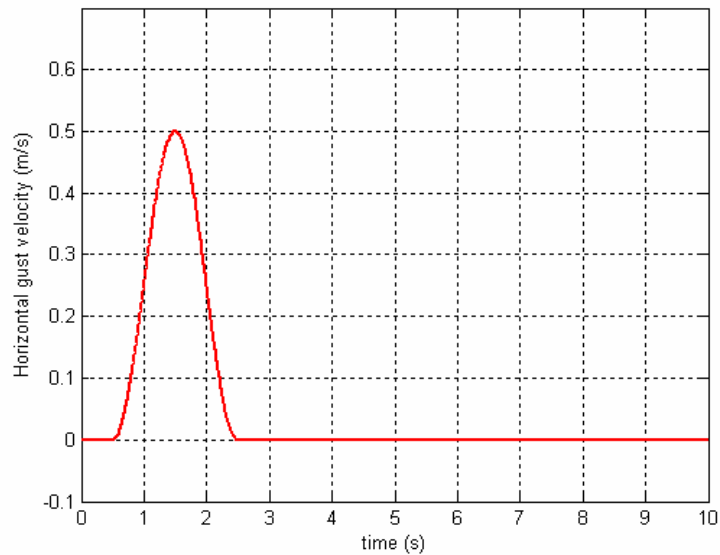


Fig 16.31. Horizontal gust velocity.

The response is completely different when the gust is horizontal. The unwanted pitch moment that was identified for horizontal, steady flight will be present, plus other possible effects that appear due to the fact that conditions are not steady now. It is more than likely that the quadrotor will depart from equilibrium and that control will be lost. This is what happens in fact, as the figure below shows:

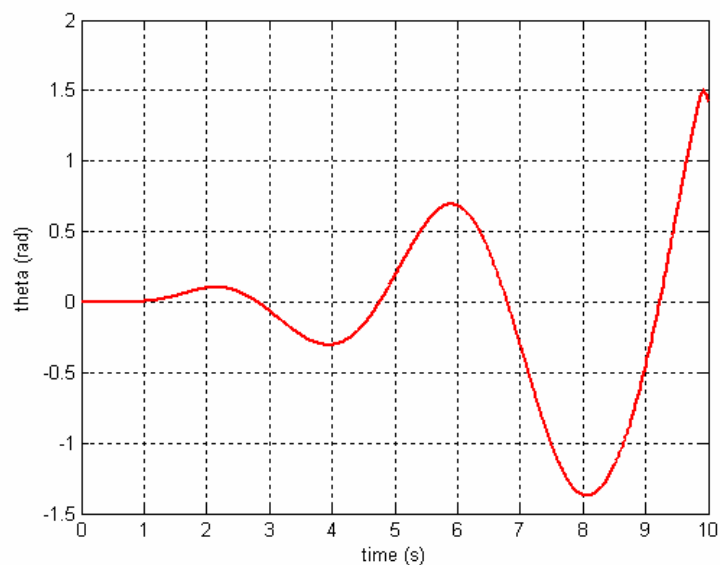


Fig 16.32. Horizontal gust: pitch angle.

The air is blowing from the front. Thus, an in-plane force f_x that points to the rear will appear at each rotor. Since the c.g. of the vehicle is below the HP, this force will create a pitch up moment. Once the quadrotor starts to pitch up, equilibrium is lost and the vehicle starts to oscillate as described in sub-section 16.4.

As explained in that sub-section, the potential benefit of raising the c.g. so that it is levelled with the HP is obvious. It is clear that the current configuration of the XPro, in which the heaviest element (the battery) is in the lowest position, is not the most convenient from this point of view.

16.12 Effect of the armature inductance L

As it was explained in Section 7, the armature inductance L affected the transient response of the motors, introducing a certain time lag. The influence of L can be assessed in different ways. One way could be to repeat the pitch up manoeuvre (with the gimbal support) using the double pulse signal and three different values of the inductance: L , $10L$ and $100L$, where L is the estimated inductance for the actual motor (1mH). The figure below shows the result for the pitch angle θ :

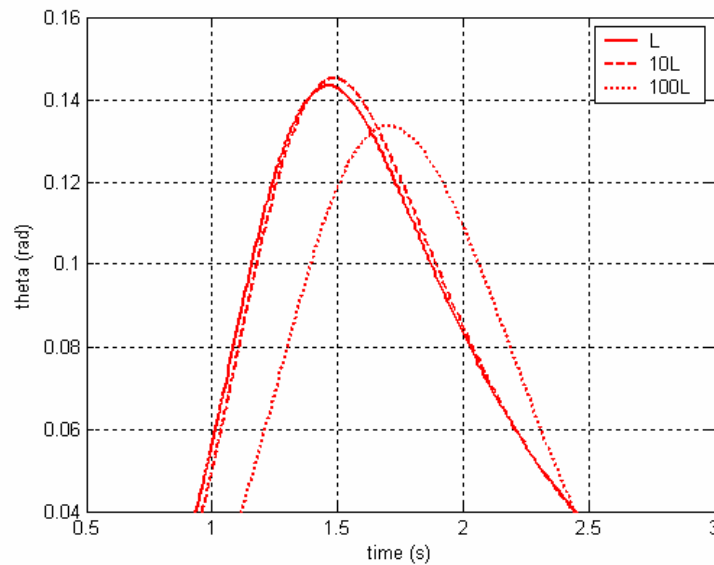


Fig 16.33. Effect of the inductance on the pitch up manoeuvre (double pulse input, gimbal support).

It can be seen that the difference in the time lag (the lateral separation between the peaks) is negligible between the L and $10L$ curves. It is necessary to increase the inductance in another order of magnitude ($100L$) to have a significant variation of the time lag. But the inductance is never going to be so high. Therefore we can conclude that the effect of the inductance on transients is very limited. The inertias of the armature and the load (the rotor) are much more important during the motor transients.

Because of this, many published quadrotor models ignore the inductance (see Refs 16.1 and 16.2, for example). However, it was necessary to confirm it, as we have done here.

It should be noted that we have assumed that the inductance is the same in the four rotors. If it is not (because of manufacturing tolerances, wear, etc) then the resulting “asymmetry” will make it more difficult to keep the quadrotor in equilibrium (see next sub-section).

16.13 Effect of asymmetries

With the term “asymmetries” we refer to small differences in the physical properties of elements of the vehicle that are supposed to be identical. These differences might affect the mass (for example, two arms that do not have the same mass), the geometry (misalignments), the electrical properties of the motors, etc. The reason why we call them “asymmetries” is because they effectively break the axial-symmetry that the quadrotor is supposed to have.

It will be shown, by means of several examples, that the quadrotor is extremely sensitive to these disturbances, which usually lead to it being incapable of remaining in equilibrium. A rigorous study of equilibrium points in the presence of these disturbances, at least from a mathematical point of view, would be very interesting.

It should be noted that what follows are just some examples of these disturbances. A complete study of all the possible asymmetries is not realizable since there are nearly infinite in number.

Any controller intended to be used to stabilize the quadrotor will have to compensate for the effects of these asymmetries.

Mass differences

Mass asymmetries will modify the total weight, the position of the centres of mass and the inertia tensors. In the default configuration, the XPro is already “asymmetrical”: the c.g. has a lateral offset (less than a millimetre, according to the CAD model) and the products of inertia of the airframe are non-zero. The second effect has been modelled while the first has been neglected until now.

If we include a lateral offset of the c.g. of 10mm, the *trim* command is still able to find a solution for hover. This solution indicates that the quadrotor has to be laterally tilted so that the moments are balanced. However, when we run the model using this solution as the starting condition, the quadrotor is not capable of remaining stable and departs from equilibrium. This is identical to what happened when we used the *trim* command to try to find a trim solution in forward flight, and the possible explanations are the same (errors in the proposed solution, sensitivity of it to numerical errors in the computing algorithm...).

Differences in the properties of the motors

In Ref 16.4 it is stated that small differences in the response of each of the motors are responsible for the unstable dynamics of a quadrotor. Although we have seen that there are many factors that contribute to making the quadrotor difficult to control (unwanted pitch/roll moments, cross-coupling between degrees of freedom...) it is likely that the differences in the response of the motors will be at least as important as those other factors.

Differences in the inductance:

It was confirmed that an increase in the inductance L of any of the motors relative to the others leads to unstable pitch oscillations when an identical pulse signal is fed into the four motors (“heave” manoeuvre).

Obviously, the smaller the relative differences between the inductances, the smaller too the amplitude of the oscillations in θ . In other words, the unstable behaviour will become noticeable later.

Differences in the internal resistance:

It was confirmed that when an identical pulse signal is sent to the four motors, if there is just a small difference in the resistance R_a of the front motor relative to the others (for example, a 5%) there will be intense, divergent oscillations first in pitch and then in roll and yaw. Of course, this could be avoided by modifying the amplitude of the signal sent to the front motor, relative to the other signals. However, since in reality the values of the internal resistance of each motor will not be known with precision, it will not be possible to apply the exact correction to each signal.

16.14 Modification of the previous results due to other effects

The quadrotor model that has been developed is very detailed. However, there are still some effects that have not been modelled, for different reasons. Other effects have been modelled but in a limited way, as we have seen (gusts, for instance).

Aerodynamic moments over the airframe

As explained in Section 11, the aerodynamic moments over the airframe, $\mathbf{M}_{\text{airframe}}^0$, can have the same order of magnitude as other moments studied here. Hence, their inclusion in the model could modify some of the results which have been obtained in this Section. In the absence of interference from the rotors, these moments over the airframe have always a damping effect, i.e., they oppose to the angular motion of the vehicle.

Aerodynamic interference

It was commented in Section 11 that the presence of the rotors significantly affected the aerodynamic forces and moments over the airframe. Conversely, the presence of the airframe modifies the predicted forces and moments at the rotors. According to Hoffmann *et al* (Ref 16.3), rotor thrust and torque might become unsteady as a result of vehicle body interference. This will lead to unsteady moments around the three axes. These moments can appear at any time during any of the manoeuvres described here.

Fortunately, according to Hoffmann *et al*, aerodynamic interference can be minimized with an adequate design of the vehicle; for example, by locating the rotors far enough from the centre of the airframe. It still has to be investigated whether it is necessary to introduce any such modifications in the XPro design.

Rotor instabilities

The unsteady behaviour of the rotor in certain situations is not only due to the aerodynamic interference of the airframe. When the rotor is isolated, like in the wind tunnel, this behaviour can also appear, as it has been confirmed in our tests.

One of the most obvious signs of this unsteadiness is the random fluctuation of the tilt angle of the TPP. These fluctuations are negligible in many situations but there were certain combinations of wind speed and angle of attack that make them become very intense. A detailed study of the causes of these fluctuations is out of the scope of this Report. But at least we know one of them, which is the unsteadiness of the airflow under the Vortex Ring and Turbulent Wake States (VRS and TWS).

Whatever reason might cause the random oscillations of the TPP, the consequence is the same: a random in-plane force that will create random moments around the three axes of the vehicle.

The only way to prevent these effects from happening is to avoid those situations in which the oscillations of the TPP are likely to occur, however, this might not be so easy to do. Besides, it requires knowing exactly which situations are those.

16.15 Conclusions

The main aim of this Section was to analyze the results produced by the Simulink model under several situations in order to determine whether they were realistic or not. It was hoped that this would serve as a “limited” model validation. This analysis has been done and all the results have been found to be supported by solid physical causes.

However, inevitably some effects have not been included in the model, and these effects could modify the results that have been obtained here. The influence of these effects has been assessed qualitatively, but their influence in quantitative terms is still unknown. It

is evident that the final answer to this question will not come without real flight data. Ultimately, these data will provide the means to carry out a proper validation of the model.

The second aim of this Section was to extract some relevant conclusions about the flight dynamics of quadrotors in general and the XPro in particular. To this respect, much is the information that has been gathered.

It has been confirmed that it is essential to model the in-plane forces and moments, as well as blade flapping, because of their importance in quadrotor flight dynamics.

It has been found that the use of step signals is the simplest way to control altitude and attitude. The dependence of C_T with λ_z has been identified as an important source of damping.

It has been observed that pitch/roll manoeuvres lead to divergent pitch/roll angles unless the loss of altitude is avoided. To this respect, it has been confirmed that raising the c.g. can limit this effect, because the moment arm of the in-plane force f_x is reduced. For the same reason, raising the c.g. is also beneficial to reduce the pitch up moment that appears in forward flight or in presence of horizontal gusts.

Finally, it has been shown that mass asymmetries create unwanted moments that are difficult to cancel even in hover. The same applies to the small variations of L or R_a from one motor to another.

17. CONCLUSIONS

17.1 Revision of the aims of the Research Project

Although the quadrotor concept is relatively old, it has gained popularity only very recently. Because of the novelty of this type of rotorcraft, there are many aspects related to it that need investigation. The most important issue is Stability and Control, because it is there where most of the challenges have arisen.

Any study of Stability and Control will require accurate models of the flight characteristics of quadrotors, and it is in this context that this Research Project was proposed.

The aim of this Research Project as explained in the Introduction was to produce a quadrotor model that could be later used as a tool for the study of Stability and Control. This model would be programmed in Matlab/Simulink and would be based around the Draganfly XPro quadrotor. In order to enable this quadrotor to fly autonomously, several controllers have been proposed. It was expected that these controllers could be tested in the model before trying to implement them in the real vehicle. Hence, the accuracy of the model (and thus the level of detail) had to be in accordance with this task. Ideally, the model should have enough flexibility to be adapted in the future to simulate other quadrotors apart from the XPro.

Although this was the global aim of the Project, it was also expected that in developing the model all the published information about quadrotor flight dynamics could be gathered. This was relevant because there is still not much published information about quadrotors, and that which is available is usually scattered and incomplete. It was felt that all this information could be united in a single piece of work that could serve as a starting point for future research.

As it has been said before, controllers were to be tested afterwards on the Matlab/Simulink model. However, the model itself, as developed during the Project, was not to include any controller. In other words, it would only simulate open-loop flight dynamics. Although a real quadrotor is not likely to be flown in open loop, it was felt that having detailed information about flight handling characteristics in open loop would be very interesting, especially in order to understand the challenges that any possible controller will have to face. This was another objective of this Research Project.

17.2 Summary of the model features

A working Matlab/Simulink model of the Draganfly XPro has been produced. The most important features of this simulator are listed below.

Rotor modelling

The rotor model is based on Blade Element Theory (BET) combined with “Modified” Momentum Theory (MMT). This “Modified” Momentum Theory produces valid results even in those situations where the “Classic” theory fails (e.g. vertical descent).

Blade flapping has been included, since it has a significant influence on quadrotor flight dynamics. To model it, the real blade has been replaced by a perfectly rigid blade with an offset hinge and a torsional spring. Rotor in-plane forces and moments have been included too. The author has not found any other model that has included all these in-plane forces and moments with the same level of detail.

The influence of vehicle angular rates on blade flapping dynamics has also been modelled.

The rotor model has been partially validated using wind tunnel tests data. Thrust and torque predictions have been found to be satisfactory. Predictions of flapping and coning angles have been compared to a limited set of experimental data. It has been found that these angles have been overestimated, although the trends are well represented. On the other hand, no reliable measures of the in-plane forces and moments were available to compare them with the results from the model.

Motor model

Linear equations have been used, as in all the published reports about quadrotors powered by d.c. motors. Correlation with experimental results is good, especially between 4 and 8 volts.

In most of the published models the inductance L is ignored. In the model used here, however, the inductance has been included to be able to assess its importance. It can now be confirmed that L is indeed negligible.

Dynamic model

The equations of motion have been written using Newton-Euler formulation. The effect of the moving parts on the dynamics of the whole vehicle has been considered. This is not a novelty in the case of the rotors but it is regarding the armatures. The rotating motion of these elements generates gyroscopic and inertial torques that affect the dynamics of the quadrotor. Although the rotor has a larger inertia, the armature is much heavier and rotates faster, and thus the effect of both can be of a similar order of magnitude.

Environment

Horizontal and vertical gusts have been included. In addition, the Simulink program is flexible enough to accommodate more sophisticated models of gusts.

Ground effect has not been included, but provisions have been made so that an externally developed model of this effect can be easily integrated into the simulation.

Matlab/Simulink programming

A variable-step solver is used to integrate the equations. This means that the simulation will run at variable speed. Under certain conditions, especially when the state-space vector is rapidly changing, the step size can be very small and the simulation will run slower than real time. In other situations it will run faster. Usually, execution speeds range between 0.1 and 1 seconds of computing time per second of simulated time. If the inductance L is neglected the simulation runs much faster.

The quadrotor simulation has been designed in a modular way, so that changes can be introduced easily. The amount of features that are “hardcoded” has been kept to a minimum. In addition, all the model parameters (masses, blade geometry, etc) are kept on a separate file that can be modified to simulate other quadrotors besides the XPro.

Miscellaneous

The quadrotor is a very unstable vehicle. The lack of damping and the cross-coupling between degrees of freedom makes it very sensitive to disturbances. Among these disturbances are the “asymmetries”, that is, the differences between elements of the vehicle that are expected to be identical. For example, differences in the mass of the rotors, or in the electrical properties of the motors. Because of their impact on Stability and Control, it is important to be able to introduce these “asymmetries” in the simulation. The Matlab/Simulink model offers this capability. Thanks to it, it has been possible to conduct some simulations to assess the effect of these “asymmetries” (see Section 16).

17.3 Important findings

The simulations conducted with the Matlab/Simulink model provided useful information about open loop flight dynamics. Additional information, in this case about the aerodynamics of the rotor, was obtained from the wind tunnel tests.

The fact that attitude and linear velocity could not be controlled independently in a quadrotor was already known. This was the reason why the quadrotor has been defined as an underactuated vehicle. One of the most important findings of this Project was that there is another phenomenon that contributes to the cross-coupling between attitude and linear velocity. This is the existence of forces and moments in the rotor Hub Plane (the plane perpendicular to the hub axis). These “in-plane” forces and moments are inextricably linked to blade flapping dynamics, although there are some other factors involved.

There are several examples that illustrate the influence of the in-plane forces and moments in the cross-coupling between attitude and linear velocity. In forward flight, they create pitch moments at the c.g. of the vehicle, which might be impossible to

balance. In vertical flight any disturbance in the pitch or roll angles will result in non-zero in-plane forces that will create pitch/roll moments around the c.g.

Another important result was to be able to confirm the importance of rotor thrust as a source of damping. Thrust is highly dependent on the component of the air velocity vector which is perpendicular to the rotor. When the air blows from above, thrust decreases, whereas if the air is blowing from below, it increases. As a result, thrust opposes to disturbances in the vertical speed of the vehicle. Besides, it has a damping effect when the quadrotor pitches or rolls, because it creates a restoring moment around the c.g. of the vehicle.

Thanks to this characteristic of rotor thrust, it is possible to reach and then maintain a specific altitude by means of a single pulse signal (two step signals).

Other relevant findings are related to rotor aerodynamics. For instance, it was discovered that the aerodynamic model used for the rotor, based on Blade Element Theory combined with “Modified” Momentum Theory, failed when the rotor was spinning at very low speeds (below $80\text{--}100\text{rad/s}$). In these conditions, contrary to what happened at higher speeds, thrust and torque coefficients were found to depend on the spinning speed, according to experimental data. It is this dependence that the rotor model failed to predict.

17.4 Comparison between the original aims of the Project and what was finally achieved. Assessment of the results obtained and the work done.

The quadrotor model which was developed had a higher level of detail than many published models (Refs 1.2, 1.4, 1.7, 1.9 to 1.11 and 1.13). However, the lack of real flight data made it impossible to validate the model in a complete and rigorous way.

The simulation results were studied and it was concluded that these results were in accordance with the “expected” flight behaviour. Nevertheless, this cannot be a substitute for full model validation. In reality, effects which are not included in the model might be dominant (such as unsteady aerodynamics or rotor-airframe interference), leading to results different from those predicted. Although it is expected that this will not be the case, this cannot be confirmed without real flight data.

It is very unlikely that the quadrotor will be flown in open loop, because of the risk. Hence, all the experimental data will be necessarily obtained in closed loop conditions. Before comparing these data with the model, the loop will have to be modelled too.

Model validation, although desirable, was not among the objectives of the Research Project. The main goal was to produce the model, and this has been achieved. In fact, as it has just been said, the simulation has a level of detail above that of other known quadrotor models. It still has to be determined, though, if the accuracy of the model is in accordance with its purpose, which was to be used to test control algorithms. There is no simple answer to this question. On the one hand, it is clear that, thanks to its higher level of detail, this model will be more adequate for this task than others. On the other

hand, it might occur that this level of detail is still not enough for the purpose of testing controllers.

A very specific issue has to do with modelling in-plane forces and moments. It has been found that these have a great influence on flight dynamics and therefore it is essential to model them. But for the same reason, failure to calculate them accurately might lead to incorrect predictions of the flight response. This is a primary source of concern, because in-plane forces and moments are very sensitive to the assumptions made during its calculation, and thus it is easy to overestimate or underestimate them. Moreover, there are many effects not included in the model which can be affecting them. Because of this, all the results in which the magnitude of these forces and moments is decisive should be treated cautiously. Nevertheless, it is believed that, qualitatively, the simulation results will be the same regardless of the accuracy of the estimates of the in-plane forces and moments.

To better understand this, an example can be used. In forward flight, it is known that the referred forces and moments create a pitch up moment around the c.g. of the vehicle. The existence of this pitch up moment will be predicted by the model. But the model will also indicate the value of this moment. It is that value that has to be treated cautiously. Fortunately, if we want to test a control algorithm what we need is a model that can predict the existence of that pitch up moment, the rest is not so important.

Anyway, it has to be borne in mind that a moderate increase in the level of detail will probably require substantially larger resources. The author considers that this is a very important conclusion. It is felt that the actual model is already pushing to the limits the theories on which it is based (BET and MMT, as for the rotor). Higher accuracy will mean moving to more sophisticated theories (wake methods, CFD) or adopting an entirely different approach based on system identification. In both cases, but particularly in the second, vast arrays of experimental data will be needed, and no doubt that to obtain these data larger and better testing equipment will be needed.

Besides, more accuracy will probably imply less flexibility. The model that has been developed here can be easily adapted to simulate other quadrotors, or different configurations of the same vehicle. But it is unlikely that models based on more complex theories or on system identification techniques will so flexible. This is particularly true for the latter.

17.5 Suggestions for future work

Additions to the physical model

Several effects have been omitted in the quadrotor model. These are listed below:

- Reverse flow region
- Blade tip losses
- Blade Feathering and Lead-Lag
- Nonlinearities in the motor model

- Rotor instabilities (thrust and torque fluctuations)
- Rotor-airframe aerodynamic interference
- Aerodynamic forces and moments over the airframe
- Airframe flexibility (vibrations)

The inclusion of any of these in the future would be an interesting improvement over the current model. Nevertheless, some of these effects will be definitely more important than the others, and so they should receive more attention. According to some recently published papers (Ref 1.7), rotor instabilities and rotor-airframe interference might play a very significant role in quadrotor flight dynamics. On the other hand, blade lead-lag might introduce some vibrations in the hub, but it is not likely to have a significant impact on flight dynamics.

It should be borne in mind that most of these effects cannot be included just by making some minor modifications into the model. With the possible exception of the first four, all the other effects will require sophisticated theories and/or large amounts of experimental data in order to be adequately modelled. In some cases this effort might be justified by the subsequent improvement in the correlation between simulation results and real flight data, but in others the gain might be minimal.

Anyway, there will always be a limit as to the level of detail of the simulation, due to the existing constraints (computational resources, lack of experimental data, time available, etc).

Quality and quantity of experimental data

Although the rotor model is theoretical, many of its parameters ($a, c_{d0}, c_{d1}, c_{d2}, k_{\beta} \dots$) have been inferred from experimental data. Besides, experimental data have been used to validate the rotor model.

Hence, it is obvious that any improvement in the amount and quality of the data available will lead to better estimates of the parameters needed and will allow a more rigorous validation of the model. The latter applies specifically to the measures of the in-plane forces and moments, as well as to the coning and flapping angles. The balance which was used in the wind tunnel tests did not have the necessary accuracy to produce reliable measures of those in-plane forces and moments. As for the coning and flapping angles, the number of measures available was too limited. Both the in-plane forces and moments and the flapping angles play a very important role in Stability and Control, as it has been shown. Therefore, it is essential to confirm that the simulation is estimating them accurately, and to do so, first we need large amounts of reliable experimental data.

Improvements in the Matlab/Simulink simulation

A significant improvement would consist in adding graphics to the simulation. To this respect, the easiest methods are to use VRML or to link the model to the Flight Gear simulator.

Future research on quadrotor flight dynamics

There are many areas where further investigation is required in order to improve the understanding of quadrotor flight dynamics. Some of them have already been identified in this Report.

Firstly, it is necessary to study in more detail the points of equilibrium of the system in open loop. Until now, only hover has been studied thoroughly. It would be very interesting to study equilibrium in forward flight, or in hover but under mass asymmetries (c.g. lateral offset). It has been shown that it is not easy to trim the quadrotor in these conditions, so any study about this topic would be welcome.

In order to develop suitable controllers for the quadrotor, the model will have to be linearized around one or more of the points of equilibrium previously mentioned. Linearization is indeed an unavoidable task.

Once the controllers have been selected and optimized, they will have to be tested in the nonlinear model. This will also allow comparing open-loop and closed-loop flight dynamics.

Validation of the open-loop, nonlinear model which has been developed here probably will not be possible, since the real flight data required for that will be obtained with a quadrotor flying in closed-loop. However, once the loop and the controller have been added to the model, validation will be possible at last.

It is likely that comparison with real flight data will reveal several discrepancies. These may be due to unforeseen effects or to the limitations of the theories on which the model is based. However, the author is confident that the flexibility of the model will allow modification to correct these problems. Even if that is not possible and an entirely new, purely empirical model is needed, the author hopes that the present model will remain a useful tool to understand how the different parameters influence the flight characteristics of the quadrotor.

Future research on other areas

In the study of quadrotors there are other subjects that could be explored, not linked with flight dynamics but with performance and operational capabilities. For example, it would be interesting to study the impact on performance of replacing the two-blade rotors with three-blade ones. It is obvious that this would increase the total thrust and therefore the payload capacity. On the other hand, it would increase the power consumption, reducing flight endurance. What needs to be investigated is the ratio between the new and the old power consumption, because if it is not very high, maybe it would be interesting to use three-blade rotors.

Another possible improvement in the performance of the quadrotor would come with the installation of brushless motors instead of the original ones. It would have to be investigated if their advantages compensated the extra weight and cost.

The same could be said of the use of ducted rotors. A ducted rotor might have some aerodynamic advantages. On the other hand, it weighs more and is structurally more complex.

Another issue would be the use of alternative systems for attitude control. In Section 2 it was mentioned that it was possible to control attitude by modifying the pitch angle of the blades. This method offered the advantage of a nearly instantaneous response, but it also increased the mechanical complexity of the rotor. A study about this control method would be welcome.

Of course, there are many other areas of interest, but if they were all to be included here the list would become endless. The potential applications of the quadrotor are enormous, so any new study about it will be useful.

REFERENCES

1. INTRODUCTION

- 1.1 Pounds, P., Mahony, R., Hynes, P. and Roberts, J. (2002). **Design of a Four-Rotor Aerial Robot**. In: Proc. Australasian Conference on Robotics and Automation, Auckland, 27-29 November 2002.
- 1.2 Pounds, P., Mahony, R., Gresham, J., Corke, P. and Roberts, J. **Towards Dynamically-Favourable Quad-Rotor Aerial Robots**. In: Proc. Australasian Conference on Robotics and Automation, Canberra, December 2004.
- 1.3 Pounds, P. and Mahony, R. **Small-scale Aeroelastic Rotor Simulation, Design and Fabrication**. In: Proc. Australasian Conference on Robotics and Automation, Sydney, 2005.
- 1.4 Pounds, P., Mahony, R. and Corke, P. **Modelling and Control of a Quad-Rotor Robot**. In: Proc. Australasian Conference on Robotics and Automation, 2006.
- 1.5 McKerrow, P. (2004). **Modelling the Draganflyer four-rotor helicopter**. In: Proc. IEEE International Conference on Robotics & Automation, New Orleans, LA, April 2004.
- 1.6 Hoffmann G.M., Rajnarayan, D.G., Waslander, S.L., Dostal, D., Jang, J.S. and Tomlin, C.J. **The Stanford Testbed of Autonomous Rotorcraft for Multi Agent Control (STARMAC)**. In: Proc. of the 23rd Digital Avionics Systems Conference, Salt Lake City, Utah, November, 2004.
- 1.7 Hoffmann, G.M., Huang, H., Waslander, S.L. and Tomlin, C.J. (2007). **Quadrotor Helicopter Flight Dynamics and Control: Theory and Experiment**. AIAA.
- 1.8 Altug, E., Ostrowski J.P. and Taylor, C.J. (2003). **Quadrotor control using dual camera visual feedback**. In: Proc. IEEE International Conference on Robotics & Automation, Taipei, Taiwan, September 2003.
- 1.9 Bouabdallah, S., Murrieri, P. and Siegwart, R. (2004). **Design and Control of an Indoor Micro Quadrotor**. In: Proc. IEEE International Conference on Robotics & Automation, New Orleans, LA, April 2004.
- 1.10 Bouabdallah, S., Noth, A. and Siegwart, R. **PID vs LQ Control Techniques Applied to an Indoor Micro Quadrotor**. <http://ieeexplore.ieee.org/iel5/9577/30277/01389776.pdf>. (accessed 10th January 2007).

- 1.11 Chen, M. and Huzmezan, M. (2003). **A Simulation Model and H_{∞} Loop shaping Control of a Quad Rotor Unmanned Air Vehicle**. In: Proc. of the IASTED International Conference on Modelling, Simulation and Optimization, Banff, Canada, 2-4 July 2003.
- 1.12 Klauske, L., Lorenz, T., Colberg, N., Janke, M., Mönich, U., Nothing, N., Thiele, L., Venzke, F., Wernicke, T., Zeiler, S. and Kusch, R. **DSP-Copter - A Quadrotor Helicopter Controlled by a Digital Signal Processor**. https://www.emsp.tu-berlin.de/Members/Kusch/DSPcopter_digest.pdf. (accessed 10th January 2007).
- 1.13 Tayebi, Abdelhamid and McGilvray, Stephen. (2006) **Attitude Stabilization of a VTOL Quadrotor Aircraft**. IEEE Transactions on Control Systems Technology, Vol. 14, No. 3, p. 562-571.
- 1.14 Waslander, S.L., Hoffmann, G.M., Jang, J.S. and Tomlin, C.J. **Multi-Agent Quadrotor Testbed Control Design: Integral Sliding Mode vs. Reinforcement Learning**. In: Proceedings of IEEE/RSJ International Conference on Intelligent Robots and Systems, Edmonton, Alberta, Canada, August, 2005.

2. FUNDAMENTALS OF THE QUADROTOR

- 2.1 Leishman, J.G. (2006). **Principles of helicopter aerodynamics**, 2nd ed. Cambridge University Press, Cambridge.
- 2.2 Prouty, R. (1990). **Helicopter Performance, Stability and Control**, reprint edition with corrections. Krieger, Florida.
- 2.3 Espino, J.L. and Cuerva, A. and Meseguer, J. (2004). **Helicópteros y Aeronaves Diversas II**. Escuela Técnica Superior de Ingenieros Aeronáuticos, Madrid.
- 2.4 Borenstein, Johann. (1996). **The Hoverbot-An Electrically Powered Flying Robot**. <http://www.eecs.umich.edu/~johannb/paper99.pdf>. (accessed 10th January 2007).
- 2.5 Unknown author. **Draganflyer V Ti**. Draganfly Innovations Inc, Saskatoon.
- 2.6 Piasecki Aircraft Corporation. **PA-39**. <http://www.piasecki.com/pa-39.htm>. (accessed 17th August 2007).
- 2.7 Unknown author. (1997). **Jane's helicopter markets and systems**, Jane's Information Group.

- 2.8 Pounds, P., Mahony, R., Hynes, P. and Roberts, J. (2002). **Design of a Four-Rotor Aerial Robot**. In: Proc. Australasian Conference on Robotics and Automation, Auckland, 27-29 November 2002.
- 2.9 Planet Aerospace. **The Quattrocopter**. <http://www.planet-aerospace.com/pas/content/OF00000200000057/6/04/200009046.pdf>. (accessed 10th January 2007).
- 2.10 EADS. **Quattrocopter A Unique Micro Aerial Vehicle**. <http://www.eads.net/xml/content/OF00000000400004/3/45/559453.pdf>. (accessed 10th January 2007).
- 2.11 Atair Aerospace. **Quad Copter**. <http://www.atairaerospace.com/dev/quad-copter/>. (accessed 10th January 2007).
- 2.12 **Human Powered Helicopters**. <http://www.humanpoweredhelicopters.org>. (accessed 26th January 2007).

3. THE DRAGANFLY XPRO

- 3.1 Unknown author. (2003). **DraganFly XPro Flyer Assembly and Maintenance Manual**. Spectrosolutions Inc.

4. EQUATIONS OF MOTION

- 4.1 Ginsberg, J.H. (1995). **Advanced Engineering Mechanics**, 2nd ed. Cambridge University Press, Cambridge.
- 4.2 Cook, M.V. (1997). **Flight Dynamics Principles**. Arnold, London.

5. ESTIMATION OF MASS AND INERTIAL PROPERTIES

- 5.1 Green, M.W. (1927). **NACA TN 265: Measurement of the moments of inertia of full scale airplanes**. NACA.
- 5.2 Miller, M.P. (1930). **NACA TN 351: An accurate method of measuring the moments of inertia of airplanes**. NACA.
- 5.3 Miller, M.P. and Soulé, H.A. (1934). **NACA TN 467: The experimental determination of the moments of inertia of airplanes**. NACA.

- 5.4 Gracey, W. (1948). **NACA TN 1629: The experimental determination of the moments of inertia of airplanes by a simplified compound-pendulum method.** NACA.
- 5.5 Turner, H.L. (1950). **NACA TN 2201: Measurement of the moments of inertia of an airplane by a simplified method.** NACA.

6. EQUATIONS OF THE MOTORS

- 6.1 Edwards, J.D. (1986). **Electrical machines: an introduction to principles and characteristics**, 2nd ed. Macmillan.
- 6.2 Zaccarian, Luca. **DC motors: dynamic model and control techniques.** <http://robot2.disp.uniroma2.it/~zack/LabRob/DCmotors.pdf>. (accessed 10th January 2007).

7. ESTIMATION OF THE CONSTANTS OF THE MOTORS

8. OVERVIEW OF THE ROTOR MODELS

- 8.1 Leishman, J.G. (2006). **Principles of helicopter aerodynamics**, 2nd ed. Cambridge University Press, Cambridge.
- 8.2 Pounds, P., Mahony, R., Gresham, J., Corke, P. and Roberts, J. **Towards Dynamically-Favourable Quad-Rotor Aerial Robots.** In: Proc. Australasian Conference on Robotics and Automation, Canberra, December 2004.
- 8.3 Pounds, P., Mahony, R. and Corke, P. **Modelling and Control of a Quad-Rotor Robot.** In: Proc. Australasian Conference on Robotics and Automation, 2006.
- 8.4 Prouty, R. (1990). **Helicopter Performance, Stability and Control**, reprint edition with corrections. Krieger, Florida.
- 8.5 Hoffmann, G.M., Huang, H., Waslander, S.L. and Tomlin, C.J. (2007). **Quadrotor Helicopter Flight Dynamics and Control: Theory and Experiment.** AIAA.
- 8.6 Newman, S. (1994). **The Foundations of Helicopter Flight.** Edward Arnold, London.

- 8.7 Padfield, Gareth D. (1996). **Helicopter Flight Dynamics**. Blackwell, Oxford.
- 8.8 Bramwell, A.R.S. (1976). **Helicopter Dynamics**. Arnold, London.
- 8.9 Bramwell, A.R.S., Balmford, D. and Done, G. (2001). **Bramwell's Helicopter Dynamics**, 2nd ed. Butterworth-Heinemann, Oxford.
- 8.10 Wheatley, J.B. (1934). **Technical Report 487: An aerodynamic analysis of the autogiro rotor with a comparison between calculated and experimental results**. NACA.
- 8.11 Bailey, F.J. **Technical Report 716: A simplified theoretical method of determining the characteristics of a lifting rotor in forward flight**. NACA.

9. MODELLING OF THE ROTOR

- 9.1 Newman, S. (1994). **The Foundations of Helicopter Flight**. Edward Arnold, London.
- 9.2 Padfield, Gareth D. (1996). **Helicopter Flight Dynamics**. Blackwell, Oxford.
- 9.2 Bramwell, A.R.S., Balmford, D. and Done, G. (2001). **Bramwell's Helicopter Dynamics**, 2nd ed. Butterworth-Heinemann, Oxford.
- 9.3 Cooke, Alastair K. and Fitzpatrick, Eric W.H. (2002). **Helicopter test and evaluation**. Blackwell and QinetiQ, Oxford.
- 9.4 Prouty, R. (1990). **Helicopter Performance, Stability and Control**, reprint edition with corrections. Krieger, Florida.
- 9.5 Young, M.I. (1962). **A Simplified Theory of Hingeless Rotors with Application to Tandem Rotors**. Proceedings of the 18th Annual National Forum of the AHS.
- 9.6 Leishman, J.G. (2006). **Principles of helicopter aerodynamics**, 2nd ed. Cambridge University Press, Cambridge.
- 9.7 Harris, F.D. (1972). **Articulated rotor blade flapping motion at low advance ratio**. *Journal of the American Helicopter Society*, January.
- 9.8 Yntema, Robert T. (1955). **Technical Note 3459: Simplified procedures and charts for the rapid estimation of bending frequencies of rotating beams**. NACA.

10. INDUCED FLOW

- 10.1 Johnson, W. (1980). **Helicopter Theory**. Princeton University Press, Princeton.
- 10.2 Chen, R.T.N. (1989). **A Survey of Nonuniform Inflow Models for Rotorcraft Flight Dynamics and Control Applications**. NASA.
- 10.3 Glauert, H. (1926). **A General Theory of the Autogyro**. R&M No.1111, British A.R.C.
- 10.4 Coleman, R. P., Feingold, A. M. and Stempin, C. W. (1945). **ARR L5E10: Evaluation of the Induced-Velocity Field of an Idealized Helicopter Rotor**, NACA.
- 10.5 Prouty, R. (1990). **Helicopter Performance, Stability and Control**, reprint edition with corrections. Krieger, Florida.
- 10.6 Leishman, J.G. (2006). **Principles of helicopter aerodynamics**, 2nd ed. Cambridge University Press, Cambridge.
- 10.7 Wolkovitch, J. (1972). **Analytical Prediction of Vortex-Ring Boundaries for Helicopters in Steep Descents**. *Journal of the American Helicopter Society*, 17, No. 3, July.
- 10.8 Peters, D.A. and Chen, S. (1982). **Momentum Theory, Dynamic Inflow, and the Vortex-Ring State**. *Journal of the American Helicopter Society*, July.
- 10.9 Johnson, E.N. and DeBitteto, P.A. (1997). **Modeling and Simulation for Small Autonomous Helicopter Development**. AIAA.
- 10.10 Chen, C. (2006). **Development of a simplified inflow model for a helicopter rotor in descent flight**. Georgia Institute of Technology.
- 10.11 López Ruiz, J.L. (1993). **Helicópteros. Teoría y Diseño Conceptual**. Escuela Técnica Superior de Ingenieros Aeronáuticos, Madrid.
- 10.12 Espino, J.L. and Cuerva, A. and Meseguer, J. (2004). **Helicópteros y Aeronaves Diversas II**. Escuela Técnica Superior de Ingenieros Aeronáuticos, Madrid.

11. AERODYNAMICS OF THE AIRFRAME

- 11.1 Padfield, Gareth D. (1996). **Helicopter Flight Dynamics**. Blackwell, Oxford.
- 11.2 Leishman, J.G. (2006). **Principles of helicopter aerodynamics**, 2nd ed. Cambridge University Press, Cambridge.

12. WIND TUNNEL TESTS

13. ANALYSIS OF THE EXPERIMENTAL DATA. ROTOR MODEL VALIDATION

- 13.1 Bramwell, A.R.S., Balmford, D. and Done, G. (2001). **Bramwell's Helicopter Dynamics**, 2nd ed. Butterworth-Heinemann, Oxford.
- 13.2 Leishman, J.G. (2006). **Principles of helicopter aerodynamics**, 2nd ed. Cambridge University Press, Cambridge.
- 13.3 Prouty, R. (1990). **Helicopter Performance, Stability and Control**, reprint edition with corrections. Krieger, Florida.
- 13.4 Felker, F.F. and McKillip, R.M. (1994). **Comparisons of Predicted and Measured Rotor Performance in Vertical Climb and Descent**. AIAA.

14. BUILDING THE MATLAB/SIMULINK MODEL OF THE QUADROTOR

- 14.3 Hanselman, Duane and Littlefield, Bruce. (2001). **Mastering Matlab 6**. Pearson Prentice Hall, New Jersey.
- 14.2 Dabney, James B. and Harman, Thomas L. (2004). **Mastering Simulink**. Pearson Prentice Hall, New Jersey.
- 14.3 Unknown author. (2003). **DraganFly XPro Flyer Assembly and Maintenance Manual**. Spectrosolutions Inc.

15. LIMITATIONS OF THE MODEL

16. RUNNING THE MATLAB/SIMULINK MODEL OF THE QUADROTOR

- 16.1 Bouabdallah, S., Murrieri, P. and Siegwart, R. (2004). **Design and Control of an Indoor Micro Quadrotor**. In: Proc. IEEE International Conference on Robotics & Automation, New Orleans, LA, April 2004.

- 16.2 Tayebi, Abdelhamid and McGilvray, Stephen. (2006) **Attitude Stabilization of a VTOL Quadrotor Aircraft**. IEEE Transactions on Control Systems Technology, Vol. 14, No. 3, p. 562-571.
- 16.3 Hoffmann, G.M., Huang, H., Waslander, S.L. and Tomlin, C.J. (2007). **Quadrotor Helicopter Flight Dynamics and Control: Theory and Experiment**. AIAA.
- 16.4 Unknown author. **Draganflyer V Ti**. Draganfly Innovations Inc, Saskatoon.

17. CONCLUSIONS

APPENDIX A: MATLAB/SIMULINK MODEL

Version August 2007

Installation

1. Copy the contents of the folder Quadrotor_model into the chosen directory.
2. Open Matlab and select the previous directory.
3. Run the INITIALIZATION.m file. This will load into the workspace the variables required by the model.
4. Open QuadrotorSimulator.mdl and run it.

About the model

The “XPro” block simulates the Flight Dynamics of the Draganflyer XPro. The inputs are the voltages fed into each of the motors:

- v1: front motor
- v2: right motor
- v3: rear motor
- v4: left motor

The DC motors are rated from 0 to 12 volts, but the experimental results show that the normal operational envelope is 4 to 10 volts. The voltage corresponding to hover, in the real quadrotor, is approximately 7.5 volts. The value estimated by the model is slightly higher.

There are three additional inputs: the components of the velocity vector of the mass of air, relative to the ground:

- Vgust_x
- Vgust_y
- Vgust_z

The state-space vector is: $p, q, r, \phi, \theta, \psi, u, v, w, x_e, y_e, z_e, \Omega_1, \tau_1, \Omega_2, \tau_2, \Omega_3, \tau_3, \Omega_4, \tau_4$

Where:

p, q, r Body angular rates

ϕ, θ, ψ Euler angles (roll , pitch, yaw, respectively)

u, v, w	Components of the velocity of the point O in body axes (the point O is defined as the intersection between the central vertical axis of the quadrotor and the bottom plate)
x_e, y_e, z_e	Coordinates of the point O , in ground axes (notice that the Z axis points downwards)
$\Omega_1, \Omega_2, \Omega_3, \Omega_4$	Rotating speeds of the rotors, numbered with the same procedure as the motors
$\tau_1, \tau_2, \tau_3, \tau_4$	EM torques at each of the motors

All magnitudes are in S.I.

It should be noted that the front and rear rotors turn counter clockwise, whereas the left and right do it clockwise. This is represented by the sign of the rotating speeds, positive for Ω_1, Ω_3 and negative for Ω_2, Ω_4 . The same applies for $\tau_1, \tau_2, \tau_3, \tau_4$.

Initialization

The initial settings required by the model are provided by the INITIALIZATION.m file. Before running the model, ensure that the “Load from workspace” option is checked.

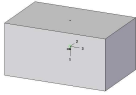
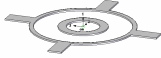
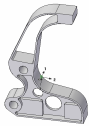
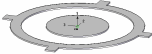
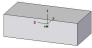

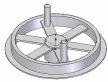
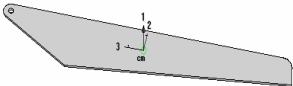
To change the initial state-space vector, modify the INITIALIZATION.m file. Please note that if the initial state-space vector is modified, the initial voltages settings should be changed in accordance.


The parameters of the physical model are stored in the DATA.m file.

The rest of the files should not be modified.

APPENDIX B: MASS AND INERTIAL PROPERTIES

MASS PROPERTIES

Item	Mass (grams)
Battery 	634
CFRP plate 	45
Arm bracket (4) 	26
Electronics Plate 	129 (including electronic components)
Receiver 	19
Arm (4) 	119
Gear (4) 	30
Blade (8) 	13

Motor (4) 	156
Other elements (Blade joints, screws, dome, etc)	101

Total: 2.356 kg

INERTIAL PROPERTIES (CAD MODEL)

Properties calculated with the Solid Edge model of the XPro. Only the default equipment of the XPro is considered.

Rigid airframe

x, y, z are the coordinates of the centre of mass of the rigid airframe on the set of axes $Oxyz$. Hence, $\mathbf{OG} = x\mathbf{i} + y\mathbf{j} + z\mathbf{k}$

$I_x, I_y, I_z, I_{xy}, I_{yz}, I_{xz}$ are the components of the inertia tensor of the rigid airframe *on a set of axes parallel to $Oxyz$ and with origin in the centre of mass of the rigid airframe.*

Mass	1.6571 kg
x	0.00 mm
y	-0.40 mm
z	-59.58 mm
I_x	0.062534 kgm ²
I_y	0.063547 kgm ²
I_z	0.119814 kgm ²
I_{xy}	-0.000027 kgm ²
I_{xz}	-0.000310 kgm ²
I_{yz}	0.000096 kgm ²

Hub

x, y, z are the coordinates of the centre of mass G_i of the front rotor in the $Oxyz$ frame.

I_x, I_y, I_z are the principal moments of inertia of the hub.

Mass	0.0578 kg
x	453.42 mm
y	-0.04 mm
z	-149.60 mm
I_x	0.000019 kgm ²
I_y	0.000019 kgm ²
I_z	0.000032 kgm ²

Blade

I_{yb} is the inertia of the blade around the effective hinge.

I_{zb} is the inertia of the blade around the axis of the hub.

Mass	0.013 kg
I_{yb}	0.000211 kgm ²
I_{zb}	0.000378 kgm ²

Armature

x, y, z are the coordinates of the centre of mass G_j of the front armature in the $Oxyz$ frame.

I_x, I_y, I_z are the principal moments of inertia of the armature.

Mass	0.1171 kg
x	520.51 mm
y	0.04 mm
z	-100.55 mm
I_x	0.000031 kgm ²
I_y	0.000031 kgm ²
I_z	0.000014 kgm ²

Complete vehicle

x, y, z are the coordinates of the centre of mass of the complete quadrotor on the set of axes $Oxyz$. Hence, $\mathbf{OG}_T = x\mathbf{i} + y\mathbf{j} + z\mathbf{k}$

$I_x, I_y, I_z, I_{xy}, I_{yz}, I_{xz}$ are the *mean* components of the tensor of inertia of the complete quadrotor on a set of axes parallel to $Oxyz$ and with origin in O .

Mass	2.356 kg
x	0.00 mm
y	-0.30 mm
z	-77.32 mm
I_x	0.1676 kgm ²
I_y	0.1686 kgm ²
I_z	0.29743 kgm ²
I_{xy}	0.0000 kgm ²
I_{xz}	-0.00030 kgm ²
I_{yz}	0.00014 kgm ²

APPENDIX C: TECHNICAL DATA OF THE MOTOR



RS-545SH

OUTPUT:5.0W-75W (APPROX)



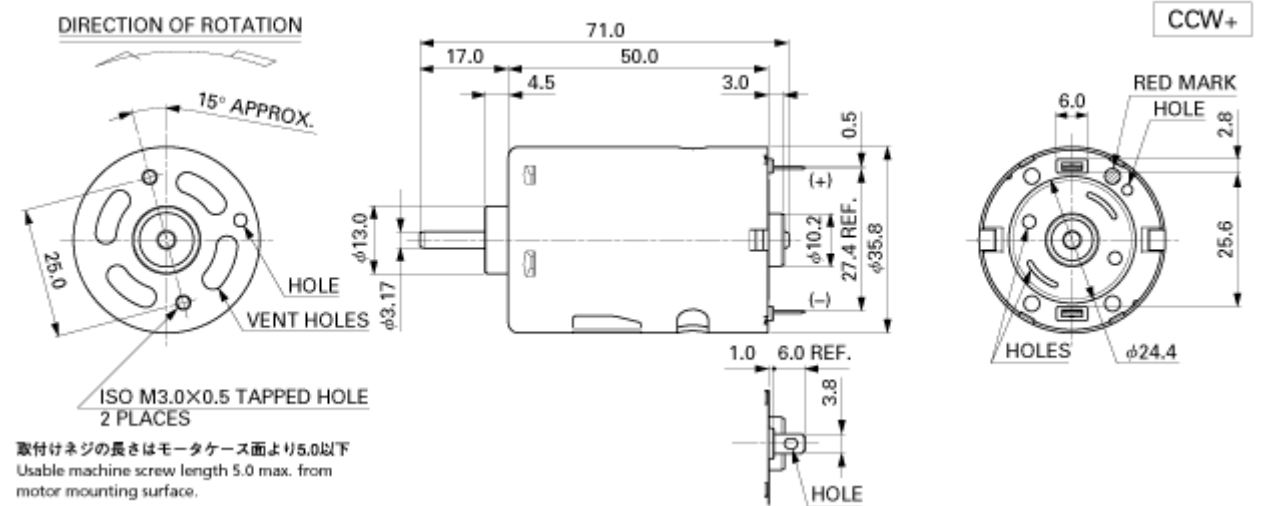
WEIGHT: 156g (APPROX)

Typical Applications :Automotive Products> Automatic Cruise Control
Home Appliances> Hair Dryer / Massager / Vibrator / Vacuum Cleaner / Bilge Pump

*By clicking the "MODEL", you can display the Performance Chart Simulation.

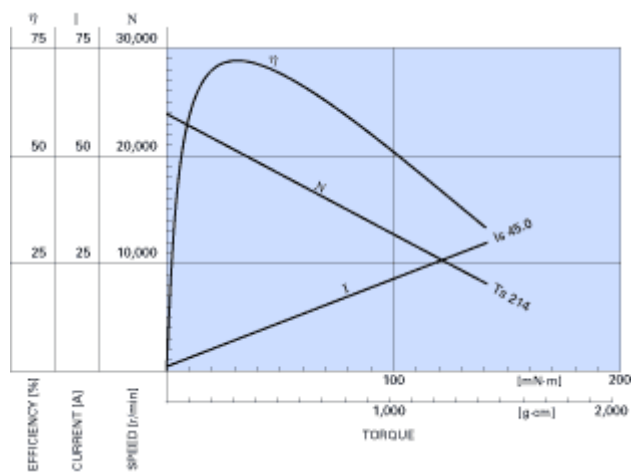
MODEL		VOLTAGE		NO LOAD		AT MAXIMUM EFFICIENCY					STALL		
		OPERATING RANGE	NOMINAL	SPEED	CURRENT	SPEED	CURRENT	TORQUE		OUTPUT	TORQUE		CURRENT
			V	r/min	A	r/min	A	mN·m	g·cm	W	mN·m	g·cm	A
RS-545SH	5018(*1)	4.5 - 12.0	12	24000	1.30	20510	7.65	31.1	317	66.7	214	2181	45.0

(*1) CCW shifted commutation (CCW+)
The terminal position against the tapped holes varies depending on CW+/NEUTRAL.



UNIT: MILLIMETERS

RS-545SH-5018	12.0V
---------------	-------



APPENDIX D: MOTOR TESTS

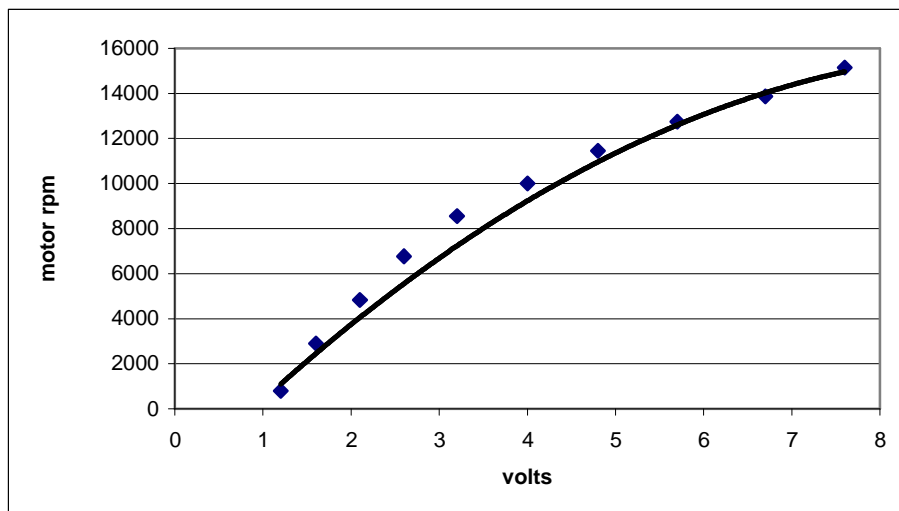
Motor tests results

Supply voltage (volts)	Armature current (amps)	Armature voltage (volts)	rotor rpm	motor rpm
1	1.2	0.64	80	800
2	1.6	1.52	244	2440
3	2.1	2.37	424	4240
4	2.6	3.22	575	5750
5	3.2	4.04	757	7570
6	4	4.8	912	9120
7	4.8	5.56	1076	10760
8	5.7	6.29	1238	12380
9	6.7	6.99	1397	13970
10	7.6	7.72	1515	15150

Estimated values of the constants

$$R_a = 0.291 \text{ ohm} \quad K = 0.00347 \text{ volts} \cdot \text{s} \cdot \text{rad}^{-1}$$

Motor-Rotor performance



Motor rpm against armature voltage, when the motor is driving the rotor. The solid line represents the “smoothed” experimental curve. The points represent the estimated results.

APPENDIX E: WIND TUNNEL TESTS

The following tables contain the raw measures of $f_x, f_z, (m_x)_{hub}, (m_y)_{hub}, m_z$, corrected for ISA conditions.

f_z and m_z have an estimated error of 10%.

The error of $f_x, (m_x)_{hub}$ and $(m_y)_{hub}$ is unknown.

α (deg)	Airspeed (m/s)	Armature voltage	Current (A)	Estimated Ω (rad/s)	f_z (N)	f_x (N)	m_z (Nm)	$(m_x)_{hub}$ (Nm)	$(m_y)_{hub}$ (Nm)
0	0	1.46	1.8	27	0.21770	-0.00174	-0.01066	0.00057	0.00138
0	0	2.34	2.2	49	0.59221	-0.00418	-0.02622	-0.00011	0.00268
0	0	3.19	2.7	69	1.11277	0.00223	-0.04792	-0.00061	0.00270
0	0	3.98	3.4	86	1.80368	0.00343	-0.07573	-0.00206	0.00528
0	0	4.8	4	105	2.59233	0.01673	-0.10577	-0.00328	0.00412
0	0	5.56	4.8	120	3.48781	0.03056	-0.14010	-0.00398	0.00491
0	0	6.32	5.6	135	4.49838	0.05284	-0.17572	-0.00435	0.00523
0	0	7.08	6.4	150	5.52147	0.06460	-0.21329	-0.00427	0.00191
0	0	7.84	7.2	165	6.60224	0.10192	-0.25288	-0.00480	0.00161
0	0	8.6	8	181	7.74448	0.13395	-0.29422	-0.00831	0.00061
0	0	9.33	8.9	194	8.93138	0.15341	-0.33712	-0.01224	-0.00596
-90	3.6	4.07	3.1	91	0.72224	0.01571	-0.05736	-0.00824	-0.00662
-90	3.6	4.89	3.7	110	1.34371	0.03344	-0.08743	-0.00859	-0.01056
-90	3.7	5.68	4.4	127	2.17300	0.05720	-0.12415	-0.01090	-0.01521
-90	3.8	6.44	5.2	142	3.05387	0.08222	-0.16233	-0.01433	-0.02027
-90	3.9	7.2	6	157	3.93443	0.10444	-0.20051	-0.01709	-0.02585
-90	4.0	7.93	6.9	171	4.95126	0.11830	-0.24283	-0.01925	-0.02998
-90	4.2	8.63	7.9	182	5.99935	0.13399	-0.28728	-0.02183	-0.03265
-90	4.3	9.42	8.6	199	6.91441	0.15271	-0.32455	-0.02305	-0.03783
-90	4.3	4.07	3.1	91	0.61472	0.02462	-0.05814	-0.01052	-0.00500
-90	4.4	4.89	3.7	110	1.20445	0.05158	-0.08841	-0.01277	-0.00856
-90	4.4	5.68	4.4	127	1.89542	0.07639	-0.12074	-0.01472	-0.01298
-90	4.5	6.47	5.1	144	2.72607	0.10104	-0.15751	-0.01826	-0.01679
-90	4.7	7.2	6	157	3.55543	0.12999	-0.19520	-0.02118	-0.02184
-90	4.8	7.96	6.8	172	4.49328	0.14720	-0.23611	-0.02355	-0.02717
-90	4.9	8.69	7.7	186	5.52131	0.16795	-0.27944	-0.02733	-0.03100
-90	5.0	9.45	8.5	201	6.46135	0.18237	-0.31839	-0.02837	-0.03570
-90	6.3	4.25	2.5	101	-0.35992	0.00295	-0.03161	-0.01393	-0.00114
-90	7.1	5.07	3.1	120	-0.24685	0.02620	-0.05251	-0.01742	-0.00382
-90	7.2	5.89	3.7	139	0.20885	0.05296	-0.08383	-0.02020	-0.00865

α (deg)	Airspeed (m/s)	Armature voltage	Current (A)	Estimated Ω (rad/s)	f_z (N)	f_x (N)	m_z (Nm)	$(m_x)_{hub}$ (Nm)	$(m_y)_{hub}$ (Nm)
-90	7.5	6.68	4.4	156	0.72167	0.07438	-0.11741	-0.02305	-0.01403
-90	7.6	7.44	5.2	171	1.39666	0.09036	-0.15544	-0.02554	-0.01848
-90	7.8	8.2	6	186	2.08504	0.11104	-0.19488	-0.02711	-0.02374
-90	7.7	8.9	7	198	3.14473	0.13425	-0.24193	-0.02923	-0.02821
-90	7.9	9.66	7.8	213	3.95030	0.14391	-0.28181	-0.03092	-0.03318
-90	8.3	4.37	2.1	108	-1.26230	-0.01696	-0.00415	-0.01467	0.00359
-90	8.5	5.25	2.5	130	-1.08282	-0.00676	-0.02674	-0.02110	0.00100
-90	8.8	6.04	3.2	147	-0.81052	0.01090	-0.05450	-0.02526	-0.00241
-90	8.9	6.86	3.8	166	-0.34944	0.03963	-0.08900	-0.02763	-0.00741
-90	9.1	7.62	4.6	181	0.17900	0.05035	-0.12611	-0.03052	-0.01208
-90	9.2	8.35	5.5	194	0.88158	0.06749	-0.16866	-0.03154	-0.01813
-90	9.3	9.11	6.3	210	1.61565	0.08118	-0.21158	-0.03328	-0.02228
-90	9.4	9.84	7.2	223	2.40929	0.09466	-0.25562	-0.03540	-0.02726
-90	11.6	4.61	1.3	122	-3.14524	-0.02280	0.03156	-0.01877	0.00760
-90	11.5	5.43	1.9	140	-3.14153	0.00429	0.00341	-0.02379	0.00389
-90	11.4	6.16	2.8	154	-3.02758	0.02441	-0.03207	-0.02799	-0.00013
-90	11.3	7.68	4.4	184	-2.28674	0.03386	-0.10868	-0.03592	-0.00688
-90	11.2	8.44	5.2	199	-1.55433	0.04970	-0.15211	-0.03714	-0.01299
-90	11.3	9.23	5.9	216	-0.96998	0.05717	-0.18959	-0.03860	-0.01801
-90	16.0	1.6	0	46	-3.46875	-0.01279	0.08080	-0.02392	0.00642
-90	18.1	3.9	0	112	-5.35217	-0.06092	0.09574	-0.03713	0.00135
90	2.5	4.01	3.3	88	1.69056	-0.07071	-0.07524	-0.00199	0.01444
90	1.9	4.83	3.9	106	2.27153	-0.11056	-0.10236	-0.02105	0.02465
90	1.6	5.62	4.6	123	3.17589	-0.11161	-0.13840	-0.02225	0.03418
90	1.4	6.38	5.4	138	4.08106	-0.11123	-0.17336	-0.02736	0.03895
90	1.5	7.17	6.1	155	5.08060	-0.09979	-0.21104	-0.03033	0.03826
90	1.9	7.9	7	169	6.20191	-0.09538	-0.25345	-0.02530	0.03688
90	2.1	8.6	8	181	7.38894	-0.09672	-0.30012	-0.02074	0.03768
90	2.6	9.3	9	192	8.58697	-0.05575	-0.34189	-0.02226	0.02356

α (deg)	Airspeed (m/s)	Armature voltage	Current (A)	Estimated Ω (rad/s)	f_z (N)	f_x (N)	m_z (Nm)	$(m_x)_{hub}$ (Nm)	$(m_y)_{hub}$ (Nm)
90	3.6	3.98	3.4	86	2.11182	-0.07769	-0.07869	-0.00038	0.02177
90	3.3	4.83	3.9	106	2.68117	-0.10833	-0.10679	-0.01315	0.02514
90	3.2	5.59	4.7	122	3.16395	-0.10197	-0.13911	-0.00161	0.04397
90	2.3	6.38	5.4	138	4.02221	-0.14648	-0.17321	-0.04959	0.06207
90	1.9	7.11	6.3	152	5.02274	-0.13089	-0.21239	-0.05672	0.07750
90	1.4	8.6	8	181	7.35406	-0.13624	-0.30069	-0.05326	0.07810
90	1.3	9.36	8.8	196	8.39174	-0.14344	-0.33830	-0.05737	0.07834
90	5.4	3.74	4.2	73	3.21425	0.08226	-0.10906	-0.00756	-0.02263
90	5.3	4.65	4.5	96	3.89302	0.06757	-0.12925	0.00363	-0.02026
90	4.9	5.53	4.9	118	4.51987	0.04356	-0.14253	-0.01530	-0.02422
90	4.8	6.32	5.6	135	5.21884	0.06740	-0.17308	-0.03214	-0.03880
90	4.6	7.08	6.4	150	5.69588	0.08946	-0.21375	-0.01155	-0.03850
90	4.4	7.84	7.2	165	6.29050	0.12852	-0.25429	-0.03439	-0.01046
90	4.0	8.6	8	181	7.36754	0.10656	-0.29200	-0.09360	-0.02296
90	3.8	9.36	8.8	196	8.40426	0.09774	-0.32941	-0.10474	-0.02951
90	7.8	3.68	4.4	69	3.93300	0.09869	-0.12273	0.00253	-0.02497
90	7.6	4.47	5.1	86	4.97378	0.11326	-0.15974	-0.00715	-0.02995
90	7.0	6.08	6.4	121	6.87321	0.07453	-0.21892	0.00420	-0.02995
90	7.0	6.81	7.3	135	7.73729	0.04965	-0.25986	-0.02011	-0.03752
90	6.8	7.78	7.4	162	8.46867	0.07801	-0.25870	-0.03739	-0.04712
90	6.7	8.57	8.1	179	9.41970	0.10621	-0.29921	-0.04333	-0.06090
90	6.5	9.36	8.8	196	9.91129	0.10205	-0.33582	-0.03572	-0.08824
90	11.8	3.56	4.8	62	4.91966	0.16853	-0.14299	0.04245	-0.00386
90	11.8	4.38	5.4	81	5.97151	0.16833	-0.17517	0.04855	-0.00102
90	11.4	5.11	6.3	94	7.30721	0.11841	-0.21269	0.02466	-0.02495
90	11.0	5.9	7	111	8.74105	0.11650	-0.25345	-0.00710	-0.05540
90	10.9	6.39	8.7	111	10.44180	0.19695	-0.32931	0.02658	-0.04015
90	10.4	7.06	9.8	121	11.23842	0.13614	-0.36868	0.03516	-0.04014
90	15.3	3.44	5.2	56	6.03153	0.18332	-0.16331	0.06351	-0.00650

α (deg)	Airspeed (m/s)	Armature voltage	Current (A)	Estimated Ω (rad/s)	f_z (N)	f_x (N)	m_z (Nm)	$(m_x)_{hub}$ (Nm)	$(m_y)_{hub}$ (Nm)
90	15.1	4.23	5.9	72	7.22488	0.21967	-0.19548	0.07174	-0.01313
90	15.1	5.02	6.6	89	8.59863	0.25746	-0.22939	0.08167	-0.00362
90	15.2	5.78	7.4	104	10.29941	0.30653	-0.27126	0.08113	-0.01095
90	15.1	6.39	8.7	111	12.15785	0.25588	-0.32159	0.05618	-0.04676
90	14.8	7.12	9.6	125	13.88792	0.18048	-0.36898	0.02959	-0.08977
-75	4.4	4.1	3	93	0.59624	0.10614	-0.05578	0.00190	0.00174
-75	4.5	4.95	3.5	113	1.18324	0.16002	-0.08358	0.00172	0.00299
-75	4.5	5.74	4.2	130	1.93073	0.21222	-0.11682	0.00111	0.00376
-75	4.5	6.47	5.1	144	2.89733	0.26756	-0.15708	-0.00093	0.00215
-75	4.6	7.2	6	157	3.84534	0.30292	-0.19736	-0.00651	0.00347
-75	4.7	7.93	6.9	171	4.90704	0.34719	-0.24250	-0.01341	0.00191
-75	4.8	8.66	7.8	184	5.98220	0.37277	-0.28658	-0.02024	0.00223
-75	4.9	9.42	8.6	199	6.93933	0.40817	-0.32671	-0.02357	0.00019
-75	6.0	4.22	2.6	100	-0.13122	0.07784	-0.04163	0.00503	-0.00210
-75	6.2	5.01	3.3	117	0.29728	0.10009	-0.07057	0.00677	-0.00118
-75	6.2	5.8	4	134	0.92010	0.12453	-0.10491	0.00644	0.00039
-75	6.3	6.56	4.8	149	1.66845	0.14690	-0.14319	0.00489	0.00192
-75	6.4	7.29	5.7	162	2.47742	0.16888	-0.18334	0.00185	0.00263
-75	6.5	8.08	6.4	179	3.32906	0.20093	-0.22393	-0.00268	-0.00021
-75	6.5	8.78	7.4	191	4.36429	0.19650	-0.27006	-0.01249	0.00187
-75	6.5	9.54	8.2	206	5.39237	0.24025	-0.31239	-0.01492	-0.00175
-75	7.9	4.34	2.2	107	-1.00070	0.08577	-0.01728	0.00100	-0.00615
-75	8.1	5.19	2.7	127	-0.71063	0.11652	-0.04433	0.00422	-0.00356
-75	8.2	5.95	3.5	142	-0.26472	0.13136	-0.07763	0.00500	-0.00018
-75	8.3	6.74	4.2	159	0.29729	0.15088	-0.11368	0.00368	0.00220
-75	8.4	7.5	5	174	0.90638	0.16758	-0.15064	0.00065	0.00365
-75	8.8	8.26	5.8	189	1.43183	0.20959	-0.18858	-0.00672	0.00227
-75	8.9	9.02	6.6	204	2.22960	0.19083	-0.23265	-0.01224	0.00572
-75	8.9	9.78	7.4	220	3.08596	0.22553	-0.27572	-0.01510	0.00233

α (deg)	Airspeed (m/s)	Armature voltage	Current (A)	Estimated Ω (rad/s)	f_z (N)	f_x (N)	m_z (Nm)	$(m_x)_{hub}$ (Nm)	$(m_y)_{hub}$ (Nm)
-60	3.8	4.1	3	93	1.17672	-0.00977	-0.06858	0.01501	0.02172
-60	4.0	4.92	3.6	112	1.84222	0.18905	-0.10200	0.01412	0.01200
-60	4.2	5.68	4.4	127	2.66077	0.09674	-0.13489	0.03414	0.03420
-60	4.2	6.41	5.3	140	3.67626	0.22534	-0.17624	0.02495	0.03332
-60	4.3	7.17	6.1	155	4.65701	0.70505	-0.22072	-0.01050	-0.00239
-60	4.5	7.9	7	169	5.47662	0.15716	-0.25517	0.01470	0.06060
-60	4.5	8.63	7.9	182	6.81099	0.17239	-0.30087	0.00985	0.06747
-60	4.5	9.39	8.7	198	7.73580	0.19408	-0.34043	0.01694	0.06798
-60	7.3	4.25	2.5	101	-0.41860	0.18644	-0.04301	0.01359	-0.00598
-60	7.4	5.1	3	122	-0.04506	0.40136	-0.07309	0.00421	-0.01605
-60	7.6	5.83	3.9	135	0.46888	0.33797	-0.10765	0.02251	0.00152
-60	7.7	6.62	4.6	152	1.11258	0.29897	-0.14444	0.01543	0.01430
-60	8.6	7.38	5.4	167	1.31817	0.53241	-0.17678	0.00003	0.00263
-60	8.9	8.2	6	186	1.98822	0.47525	-0.21401	-0.02203	0.01438
-60	9.1	8.96	6.8	201	2.70949	0.38427	-0.25344	-0.01978	0.03103
-60	9.1	9.69	7.7	215	3.60077	0.44103	-0.29862	-0.01535	0.03202
-45	4.2	3.98	3.4	86	1.16911	0.20653	-0.07460	0.03873	0.00580
-45	4.1	4.83	3.9	106	1.82414	0.24215	-0.10114	0.04417	0.01255
-45	4.1	5.62	4.6	123	2.64577	0.28521	-0.13508	0.04824	0.02154
-45	4.1	6.41	5.3	140	3.53701	0.33948	-0.17101	0.05024	0.02996
-45	4.2	7.17	6.1	155	4.53546	0.38456	-0.21025	0.05005	0.03682
-45	4.1	7.9	7	169	5.68540	0.42963	-0.25512	0.04706	0.04328
-45	4.2	8.6	8	181	6.80585	0.47667	-0.29974	0.04307	0.05066
-45	4.1	9.33	8.9	194	7.99062	0.50765	-0.34544	0.03505	0.05320
-45	5.8	4.04	3.2	90	0.67929	0.28666	-0.07018	0.04846	0.00032
-45	5.9	4.89	3.7	110	1.24949	0.33330	-0.09840	0.05803	0.00813
-45	6.0	5.65	4.5	125	1.97365	0.38074	-0.13315	0.06333	0.01813
-45	5.9	6.41	5.3	140	2.89896	0.42505	-0.17188	0.06455	0.02756
-45	5.9	7.17	6.1	155	3.75558	0.48349	-0.21075	0.06449	0.03761
-45	6.1	7.93	6.9	171	4.70728	0.54367	-0.25316	0.06129	0.04580

α (deg)	Airspeed (m/s)	Armature voltage	Current (A)	Estimated Ω (rad/s)	f_z (N)	f_x (N)	m_z (Nm)	$(m_x)_{hub}$ (Nm)	$(m_y)_{hub}$ (Nm)
-45	6.7	8.63	7.9	182	5.52343	0.64266	-0.29683	0.05856	0.05611
-45	6.8	9.39	8.7	198	6.57415	0.70010	-0.34077	0.04859	0.06328
-45	10.3	4.31	2.3	105	-0.74212	0.58471	-0.03300	0.03244	-0.03377
-45	10.6	5.1	3	122	-0.36895	0.66786	-0.06277	0.05793	-0.01636
-45	10.7	5.89	3.7	139	0.11329	0.72855	-0.09646	0.06639	0.00542
-45	10.8	6.65	4.5	154	0.74414	0.78941	-0.13602	0.06933	0.02174
-45	11.0	7.38	5.4	167	1.38248	0.85676	-0.17624	0.06893	0.03595
-45	11.0	8.14	6.2	182	2.22423	0.92475	-0.22163	0.06569	0.04639
-45	11.2	8.87	7.1	196	3.06162	1.01208	-0.26811	0.06151	0.05485
-30	3.7	4.01	3.3	88	1.50843	0.22668	-0.08054	0.05884	0.01745
-30	3.8	4.83	3.9	106	2.20002	0.26574	-0.10918	0.06822	0.03022
-30	3.6	5.65	4.5	125	3.04216	0.29106	-0.14193	0.07160	0.04237
-30	3.5	6.38	5.4	138	4.01904	0.30640	-0.18037	0.07224	0.05540
-30	3.3	7.14	6.2	154	5.00505	0.32974	-0.21911	0.07250	0.06605
-30	3.2	7.9	7	169	6.11759	0.33450	-0.26107	0.06795	0.07488
-30	3.0	8.63	7.9	182	7.30152	0.34078	-0.30572	0.05917	0.07858
-30	2.9	9.36	8.8	196	8.41058	0.34401	-0.34701	0.05020	0.07874
-30	7.4	4.04	3.2	90	0.89937	0.52554	-0.08240	0.08999	0.00451
-30	7.1	4.86	3.8	108	1.56289	0.56076	-0.11111	0.10730	0.02557
-30	6.6	5.62	4.6	123	2.48820	0.57478	-0.14652	0.10926	0.04331
-30	6.9	6.41	5.3	140	3.30389	0.68368	-0.18451	0.11640	0.06085
-30	7.0	7.17	6.1	155	4.13388	0.78174	-0.22164	0.12081	0.07720
-30	6.9	7.9	7	169	5.08633	0.84899	-0.26129	0.11449	0.08992
-30	7.2	8.66	7.8	184	6.05662	0.96497	-0.30602	0.11584	0.10830
-30	6.9	9.39	8.7	198	7.14622	1.00184	-0.34922	0.10221	0.11923
-15	3.5	3.98	3.4	86	1.90666	0.18733	-0.08380	0.07241	0.03404
-15	3.3	4.8	4	105	2.69548	0.17206	-0.11176	0.08306	0.05913
-15	3.2	5.59	4.7	122	3.58103	0.17223	-0.14508	0.08835	0.07814
-15	2.9	6.32	5.6	135	4.53604	0.19254	-0.18156	0.08934	0.09169

α (deg)	Airspeed (m/s)	Armature voltage	Current (A)	Estimated Ω (rad/s)	f_z (N)	f_x (N)	m_z (Nm)	$(m_x)_{hub}$ (Nm)	$(m_y)_{hub}$ (Nm)
-15	2.7	7.08	6.4	150	5.54950	0.19995	-0.21966	0.08751	0.09715
-15	2.5	7.84	7.2	165	6.60143	0.20376	-0.25820	0.08514	0.10105
-15	2.5	8.57	8.1	179	7.71691	0.23943	-0.29890	0.07916	0.09999
-15	2.4	9.3	9	192	8.78378	0.28464	-0.33918	0.07798	0.09897
-15	6.0	3.95	3.5	84	1.66943	0.53087	-0.08686	0.11827	0.00198
-15	6.2	4.77	4.1	103	2.33309	0.61109	-0.11493	0.14343	0.02608
-15	6.3	5.56	4.8	120	3.09484	0.69116	-0.14723	0.15748	0.04581
-15	6.4	6.32	5.6	135	3.96380	0.79131	-0.18420	0.16896	0.06967
-15	6.2	7.05	6.5	149	4.79799	0.85647	-0.21913	0.17038	0.08836
-15	6.0	7.81	7.3	164	5.74021	0.92065	-0.26175	0.16616	0.10375
-15	6.1	8.57	8.1	179	6.74134	1.02959	-0.30263	0.16648	0.12527
-15	6.0	9.3	9	192	7.66997	1.11060	-0.34264	0.15719	0.13776
-15	7.9	3.95	3.5	84	1.63713	0.70850	-0.09372	0.14659	0.00024
-15	7.9	4.74	4.2	101	2.29292	0.79397	-0.11965	0.17548	0.02852
-15	7.9	5.56	4.8	120	3.09791	0.87144	-0.15374	0.18746	0.05752
-15	7.8	6.32	5.6	135	3.93151	0.95407	-0.19055	0.19406	0.08497
-15	7.5	7.08	6.4	150	4.82190	1.02221	-0.22845	0.19392	0.10906
-15	7.3	7.78	7.4	162	5.71795	1.05030	-0.27156	0.18325	0.12641
-15	7.6	8.57	8.1	179	6.73494	1.25299	-0.31443	0.18902	0.15821
-15	7.5	9.3	9	192	7.72547	1.35465	-0.35727	0.17823	0.17539
-5	3.9	3.98	3.4	86	1.90236	0.29198	-0.08869	0.09093	0.01755
-5	3.7	4.77	4.1	103	2.55771	0.29833	-0.11701	0.10209	0.04081
-5	3.5	5.59	4.7	122	3.34896	0.33918	-0.15167	0.10711	0.06006
-5	3.2	6.35	5.5	137	4.21841	0.37229	-0.18987	0.10893	0.07681
-5	3.1	7.08	6.4	150	5.15595	0.40990	-0.22837	0.11010	0.08693
-5	3.0	7.84	7.2	165	6.17107	0.42765	-0.26855	0.10561	0.09296
-5	3.1	8.6	8	181	7.20280	0.50004	-0.31018	0.10297	0.10346
-5	3.2	9.33	8.9	194	8.23343	0.57554	-0.35146	0.10004	0.11379
0	3.9	3.92	3.6	83	1.95099	0.35322	-0.08767	0.09209	0.00412

α (deg)	Airspeed (m/s)	Armature voltage	Current (A)	Estimated Ω (rad/s)	f_z (N)	f_x (N)	m_z (Nm)	$(m_x)_{hub}$ (Nm)	$(m_y)_{hub}$ (Nm)
0	3.7	4.74	4.2	101	2.59457	0.39047	-0.11688	0.10811	0.02650
0	3.5	5.53	4.9	118	3.26310	0.52245	-0.15072	0.10601	0.03994
0	3.2	6.29	5.7	133	4.07620	0.49892	-0.18586	0.11313	0.06487
0	3.1	7.05	6.5	149	4.90804	0.57646	-0.22135	0.11410	0.07226
0	3.0	7.84	7.2	165	5.93539	0.57008	-0.26362	0.08051	0.08511
0	2.9	8.57	8.1	179	7.03926	0.66509	-0.30446	0.09009	0.08252
0	2.8	9.33	8.9	194	8.05327	0.55058	-0.34385	0.08266	0.09775
0	5.9	3.89	3.7	81	2.27399	0.42190	-0.10177	0.12217	0.00885
0	5.9	4.71	4.3	100	2.94892	0.39351	-0.13136	0.14294	0.04059
0	5.9	5.5	5	117	3.82761	0.66920	-0.16946	0.13567	0.05213
0	5.6	6.23	5.9	130	4.74868	0.53983	-0.20461	0.15219	0.11181
0	5.4	6.99	6.7	145	5.54201	0.66186	-0.23953	0.13598	0.13904
0	4.8	7.75	7.5	160	6.29007	0.54481	-0.27787	0.12053	0.18259
0	4.6	8.54	8.2	177	7.31435	0.75700	-0.31856	0.11644	0.18547
0	4.3	9.3	9	192	8.07602	0.72873	-0.35339	0.10221	0.20005
0	7.2	3.89	3.7	81	2.32499	0.67117	-0.10119	0.16064	-0.01775
0	7.3	4.68	4.4	98	3.01940	0.69111	-0.13141	0.18899	0.00973
0	7.2	5.47	5.1	115	3.85890	0.83045	-0.16905	0.19219	0.03331
0	7.4	6.2	6	128	4.90402	0.87421	-0.20773	0.21526	0.07439
0	7.6	6.96	6.8	143	5.85006	0.89220	-0.24795	0.19609	0.11998
0	7.7	7.69	7.7	157	6.83411	0.85594	-0.28719	0.19489	0.16414
0	7.5	8.45	8.5	172	7.95841	1.21557	-0.32897	0.17932	0.16975
0	6.9	9.24	9.2	189	8.59918	1.16064	-0.35956	0.14916	0.20433
0	12.2	3.8	4	76	2.87865	1.54215	-0.12502	0.28379	-0.03716
0	12.0	4.59	4.7	93	3.48869	1.56531	-0.15542	0.30762	-0.02067
0	12.0	5.41	5.3	111	4.30021	1.60899	-0.18742	0.34367	0.00493
0	11.9	6.14	6.2	125	5.36828	1.70512	-0.22997	0.35983	0.05561
0	12.0	7.14	6.2	154	6.30668	1.72667	-0.26638	0.35378	0.08882
0	12.4	7.6	8	152	7.24763	1.85644	-0.31248	0.35359	0.14923
0	12.1	8.36	8.8	167	8.46835	2.13418	-0.35414	0.33798	0.17565

α (deg)	Airspeed (m/s)	Armature voltage	Current (A)	Estimated Ω (rad/s)	f_z (N)	f_x (N)	m_z (Nm)	$(m_x)_{hub}$ (Nm)	$(m_y)_{hub}$ (Nm)
0	12.6	9.09	9.7	181	9.65267	2.08028	-0.39496	0.32713	0.24857
0	15.5	3.74	4.2	73	3.49040	2.37769	-0.14389	0.37485	-0.05918
0	15.5	4.56	4.8	91	4.00647	2.46960	-0.17338	0.40907	-0.03762
0	15.5	5.35	5.5	108	4.72297	2.50540	-0.20873	0.44841	-0.00245
0	15.6	6.11	6.3	123	5.80327	2.66835	-0.25264	0.48128	0.05280
0	15.3	6.84	7.2	137	6.70651	2.73156	-0.29155	0.47882	0.11251
0	15.2	7.51	8.3	147	7.64782	2.86407	-0.33863	0.43821	0.16975
5	3.3	3.98	3.4	86	2.15718	0.32327	-0.09011	0.05643	0.01110
5	3.2	4.74	4.2	101	2.82536	0.51988	-0.12142	0.07206	0.01776
5	3.1	5.56	4.8	120	3.48104	0.67455	-0.15409	0.08293	0.02665
5	2.9	6.32	5.6	135	4.30698	0.55773	-0.18873	0.10715	0.05797
5	2.7	7.05	6.5	149	5.28783	0.60241	-0.22762	0.09517	0.05914
5	2.5	7.84	7.2	165	6.28306	0.65505	-0.26743	0.04995	0.05272
5	2.4	8.6	8	181	7.53828	0.79277	-0.30991	0.04809	0.03984
5	2.4	9.33	8.9	194	8.47336	0.64780	-0.34559	0.07891	0.05841
15	3.4	3.92	3.6	83	2.23449	0.18094	-0.09133	0.06947	0.02035
15	3.2	4.74	4.2	101	2.84813	0.19120	-0.12062	0.07729	0.05722
15	3.0	5.53	4.9	118	3.50693	0.23679	-0.15506	0.08747	0.08287
15	2.9	6.29	5.7	133	4.26525	0.29177	-0.19129	0.10150	0.10681
15	2.8	7.05	6.5	149	5.09866	0.32846	-0.22877	0.10791	0.12053
15	2.7	7.81	7.3	164	6.10962	0.36786	-0.26958	0.11053	0.12217
15	2.6	8.54	8.2	177	7.24144	0.41998	-0.31314	0.11156	0.12493
15	2.6	9.27	9.1	191	8.30927	0.47671	-0.35400	0.10923	0.12581
15	5.3	3.89	3.7	81	2.45910	0.43309	-0.09632	0.11548	-0.01037
15	5.2	4.68	4.4	98	3.22056	0.45143	-0.12538	0.12927	0.00236
15	5.0	5.47	5.1	115	4.22179	0.50071	-0.16286	0.13141	0.03946
15	4.6	6.23	5.9	130	5.05629	0.54072	-0.19693	0.10632	0.07885
15	3.9	6.99	6.7	145	5.55644	0.59832	-0.23083	0.10703	0.10600
15	3.8	7.75	7.5	160	6.29296	0.70554	-0.27065	0.11464	0.12643

α (deg)	Airspeed (m/s)	Armature voltage	Current (A)	Estimated Ω (rad/s)	f_z (N)	f_x (N)	m_z (Nm)	$(m_x)_{hub}$ (Nm)	$(m_y)_{hub}$ (Nm)
15	3.7	8.51	8.3	176	7.16687	0.79763	-0.30998	0.12162	0.14314
15	3.7	9.27	9.1	191	8.09599	0.87871	-0.35036	0.11797	0.15219
15	7.5	3.86	3.8	79	2.73693	0.65522	-0.10767	0.16290	-0.03814
15	7.4	4.65	4.5	96	3.52995	0.69297	-0.13622	0.18316	-0.01891
15	6.9	5.44	5.2	113	4.53122	0.66153	-0.17015	0.19212	0.02258
15	7.0	6.17	6.1	127	5.66875	0.75169	-0.21005	0.20127	0.04936
15	6.7	6.93	6.9	142	6.70291	0.82757	-0.24827	0.18205	0.07348
15	6.6	7.66	7.8	155	7.74704	0.94371	-0.28892	0.14717	0.11369
15	6.6	8.36	8.8	167	8.89399	1.06698	-0.33090	0.13330	0.14828
15	6.0	9.15	9.5	184	9.62502	1.11655	-0.36682	0.10176	0.18400
30	3.3	3.95	3.5	84	2.42383	0.17432	-0.08887	0.05128	0.00386
30	3.1	4.74	4.2	101	3.09492	0.21424	-0.11935	0.04953	0.03921
30	2.9	5.5	5	117	3.72242	0.25823	-0.15483	0.05403	0.07749
30	2.8	6.32	5.6	135	4.36656	0.34710	-0.18752	0.07046	0.09710
30	2.8	7.08	6.4	150	5.14730	0.41401	-0.22200	0.07370	0.10675
30	2.6	7.81	7.3	164	6.12088	0.49620	-0.26182	0.07668	0.09852
30	2.6	8.57	8.1	179	7.13720	0.57476	-0.30283	0.08236	0.09788
30	2.6	9.33	8.9	194	8.14475	0.65157	-0.34121	0.08216	0.09531
30	7.5	3.8	4	76	3.17847	0.61412	-0.11438	0.14756	-0.04965
30	7.4	4.62	4.6	95	3.97201	0.62547	-0.13812	0.15292	-0.02320
30	7.4	5.44	5.2	113	4.96129	0.62390	-0.16764	0.15132	0.00262
30	7.4	6.2	6	128	6.13878	0.65451	-0.20217	0.14708	0.02451
30	7.1	6.99	6.7	145	7.30695	0.67432	-0.23425	0.13116	0.03417
30	6.9	7.63	7.9	154	8.77217	0.83517	-0.28892	0.14205	0.07429
30	6.9	8.3	9	164	10.01452	1.02848	-0.34220	0.09628	0.12762
45	3.4	3.92	3.6	83	2.37074	0.08577	-0.08713	0.01462	0.02033
45	3.1	4.71	4.3	100	3.33270	0.09213	-0.11848	0.02293	0.04943
45	2.9	5.53	4.9	118	3.92548	0.08921	-0.14789	-0.01028	0.07942
45	2.7	6.32	5.6	135	4.57869	0.09683	-0.18559	0.00485	0.07066

α (deg)	Airspeed (m/s)	Armature voltage	Current (A)	Estimated Ω (rad/s)	f_z (N)	f_x (N)	m_z (Nm)	$(m_x)_{hub}$ (Nm)	$(m_y)_{hub}$ (Nm)
45	2.7	7.05	6.5	149	5.27077	0.16311	-0.22019	0.03811	0.09421
45	2.7	7.84	7.2	165	6.14154	0.25626	-0.25945	0.05990	0.11716
45	2.7	8.6	8	181	7.19302	0.32723	-0.30205	0.06065	0.13342
45	2.7	9.3	9	192	8.21846	0.36267	-0.34711	0.04333	0.12226
45	5.2	3.86	3.8	79	2.77842	0.28600	-0.09765	0.04954	-0.01011
45	5.1	4.71	4.3	100	3.50383	0.25850	-0.11838	0.02791	0.00082
45	4.9	5.5	5	117	4.59632	0.31109	-0.14665	0.02197	0.01044
45	4.4	6.23	5.9	130	5.97110	0.40714	-0.18938	0.03230	0.04836
45	4.3	6.99	6.7	145	6.93882	0.51822	-0.22359	0.00215	0.08325
45	4.2	7.75	7.5	160	7.72068	0.55839	-0.25728	-0.04380	0.09346
45	4.0	8.54	8.2	177	8.36163	0.55965	-0.29389	-0.08953	0.06799
45	3.9	9.24	9.2	189	9.04992	0.56330	-0.33542	-0.08217	0.02210
45	7.2	3.74	4.2	73	3.40023	0.45439	-0.11691	0.10554	-0.04816
45	7.2	4.59	4.7	93	4.13634	0.44509	-0.13901	0.10338	-0.02577
45	6.8	5.44	5.2	113	5.03973	0.41564	-0.16475	0.07001	-0.00162
45	6.6	6.14	6.2	125	6.34615	0.48696	-0.20557	0.05592	0.04093
45	6.2	6.87	7.1	138	7.59927	0.54902	-0.24122	0.03060	0.04174
45	5.7	7.69	7.7	157	8.98953	0.65896	-0.26984	0.04496	0.05076
45	5.6	8.3	9	164	10.23398	0.84149	-0.32625	-0.00270	0.11429
60	3.0	4.01	3.3	88	2.24495	0.03851	-0.07803	-0.00755	0.01626
60	2.8	5.62	4.6	123	3.23672	-0.03059	-0.13315	-0.03261	0.01107
60	2.7	6.35	5.5	137	4.14763	-0.02738	-0.16999	-0.02795	-0.00302
60	2.7	7.14	6.2	154	5.25506	-0.00421	-0.21394	-0.00517	0.00489
60	2.5	7.84	7.2	165	6.37763	0.03594	-0.25521	-0.00403	0.01217
60	2.5	8.54	8.2	177	7.36032	0.09656	-0.29761	0.01186	0.02870
60	2.7	9.3	9	192	8.41157	0.16868	-0.34759	0.00766	0.04307
60	6.2	3.8	4	76	3.30032	0.24132	-0.10912	0.04664	-0.02551
60	5.9	4.65	4.5	96	3.96595	0.20514	-0.13018	0.03706	-0.00690
60	5.8	5.5	5	117	4.89914	0.21554	-0.15434	0.02024	0.01672

α (deg)	Airspeed (m/s)	Armature voltage	Current (A)	Estimated Ω (rad/s)	f_z (N)	f_x (N)	m_z (Nm)	$(m_x)_{hub}$ (Nm)	$(m_y)_{hub}$ (Nm)
60	5.8	6.26	5.8	132	6.06871	0.26333	-0.18665	-0.00201	0.03363
60	5.4	7.05	6.5	149	7.07854	0.30548	-0.22276	-0.02129	0.04878
60	5.1	7.9	7	169	7.84324	0.32675	-0.24489	-0.04750	0.04401
60	5.2	8.6	8	181	8.85415	0.38079	-0.28376	-0.05952	0.04280
60	5.0	9.36	8.8	196	9.26337	0.30843	-0.32688	-0.08367	-0.00282
75	3.2	4.01	3.3	88	2.13634	-0.03018	-0.07561	-0.01310	0.01111
75	3.0	4.83	3.9	106	2.59145	-0.05002	-0.10140	-0.01797	0.01285
75	2.7	5.62	4.6	123	3.24322	-0.06781	-0.13682	-0.03788	0.02109
75	2.1	6.35	5.5	137	4.19790	-0.05456	-0.17213	-0.02235	0.01706
75	2.2	7.14	6.2	154	5.23542	-0.06905	-0.21033	-0.04064	0.00994
75	2.3	7.87	7.1	167	6.39767	-0.05987	-0.25399	-0.03038	0.00842
75	2.4	8.6	8	181	7.53923	-0.01898	-0.29857	-0.03210	0.01168
75	2.4	9.3	9	192	8.68160	0.03457	-0.34154	-0.03007	0.01095
75	4.9	3.86	3.8	79	2.93882	0.13305	-0.10054	0.01228	-0.02269
75	4.9	4.71	4.3	100	3.72950	0.15441	-0.12048	0.00665	-0.01041
75	4.7	5.56	4.8	120	4.47531	0.15396	-0.13703	-0.02071	-0.01152
75	4.8	6.35	5.5	137	5.50429	0.20413	-0.16677	-0.03321	-0.01594
75	4.9	7.14	6.2	154	6.45469	0.23604	-0.20106	-0.05442	-0.02436
75	4.8	7.87	7.1	167	7.18067	0.25271	-0.24284	-0.05687	-0.04825
75	4.8	8.6	8	181	7.81690	0.28363	-0.28465	-0.04809	-0.05341
75	4.7	9.3	9	192	8.23332	0.31004	-0.32654	-0.10111	-0.05218
75	7.1	3.74	4.2	73	3.70093	0.22291	-0.11900	0.02378	-0.03406
75	6.6	4.59	4.7	93	4.29190	0.14915	-0.14226	0.01833	-0.02678
75	6.3	5.41	5.3	111	5.23907	0.17046	-0.16689	0.02058	-0.01010
75	6.3	6.2	6	128	6.25706	0.19168	-0.19482	-0.01043	0.01056
75	6.0	7.08	6.4	150	7.01828	0.20606	-0.22106	-0.03902	0.00343
75	5.6	7.9	7	169	7.73287	0.24328	-0.24350	-0.07041	-0.02642
75	5.1	8.63	7.9	182	7.91152	0.23738	-0.28632	-0.05258	-0.04251
75	5.3	9.36	8.8	196	8.82425	0.27650	-0.32828	-0.05079	-0.05381

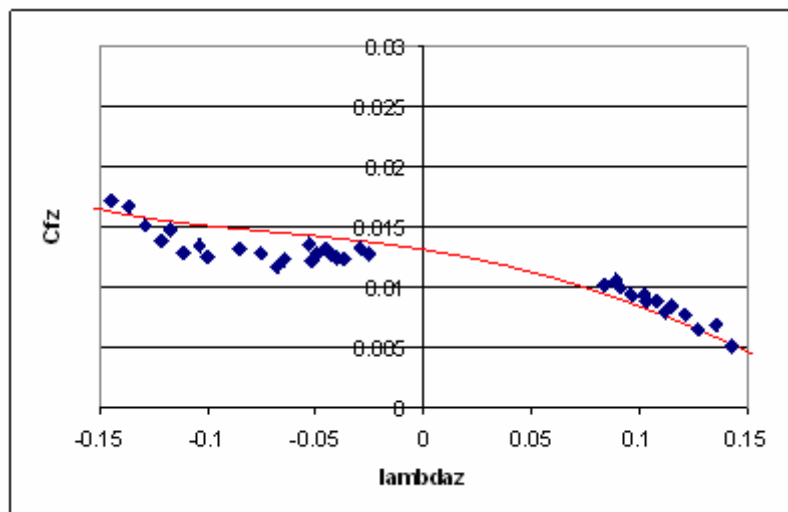
APPENDIX F: COEFFICIENTS OF FORCES AND MOMENTS

The following pages contain the graphs with the experimental values of $C_{fz}, -C_{mz}, C_{fx}, (C_{mx})_{hub}, (C_{my})_{hub}$ compared with the predictions obtained from the Matlab/Simulink model (solid line).

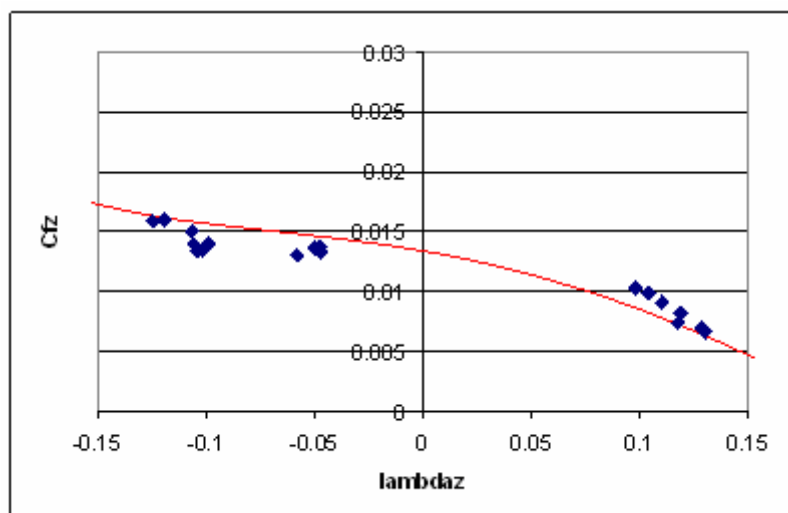
Please note that the rotor used in the tests turned clockwise.

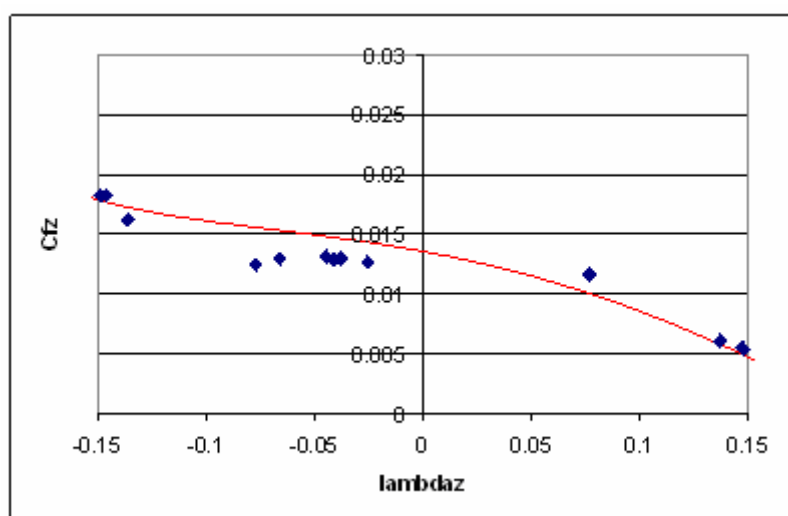
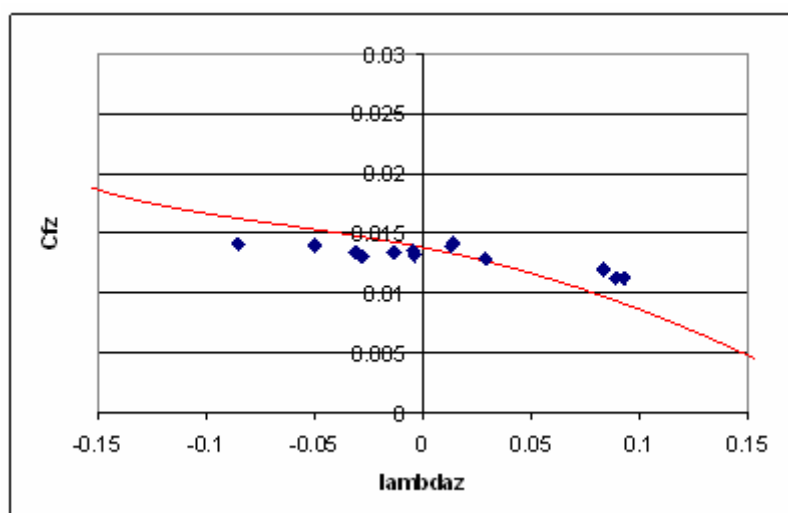
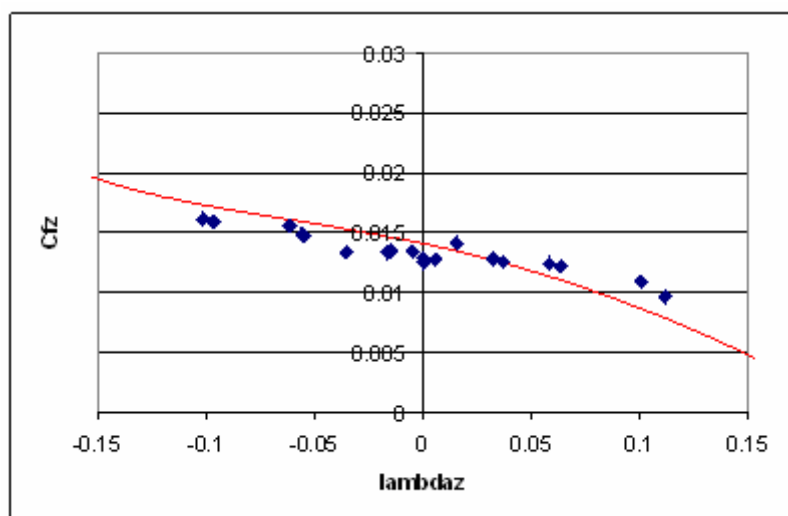
$$C_{fz}$$

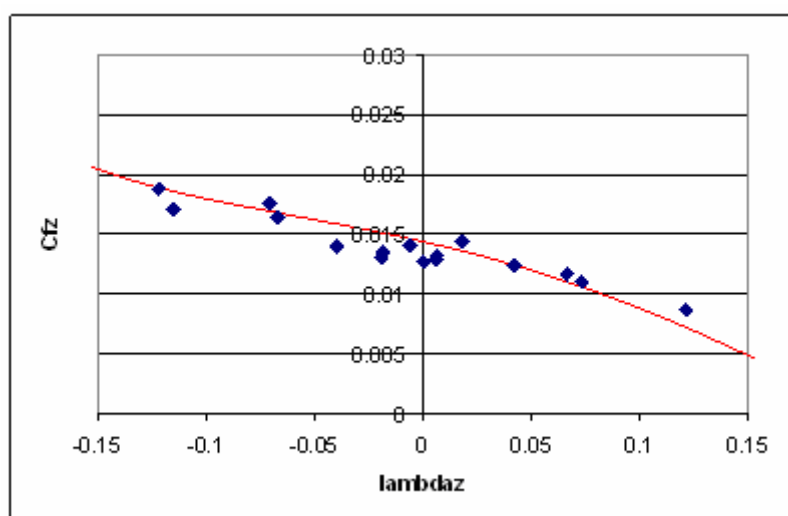
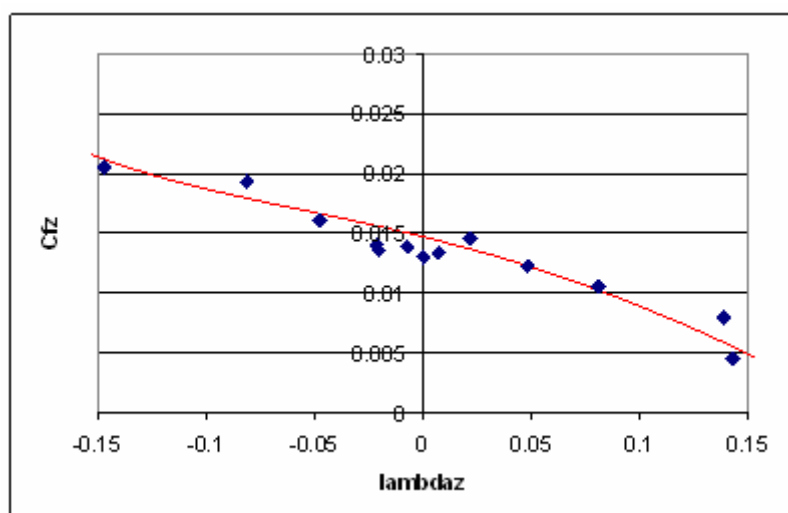
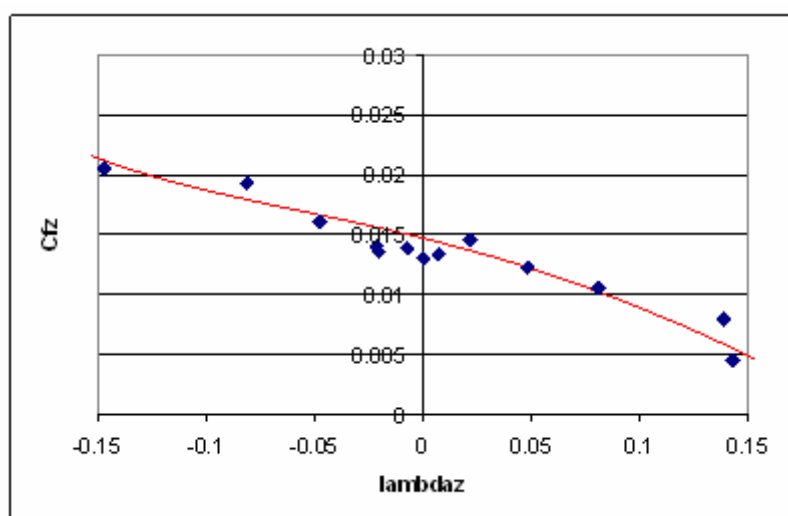
mu=0

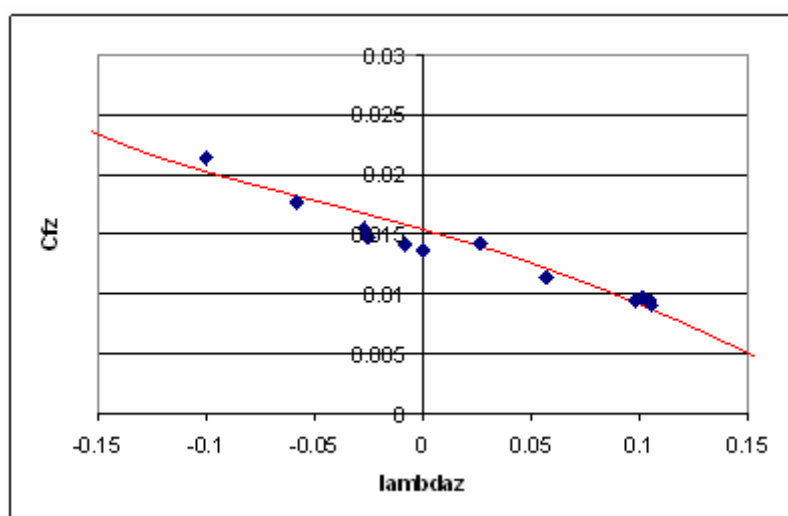
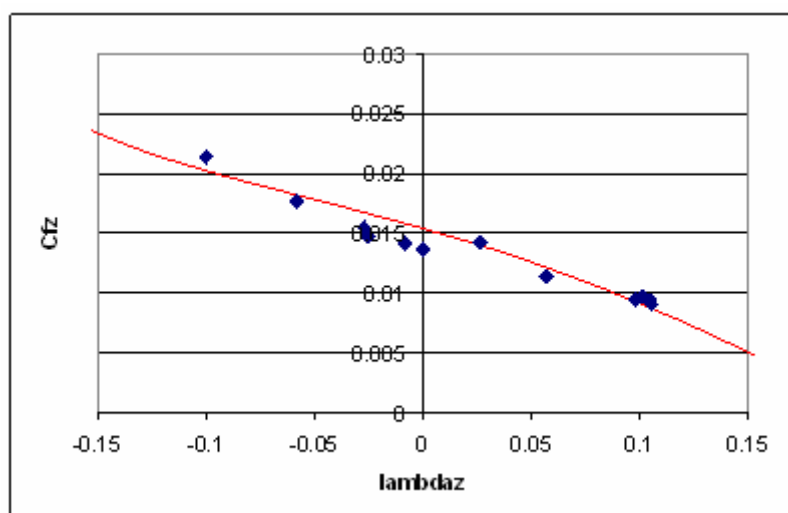
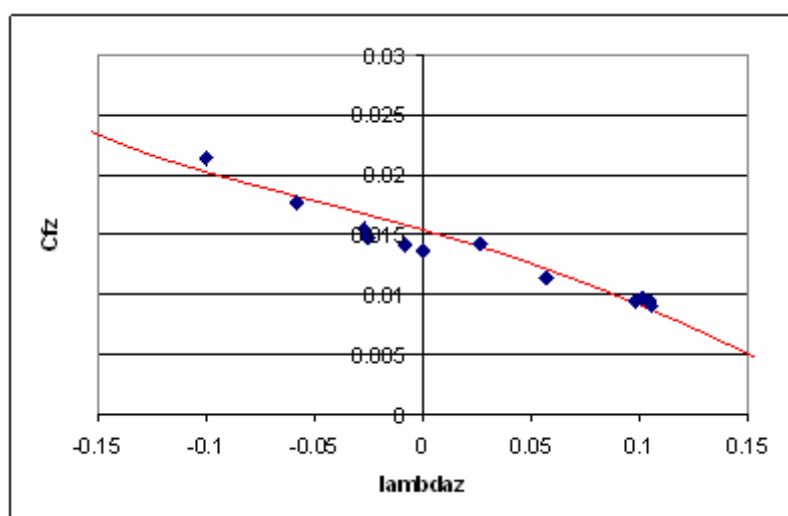


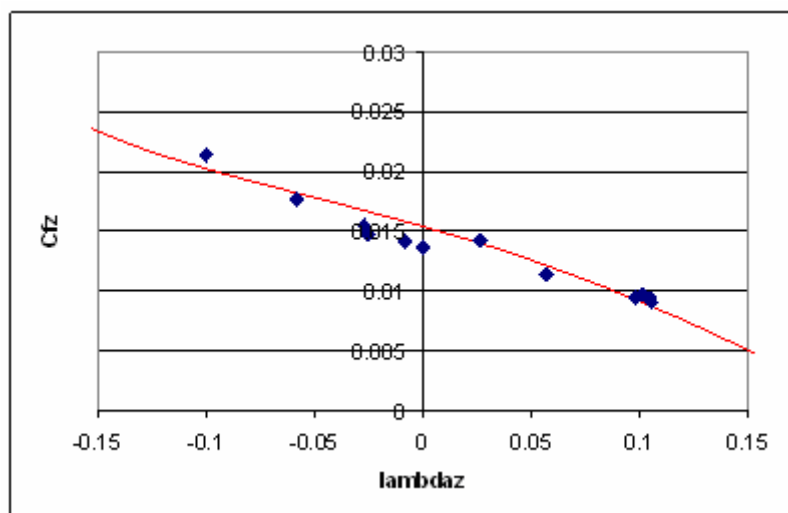
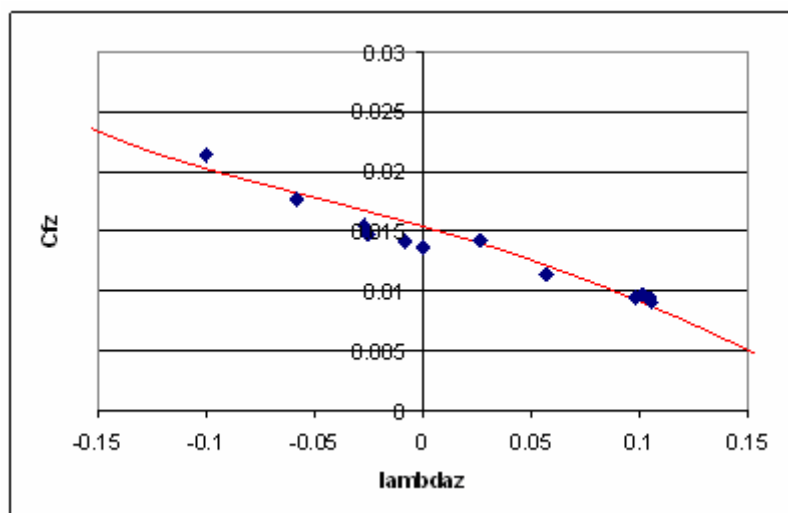
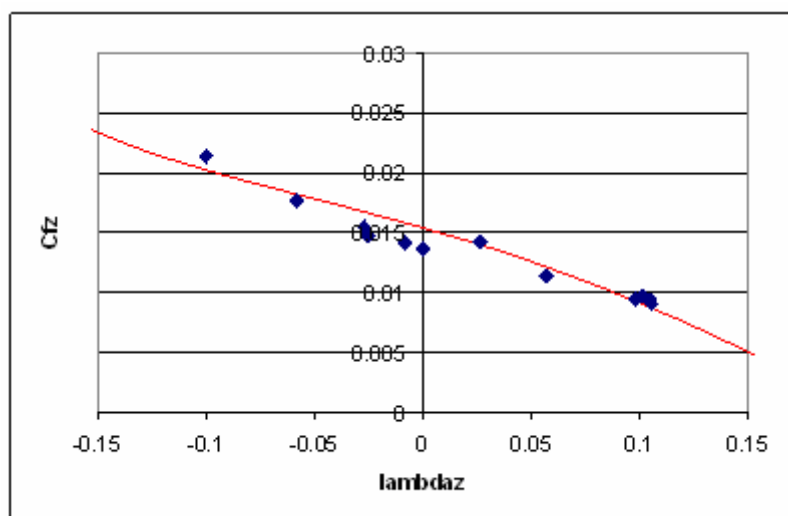
mu=0.03

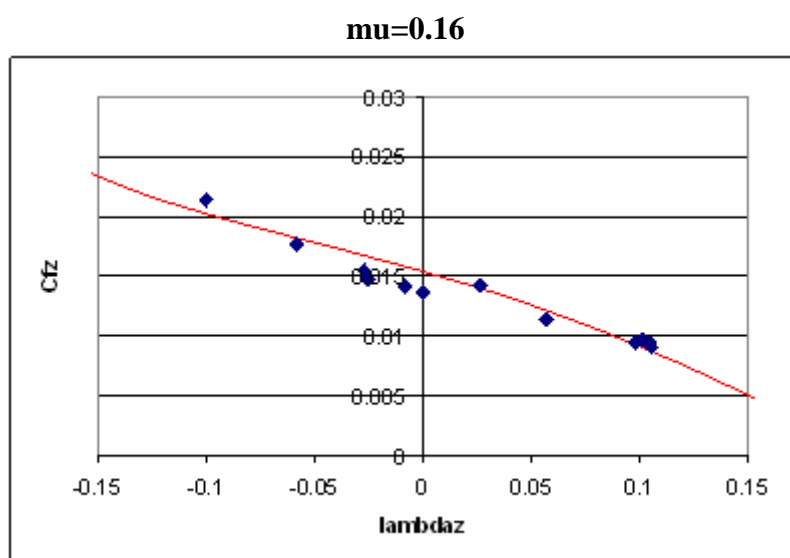


$\mu=0.04$  $\mu=0.05$  $\mu=0.06$ 

$\mu=0.07$  $\mu=0.08$  $\mu=0.09$ 

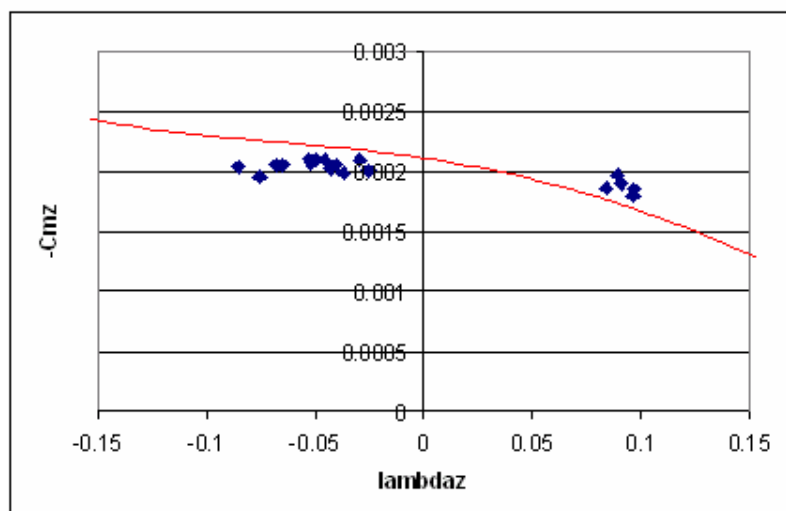
$\mu=0.10$  **$\mu=0.11$**  **$\mu=0.12$** 

$\mu=0.13$  $\mu=0.14$  $\mu=0.15$ 

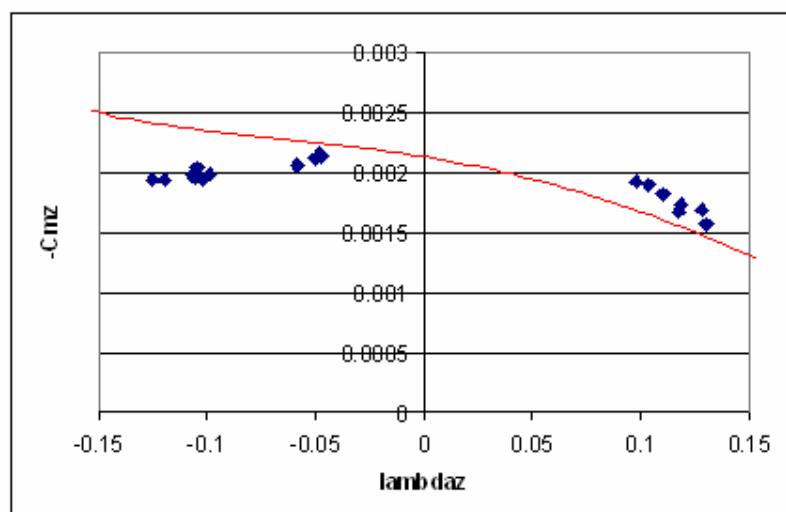


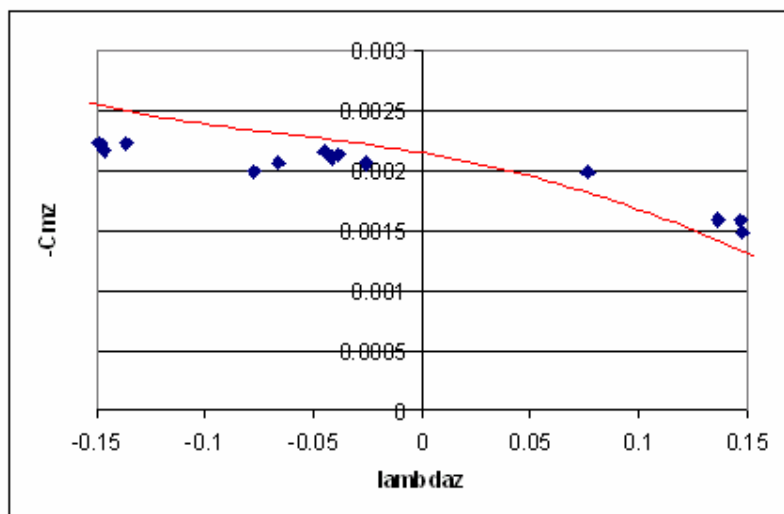
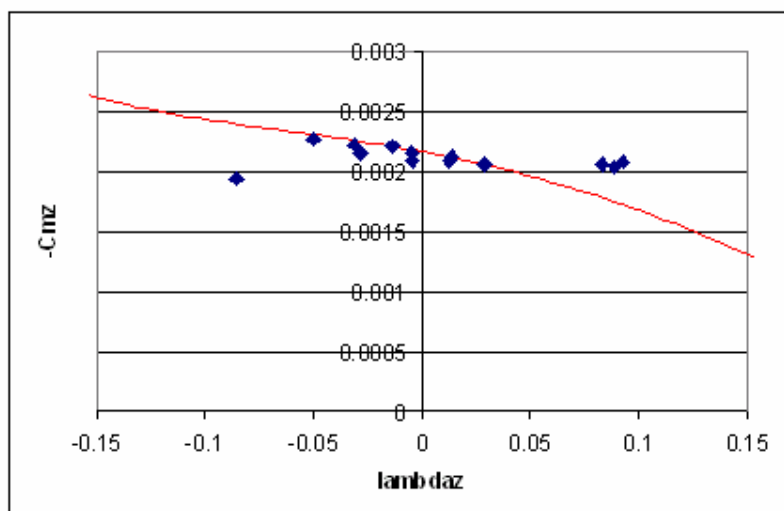
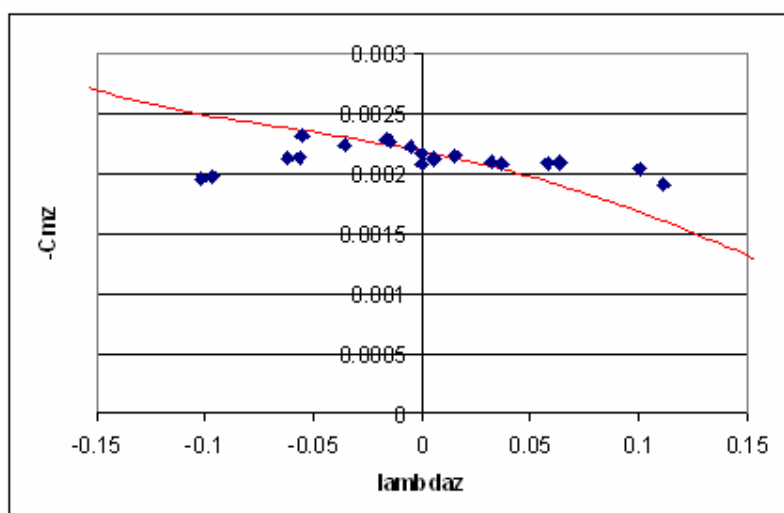
$$-C_{mz}$$

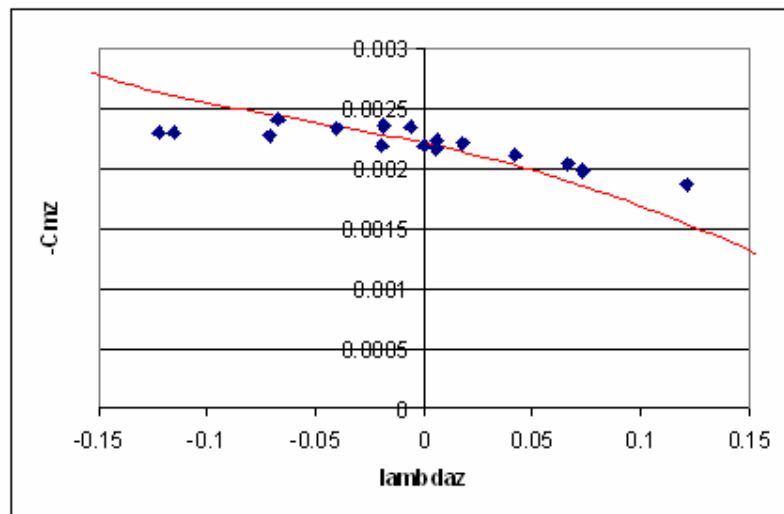
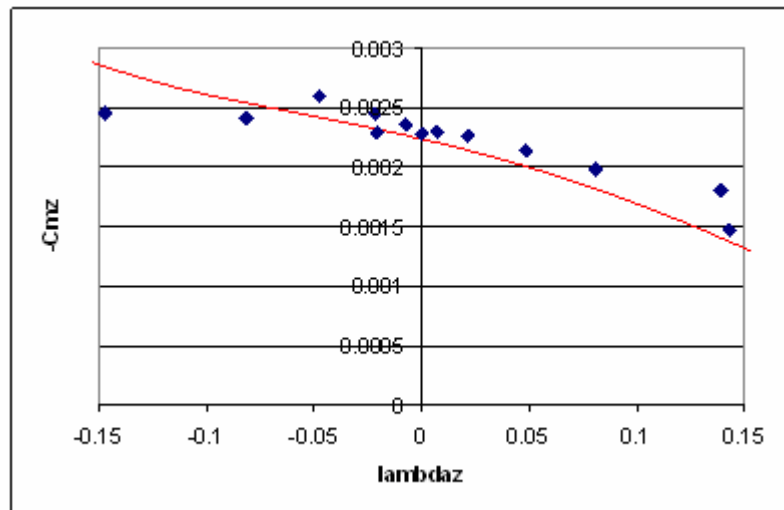
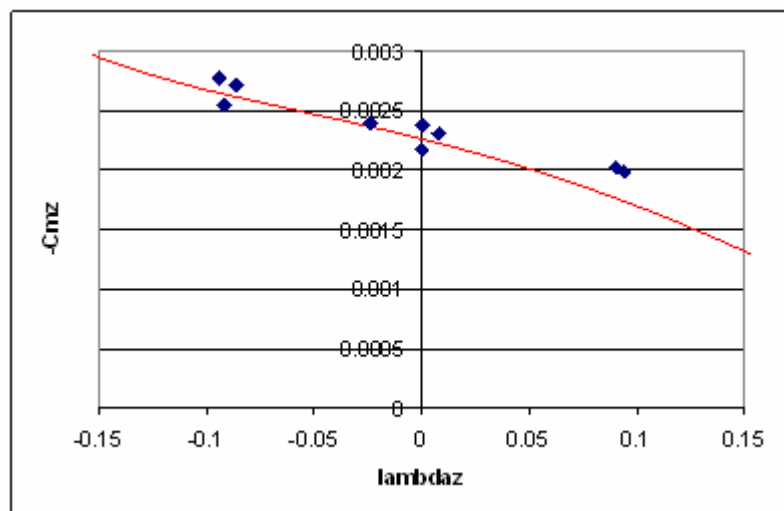
mu=0

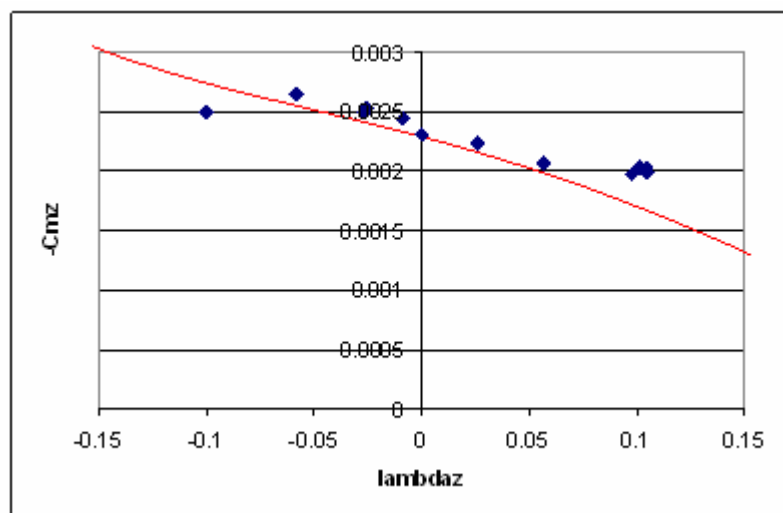
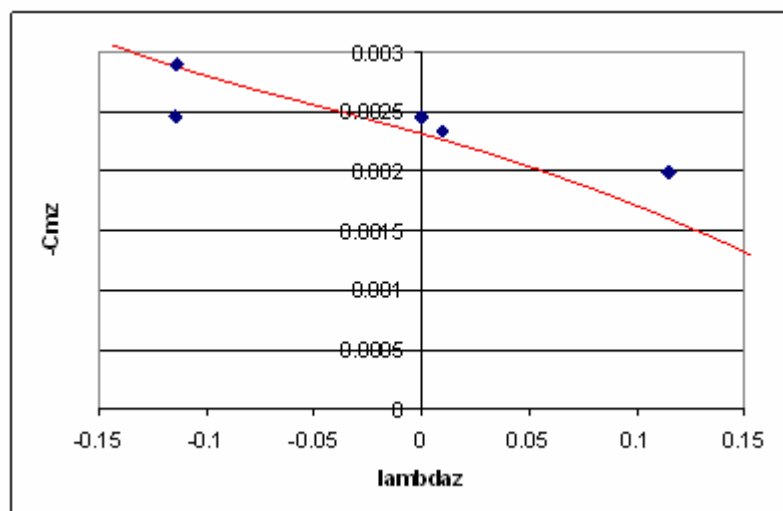
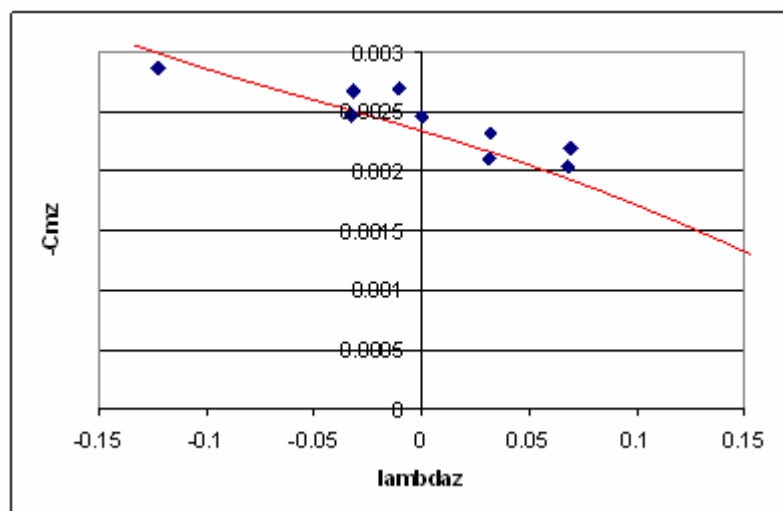


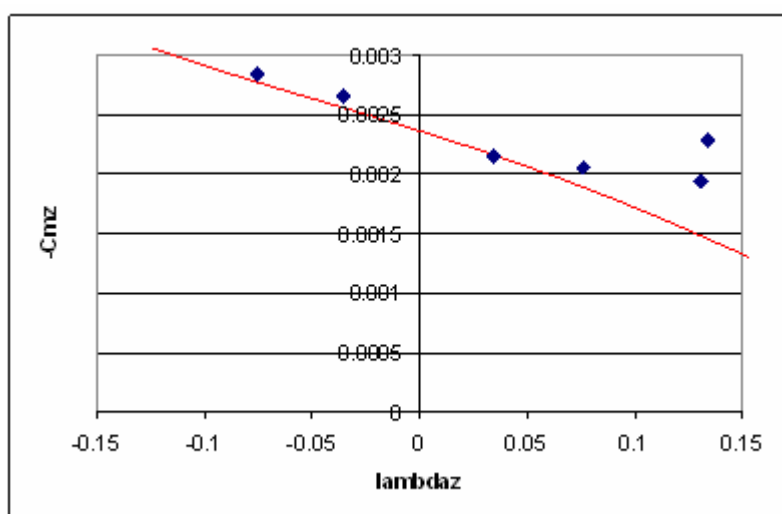
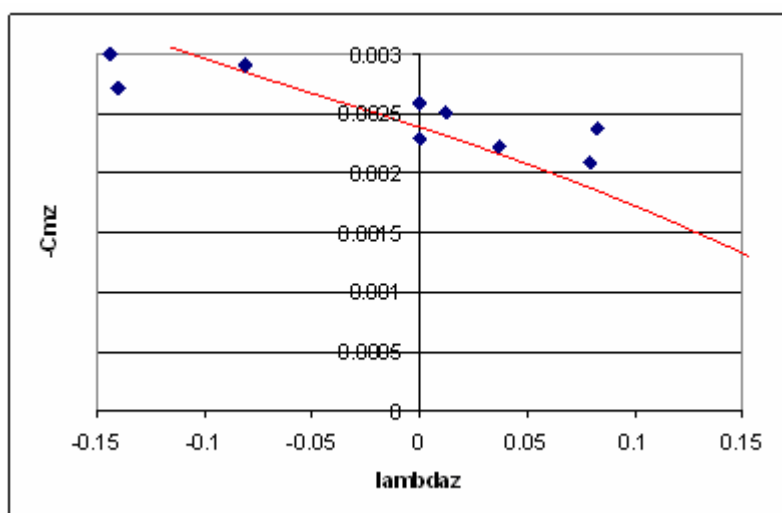
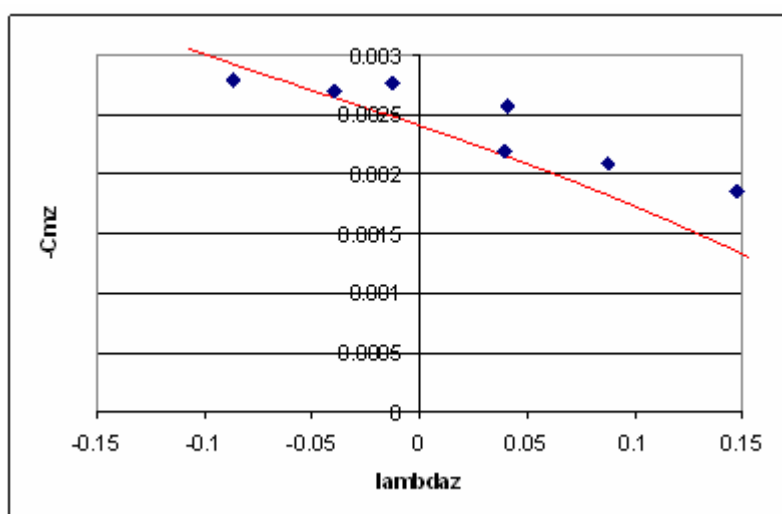
mu=0.03

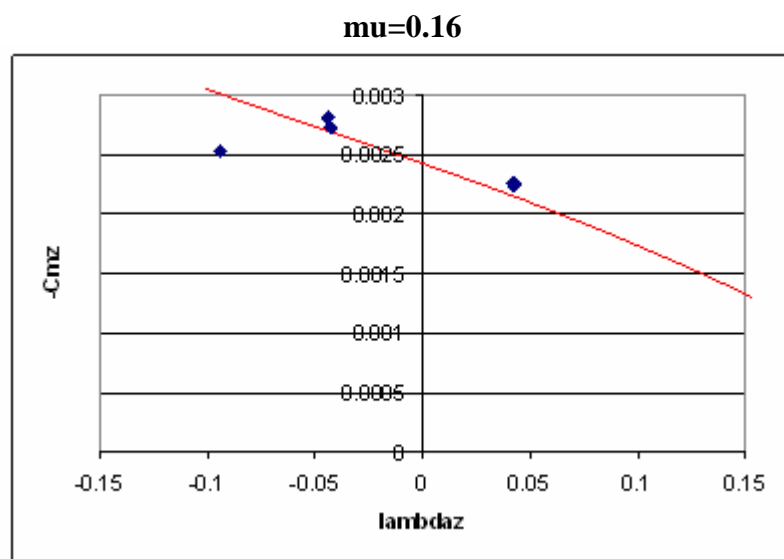


$\mu=0.04$  $\mu=0.05$  $\mu=0.06$ 

$\mu=0.07$  $\mu=0.08$  $\mu=0.09$ 

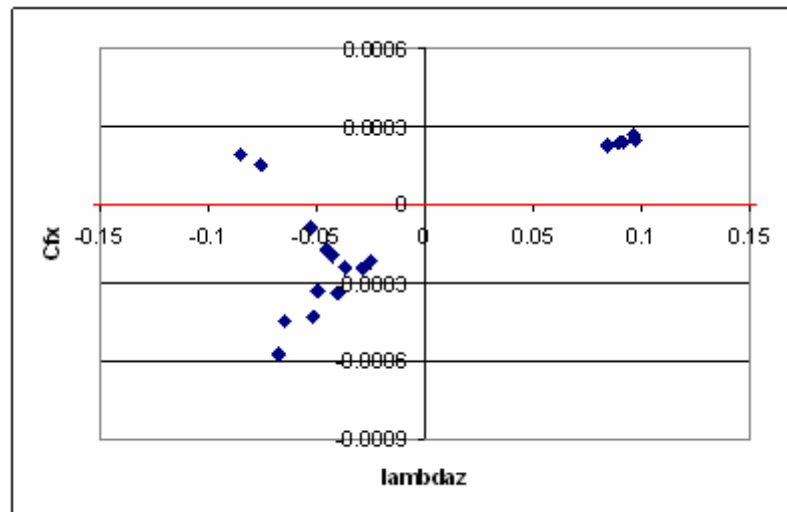
$\mu=0.10$  $\mu=0.11$  $\mu=0.12$ 

mu=0.13**mu=0.14****mu=0.15**

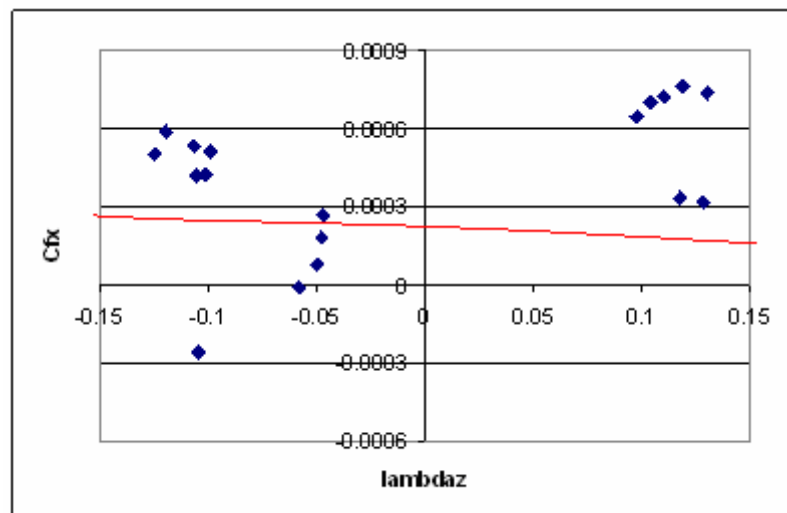


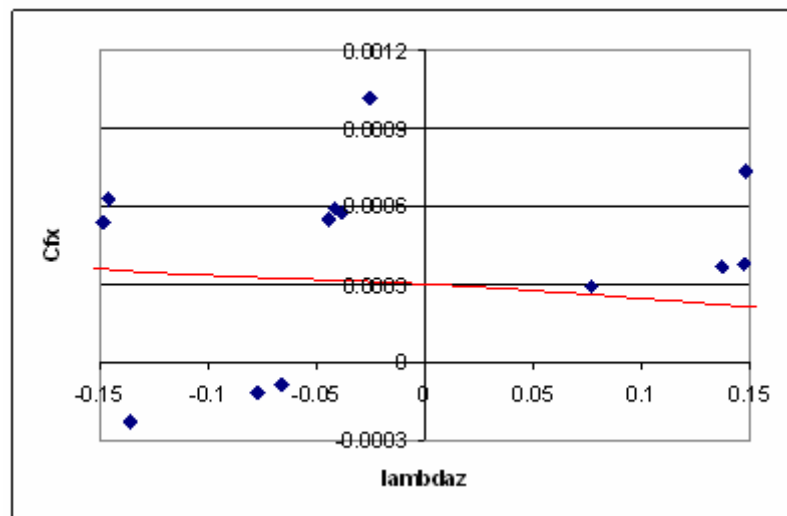
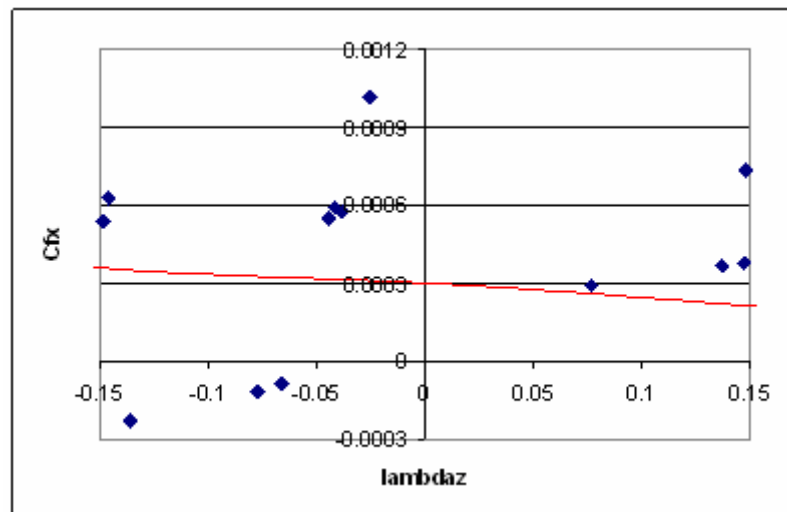
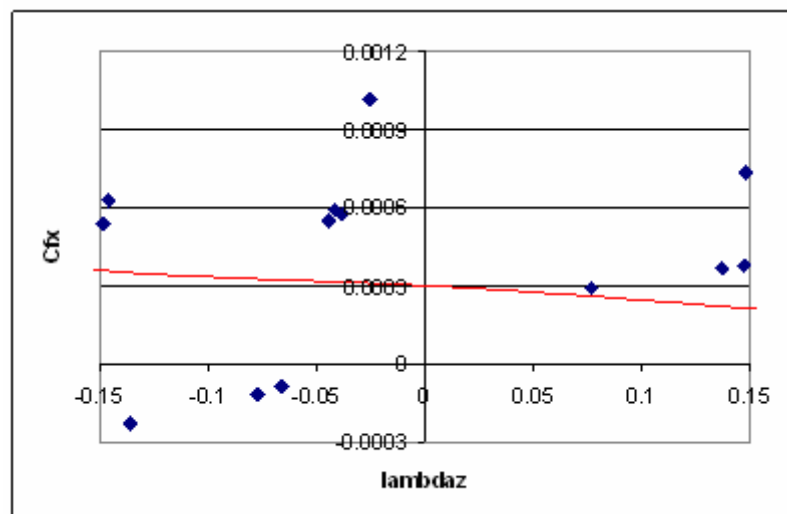
$$C_{fx}$$

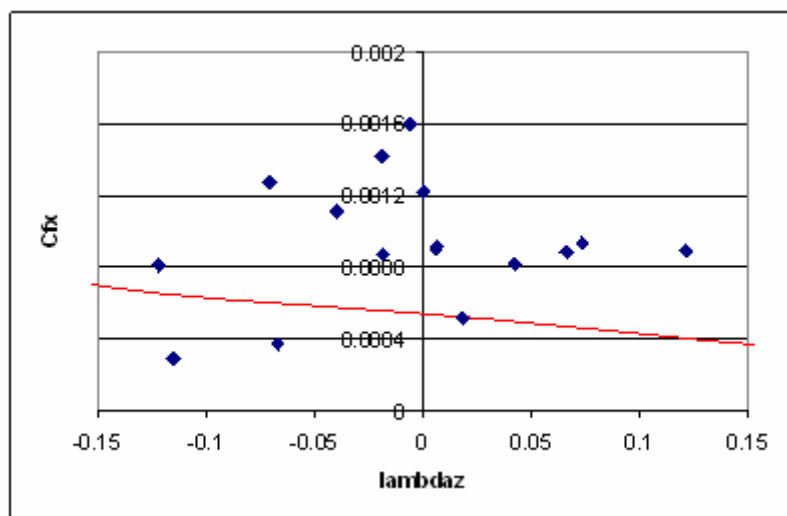
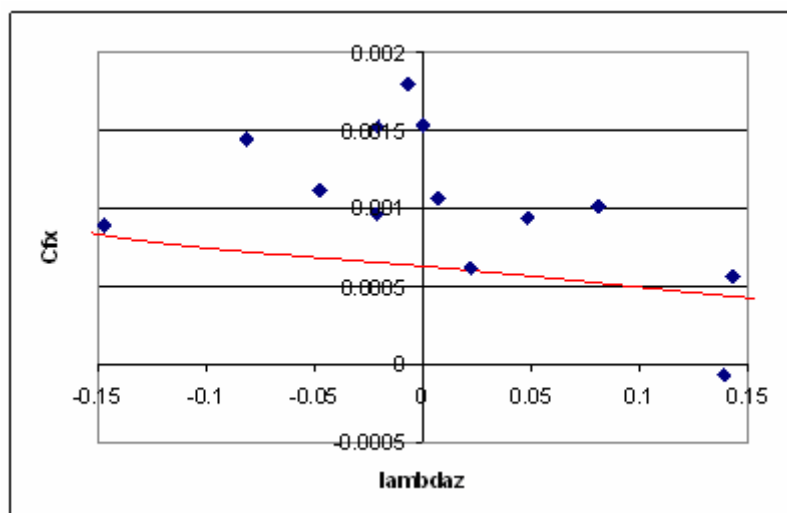
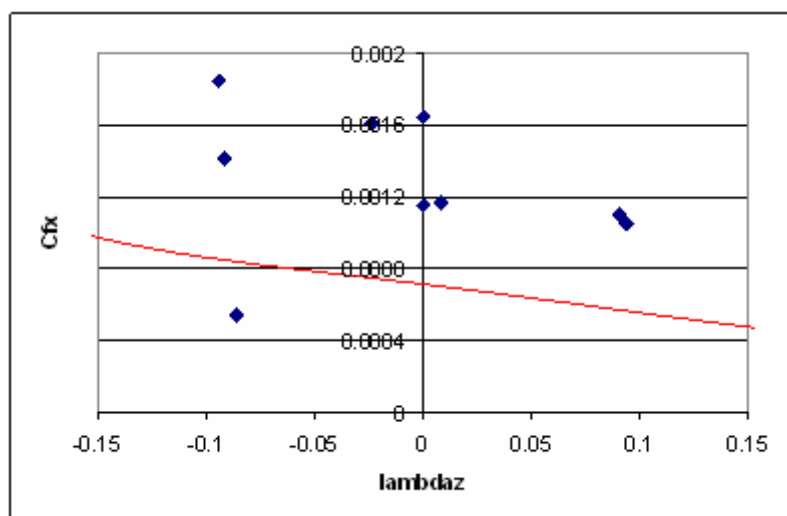
mu=0

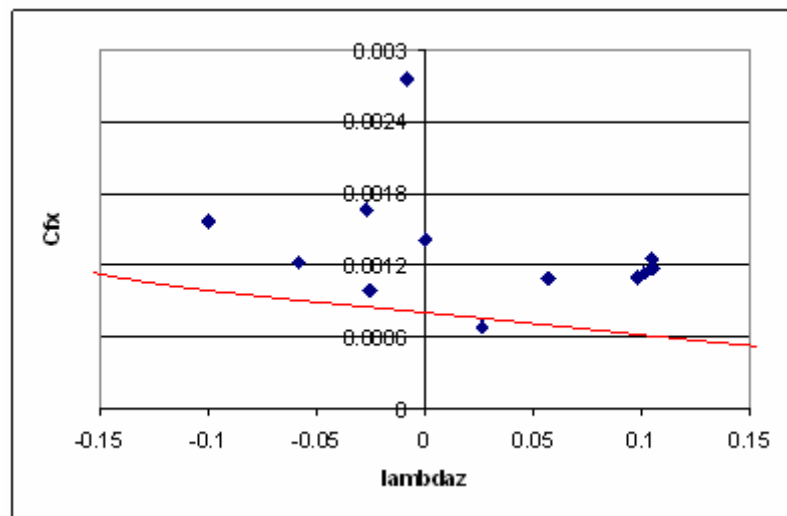
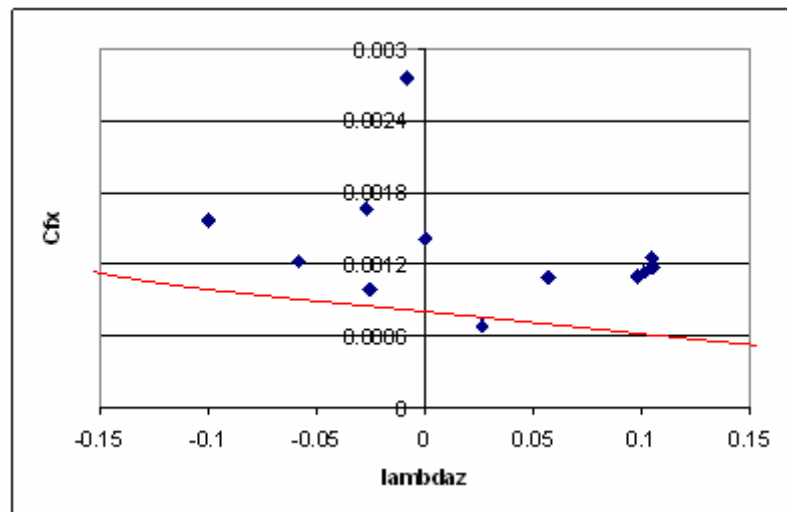
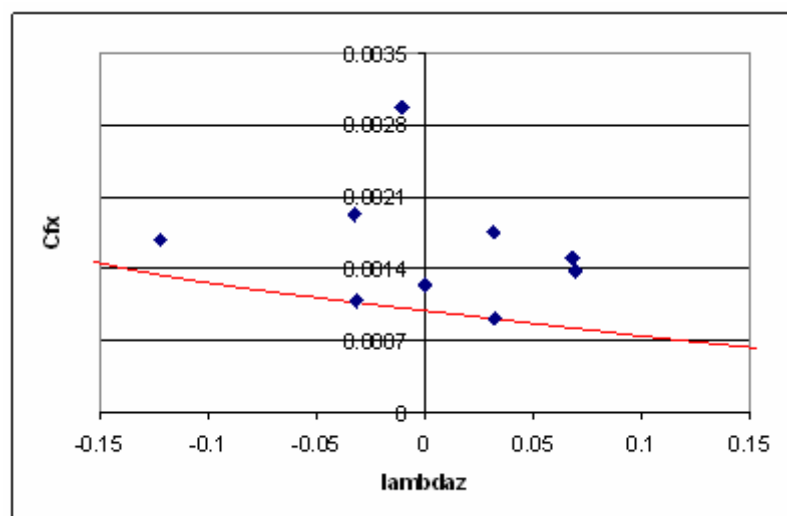


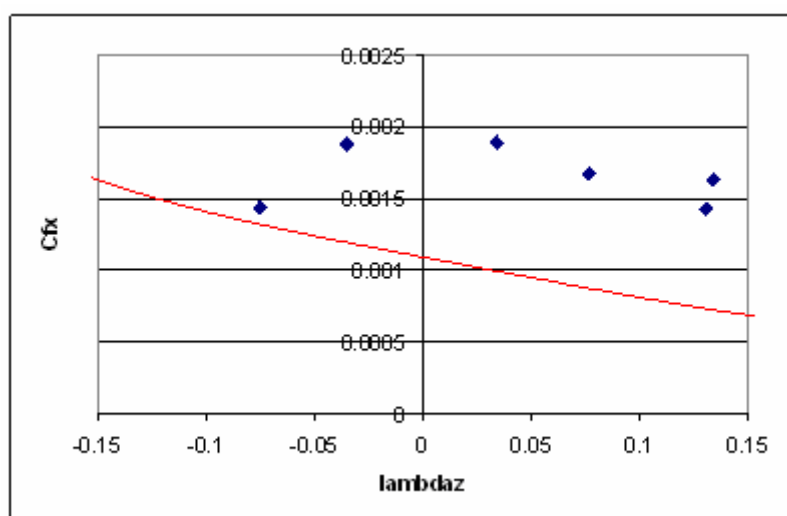
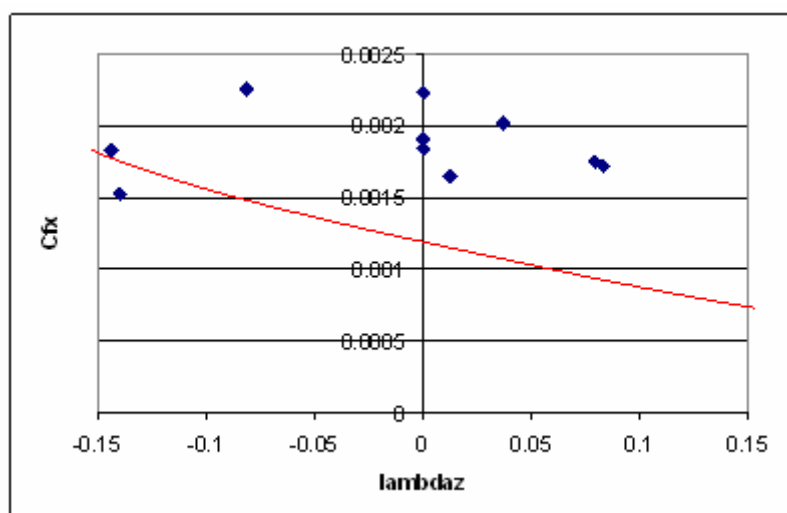
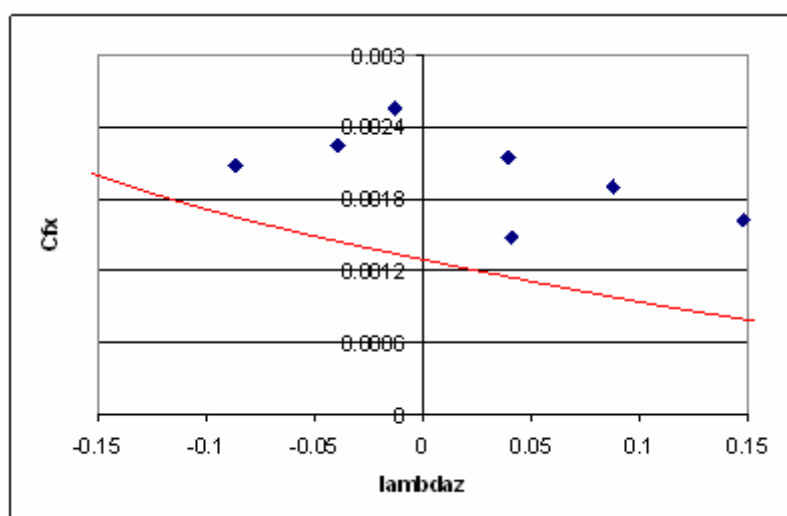
mu=0.03

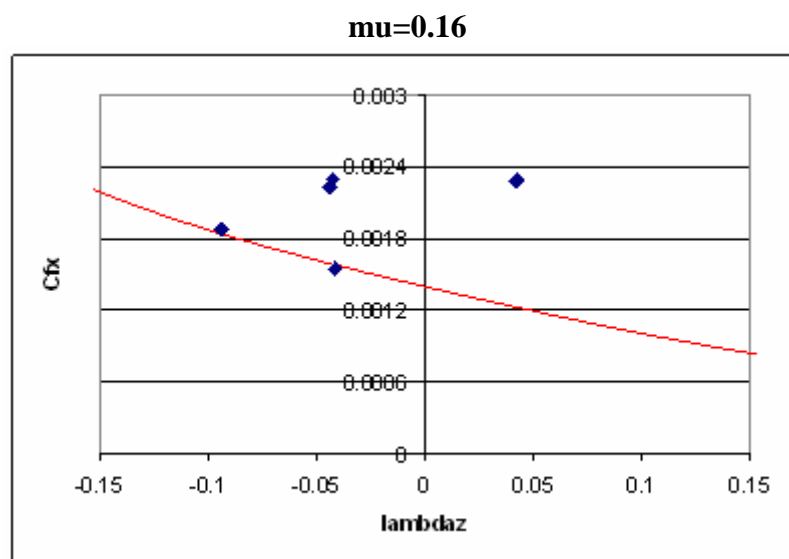


$\mu=0.04$  $\mu=0.05$  $\mu=0.06$ 

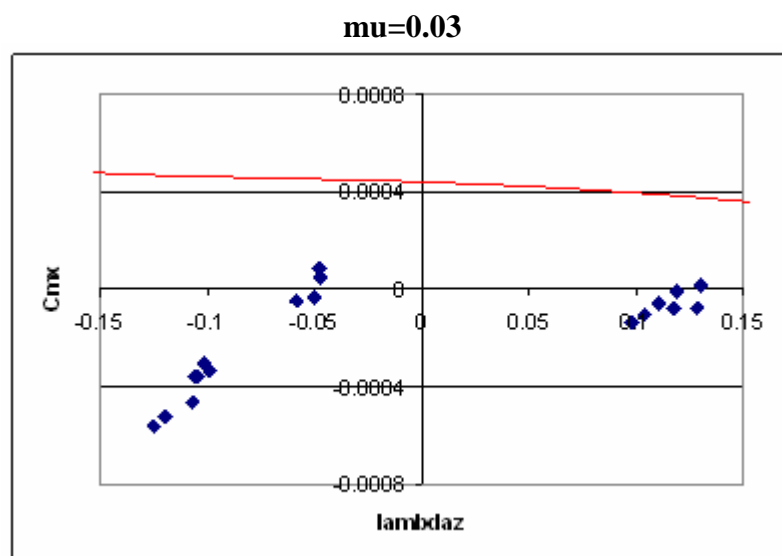
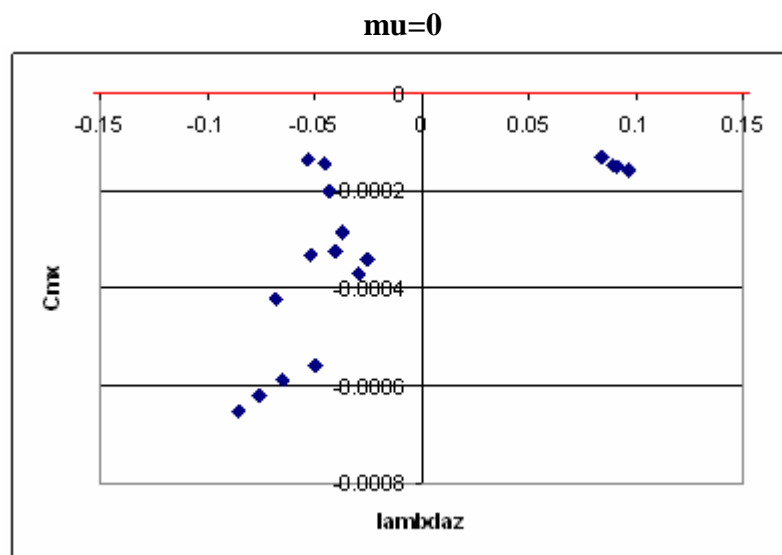
$\mu=0.07$  $\mu=0.08$  $\mu=0.09$ 

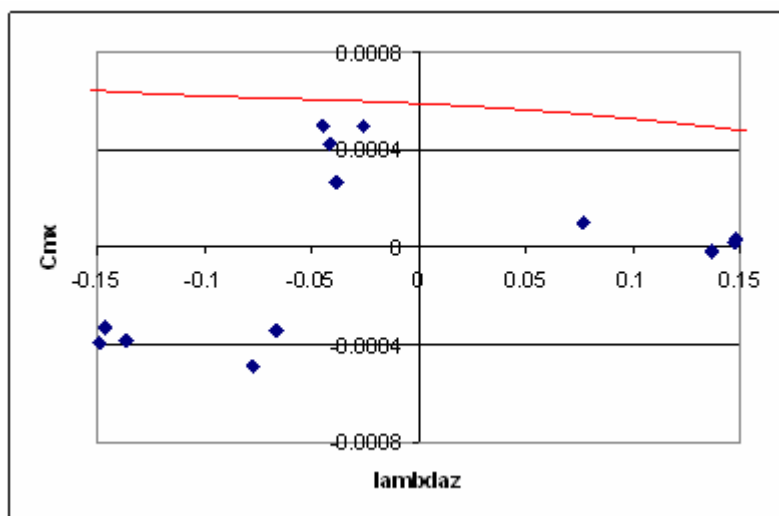
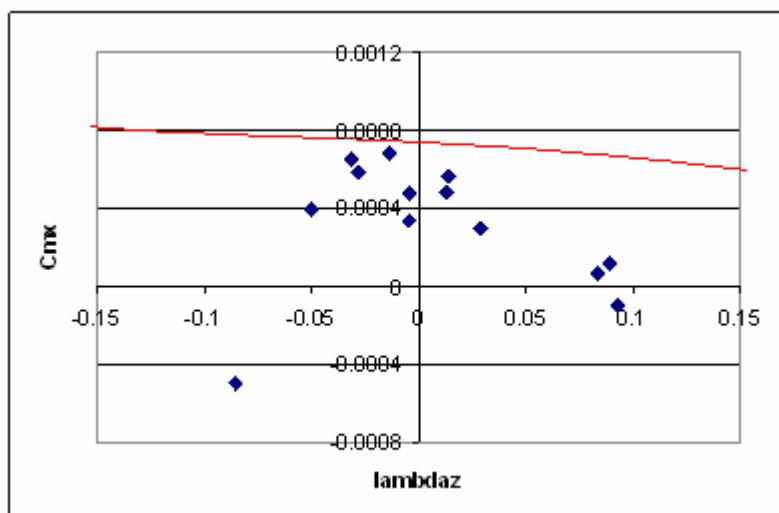
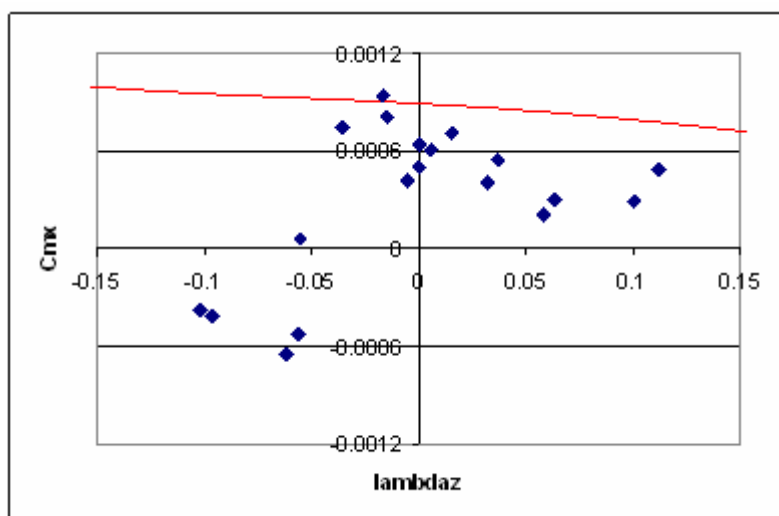
$\mu=0.10$  $\mu=0.11$  $\mu=0.12$ 

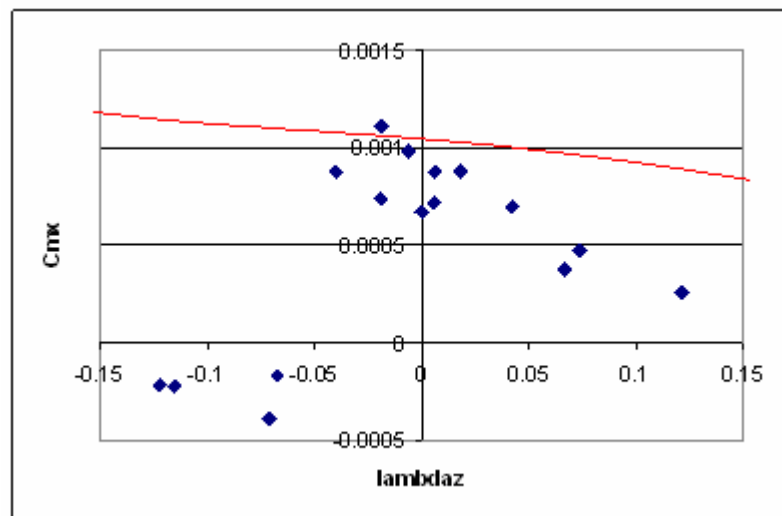
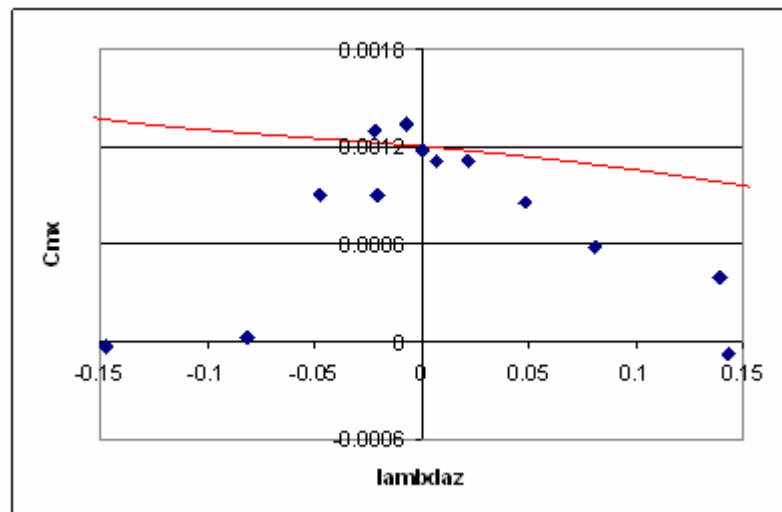
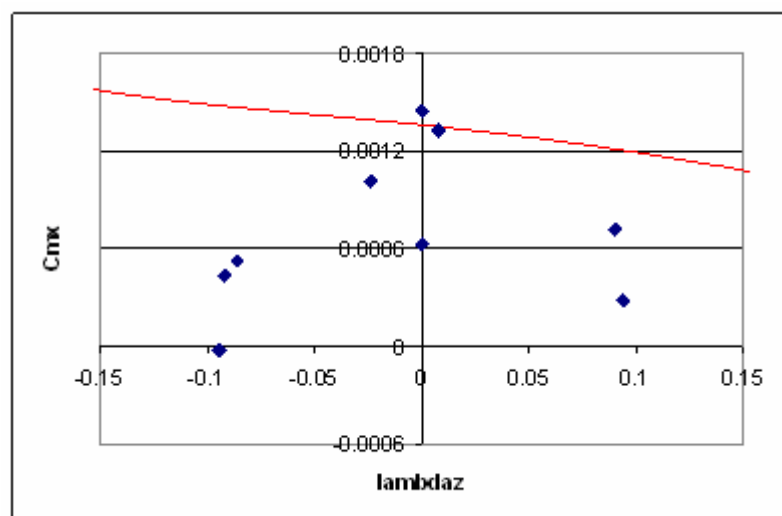
$\mu=0.13$  **$\mu=0.14$**  **$\mu=0.15$** 

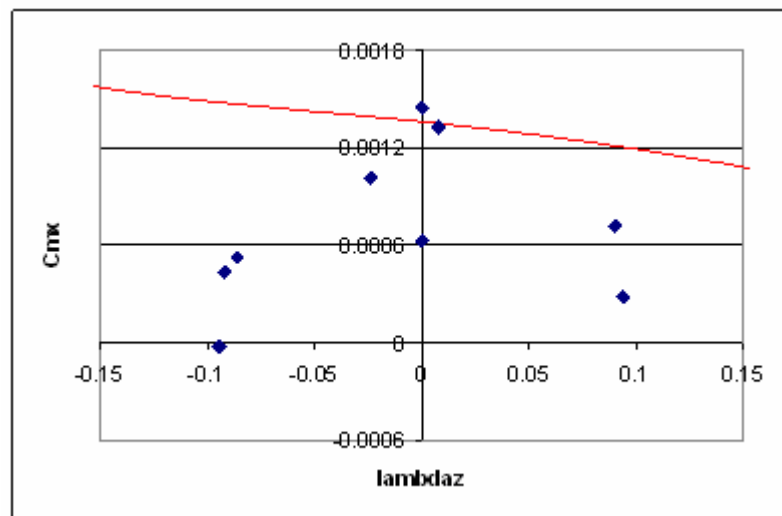
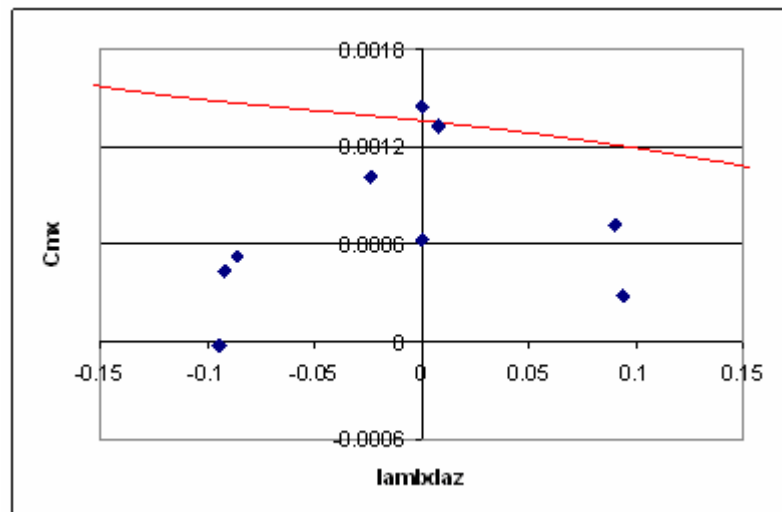
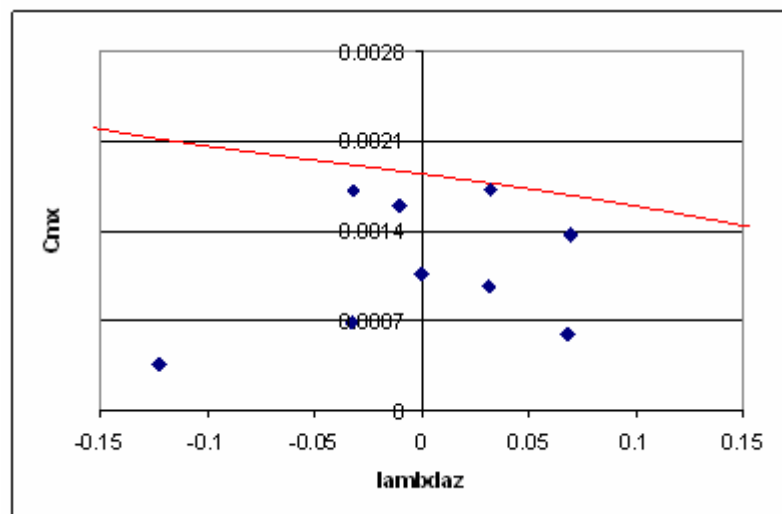


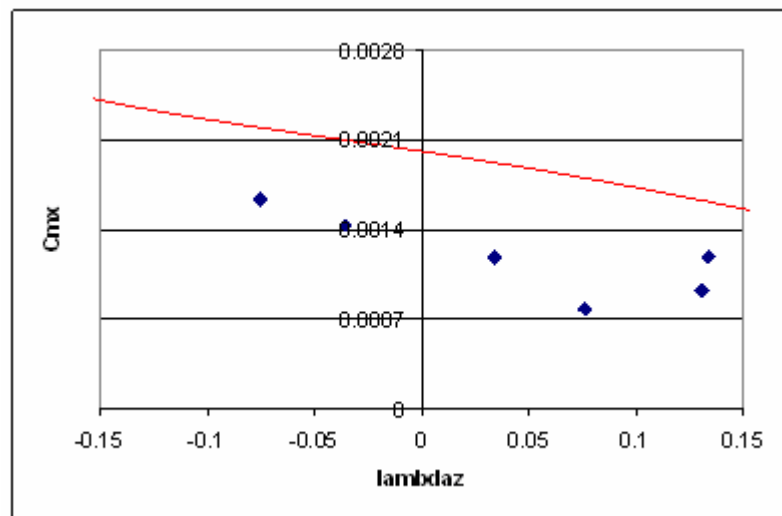
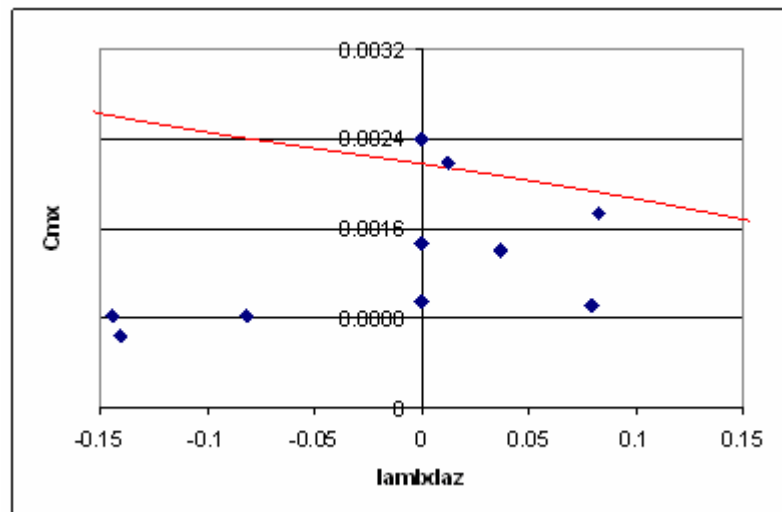
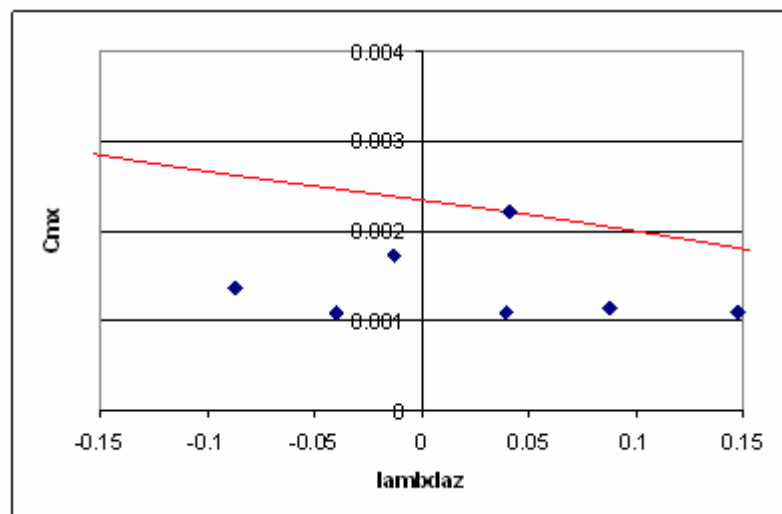
$$(C_{mx})_{hub}$$

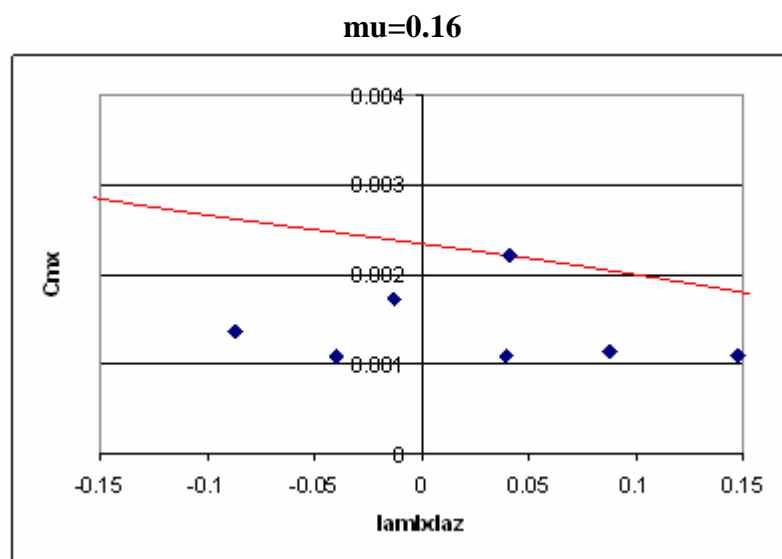


$\mu=0.04$  $\mu=0.05$  $\mu=0.06$ 

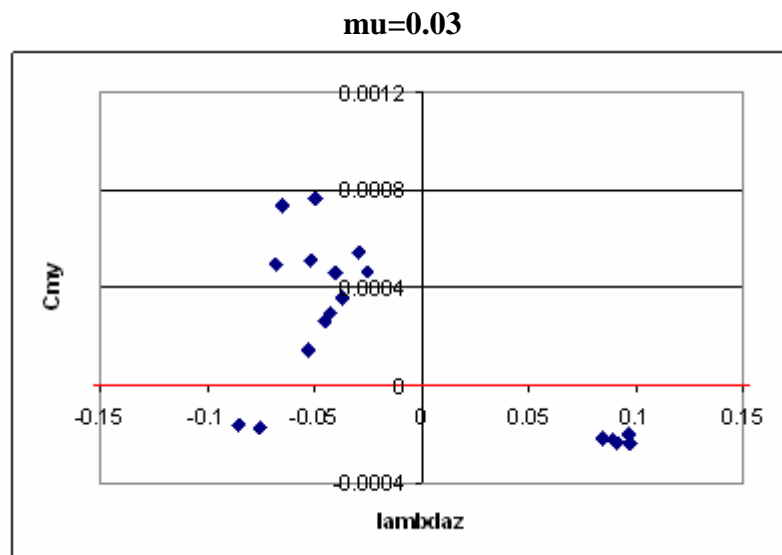
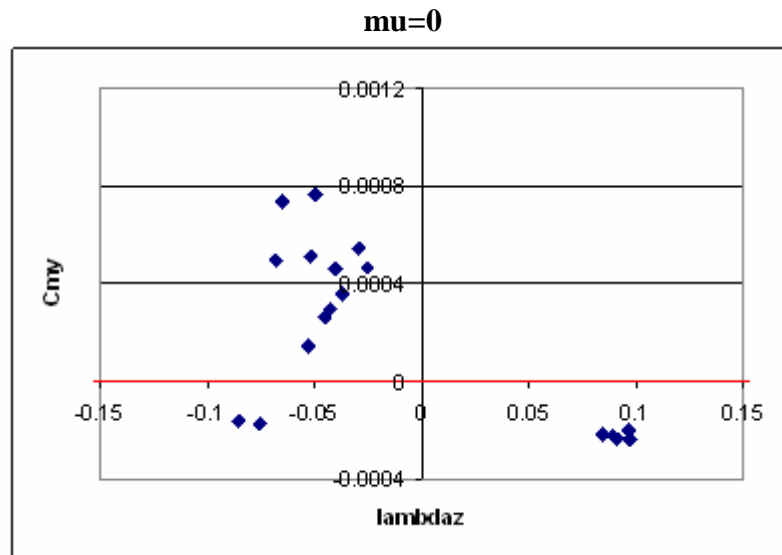
$\mu=0.07$  $\mu=0.08$  $\mu=0.09$ 

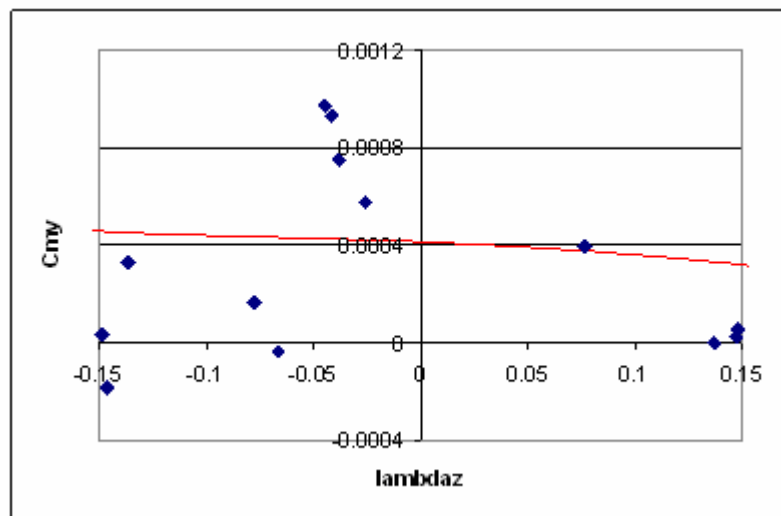
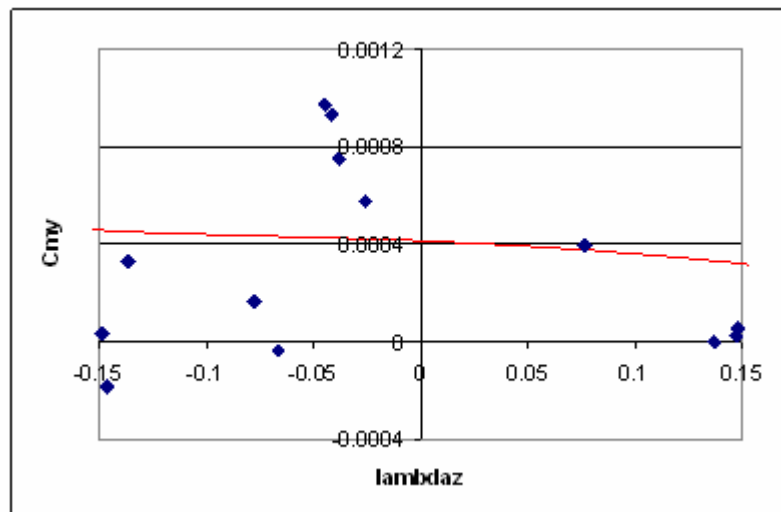
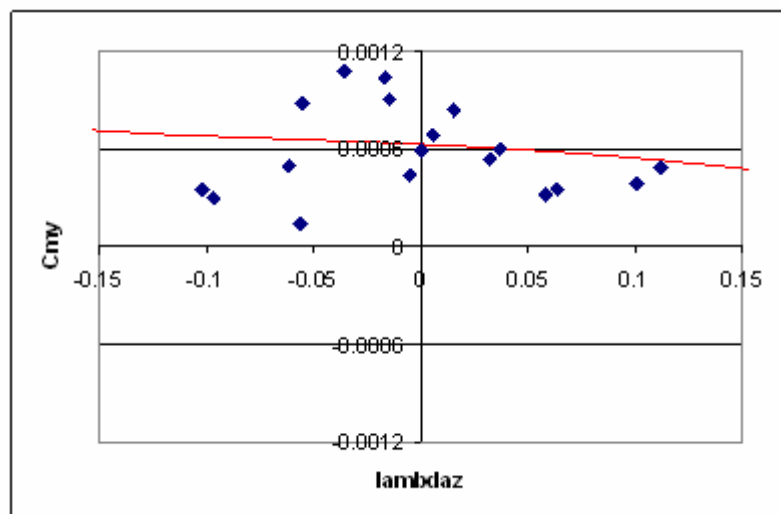
mu=0.10**mu=0.11****mu=0.12**

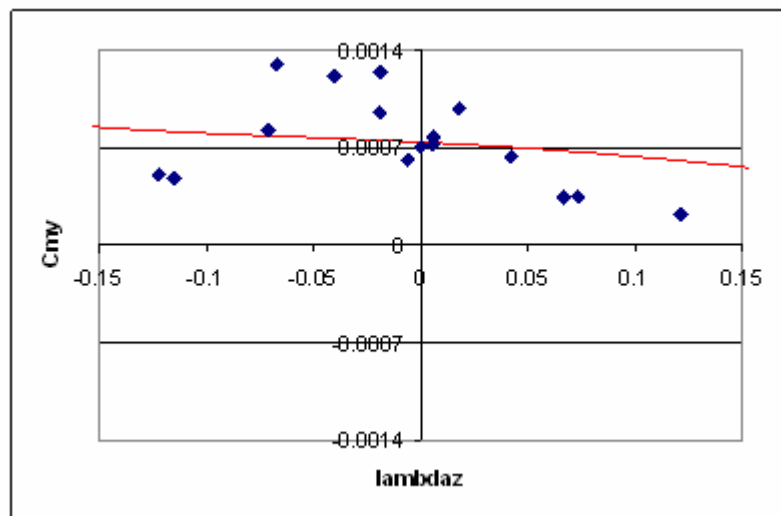
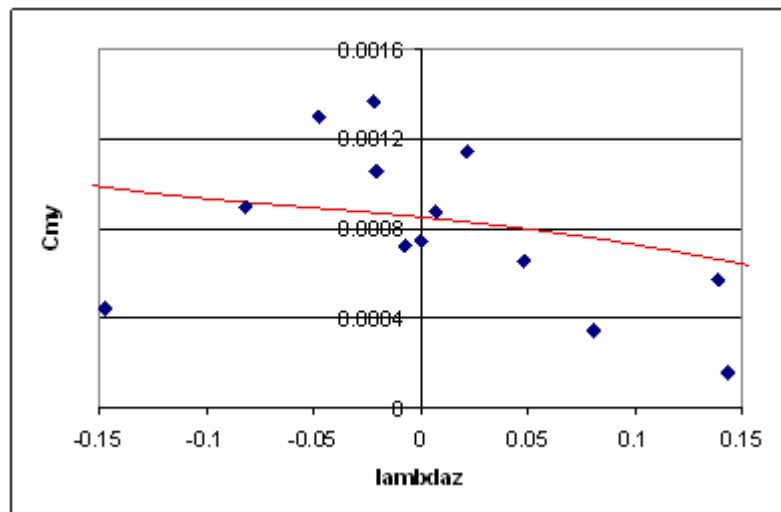
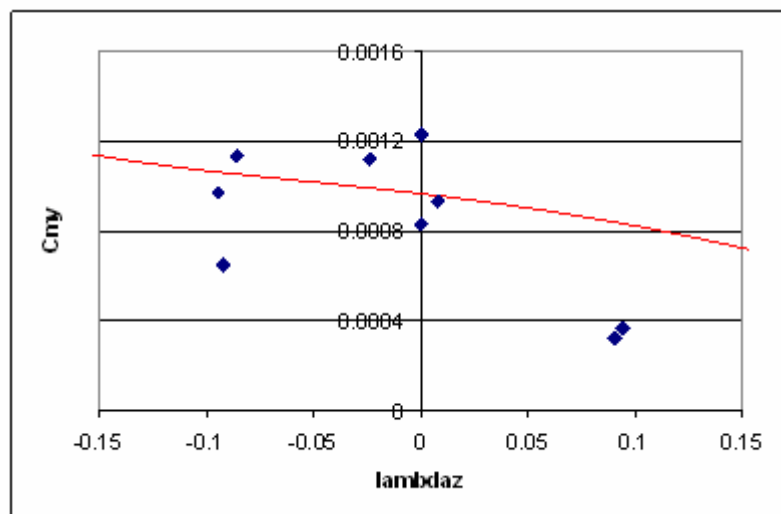
mu=0.13**mu=0.14****mu=0.15**

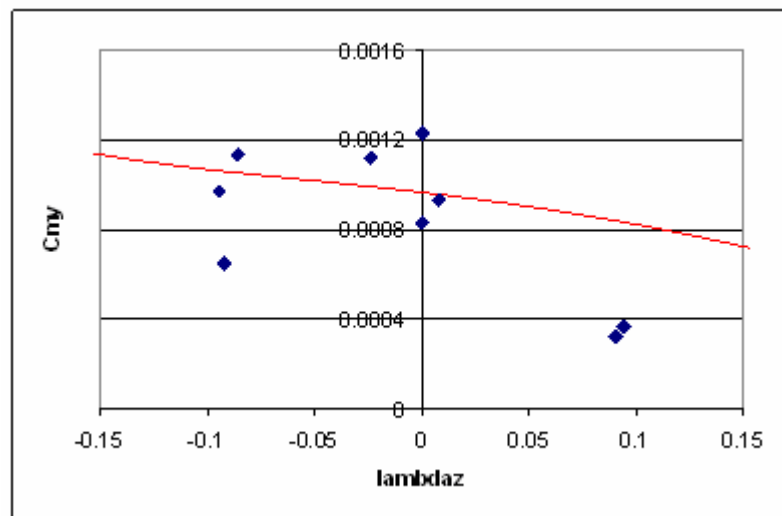
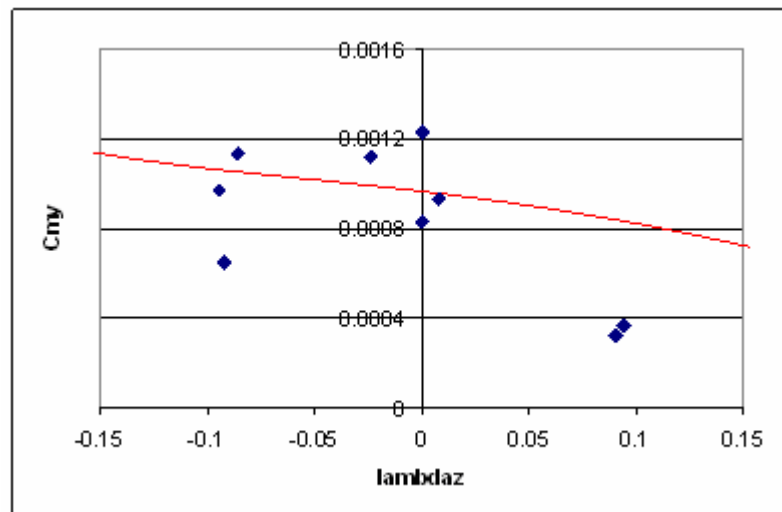
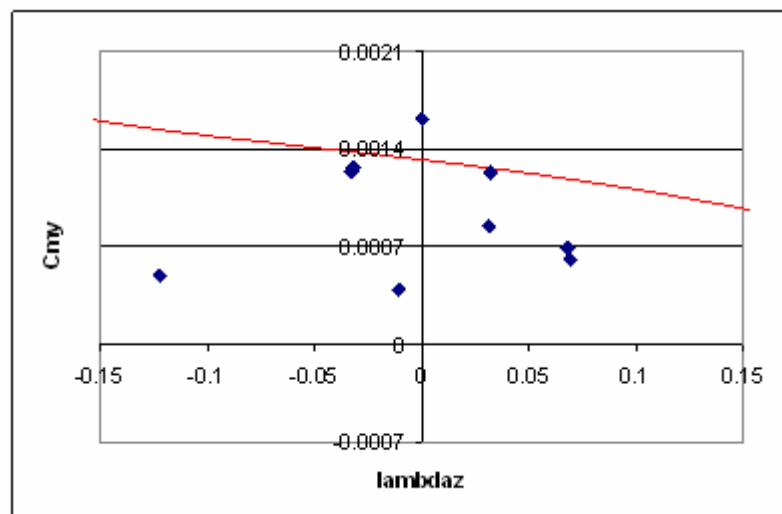


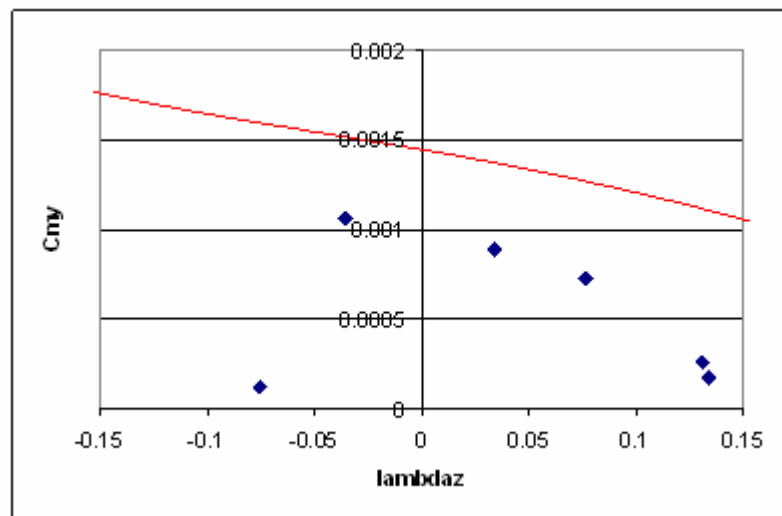
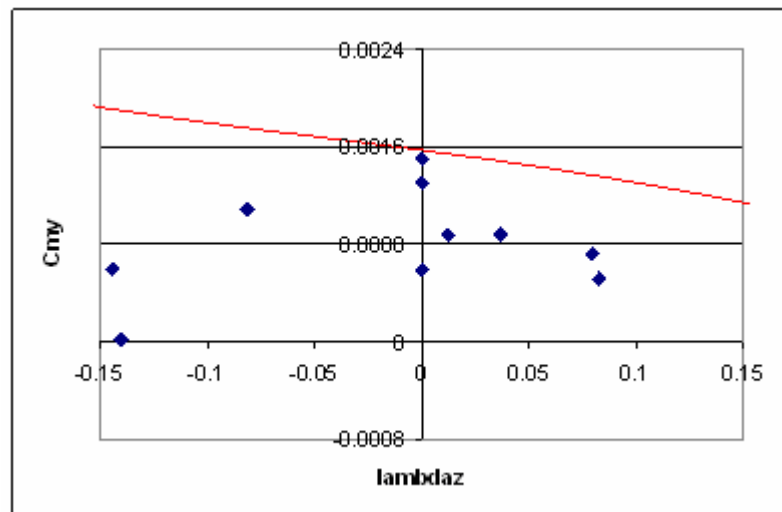
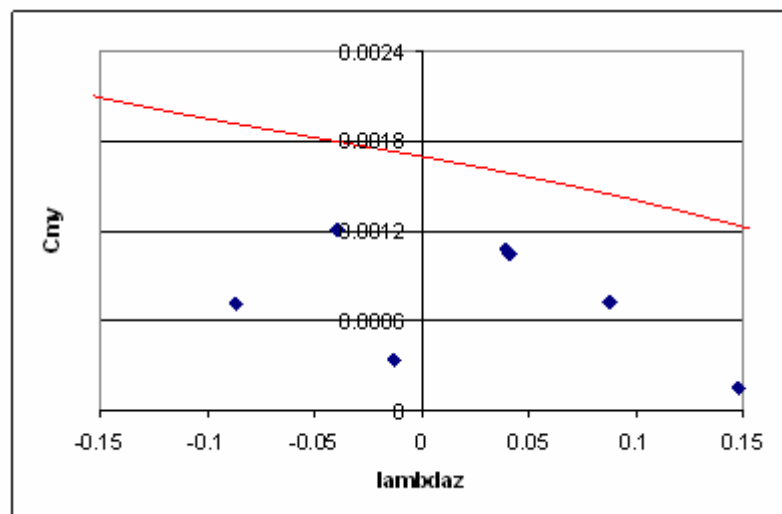
$$(C_{my})_{hub}$$

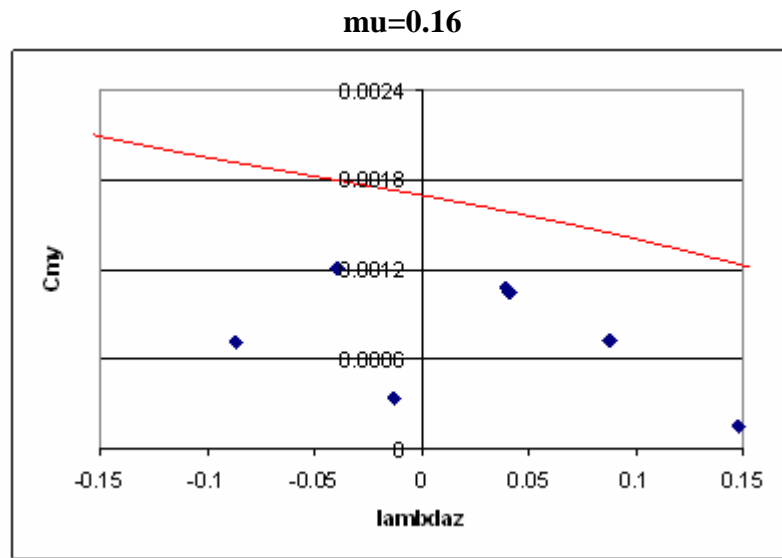


$\mu=0.04$  $\mu=0.05$  $\mu=0.06$ 

$\mu=0.07$  $\mu=0.08$  $\mu=0.09$ 

$\mu=0.10$  **$\mu=0.11$**  **$\mu=0.12$** 

$\mu=0.13$  **$\mu=0.14$**  **$\mu=0.15$** 



APPENDIX G: MATLAB FILES

The main files requires by the Simulink model are included in this Appendix.

DATA.m

% COMPLETE LIST OF PARAMETERS OF THE SIMULATOR

% *****

% ELECTRIC

K1 = 0.003472471;

Ra1 = 0.290909091;

L1 = 0.001;

vinf1 = 1.4; % lower limit for the voltage, estimated from the lower voltage used in the wind tunnel tests

vsup1 = 12*1.1; % upper limit, calculated by adding a 10% of the nominal voltage (12V)

K2 = 0.003472471;

Ra2 = 0.290909091;

L2 = 0.001;

vinf2 = 1.4; % lower limit for the voltage, estimated from the lower voltage used in the wind tunnel tests

vsup2 = 12*1.1; % upper limit, calculated by adding a 10% of the nominal voltage (12V)

K3 = 0.003472471;

Ra3 = 0.290909091;

L3 = 0.001;

vinf3 = 1.4; % lower limit for the voltage, estimated from the lower voltage used in the wind tunnel tests

vsup3 = 12*1.1; % upper limit, calculated by adding a 10% of the nominal voltage (12V)

K4 = 0.003472471;

Ra4 = 0.290909091;

L4 = 0.001;

vinf4 = 1.4; % lower limit for the voltage, estimated from the lower voltage used in the wind tunnel tests

vsup4 = 12*1.1; % upper limit, calculated by adding a 10% of the nominal voltage (12V)

% *****

% DIMENSIONS, MASSES AND INERTIAL PROPERTIES

% Masses

mb = 0.013; % Blade

mi = 0.0318; % Hub (=Gear)

mj = 0.1171; % Armature

m = 1.6571; % Airframe

% Rigid airframe

OG = [0 0 -0.05958];

% Hubs

m1 = mi;

OG1 = [0.4534 0 -0.1385];

OO1 = [0.4534 0 -0.1616];

m2 = mi;

OG2 = [0 0.4534 -0.1385];

OO2 = [0 0.4534 -0.1616];

m3 = mi;

OG3 = [-0.4534 0 -0.1385];

OO3 = [-0.4534 0 -0.1616];

```

m4 = mi;
OG4 = [0 -0.4534 -0.1385];
OO4 = [0 -0.4534 -0.1616];

%Armatures
m11 = mj;
OG11 = [0.52051 0 -0.10055];

m22 = mj;
OG22 = [0 0.52051 -0.10055];

m33 = mj;
OG33 = [-0.52051 0 -0.10055];

m44 = mj;
OG44 = [0 -0.52051 -0.10055];

%Inertia tensor of the rigid airframe on a set of axes parallel to Oxyz and with origin in the centre of mass
of the rigid airframe
IG = [0.062534 0.000027 0.000310;
      0.000027 0.063547 -0.000096;
      0.000310 -0.000096 0.119814];

%Inertia tensor of the hub on principal axes of inertia and with origin in Gi
Ih = [0.000019 0 0;
      0 0.000019 0;
      0 0 0.000032];

%Inertia tensor of the armature on principal axes of inertia and with origin in Gj
Ia = [0.000031 0 0;
      0 0.000031 0;
      0 0 0.000014];

% *****

%OTHER PARAMETERS

g = 9.8;
gr = 10;
F = 2.03467E-06;
rho = 1.225;

% *****

%MODELLING OF THE BLADES

factor = 1.2; %Empirical correction for the induced velocity. Run inflow.m after running DATA.m if this
parameter is changed.
a = 5.5; %Aerofoil lift slope
cd0 = 0.05;
cd1 = 0.7;
cd2 = 0;
c = 0.04; %Mean chord 0.032
R = 0.258; %Rotor disc radius (including the hinge offset)
b = 2; %Number of blades
sigma = b*c/(pi*R); %Rotor solidity
theta0 = 0.37; %Pitch at the root

```

```

theta1 = -0.09; %Twist
eb = 0.026; %Offset of the joint between the blade and the gear. Needed for aerodynamic purposes
rG = 0.111; %Distance from the joint to the centre of mass of the blade
A1 = 0; %Cyclic pitch parameter
B1 = 0; %Cyclic pitch parameter
Izb = 0.000378; %Inertia of the blade around the z axis, relative to the centre of the hub
omn = 109; %Natural flapping frequency of the non-rotating blade (rad/s) 109
Ib = 0.000211; %Blade flapping inertia around the hinge
Mb = mb*g*rG; %First static moment around the hinge
kbeta = Ib*omn^2;
lock = (rho*a*c*R^4)/Ib; %Lock Number

```

```

% ****

```

calc.m

% ADDITIONAL PROPERTIES TO BE CALCULATED

run DATA

mT = 4*b*mb+m1+m2+m3+m4+m11+m22+m33+m44+m; % Total mass

% Centre of mass of the complete vehicle

OGT = (1/mT)*(b*mb*OO1+b*mb*OO2+b*mb*OO3+b*mb*OO4+m1*OG1+m2*OG2+m3*OG3...
+m4*OG4+m11*OG11+m22*OG22+m33*OG33+m44*OG44+m*OG);

% This centre of mass is with the rotors stopped (when the centre of mass of the blades of each rotor is at Oi)

M = [b*mb b*mb b*mb b*mb m1 m2 m3 m4 m11 m22 m33 m44 m mT];

cm = [OO1;OO2;OO3;OO4;OG1;OG2;OG3;OG4;OG11;OG22;OG33;OG44;OG;OGT];

% Here, for simplicity, we have assumed that the centre of mass of the blades of each rotor is at Oi

I1 = IG+4*(Ih+Ia);

for i=1:13

AA = M(i)*[cm(i,2)^2+cm(i,3)^2 -cm(i,1)*cm(i,2) -cm(i,1)*cm(i,3);-cm(i,1)*cm(i,2)
cm(i,1)^2+cm(i,3)^2 -cm(i,2)*cm(i,3);-cm(i,1)*cm(i,3) -cm(i,2)*cm(i,3) cm(i,1)^2+cm(i,2)^2];

I1 = I1+AA;

end

for i=14:14

AA = M(i)*[cm(i,2)^2+cm(i,3)^2 -cm(i,1)*cm(i,2) -cm(i,1)*cm(i,3);-cm(i,1)*cm(i,2)
cm(i,1)^2+cm(i,3)^2 -cm(i,2)*cm(i,3);-cm(i,1)*cm(i,3) -cm(i,2)*cm(i,3) cm(i,1)^2+cm(i,2)^2];

I1 = I1-AA;

end

I2 = I1;

I1 = I1+b*Izb*[0 0 0;0 0 0;0 0 1];

I3 = -Ih-gr*Ia;

I4 = I3-b*Izb*[0 0 0;0 0 0;0 0 1];

C4_1 = [-F*gr/(Ia(3,3)*gr+Ih(3,3)/gr+b*Izb/gr) 1/(Ia(3,3)*gr+Ih(3,3)/gr+b*Izb/gr);-gr*(K1^2)/L1 -
Ra1/L1];

C4_2 = [-F*gr/(Ia(3,3)*gr+Ih(3,3)/gr+b*Izb/gr) 1/(Ia(3,3)*gr+Ih(3,3)/gr+b*Izb/gr);-gr*(K2^2)/L2 -
Ra2/L2];

C4_3 = [-F*gr/(Ia(3,3)*gr+Ih(3,3)/gr+b*Izb/gr) 1/(Ia(3,3)*gr+Ih(3,3)/gr+b*Izb/gr);-gr*(K3^2)/L3 -
Ra3/L3];

C4_4 = [-F*gr/(Ia(3,3)*gr+Ih(3,3)/gr+b*Izb/gr) 1/(Ia(3,3)*gr+Ih(3,3)/gr+b*Izb/gr);-gr*(K4^2)/L4 -
Ra4/L4];

blades.m

```

%S-FUNCTION blades

function [sys,x0,str,ts] =
blades(t,x,e,flag,a,cd0,cd1,cd2,sigma,b,theta0,theta1,A1,B1,mb,Mb,Ib,lock,eb,kbeta,omn,R,rG,c,rho,g,p)

%p=1 for counterclockwise propellers and clockwise for clockwise propellers

switch flag,
    case 0,
        [sys,x0,str,ts] = mdlInitializeSizes;
    case 1,
        sys = mdlDerivatives(t,x,e,flag);
    case 2,
        sys = mdlUpdate(t,x,e,flag);
    case 3,
        sys =
mdlOutputs(t,x,e,flag,a,cd0,cd1,cd2,sigma,b,theta0,theta1,A1,B1,mb,Mb,Ib,lock,eb,kbeta,omn,R,rG,c,rho
,g,p);
    case 4,
        sys = mdlGetTimeOfNextVarHit(t,x,e,flag);
    case 9,
        sys = mdlTerminate(t,x,e,flag);
    otherwise
        error(['Unhandled flag = ',num2str(flag)]);
end

% *****

function [sys,x0,str,ts] = mdlInitializeSizes()
sizes = simsizes;
sizes.NumContStates = 0;
sizes.NumDiscStates = 0;
sizes.NumOutputs = 9;
sizes.NumInputs = 8;
sizes.DirFeedthrough = 1;
sizes.NumSampleTimes = 1;
sys = simsizes(sizes);
x0 = [];
str = [];
ts = [0,0];

% *****

function sys = mdlDerivatives(t,x,e,flag)
sys = [];

% *****

function sys = mdlUpdate(t,x,e,flag)
sys = [];

% *****

```

```

function sys =
mdlOutputs(t,x,e,flag,a,cd0,cd1,cd2,sigma,b,theta0,theta1,A1,B1,mb,Mb,Ib,lock,eb,kbeta,omn,R,rG,c,rho
,g,p)

li = e(1);
lz = e(2);
mu = e(3);
pw = e(4);
qw = e(5);
om = e(6);
axialp = e(7);
beta = e(8);

squareL1 = 1.35+(omn/om)^2; %Southwell's equation.
eeff = Ib*R*(squareL1-1-kbeta/(Ib*om^2))/(mb*rG*R);

Kc = 0;

CT = 0.25*a*sigma*(1-eb/R)*((2/3+mu^2)*theta0+0.5*(1+mu^2)*theta1-lz-B1*mu-li);

f9 = 1+0.5*mu^2;
f9b = 1-0.5*mu^2;
f10 = 1/2*lock*Ib*(om^2)*(1-eb/R)^2;

M11 = -(Ib*om^2+kbeta+eeff*Mb*om^2/g);
M12 = f10*(mu/4)*(eeff/R);
M13 = 0;
M21 = 0;
M22 = -f10*(1/4-mu^2/8-1/6*eeff/R-1/12*(eeff/R)^2);
M23 = eeff*Mb*om^2/g+kbeta;
M31 = -f10*mu*(1/3+1/6*eeff/R);
M32 = eeff*Mb*om^2/g+kbeta;
M33 = f10*(1/4+mu^2/8-1/6*eeff/R-1/12*(eeff/R)^2);
F1 = -f10*(1/4*theta0*(1+mu^2+2/3*eeff/R+1/3*(eeff/R)^2)+theta1*(1/5+mu^2/6*(1-eeff/R)-
1/10*eeff/R-1/15*(eeff/R)^2-1/30*(eeff/R)^3)-(lz+li+B1*mu)*(1/3+1/6*eeff/R));
F2 = -f10*(2*theta0*mu*(1/3+1/6*eeff/R)+2*theta1*mu*(1/4-1/6*eeff/R-1/12*(eeff/R)^2)-
B1*(1/4+3/8*mu^2+1/6*eeff/R+1/12*(eeff/R)^2)-1/2*mu*(lz+li));
F3 = -f10*(-A1*(1/4+mu^2/8+1/6*eeff/R+1/12*(eeff/R)^2)-1/3*li*Kc*(1/4-1/6*eeff/R-
1/12*(eeff/R)^2));

a0 = det([F1 M12 M13;F2 M22 M23;F3 M32 M33])/det([M11 M12 M13;M21 M22 M23;M31 M32
M33]);
a1s_a = det([M11 F1 M13;M21 F2 M23;M31 F3 M33])/det([M11 M12 M13;M21 M22 M23;M31 M32
M33]);
b1s_a = det([M11 M12 F1;M21 M22 F2;M31 M32 F3])/det([M11 M12 M13;M21 M22 M23;M31 M32
M33]);

N22 = -1/4*f10*(1-mu^2/2);
N23 = eeff*Mb*om^2/g+kbeta;
N32 = eeff*Mb*om^2/g+kbeta;
N33 = 1/4*f10*(1+mu^2/2);
G2 = -1/4*f10*pw/om+2*Ib*qw*om;
G3 = -1/4*f10*qw/om-2*Ib*pw*om;

a1s_b = det([G2 N23;G3 N33])/det([N22 N23;N32 N33]);
b1s_b = det([N22 G2;N32 G3])/det([N22 N23;N32 N33]);

a1s = a1s_a+a1s_b;

```

```

b1s = b1s_a+b1s_b;

f29 = 1+1.5*mu^2;

f30 = 1/2-19/36*mu^2+3/4*mu^4;
f31 = 2/5-2/5*mu^2+1/2*mu^4;
f32 = (1/3)*(2-mu^2);
f33 = 1/2+2/9*mu^2-mu^4/24+9/8*mu^6;
f34 = 1/3+mu^2/4+9/16*mu^4;
f35 = 1+2*mu^2+3/4*mu^4;
f36 = 4/5+2/5*mu^2-mu^4/5+3/2*mu^6;
f37 = 4/3+4/3*mu^2-mu^4;
f38 = 1+mu^2-3/4*mu^4;
f39 = 1/18+mu^2/6-mu^4/8;
f40 = 1/8+mu^2/16;
f41 = mu/3+mu^3/6;

f50 = 1/9-mu^2/2;
f51 = -7/9+5/3*mu^2-15/4*mu^4;
f52 = -1/2+3/2*mu^2-9/8*mu^4;
f53 = -4/3+3*mu^2-9/2*mu^4;
f54 = -2+5*mu^2;
f55 = -2+3*mu^2;
f56 = 2/9*mu+mu^3/3;
f57 = 1/6+5/12*mu^2;

CQ = 0.25*sigma*(0.5*cd0*(1+mu^2)+(cd1/f29)*(theta0*f30+theta1*f31+(-lz+mu*a1s-li)*f32)...
+(cd2/(f29^2))*(theta0^2*f33+theta1^2*f34+(-lz+mu*a1s-li)^2*f35+theta0*theta1*f36+theta0*(-
lz+mu*a1s-li)*f37+theta1*(-lz+mu*a1s-li)*f38)...
+(cd2/(f9^2))*mu^2*(a0^2*f39+li^2*f40+a0*li*f41));

CH = 0.25*sigma*mu*(cd0+(cd1/f29)*(theta0*f50-0.5*theta1*mu^2+(-lz+mu*a1s-
li)/3)+(cd2/(f29^2))*(theta0^2*f51+theta1^2*f52-2*(-lz+mu*a1s-li)^2)...
+theta0*theta1*f53+theta0*(-lz+mu*a1s-li)*f54+theta1*(-lz+mu*a1s-li)*f55-
mu^2*(cd2/(f9^2))*(a0^2*f56+1/8*mu*li^2+a0*li*f57));

coef_f = rho*(pi*R^2)*(om*R)^2;
coef_m = rho*R*(pi*R^2)*(om*R)^2;

T = coef_f*CT;
H = coef_f*CH;
Q = coef_m*CQ;

fx = H*cos(a1s)+T*tan(a1s)*(1/sqrt(1+tan(a1s)^2+tan(p*b1s)^2)); %aprox H+T*tan(a1s)
fy = T*tan(p*b1s)*(1/sqrt(1+tan(a1s)^2+tan(p*b1s)^2));
fz = T*(1/sqrt(1+tan(a1s)^2+tan(p*b1s)^2))-H*sin(a1s);

mx = (1/2*b*eeff*(om^2)*Mb/g+kbeta)*p*b1s-p*Q*tan(a1s)*(1/sqrt(1+tan(a1s)^2+tan(p*b1s)^2));
my = (1/2*b*eeff*(om^2)*Mb/g+kbeta)*a1s+p*Q*tan(p*b1s)*(1/sqrt(1+tan(a1s)^2+tan(p*b1s)^2));
mz = p*Q/sqrt(1+tan(a1s)^2+tan(p*b1s)^2);

Fx = axialp*(-fx*cos(beta)-fy*sin(beta));
Fy = axialp*(fy*cos(beta)-fx*sin(beta));
Fz = -fz;

Mx = axialp*(mx*cos(beta)-my*sin(beta));
My = axialp*(my*cos(beta)+mx*sin(beta));
Mz = mz;

```

```
sys = [Fx,Fy,Fz,Mx,My,Mz,a0,a1s,b1s];

% *****

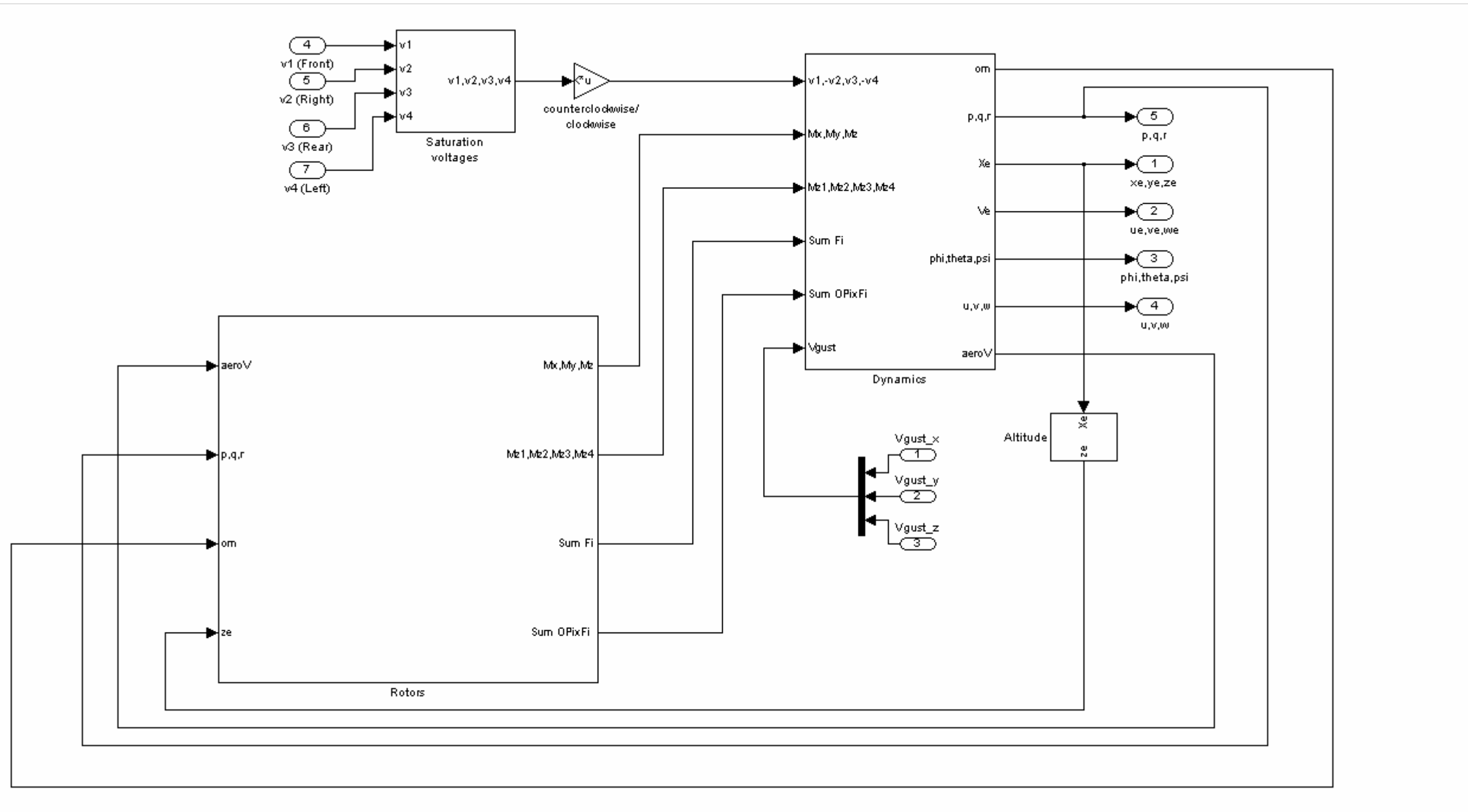
function sys = mdlGetTimeOfNextVarHit(t,x,e,flag)
sampletime = [];

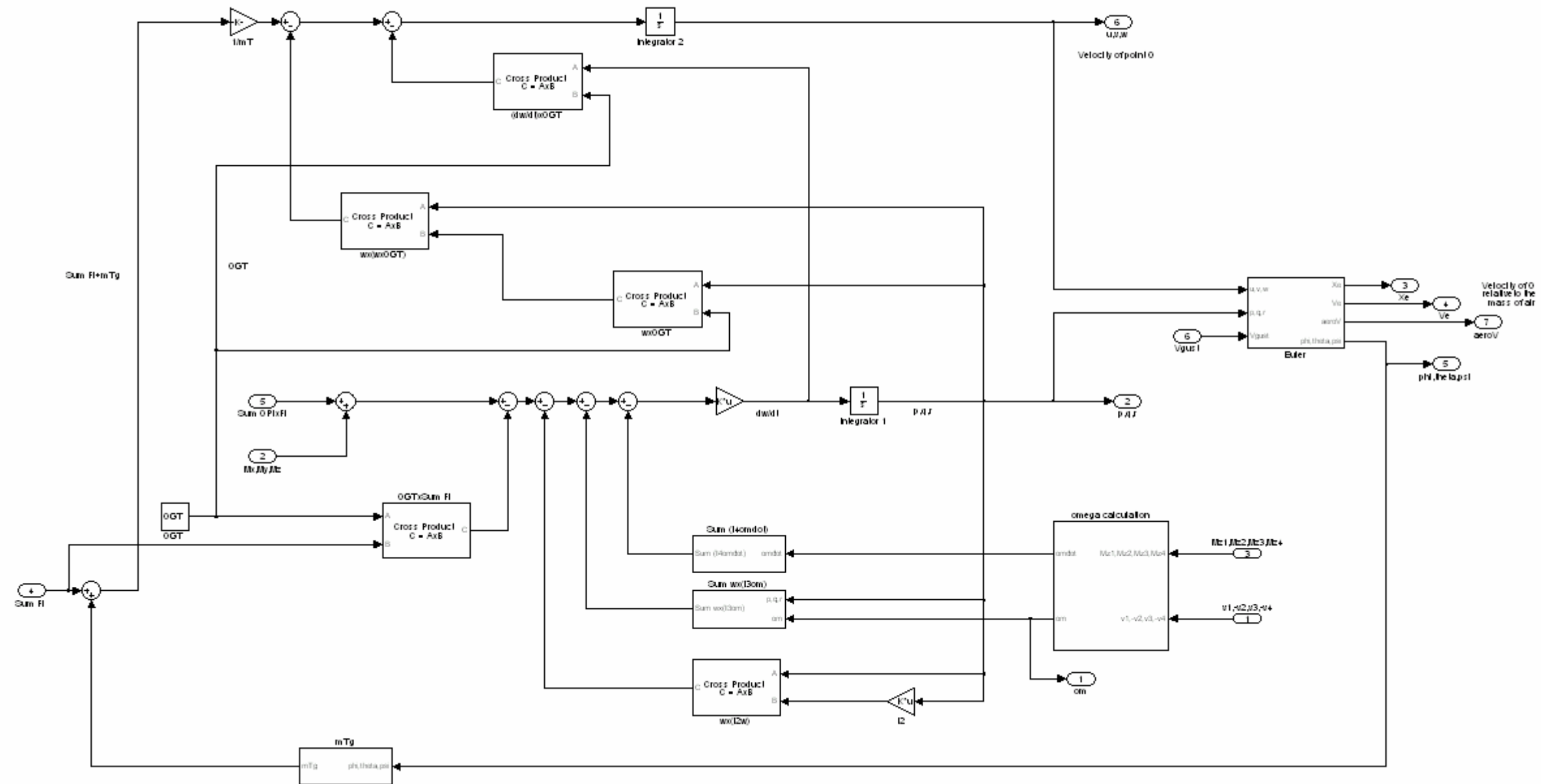
% *****

function sys = mdlTerminate(t,x,e,flag)
sys = [];
```

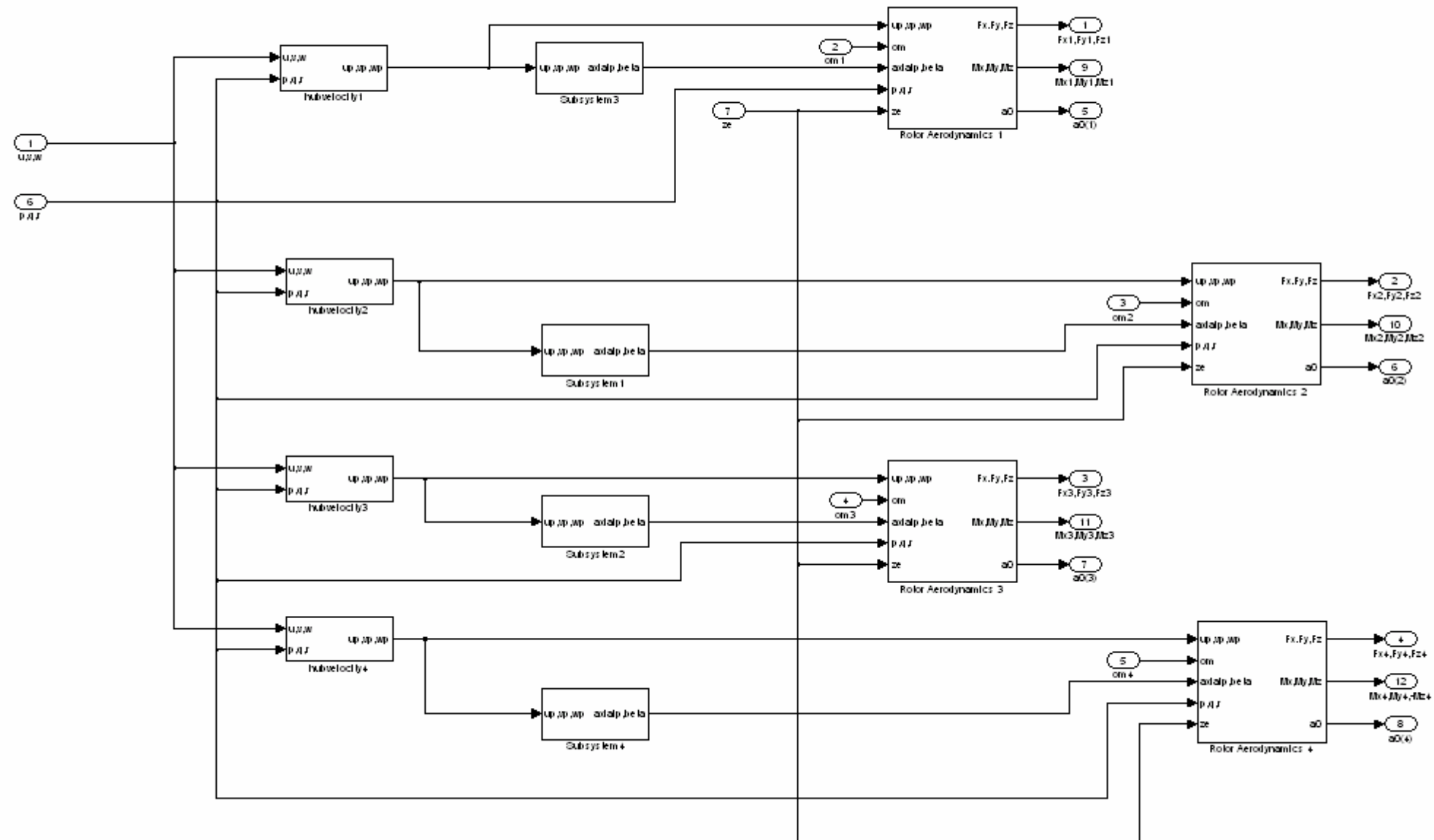

APPENDIX H: SIMULINK BLOCKS

The following pages contain several figures with the basic blocks of the Simulink model.

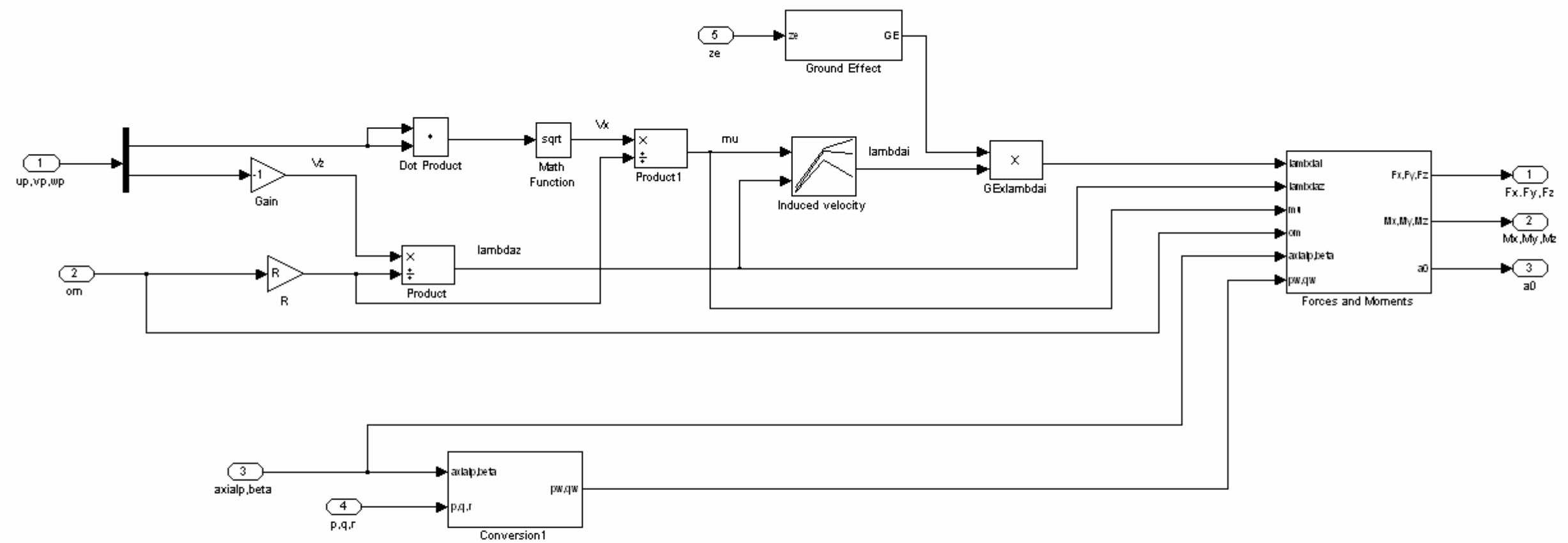
**Block: Quadrotor**



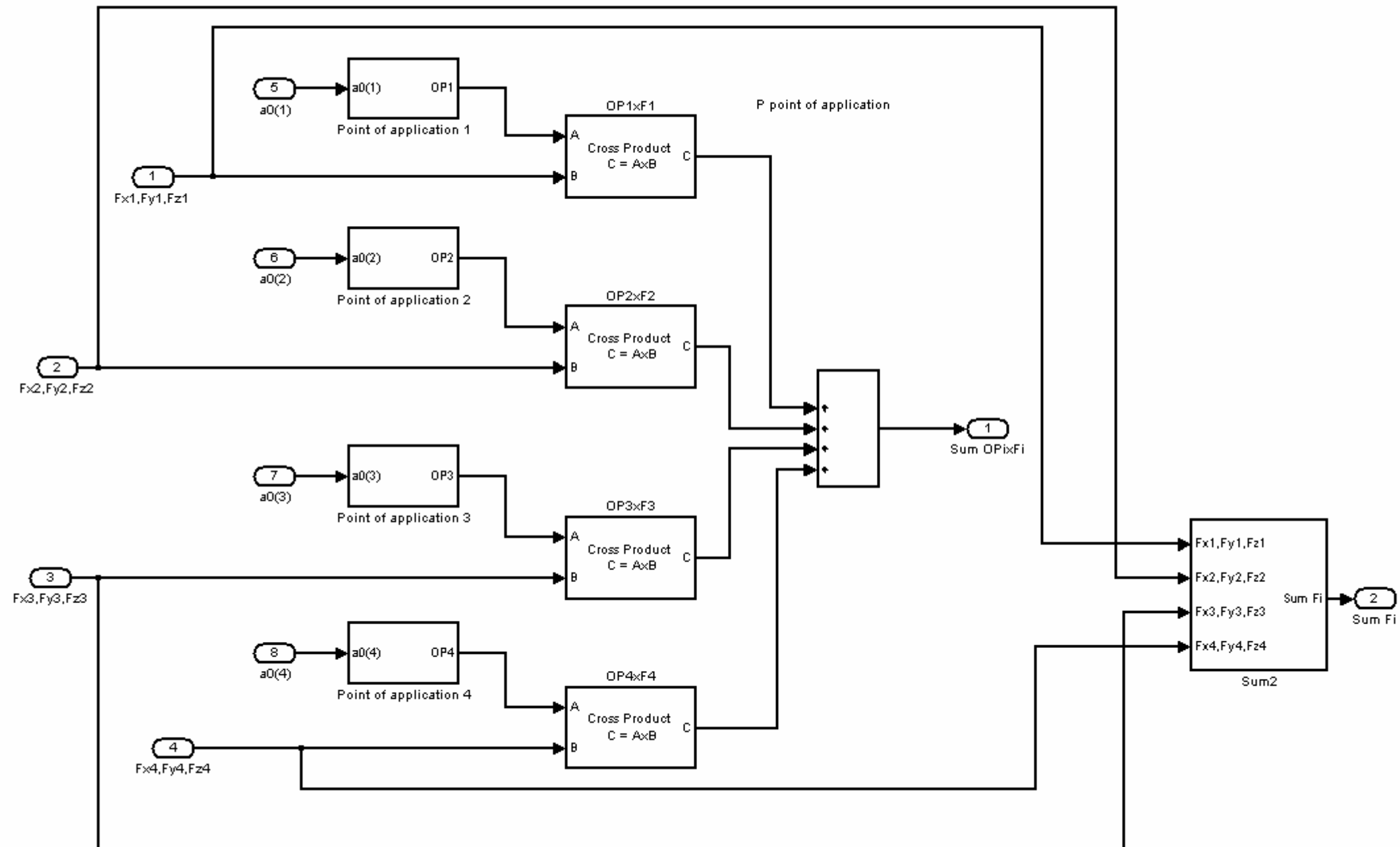
Block: Dynamics

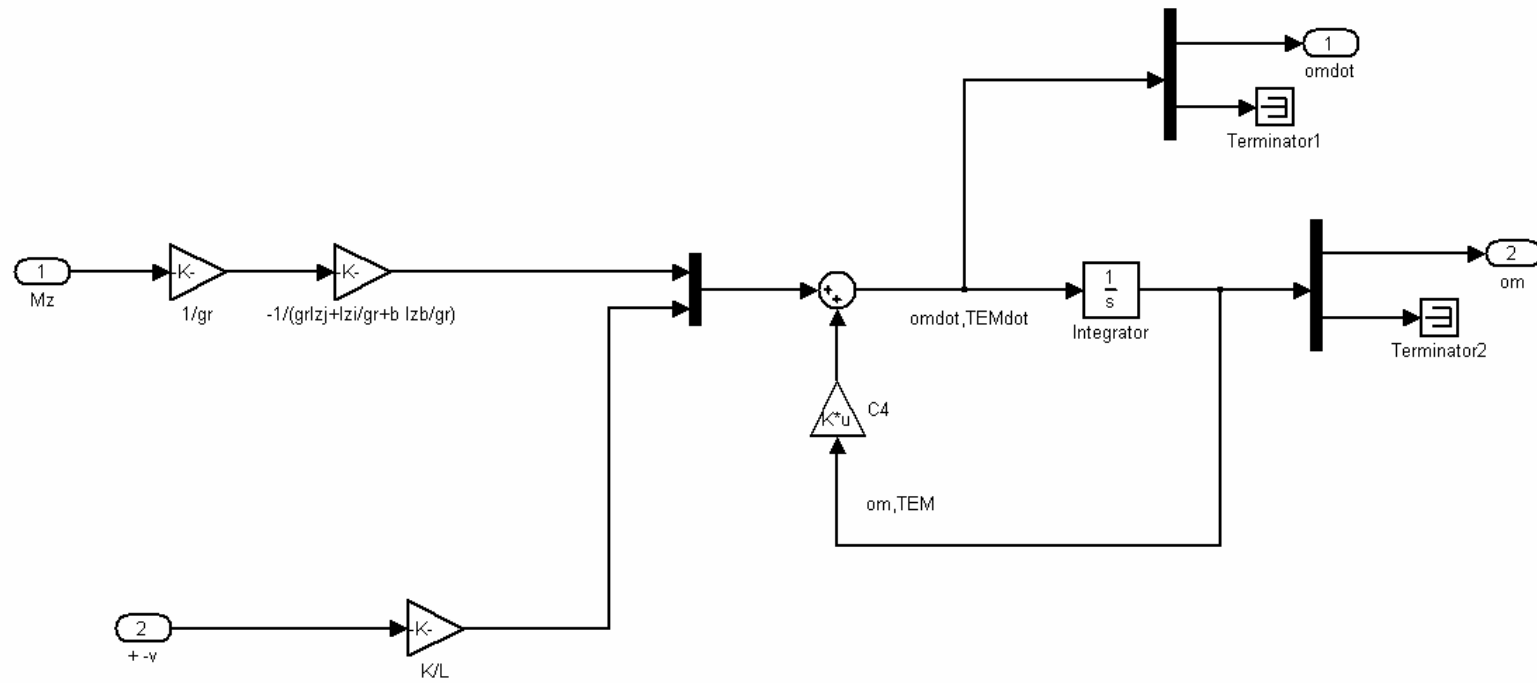


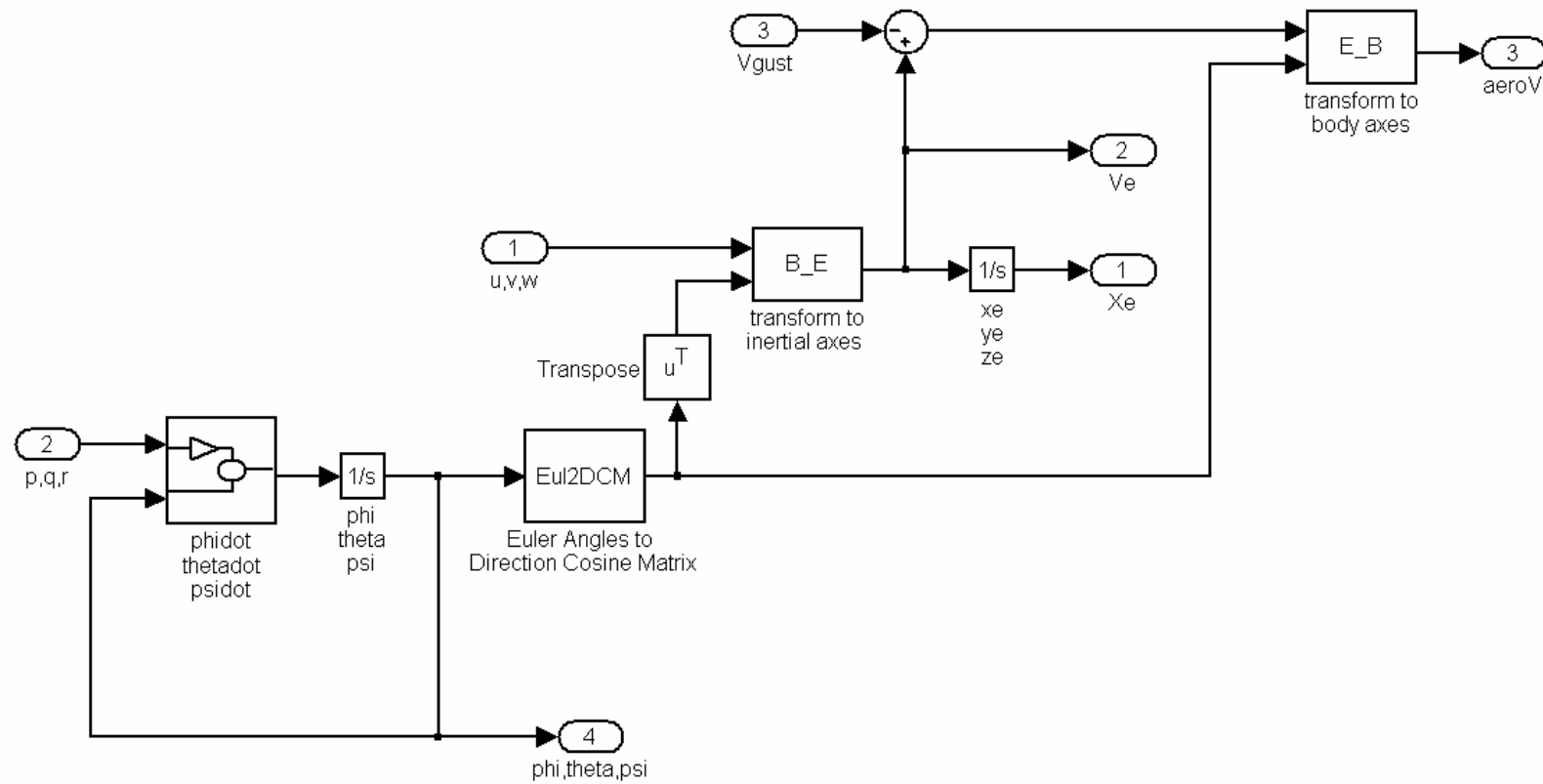
Block: Model of the Rotor



Block: Rotor Aerodynamics

**Block: Calculations**

**Block: Motor**

**Block: Euler**

THIS PAGE INTENTIONALLY LEFT BLANK